Mineralogy and chemical mobility in a weathered ash dump site, South Africa

By

OLUFUNKE IDOWU OJO

B.Sc. (Hons.) Geology

Submitted in fulfilment of the requirements for the degree of Magister Scientiae in Environmental Science

Earth Sciences Department

University of the Western Cape

Supervisor

Dr. A. Akinlua

Co-Supervisors

Dr. L.F. Petrik and Mr. A.C.T. Scheepers

April 2010

ABSTRACT

Coal fly ash generated from coal fired plants poses potential health risks to humans and plants in the environment due to the surface enrichment of the ash with various toxic trace elements during combustion. Only a small portion of the fly ash produced every year as a result of the increase in the demand for electricity, is being utilized. The bulk of the ash is disposed of in ash dams and landfills. Rain water as well as waste water from the ash slurry serves as leaching medium for the toxic elements into the environment, especially into the groundwater.

This study aims at understanding the chemical and mineralogical composition of the weathered fly ash, the distributive pattern of species down the ash dump, the various mineral phases with which the elements are associated and the change in mineralogy as a result of weathering over time. Methods employed in this study included the use of XRF and total acid digestion of the samples followed by ICP AES/MS analysis of the leachates to identify and quantify the major, minor and trace elements in the ash samples, pore water chemistry of the samples to determine the species soluble in water at various horizons in the drilled core, XRD and SEM/EDS to determine the mineralogy and morphology of the fly ash samples and a 5 step sequential extraction procedure to understand the various mineral phases with which the elements in the fly ash are associated.

Fly ash samples were obtained from a core drilled to 32 m at Kragbron in the Free State Province of South Africa. Geology of the area falls under the Karoo Supergroup and the study site is underlain with Jurassic dolerite rock of the Karoo Supergroup. The ash was disposed at the dump as slurry in a layered form.

The bulk chemical composition as determined by XRF showed Al_2O_3, SiO_2, Fe_2O_3 and CaO as the major oxide constituents in the fly ash samples. Kragbron ash belongs to Class F according to ASTM C618, as the sum of the percentage composition of SiO_2, Al_2O_3 and Fe_2O_3 revealed by XRF was greater than 70 % and the lime content was less

than 10 %. Loss on ignition values in most of the samples (between 15 m and 22 m) was higher than specified by ASTM C618. This was as a result of the different coals used in the combustion units at the power stations.

Comparison between the results obtained from XRF and the ICP analysis of the fly ash digestates was good in some of the elements. Al, Si and Na concentration was higher with XRF than with ICP. This was expected because the elements are present in reasonable amounts in fly ash. The concentration of Ca, Fe, Mg, K and Ti was higher with ICP than with XRF. This ought not to be as these elements are also present in appreciable quantities in fly ash. Results obtained with XRF showed more accuracy because the technique gives total composition of the solid sample and chances of contamination are minimal.

Results obtained from XRD showed mullite, quartz and calcite to be the major crystalline mineral phases identified in most of the ash samples. Hematite and calcite were observed at 22 m depth in the ash dump. The inclusion of hematite at 22 m could be due to mixing with parts of the bedrock during the initial construction of the ash dump as hematite was not identified in the previous depths. Mullite, quartz, anorthite and diopside were the minerals identified at 23 m. The presence of mullite also indicates a mixture of ash and bedrock components. Literature revealed the bedrock to be dolerite. Major minerals revealed by XRD from 24 m to 32 m were quartz, diopside and anorthite commonly found in dolerites.

The pH pattern observed in the profile showed strong weathering at the surface of the dump between 1 m and 5 m and it was alkaline for all the samples. Electrical conductivity (EC) was very high at 16 m depth and the trend coincided with that which was observed in Ca, Na, K, Ba, SO_4^{2-} and Cl^- indicating the presence of these elements in highly soluble forms at that depth. Al was observed in high concentrations at 15 m and 18 m due to its presence in soluble hydroxide form. Se, As, Cr, Zn, Cu and V showed a considerable release in the fly ash pore water leachates. Ti, Pb, Co, Fe, Mn and Mg were present in water insoluble phases in the fly ash samples.

High cation exchange capacity (CEC) values were obtained between 14 m and 22 m depth of the ash column. This showed a transient mineral phase region in the ash column where mobile species are trapped through remineralization processes.

Sequential extraction of the ash core samples revealed that most of the major elements were associated with the carbonate, iron and manganese and residual phase fractions. The bulk of Al, Si, Fe, Ti, Sr, Na and Ba i.e. > 60 % remained locked up in the residual fraction phase present in the ash samples. Ca and K had more than 50 % of their 100 % released in the exchangeable fraction phase. Na was present in appreciable quantity in the water soluble phase (about 18 %). The trend observed for Ca, Mg, K, Sr and Si in the exchangeable fraction phase and Al, Si, Ca, Mg, Ba and Sr in the carbonate fraction phase showed a similarity with the trend observed in the CEC between 14 m and 22 m, thus making these elements a part of the remineralization process due to surface adsorption and exchange processes. The presence of toxic elements like Pb, V, Cr, Zn, Cd and Cu was observed to be strongly associated with the glassy and silicate phase of the residual fraction. Trace elements such as B, Mn, Co, Ni, V, Cu, Zn, Cr, Mo and Pb had their bulk in the residual fraction phase, well above 60 %. As and Se showed high potentials to be released into the environment under normal conditions from the trends exhibited in the water soluble and the exchangeable phase fractions.

The study showed the dissolution and mobility of soluble species down the ash column under both high and low pH. The formation of secondary minerals acted as a trap preventing the free movement of these elements down the dump. But with continuous weathering over time and a low pH, the elements would become mobile again and could pose a threat to soils and subsurface waters.

DECLARATION

I, Olufunke Idowu Ojo, declare that ***Mineralogy and chemical mobility in a weathered ash dump site, South Africa*** is my own work and it has not been submitted for any degree or examination in any other university. All sources I have quoted and used have been indicated and acknowledged as complete references.

Signed .....

Olufunke Idowu, Ojo

DEDICATION

This project is dedicated

To

The Almighty Supreme One,

Who never fails nor forgets....

ACKNOWLEDGEMENTS

My deepest appreciation goes to the Almighty God, who in His infinite mercies saw to the success and completion of this program.

A big thank you to – Prof. D. Mazvimavi, Dr. A. Akinlua, Dr. L.F. Petrik and Mr. A.C.T. Scheepers for their untiring efforts, input and belief in me during the course of this program.

My appreciation goes to all members of ENS Group, Chemistry Department, UWC, for giving me a sense of belonging.

My gratitude goes to ESKOM generations for the funding of this research work.

I also wish to express my sincere appreciation to the following persons for the crucial role played in my life during the duration of the program:

My parents, Engr. and Mrs. K.S. Ojo, for their support in prayers, financially and in all other areas.

My brothers, Babajide Ojo and Ayodeji Ojo, for bearing this burden with me.

My sisters, Mrs. Taiwo Ogunika and Mrs. Kehinde Akinro for their love and support.

My dearest friend and sister, Mrs. Olajumoke Caxton-Martins, for the unforgettable role you played in my life during your short stay at UWC.

Ayobade Oladotun, Olushola Adeniyi, Mudzonga Rumbie, Palesa Leuta and Yafah Hoosain, for being friends indeed.

Alloysius Bazuaye for the difference you make in my life.

Mr. Adeniyi Adekola, Mrs. Morounke Saibu, Mr. Olushola Adesina, Mr. Oare Okosun, Mr. Bidemi Kappo, Mrs. Enih Sone and Mr. Edwin Mukong for the words of encouragement during this phase of my life.

Pastor Sola Oduwole, Pastor Richard Akinyeye, Pastor Ojo Fatoba, Pastor Rasaq Olowu, Pastor Tayo Arotiba, Deacon and Mrs Adewumi for adding to my life spiritually and making my stay in Cape Town worthwhile.

All members of the Household of God Parish, UWC for being my family in Cape Town.

May God bless each and every one of you richly, Amen.

LIST OF ABBREVIATIONS

ACAA American Coal Ash Association

ACI American Concrete Institute

ASTM American Society for Testing and Materials

CCBs Coal Combustion By-Products

EC Electrical Conductivity

FTIR Fourier Transform Infra Red Spectroscopy

IEO International Energy Outlook

IC Ion Chromatography

ICP-MS Inductively Coupled Plasma Mass Spectrometry

ICP-AES Inductively Coupled Plasma Atomic Emission Spectrometry

kbars kilobars

ppm parts per million

ppb parts per billion

r.p.m revolution per minute

SEM-EDS Scanning Electron Microscopy-Energy Dispersive Spectroscopy

TDS Total Dissolved Solids

XRD X-ray Diffraction

XRF X-ray Fluorescence

TABLE OF CONTENTS

LIST OF FIGURES

LIST OF TABLES

Chapter One

Introduction

Increase in demand for electricity in modern society has resulted in the burning of large quantities of coal to generate electricity. World coal consumption is expected to remain on the increase by 49 % from 2006 to 2030 according to the projections made in the IEO2009 reference case (IEO, 2009). Presently, South Africa accounts for 92 % of the coal consumed in Africa and it is expected to continue to account for much of the continent's total coal consumption over the projected time (IEO, 2009).

In coal fired plants, chunks of coal are crushed into fine powder and fed into a combustion unit where it is burned. Heat from the burning coal is used to generate steam that spins one or more turbines to generate electricity. This process of coal combustion produces a range of Coal Combustion By-products (CCB's). These include (a) Fly ash, a non-combustible, powdery, inorganic matter of coal (b) Bottom ash, which consist of agglomerated ash particles that are too large to be carried in the flue gases and fall through open grates to an ash hopper at the bottom of the furnace (c) Boiler slag- molten ash collected at the base of the furnaces that is quenched with water and shatters into smooth, glassy, black particles and (d) Gypsum which is formed from an oxidizing and calcium-based flue gas desulphurization process (Yazici, 2007). The relative amount of each residue depends on the power plant configuration, the emission control devices available and the parent coal (Page et al., 1979). The efficiency of the combustion process utilized also play a part in the quantity of coal combustion residues generated (Durgun and Genc, 2009).

Fly ash, one of the CCB's, is the fine portion of the coal combustion ash that is entrained in the hot flue gas as it leaves the combustion chamber. It is collected by means of electrostatic precipitators or fabric filters and constitutes about 70 % of the total amount of residue generated in coal fired power plants (Fulekar and Dave, 1986). Coal fly ash is

a mixture of metallic oxides, silicates and some unburnt coal (Rath et al., 2008). Some of the organic residues left in fly ash include poly-chlorinated dibenzodioxins and dibenzofurans (Fytianos and Schroder, 1997).

Major countries producing the bulk of CCB's are the USA, China and India. Their production was estimated to be 129, 125 and 105 million tonnes per annum respectively at the end of 2002 (Asokan et al., 2005). Despite the utilization of fly ash in various areas by these countries, the bulk of it is still disposed of by wet and dry methods. In South Africa, only about 5 % of the 22 million tonnes of ash produced annually by ESKOM is currently being utilized (Petrik et al., 2005). The rest of the ash is disposed of in ash dams, landfills and surface impoundments (Fatoba, 2007). The dangers of this practice on the environment include wind/water erosion and leaching of substances (e.g. salts, heavy metals) into the groundwater. Rain water as well as waste water from the ash slurry pose as a leaching medium for toxic elements into the environment. Fly ash particulates when released into the atmosphere can cause irritation or inflammation to eyes, skin, throat and upper respiratory tract of humans (Haynes, 2009).

1.1 Study Area

The decommissioned Taaibos and Highveld power stations were situated at Kragbron town a few kilometres away from the industrial town of Sasolburg in the northern Orange Free State. The area surrounding the old power stations has a flat topography with a small stream 500 m south of the investigated ash dam. The area forms part of the summer rainfall region of South Africa with an average rainfall of 585 mm per annum. Taaibos and Highveld power stations were commissioned in 1954 and 1959 respectively (www.vaaltriangleinfo.co.za/history/vereeniging/chapter_14/57.htm). The coal used at the power stations was from Clydesdale colliery, delivered by overland conveyor belts. The oldest layer of ash at the bottom is between 35-40 years of age while the youngest at the top is a minimum of about 15 years, since the power stations were decommissioned in 1994 (http://heritage.eskom.co.za/heritage/taaibos.htm). Wet disposal system was practiced at both power stations. The ash was hydraulically transported and disposed of in slurry form at the ash dump just like it is presently done at SASOL Synfuels (Secunda) at

70-80 % liquid/solid (L/S) ratio (Fatoba, 2007). Fresh water from the Vaal River most likely treated with chlorine was used to transport the ash to the dump.

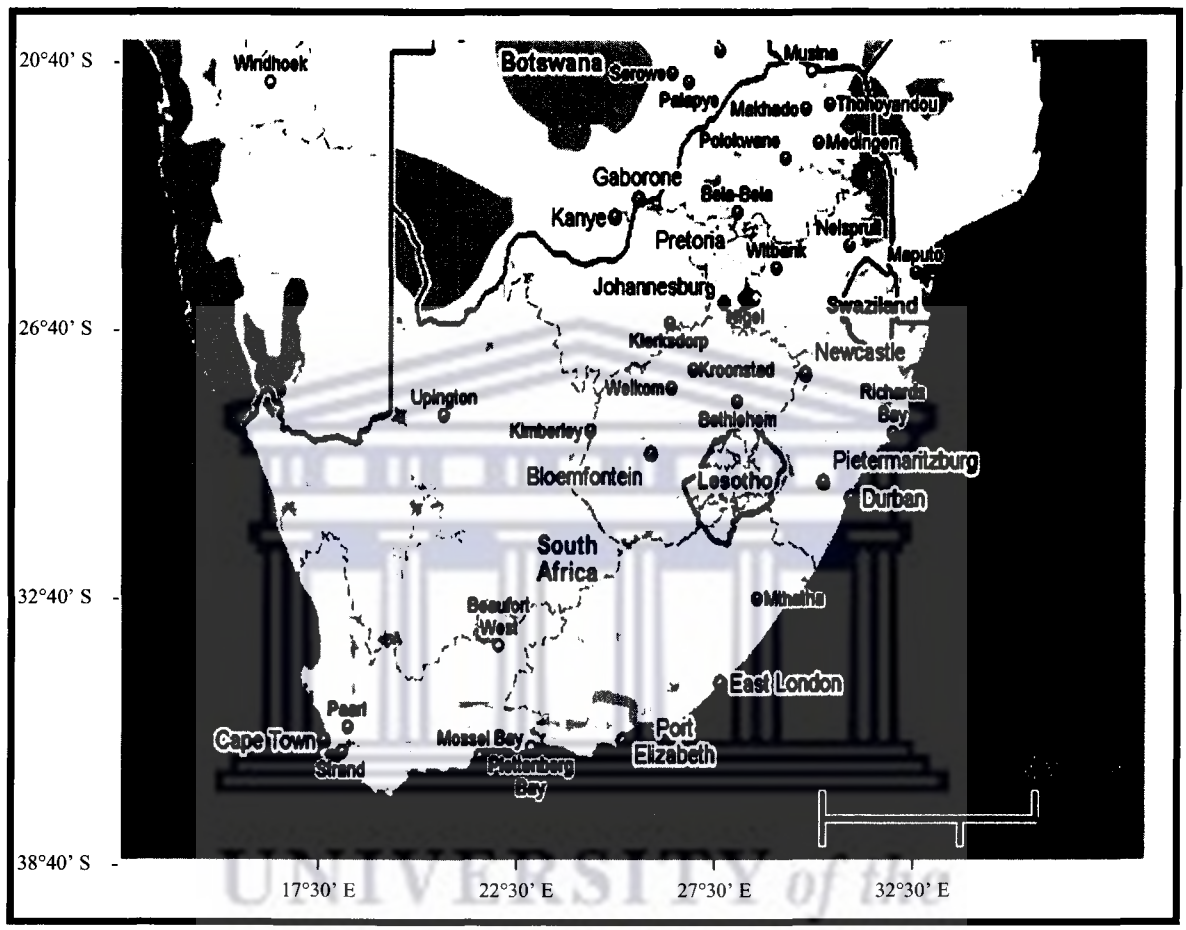

Fig. 1: Map of South Africa showing the location of the study area

1.2 Problem Statement

Coal fly ash is a highly heterogeneous constituent with variations both between and within particles (Smith, 1980). The glassy particles can adsorb different elements in various concentrations and forms, including coatings of calcium and sulfates as well as elements attached directly to the solid particles. Apart from Si, Al and Fe, fly ash may also be rich in potentially mobile major elements such as Ca, Mg, Na and K and in minor elements, such as P and B. A number of metals and metalloids present as carbonates, oxides, hydroxides and sulfates, including Cd, As, Se, Pb, Ni, Cu, Cr, Co, Mo and Be

may also occur in lower but still significant concentrations (Jankowski et al., 2006). The elements that are adsorbed on the particle surfaces are much more easily mobilized into solution during fly ash-water interaction. Leachability of elements especially trace metals to surface and ground water is of great concern. Although some of these elements might not be readily soluble in water, solids hosting them would dissolve over time as a result of continuous weathering thereby releasing the elements into solution. The presence of these trace elements may be in relatively small fractions in coal fly ashes but they are of special interest due to their cumulative build up, long life, high toxicity to man, plants and animals through air, water and soil intake (Fytianos et al., 1998).

Fly ash poses a great risk to the environment when it is exposed to aqueous materials as this causes alteration in its chemistry and also the release of some elements. This research work thus focuses mainly on the chemistry and geochemistry of the weathered fly ash when interacted with water and solutions of moderately low and high pH.

1.3 Aims and Objectives

This study aims at characterizing the fly ash in terms of its chemistry and mineralogy. Understanding the effect of exposure of the fly ash to de-ionized water, studying and quantifying the release of elements from the fly ash when exposed to solutions of different pH and understanding the mechanisms involved in the release of species during leaching are also going to be looked into.

These objectives would be achieved by answering the following research questions.

- What are the chemical and mineralogical compositions of the fly ash gotten from Kragbron dump site?

- What are the distributive weathering patterns of major and minor elements as a function of a depth profile of the ash dump?

- What are the various mineral phases with which the elements are associated in the ash samples?

- What are the changes observed in terms of mineralogy as a result of weathering?

1.4 Research Approach

The outlined objectives would be achieved by carrying out the following experiments and analytical procedures:

- Collection of samples from an old weathered ash dump by coring the ash horizon and bedrock to obtain samples from various depth profiles
- Compositional characterization of the fly ash samples obtained from Kragbron using X-ray fluorescence (XRF) and the total acid digestion of the samples, followed by ICP MS analysis. This was done in order to identify and quantify the major, minor and trace elements in the ash samples
- X-ray diffraction (XRD) and scanning electron microscopy (SEM) to determine the mineralogical composition and morphology of the fly ash samples
- Pore water chemistry of the ash samples using de-ionized water to determine the species soluble in water at various depths in the ash horizon.
- A 5 step sequential extraction procedure by Tessier, 1979 to be carried out on the fly ash samples from the various depth profiles. This would give a clear understanding of the mode of occurrence, physicochemical availability, mobilization and transport of trace elements present in the fly ash dump and it would also establish their probable impact on the environment.

Chapter Two

Literature Review

This chapter discusses in details the genesis of coal, its types and mineralogy, the generation of fly ash from coal, types of fly ash and its physical characteristics, chemical composition, mineralogy, disposal and uses of fly ash. Factors affecting the leaching of toxic elements from fly ash, the environmental impact of fly ash disposal and finally, the impacts of fly ash disposal system on ground water quality are also reviewed in this chapter.

2.1 Genesis of Coal

Coal is a sedimentary rock that forms from the compaction of plant material that has not completely decayed. Shallow swamps or bogs in a temperate or tropical climate are likely environments of deposition due to rapid plant growth and deposition in water with low oxygen content. Coal usually develops from peat, a brown, light weight, unconsolidated or semi consolidated deposit of moss and other plant remains that accumulate in wet bogs. Peat is transformed into coal by compaction and burial by sediments. Partial decay of the abundant plant material uses up any oxygen in the swamp water causing the decay to stop and the remaining organic matter preserved. Burial by sediments compresses the plant material, gradually driving out any water and other volatile compounds. The coal changes from brown to black as the amount of carbon in it increases (Plummer et al., 1999).

Coal is classified based on its heating value and relative content of elemental carbon. For example, anthracite contains the highest proportion of pure carbon (about 86 % - 98 %) and has the highest heat value - 13,500 - 15,600 Btu/lb (British thermal units per pound) while bituminous coal generally has lower concentrations of pure carbon (from 46 % to 86 %) and lower heat values (8,300 - 13,500 Btu/lb). Bituminous coal are sometimes sub-divided on the basis of their heat value, being classified as low, medium and high volatile bituminous and sub-bituminous coal. Lignite is the poorest in terms of heat value (5,500

– 8,300 Btu/lb) and generally contains about 40 % to 60 % pure carbon (http://science.jrank.org/pages/1533/coal-combustion-coal.html).

Peat represents the initial stage in coal development. When it is dry it can be burned as a fuel. On compaction, peat becomes lignite (brown coal), which may still contain visible pieces of wood. Lignite is soft and often crumbles as it dries in air. It is subject to spontaneous combustion as it oxidizes in air and this limits its use as a fuel. Sub-bituminous and bituminous coal (soft coal) are black in colour and often banded with layers of different plant material. They are dusty to handle, ignites readily and burn with a smoky flame. Anthracite (hard coal) is generally formed under the regional compression associated with folding. It is hard to ignite but it is dust free and smokeless (Plummer et al., 1999).

Coal occurs in beds that range in thickness from a few cm to 30 m or more. Underground mining is employed to extract the coal if the beds are deeply buried while strip or sub-surface or surface mining is used when the coal beds are close to the surface. About 51 % of South African coal mining is done underground and about 49 % is by open cast method.

The most abundant energy source in South Africa is coal. Most of the coal is of low quality with a low heat value and high ash content. Majority of the coal deposits suitable for cheap power generation is found in eastern and south-eastern Gauteng and in the northern Free State (http://www.eskom.co.za/live/content.php?Category_ID=96). In addition to the extensive use of coal in the domestic economy of the country, 28 % of the country's production is also exported making South Africa the fourth largest coal exporting country in the world (http://www.dme.gov.za/energy/coal.stm).

2.2 Chemistry and Mineralogy of Coal

The primary component of coal is carbonaceous material resulting from the accumulation and decay of plant matter in marine or fresh water environments and marshes (Hessley et al., 1986). As the plant matter accumulates, it becomes humified and may eventually be

consolidated into coal through a process called coalification. In the organic matrix of coal, carbon is the major element by weight, with smaller amounts of hydrogen, oxygen, nitrogen, sulphur and many trace elements (Tishmack and Burns, 2004). Coal from South African mines is generally low in sulphur (Haw and Hughes, 2007). Coal contains detrital minerals which were deposited along with the plant materials and authigenic minerals that were formed during coalification. Minerals found in coal include: aluminosilicates, mainly clay minerals; carbonates such as calcite, ankerite, siderite and dolomite; sulphides, mainly pyrite; chlorides and silicates, principally quartz (Valkovic, 1983; Harvey and Ruch, 1986). Trace elements in coal are commonly associated with one or more of these minerals. Conditions conducive for the accumulation and decay of plant materials thereby favourable for the formation of coal are typically associated with water-saturated and reducing environments. As a result of this, most of the trace elements associated with the mineral fraction of coal are expected to occur in reduced forms, primarily as sulphides or carbonates (Tishmack and Burns, 2004).

2.3 Fly Ash Generation from Coal in Eskom, South Africa

Coal fly ash is generally produced by coal-fired and steam generating plants. The earliest conventional coal-fired power stations used lump coal which was burnt on a grate in boilers to raise steam. In recent times, the coal is first milled to fine powder, which increases the surface area and allows it to burn more quickly. The systems that utilize the powdered coal are called the pulverized coal combusting systems (World Coal Institute, 2005). Most of the coal used for power generation in South Africa is of very low quality, in heat content and in general, has very high ash content. In Eskom power stations, coal is transported from the coal mine to storage bunkers at the power stations by conveyor belts after which it is fed into pulverizing mills where the coal is grinded to dust. A stream of air blasts this dust from the mills into the boiler burners in the furnace where it burns like gas. Heat released by the burning coal is received by several kilometres of tubing which form the boiler walls. Inside the tubes, water is converted to steam at high temperature and pressure. The superheated steam passes to the turbines where it discharges onto the turbine blades causing them to spin and this is used to generate electricity (http://www.eskom.co.za/content/ESK0000114Coal%20Poster.pdf).

Electrostatic precipitators or bag filters are installed in all Eskom's coal fired power stations to remove fly ash present in the gases that are released through the smoke stacks. Fly ash consists of particles resulting from the cooling of molten droplets of fused material contained in the exhaust gases leaving the combustion furnace. The fusion of silicate minerals result in glassy spherical particles (Tishmack and Burns, 2004). The type and amount of ash accumulated during coal combustion depends largely on the mineralogy of the coal being used, the combustion process and the presence of emission control devices. Also, the chemical forms in which elements are found in ash are affected by coal combustion variables such as combustion temperature and the mode of combustion e.g., pulverized coal fired, fluidized bed, cyclone, stoker (Simsiman et al., 1987). The combustion units at Taaibos and Highveld power stations were pulverized coal fired plants.

2.4 Types of Fly Ash

Fly ash can be classified as class C or F based on the silica, ferric oxide and aluminum oxide contents according to ASTM (American Society of Testing Materials) C 618 (ASTM C 618, 1993). Class C is derived from the burning of lignite and sub bituminous coal. It has a lime content of about 18 % and the sum of silica, alumina and ferric oxide is greater than or equal to 50 %. Class F is derived from the burning of anthracite and bituminous coal. It has lower lime content (< 7 %) and contains more of the silica, alumina and ferric oxide i.e. greater than or equal to 70 %. Smooth, glassy particles are also characteristics of class F fly ash.

Class C fly ash, high in calcium content is more reactive than class F ash due to the rough textured and glassy particles present in it. In addition, it can sometimes exhibit self-hardening properties when hydrated due to much higher calcium hydroxide content in it (Lothia and Joshi, 1995). Although class F fly ash by itself possesses little or no cementious value, it will in finely divided form and in the presence of moisture, chemically react with calcium hydroxide at standard temperature and pressure to form

compounds exhibiting cementious properties. The term used to describe this behaviour is 'pozzolanic'.

Class F fly ashes is composed of a substantial amount of glass mixed with some crystalline mineral phases. Some of these minerals are primary, e.g. unmelted quartz while others like mullite, spinel and haematite which were formed either during high temperature excursion or during subsequent cooling of the ash are secondary. The pozzolanic activity of class F fly ashes is associated mainly with their glass content (Swamy, 1992). The more calcium rich class C fly ashes tend to contain less of the glassy phase but develop more crystalline phases. Some of these crystalline phases often include melilite, di-calcium silicate, tri-calcium aluminate and these exhibit substantial pozzolanic properties (Swamy, 1992). Both classes of fly ash may also contain a reasonable quantity of alkali. During combustion, some of the alkali present in coal is evaporated. A portion of that which is evaporated subsequently condenses on or near the surface of the fly ash particles. Some of the alkali is incorporated in the crystalline phases of the class C fly ashes, e.g. sodium in melilite while in the aluminosilicate class F fly ashes; much of the alkali is dissolved in the glass phase. This forms the basis for the pozzolanic behaviour observed in class F fly ashes (Swamy, 1992).

Table 2.1: ASTM C 618-95 classification of fly ash

Chemical Requirements		Class F	Class C
$SiO_2 + Al_2O_3 + Fe_2O_3$	Min %	70	50
SO_3	Max %	5	5
Moisture content	Max %	3	3
Loss on ignition (LOI)	Max %	5	5
Available alkalis	Max %	1.5	1.5

2.5 Physical Characteristics of Fly Ash

Fly ash occurs as very fine, glass-like particles with size range from 0.01 to 100 μm (average diameter of < 10 μm) (Davison et al., 1974; Wigley and Williamson, 1998; Page et al., 1979) and it has a low bulk density, high surface area and light texture (Asokan et al., 2005; Jala and Goyal, 2006). Spherical-shaped particles (often hollow) constitute most of the fly ash, especially in the fine fractions (Haynes, 2009). Some irregularly-shaped particles are also present, such as the angular particles of quartz. The spherical shape of the fly ash results from the formation of tiny molten droplets as the ash travels through the boiler. The droplets form spheres because this shape minimizes the surface area relative to the volume (Gurupira et al., 2001). The spherical, hollow shaped fly ash particles are referred to as cenospheres. Cenospheres mean particles that have gas bubbles incorporated within their structure. They are formed when the ash is still in the molten state (Gurupira et al., 2001). They are filled with CO_2 and nitrogen, giving the ash its light weight characteristics. Their sizes vary from 20-200 μm in diameter and can be up to 20 % by volume or 5 % of the weight of the fly ash (Scheetz and Earle, 1998). Other spherical shaped particles of fly ash, filled with smaller amorphous particles and crystals are called plerospheres (Adriano et al., 1980).

The size distribution of fly ash is important in both the elemental retention and release into the environment. This is because the smaller the particle the higher the specific surface area (Choi et al., 2002). Iyer (2002) in his study showed that the particle size of fly ash and its surface area are important characteristics in determining the reactivity of the ash. The large surface area of the smaller ash particle makes available a large area for the adsorption of volatile elements during coal combustion. Thus, these exposed areas are prone to hydrolysis when in contact with an aqueous solution after disposal.

The colour of fly ash is usually consistent for each power plant and coal source. The colour of the fly ash varies from tan to grey to black, depending on its chemical and mineral constituents. Tan and light colours are generally associated with high lime content ash. A brownish colour is associated with the iron content of the ash. A dark grey to black colour is attributed to the unburnt carbon content. The lighter the colour, the

lower the unburnt carbon content of fly ash (Adriano et al., 1980). Deposits from South African coal are high in Ca-Al silicates and low in Fe-Al silicates. The high content of the Ca-Al in the coal gives South African fly ash a light grey colour (Laursen, 1997).

2.6 Chemical and Mineralogical Composition of Fly Ash

Chemically, 90-99 % of fly ash is composed of Si, Al, Fe, Ca, Mg, Na and K with Si and Al forming the major matrix (Adriano et al., 1980). Carbon and nitrogen are oxidized into gaseous constituents during combustion hence they are present in fly ash in negligible quantities. Fly ash varies from acidic to alkaline depending on the coal type and furnace. Various studies have shown that the alkaline nature of most fly ashes from power stations is as a result of some soluble basic oxides present such as CaO and MgO (Choi et al., 2002; Reardon et al., 1995). Fly ash obtained from the combustion of anthracite and bituminous coal generally is high in S due to the high pyrite content (FeS) and usually forms acidic solutions when mixed with water while fly ash that evolves from the burning of lignite and sub bituminous coal, low in S but high in Ca and other basic elements gives an alkaline solution when the ash is interacted with water (Furr et al., 1977; Page et al., 1979). South Africa's power plants make use of low grade bituminous coal (Dabrowski et al., 2008) thereby making the resultant solution from the ash/water reaction alkaline in nature.

During combustion, the minerals in coal can become fluid (totally melted) or volatile, and may oxidize or undergo other gas phase reactions (Kim and Kazonich, 2004). The rate of cooling in the post combustion zone determines if a particle is amorphous or acquires a crystalline structure (Kim, 2002; Matsunaga et al., 2002). If the minerals cool slowly, they can develop the characteristic crystalline structure. If cooling is rapid, they form spherical glassy particles. Both crystalline and non crystalline compounds form on the surface of fly ash particles when elements react with oxygen in the flue gases and through condensation/crystallization within melt droplets (Smith, 1980). Lime (CaO) and periclase (MgO) may occur as small crystals embedded within the glass or may be located on its surface depending on the temperature and furnace conditions where the minerals form. Low temperature minerals such as anhydrite ($CaSO_4$) may form on the

surface of the fly ash grains after leaving the high temperature zones in the furnace (Ainsworth et al., 1993; Fishman et al., 1999). Glass is amorphous vitreous silicate or aluminosilicate that is formed when liquid material is cooled rapidly, locking the elements into a disordered, non crystalline structure. Fly ash rich in glass (class F) exhibits cementitous or pozzolanic properties depending on the available lime and is widely used in concrete as a replacement for Portland cement (Helmut, 1987).

The major mineral phases that have been commonly identified in fly ash include: quartz (SiO_2); mullite, ($Al_6Si_2O_{13}$); tricalcium aluminate, $Ca_3Al_2O_6$; alite, (Ca_3SiO_5); belite (Ca_2SiO_3); magnetite, (Fe_3O_4); hematite, (Fe_2O_3); lime, (CaO); anhydrite, ($CaSO_4$); periclase, (MgO); melilite, ($Ca_2(Mg,Al)(Al,Si)_2O_7$); merwinite, ($Ca_3Mg(SiO_4)_2$ and thenardite, (Na_2SO_4) (Tishmack and Burns, 2004). Most of the quartz in fly ash originates from coal as silt and sand sized particles and it remains in the ash because it survived thermal transformation during combustion (Helmuth, 1987). Although bituminous coal ash may contain more than 50 wt% of analytical SiO_2, only about 5-10 wt% is present as quartz (McCarthy et al., 1990). Some Si is present in mullite but a greater portion of the Si is found in the amorphous glass phase (Tishmack and Burns, 2004). Mullite is the principal Al-bearing mineral in low-Ca bituminous coal. It originates from direct crystallization of clay minerals or by devitrification of glass on cooling (Hubbard et al., 1984). South African coal ashes have high quantities of mullite because low-Ca bituminous coal which is rich in Kaolinite is utilized during combustion. Fly ash of high Ca contains less amounts of mullite because of the presence of mica-illite or smectitic clays in their parent coal and also because some of the Al combines with Ca to form $Ca_3Al_2O_6$ (Tishmack and Burns, 2004). The principal Fe-oxides minerals in coal ash are magnetite (Fe_3O_4) and hematite (Fe_2O_3). Magnetite results mainly from the volatilization and oxidation of iron bearing minerals in coal, mainly pyrite (FeS_2). Hematite crystals survive the brief exposure to high temperature like quartz while pyrite is oxidized to magnetite with the release of SO_2. About a third to half of the Fe present in fly ash is in the form of magnetite and hematite, which are largely inert (McCarthy et al., 1990). The rest is contained in the glass phase and becomes available when the glass dissolves (Helmuth, 1987).

In addition to quartz, mullite and hematite, moderate- to high-Ca fly ashes contain other calcium bearing minerals which are reactive in the presence of water. The most common is $Ca_3Al_2O_6$ which occurs with Ca-aluminate-rich glass (Tishmack et al., 1999). The principal Mg phase, periclase (MgO) is about half of the Mg present in sub-bituminous and lignite fly ashes. Magnesium is also found in melilite and merwinite, neither of which is known to significantly react with water (Tishmack and Burns, 2004). Most of the S in fly ash is in the form of anhydrite, which forms as a solid on the surface of the sub-bituminous and lignite fly ash particles (McCarthy et al., 1989). Sulphur accumulates on the surface of fly ash particles from reactions between Ca, Na, O and SO_2 as the fly ash leave the hot part of the furnace and enter low temperature zones (Fishman et al., 1999). Small amounts of anhydrite have been observed in fly ash with CaO content as low as 12 % (McCarthy et al., 1989).

The most abundant phase in a class F ash is the glass that results from the melting of clays and subsequent exsolution of mullite from the melt. Major minerals in class F fly ash are quartz, the ferrite phase and mullite. Because of the higher calcium content of the class C ash, the mineral assemblage is quite different. Quartz, ferrite phase and mullite are present as in class F but the alteration of the clay content of the coal in the presence of calcium results in a suite of silicates, aluminosilicates and oxide phases instead of large amounts of glass. Only a minor amount of glass is formed which contains a rather high concentration of alumina. It is chemically, extremely reactive. Most notable among the mineral phases are lime, di-calcium silicate and tri-calcium silicate, periclase, gypsum/anhydrite can also be found (Scheetz, 2004).

Other reports have revealed that the mineralogical analysis of fly ash showed 70-90 % of the particles to be consisting of amorphous ferro-aluminosilicate glassy spheres. The glass is generated from clay minerals such as feldspar, mica, chlorite and any other easily melted minerals (Hulett et al., 1980; Spears, 2000). The crystalline phase present in fly ash consist of quartz (SiO_2), mica, chlorite, feldspars, mullite ($3Al_2O_3.2SiO_2$), spinel ($FeAl_2O_4$), haematite (Fe_2O_3) and magnetite (Fe_3O_4) depending on the mineralogy of the feed coal (Norton et al., 1986; Vassileva et al., 1997; Vassileva et al., 2005; Kutchko and

Kim, 2006). Sakorafa et al, 1996 in the study carried out on the fly ash from Megalopolis lignite field, Peloponnese (Southern Greece) reported the main minerals present in the fly ash to be quartz, anhydrite, plagioclase, haematite, gehlenite and calcite. The presence of lime, alkali feldspars, bassanite, gypsum, mica and unburnt lignite are found in minor and trace amounts. Erol et al., 2000, in their study on the fly ash obtained from çayirhan thermal power plant, Turkey, reported the presence of quartz, mullite, enstatite, anorthite and haematite as the major mineral phases present in the ash. Volatile elements released from the coal matrix during combustion enter into the vapour phase. As they cool, these gaseous compounds may condense into very small spherical particles and on the surface of other particles leading to surface enrichment of the species (Kim and Kazonich, 2004).

2.7 Fly Ash Disposal

Fly ash from coal combustion can be considered either as a waste or as a resource yet to be fully utilized. Disposal system of fly ash can be by wet or dry methods. In dry disposal, the fly ash is transported in trucks by chute or conveyor from the power plant to the site of disposal where it is disposed of in land fills and constructed embankments. The wet method adopts the washing out of the fly ash with water and piping it as slurry into artificial dams, lagoons or ash ponds. Both methods effectively lead to dumping of the fly ash in land fills or open land (Haynes, 2009). In the USA, nearly 50 % of the produced coal combustion by products (CCB's) is recycled for beneficial use. The majority of the ash is impounded in lagoons and landfills located throughout the country (Bhattacharyya et al., 2009). India uses coal-based thermal plants to generate about 75 % of its electricity. During this process, enormous amounts of fly ash are disposed of in basins or landfills near the power plant where the land gets contaminated and degraded due to the dumping of the ash (Jambhulkar and Juwarkar, 2009).

More than 90 % of South Africa's electricity requirements are provided by coal-fired power plants (DME, 2005). The use of coal of relatively low calorific value and high ash content results in the vast quantity of coal ash produced at individual power stations in the country (Kruger and Krueger, 2005).

Eskom, the South African wholly state-owned electricity utility employs two methods of disposing fly ash; these are the dry ash and dilute slurry (wet) disposal methods. In the dilute slurry disposal method, fly ash is added from the hoppers to a stirring tank with continuous addition of water to give slurry with controlled density. This is then pumped via pipes to the ash dam where the ash particles immediately settle out and the ash-water is either drained away using a penstock, or is allowed to percolate through the ash dam and collected in a toe drain. The ash water goes to the clear ash effluent dam, where it mixes with other wastewaters and after settling is pumped back for treatment using reverse osmosis (RO) and electro dialysis reversal (EDR). The waste product obtained from these treatment processes is again used for the hydraulic transportation of more ash from the hoppers. In the dry disposal method, fly ash from the precipitators is moistened with low amounts (about 16 %) of processed brine from water treatment systems and is taken to the ash dump site via conveyor belts for disposal. Irrigation of the ash with brine takes place at the ash dump. This is done to maintain the moistened condition of the ash for dust suppression (Fatoba, 2007). An example of a power station practicing dilute slurry disposal in South Africa is the Secunda power station while Tutuka power station employs the use of the dry disposal method. To ensure that the ash dams or ash piles do not pose as environmental hazard, they are covered with layers of topsoil and planted with grasses.

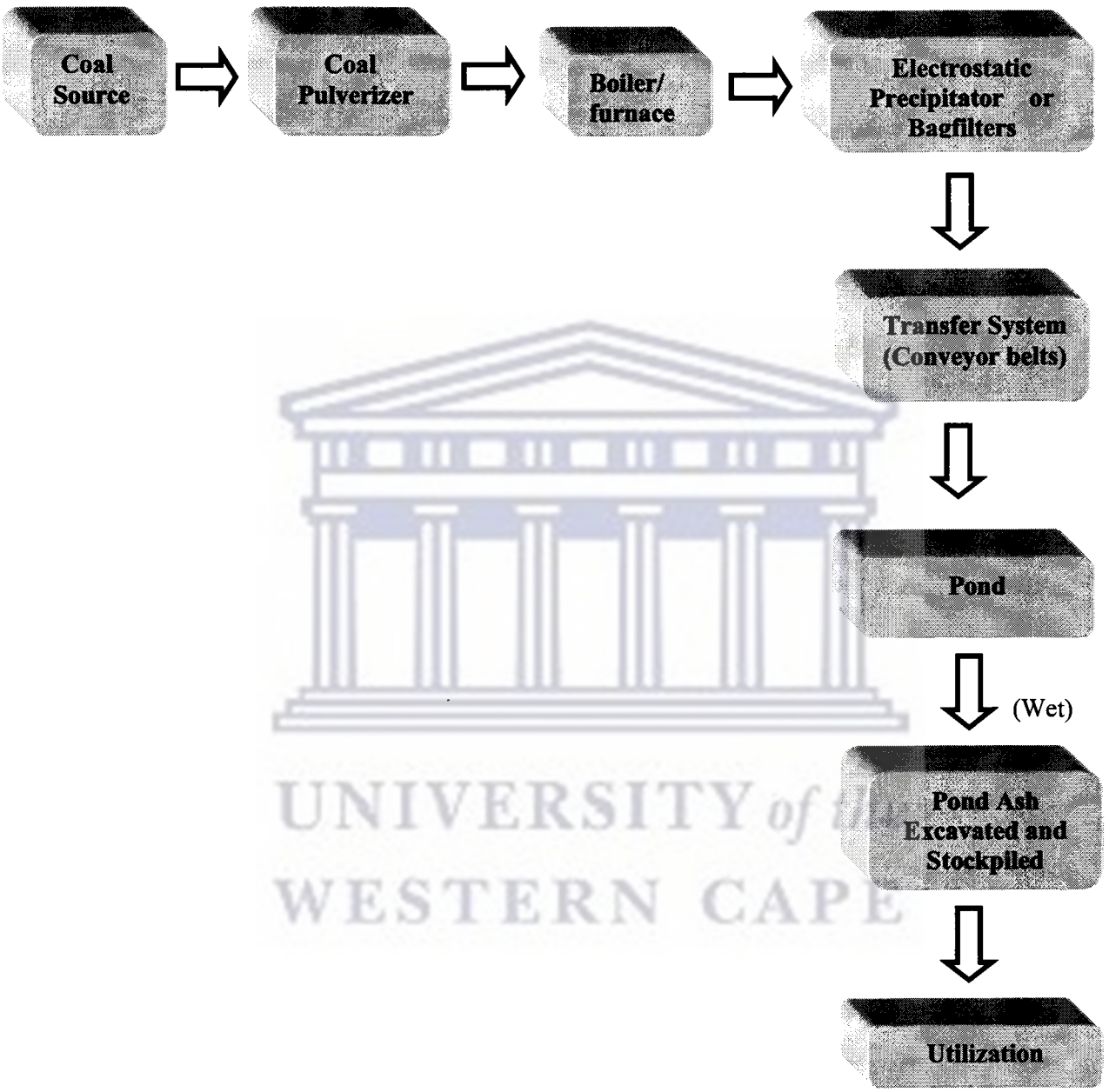

Fig. 2.1: Schematic representation of fly ash disposal and utilization at the decommissioned Taaibos and Highveld power stations

2.8 Environmental Impacts of Fly Ash Disposal

It has been estimated that in developed countries, utilization of Coal Combustion By-products (CCB's) produced amounts to slightly more than 30 % on the average (Asokan et al., 2005). But there are, however, large differences between countries. For instance, the percentage utilization of total ash generated amounted to 85 %, 73 %, 60 %, 50 %, 32 %, 25 % and 15 % in Germany, Denmark, France and UK, Poland, USA, China and India respectively (Sinha and Basu, 1998; Jala and Goyal, 2006). It is evident that, despite the high percentage of utilization in these countries, significant amounts of fly ash are still being disposed of in land fills by wet and dry methods. In South Africa, only about 5 % of the 22 Mt produced annually by Eskom is currently being utilized (Petrik et al., 2005). The rest of the ash is disposed of in landfills by wet or dry methods.

The dangers of this practice on the environment include wind/water erosion of the ash and leaching of substances (e.g. salts, heavy metals) into the groundwater. Surface fly ash particles are susceptible to wind erosion and this can be a major source of dust in the surrounding environment. Fly ash particulates when released into the atmosphere can cause irritation or inflammation to eyes, skin, throat and upper respiratory tract of humans (Haynes, 2009). In addition, metals such as Se, Cd, Cu and Zn can be ingested by humans in higher concentrations than recommended through the consumption of fish from waters close to poorly managed ash dams (Kirby et al., 2001) or from vegetables growing on the ash itself (Tsadilas et al., 2006).

Potentially toxic elements leached from fly ash (Hajarnavis and Bhide, 1999) can contaminate soils (Theis and Richter, 1979), groundwater (Theis and Gardner, 1990) and surface waters (Mills et al., 1999).

Proper measures such as lining at the bottom of the ash mound, stabilization of the ash mound and covering of the completed mound with vegetation are required to minimize environmental damage (Vidya and Snigdha, 2006). The type of climate and terrain has a significant impact on the method of disposal. In areas where water tables are high and where rain or snow is significant, extra precautions are required to ensure that the

disposed material is contained. To prevent the leachates from leaving the disposal site, liners and other barrier types need to be implemented.

2.9 Impacts of Fly Ash Disposal on Ground Water Quality

Coal ash disposal is considered to be a major environmental issue because of its potential to contaminate ground water with cations such as Al, Fe, Na, K, Ca, Sr, Ba, Zn, Cd etc, anions such as Cl^-, SO_4^{2-} and oxy-anions of Se, Mo, As, B and Cr. Leaching is the most likely means by which these metals and other constituents in fly ash would become mobile, environmental contaminants. The main leachants of the disposed ash are rainwater, mostly acidic due to gaseous power plant emissions and the slurry which carries the ash from the plant to the pond (Praharaj et al., 2002). Rain water discharge and run off from the ash mound areas into surface water bodies are a source of water pollution. A significant volume of the ash leachate percolates underground to the underlying water table if the ash pond is unlined.

The wet system of disposal in most power plants causes discharge of particulate ash directly into the nearby surface water system and may contaminate water/soil system. Also, the long storage of ash in ponds under wet conditions and humid climate can cause leaching of toxic metals from the ash, contaminate the underlying soil and ultimately the groundwater. Incorporation of engineering measures in the design of ash ponds and continuous monitoring of surface and groundwater systems would serve as a means of minimizing the impact on the environment (Vidya and Snigdha, 2006).

2.10 Factors Governing the Leaching of Species from Fly Ash

The mineralogical composition of coal fly ash plays an important role in the leaching of toxic elements (Saikia et al., 2006). Some of the trace elements in coal have organic affinity (elements associated with the organic matter in the coal) or mineral affinity (elements associated with sulfides, aluminosilicates, carbonates and other minerals in coal). Studies on the mobility of these elements during combustion have shown that their volatility depends on their affinities and concentrations, on the physical changes and chemical reactions of these elements with other volatile elements during combustion. The

release of species from coal combustion by-products in aqueous solution depend on the mineral patterns of the species existing in the residue. Their leaching abilities depend largely on their speciation and the nature on their host phases. It has been reported in literature that the glassy phases and magnetic fractions in the coal combustion residue contain most of the potentially harmful elements (Zevenbergen and Comans, 1994 and Kukier et al., 2003).

The principal mechanisms behind metal mobility are dissolution of primary solids under different environments (rain water penetration as a result of the permeability of the ash, dumping of acidic waste on the ash pile etc, leading to precipitation and sorption reactions (Van der Hoek et al., 1994, Jankowski et al., 2006); all of which are pH dependent. The amount and rates of release of species released from fly ash into solution depends on: the total concentration of the elements in the solid phases, the distribution of the elements on the fly ash particles and any incorporation of the elements into secondary solids (Eary et al., 1990). Association of elements with the water soluble phases in the fly ash causes dissolution and release of such species when in contact with aqueous solutions in the environment. Minor elements incorporated into predominantly sparingly soluble phases such as magnetite, hematite and silica glass will be released into solution only as fast as the solids bearing them dissolve , assuming aggressive and congruent dissolution over time (Eary et al., 1990).

Morphology of the combustion by-products can also affect the release of toxic species from the particles. The presence of a non porous continuous outer surface and a dense particle interior can restrict heavy metal leachability from CCB's (Ramesh and Kozinski, 2001). The particle size distributions and the specific surface area give information about the interaction between combustion by-products and aqueous solution. The initial surface area and change in surface area as the reaction progresses are also crucial in a long term leaching process.

2.11 Utilization of Fly Ash

Fly ash has found many uses which are based upon both the bulk chemical and mineralogical compositions of the ash, and upon the physical size distribution and shape of the ash. Some of the uses include application in cement and concrete products, structural fill and cover material, waste stabilization/solidification, roadway and pavement utilization, addition to construction materials as a light weight, infiltration barrier and underground void filling, soil and water and environmental improvement (Scheetz and Earle, 1998).

- **Cement and concrete products** – Fly ash has been used extensively as an additive to cement and concrete. In 1996, about 49 % of fly ash was utilized for this purpose (ACAA, 1996). An improvement of the particle size packing (due to the smaller size of the fly ash particle sizes, in comparison to the aggregate) decreases the air entrainment in the concrete. Although it has been indicated by research that decreased air entrainment adversely affects the initial freeze thaw durability of the concrete, if the fly ash concrete is allowed to fully cure, the effects are very much reduced and the concrete mix will perform satisfactorily (Xu, 1997). Fly ash increases resistance to corrosion and ingress of corrosive liquids by reacting with calcium hydroxide in the cement to become a stable, cementitious compound of calcium silicate hydrate. The reaction product also lends to the filling of capillary voids in the concrete mixture thereby reducing the permeability of the concrete (Halstead, 1986). Fly ash improves the clinker quality, mainly due to its lower alkali content. Fly ash is also beneficial in concrete due to its pozzolanic reactions with free lime, rounded particle shape and by reducing the water demand. It helps to avoid segregation and bleeding in fresh concrete as well as improving long term strength and durability. It reduces the alkali silicate reaction in addition (IEA, 2005). The use of fly ash brings about a savings on Portland cement material needed for concrete, resulting in a decrease in project cost. Also, blended cements and concretes containing large proportions of fly ash offer the benefit of CO_2 emissions avoidance by reducing the need for burning of lime.

- **Structural fill and cover material** - The use of fly ash as a fill accounted for 15.3 % of the total fly ash utilized in 1996 (ACAA, 1996). The ash can be used as a backfill material for walls, retaining structures and bridge abutments (Meyers et al., 1976). It can also be used as a material at solid waste landfills to isolate and encapsulate each successive lift i.e. an individual cover layer of material. Particle size is of great importance when considering the consolidation characteristics of the material, the smaller the particle size the easier and more quickly the physical consolidation of the ash will be. The density of the ash is of importance where the load bearing strength of the soil to be covered is low. The low density of ash is due to the presence of cenospheres or glass bubbles in the ash. By using fly ash as a lighter weight cover material, excessive settlement of failure i.e. landslide of the sub-soil is avoided due to the lighter load being placed upon it from the overlying fly ash cover material (Scheetz and Earle, 1998).

- **Waste solidification and stabilization** - The process of stabilizing a waste consists of encasing the waste in a solid block while solidification entails transforming a semi-liquid waste to a solid. The use of fly ash mixtures in this area accounted for the use of approximately 11.9 % of fly ash in 1996 (ACAA, 1996). It helps to stabilize the waste material by limiting the solubility or mobility of hazardous contaminants by sealing material in an impermeable monolith and also adjusting the pH of the waste to a range where amphoteric materials are less leachable. Fly ash produces a strong, durable solid structure waste block, exhibits hydration properties similar to those of Portland cement, and it increases material strength to improve handling characteristics of materials such as sludge and allows easier movement of waste (Scheetz and Earle, 1998).

- **Roadway and pavement utilization** - The use of fly ash as a soil stabilizer along roadway embankments, a sub grade base course material, an aggregate filler, a pavement additive and a mineral filler for concrete accounted for the use of approximately 5.5 % of the total fly ash produced in 1996 (ACAA, 1996).

Benefits of fly ash being used as a soil stabilizer include its plentiful supply from nearby electric power generation facilities and positive physical properties. Sheer strength is an important characteristic for soil stabilization fly ash utilization and it generally equals or exceeds the strength of soils typically used for embankments (Twin Cities Testing and Engineering Laboratory, 1970., Lin, 1971). This strength is partially due to some fly ashes having self hardening or a pozzolanic property, typical of the class C fly ashes and also the ash obtained from atmospheric fluidized bed boilers (Scheetz and Earle, 1998). Susceptibility to frost is one of the disadvantages associated with using ash for soil stabilization. If placed in a cold climate and exposed to frost, the fly ash will have to be stabilized with lime mixture to chemically bind the entire mixture. Alternative to this procedure is to cover the ash with sufficient soil to put the ash below the local frost line (Meyers et al., 1976). Another disadvantage is the weathering of fly ash over time.

- **Infiltration barrier and underground void filling -** Fly ash grout has been used in a number of pilot projects, conducted in joint research with the Pennsylvania State University Material Research Lab, to reduce rainfall infiltration in areas that are subject to acid mine drainage (AMD): (Scheetz et al., 1995). Acid mine drainage occurs in areas that have been previously mined for coal and contain pyrite materials in spoil heaps or in mine shafts where the pyrite material is in contact with both water and oxygen. The spoil piles and mine shafts contain iron pyrite (FeS) in the tailings that chemically react with water and oxygen. The action of *Thiobacillus* bacteria increase the rate of formation of acid mine drainage. The theory behind the fly ash capping approach to AMD control is that if the infiltration can be greatly reduced or eliminated, one contributing factor to the reactional process would be eliminated, namely oxygen, thereby stemming the formation of AMD. Mine void filling is undertaken for a number of reasons. The first is for the control of AMD, where the ground water table intersects the mining rubble. Another is that fly ash grout injection compliments AMD control by filling mine voids and providing support to areas where standing coal pillars are

crumbling and causing land subsidence on the surface. Lastly, it is used in mine fire abatement situations. Utilization of fly ash for projects such as underground void filling provide large cost savings by reducing the amount of cement needed while helping in the disposal of large volumes of the ash (Scheetz and Earle, 1998). In South Africa, co-disposal of AMD and fly ash resulted in pollution abatement, neutralization of hazardous waste streams and recovery of water as well as preparation of high capacity adsorbents (Petrik et al., 2003).

- **Fluoride retention additive in FGD gypsum** - The use of coal fly ash as a fluoride retention additive for treating flue gas desulphurization (FGD) gypsum for its disposal in landfills was studied by Álvarez-Ayuso and Querol (2008). Fluoride is an essential micronutrient that helps in preventing dental caries. Fluoride is released to the environment through natural sources (weathering of fluoride minerals, emissions from volcanoes) as well as through anthropogenic sources such as waste discharges from power plants and manufacturing industries (Álvarez-Ayuso and Querol, 2007). The risk posed by the high fluoride leaching from FGD gypsum was greatly diminished when treated with the coal fly ash. Benefits linked to using coal fly ash for this purpose include the enormous amount of aluminosilicate glass (usually higher than 50 %) in its composition (Vassilev and Vassileva, 1996; Vassileva et al., 2003), its availability in land fills and also because no additional cost on transport is required since itself is a by product from coal combustion (Álvarez-Ayuso and Querol, 2008).

- **Agricultural Amendment** – Fly ash has similar physical and chemical properties to those of soil. As such, it can be used directly as a soil amendment, in land reclamation as organic matter, lime or gypsum or in composts. The hydroxide and carbonate salts in fly ash give it the ability to neutralize acidity in soils (Matsi and Keramidas, 1999). Fly ash has also been reported to modify soil pH, improve soil texture (increasing moisture retention in poor soils and aeration) and also provide some essential plant nutrients for increasing crop production (Bilski et al, 1995). Areas where fly ash has been used successfully include rice (*Oryza sativa* cv. 'PR

106') and wheat (*Triticum aestivum* L.) (Sikka and Kansal, 1995), barley (*Hordeum vulgare* L. var. 'Leduce') (Sale et al., 1996) and tomato (*Lycopersicon esculentum* Mill. cv. 'Pusa Ruby') (Khan and Khan, 1996). In South Africa, class F fly ash when suitably augumented with quicklime, has been used to pasteurize sewage slugde. The resultant product SLASH is devoid of pathogens and is used as soil ameliorant. It enhanced the early growth of corn, showed no translocation of heavy metals to the biomass and improved the vitality and growth of spinach and asters (Reynolds et al., 1999). Another viable way of utilizing fly ash in agriculture is to incorporate it into container substrates for ornamental plant production. Jianjun and Yuncong (2006) examined the physiochemical properties of three fly ashes collected from Florida, Michigan and North Carolina and container substrates formulated by incorporating commercial dolomite and the three fly ashes respectively into a soilless basal substrate. The basal, dolomite- and fly ash- amended substrates were used to grow peace lily (*Spathiphyllum* Schott 'Ty's Pride'), a popular ornamental foliage plant, in 15-cm diameter containers in a shaded greenhouse. The three fly ashes and the commercial dolomite were able to raise pH of the basal substrate from 3.8 to about 6.8. The high quality grade of plants produced from the fly ash amended substrates was comparable to those produced from dolomite amended substrate but significantly different from those produced from the basal substrate. It was concluded that fly ash can be an alternative to commercial dolomite in amendments to soilless substrates for ornamental plant production (Jianjun and Yuncong, 2006). It will save cost, at the same time reduce the quantity of fly ash meant for disposal.

Chapter Three

Geology of the Area

The geology of Kragbron area falls under the Karoo Supergroup. The regional and local geology of the area, depositional environment, topography and the economic resources found in the area are discussed extensively in this chapter.

3.1 Regional Geology

The Karoo Supergroup ranges in age from Late Carboniferous to Middle Jurassic and attains a total cumulative thickness of approximately 12 km in the southeastern portion of the main Karoo Basin towards the eastern end of the Karoo Trough. The bulk of the Karoo strata occur in the main basin, which covers an area of approximately 700 000 km^2 but was much more extensive during the Permian. The Karoo Supergroup is world known for its terrestrial vertebrate fossils, distinctive plant assemblages, thick glacial deposits (plus glacial pavements) and extensive flood basalts with their associated dolerite dykes and sills (Johnson et al., 2006).

The main Karoo basin is largely underlain by a stable floor, comprising the Kaapvaal Craton in the north and the Namaqua-Natal Metamorphic Belt in the south, and is bounded along its southern margin by a fold-thrust belt (Cape Fold Belt). Following the deformation of the Namibian (Neoproterozoic) Saldania Belt and intrusion by the Cape Granite Suite between 560 and 500 Ma to the south of the Namaqua-Natal Belt, deposition of the Ordovician to Early Carboniferous Cape Supergroup sediments took place. The main Karoo Basin also constitutes a retro-arc foreland basin which wedges out northwards over the adjacent craton, situated behind an inferred magmatic arc and associated with the fold-thrust belt produced by northward subduction of oceanic lithosphere located south of the arc (Johnson et al., 2006).

Major lithostratigraphic units of the Karoo Supergroup include (Johnson et al., 2006):

- **Dwyka Group**: Age is from Late Carboniferous to Early Permian. It rests on glaciated Precambrian bedrock surfaces along the northern basin margin, overlies the Cape Supergroup unconformably in the south and also overlies the Natal Group and the Msikaba formation unconformably in the east. A variety of litho-facies types have been recognized and they are - the massive diamictite facies, the stratified diamictite facies, the massive carbonate-rich diamictite facies, the conglomerate facies, the sandstone facies, the mudrock with sandstone facies and the mudrock facies.

- **Ecca Group**: The Permian Ecca Group comprises of 16 formations, reflecting the lateral facies changes that characterize the succession. These include- the Prince Albert Formation, the Whitehill Formation, the Collingham Formation, the Vischkull Formation, the Laingsburg Formation, the Ripon Formation, the Fort Brown Formation, the Waterford Formation, the Tierberg Formation, the Skoorsteenberg Formation, Kookfontein Formation, Pietermaritzburg Formation, the Vryheid Formation and the Volksrust Formation.

- **Beaufort Group**: This comprises a lower Adelaide Subgroup and an upper Tarkastad Subgroup. The Adelaide Subgroup includes the Koonap, Middleton and Balfour Formations of Late Permian age in the southeastern part of the basin. In the west, the Abrahams-kraal and Teekloof Formations are the approximate equivalents of the Koonap and Middleton Formations respectively. The Normandien Formation is the only formation in the northeastern region. The Tarkastad Subgroup is Early Triassic in age and it is characterized by a greater abundance of both sandstone and red mudstone than the Adelaide Subgroup.

- Other formations found in the Main Karoo Basin include the Molteno Formation of the Late Triassic age, the Elliot Formation also of Late Triassic age and the Clarens Formation of Late Triassic to Early Jurassic age.

The Mesozoic Karoo Igneous Province is one of the world's classic continental flood basalt (CFB) provinces and its constituent extrusive and intrusive rocks occur over a very extensive area of Southern Africa. The lava outcrops of the Karoo Igneous Province are erosional remnants and the areas between them are intruded by a network of dykes, sills and discordant sheets. These dykes and sills are particularly well developed in the sedimentary sequences of the Main and subsidiary Karoo basins (Duncan and Marsh, 2006).

3.2 Local Geology

The geology of the study area (Kragbron) comprise of the Vryheid Formation under the Ecca Group and the Karoo Dolerite suite. The Vryheid Formation consists of different lithofacies arranged in upward-coarsening cycles which are essentially deltaic in origin. The base of the cycle in the eastern part of the formation consists of dark-grey, muddy siltstone resulting from shelf suspension deposition in anoxic water of moderate depth. Prodelta sediments are represented by alterations of bioturbated, immature sandstones, dark siltstones and mudstones on a centimeter to decimeter scale. The rhythmic nature of this facies reflects a seasonal variation in the fluvial input or storm/fair-weather deposition. Distal distributary mouth-bar sediments comprise repetitive units of horizontally laminated, medium grained sandstone and siltstone, bioturbated in places. Proximal mouth-bar deposits take the form of trough cross-stratified medium- to coarse-grained sandstone with polymodal palaeocurrent patterns. This facies is erosively overlain by coarse to pebbly, planar and trough cross-stratified, feldspathic sandstone with unimodal palaeocurrent patterns interpreted as distributary channel fills. The delta-front deposits have a sheet-like geometry due to sediment redistribution by basinal currents and were probably lobate in plain view. Fining-upward fluvial cycles present in the east are typically sheet-like in geometry, although some form valley-fill deposits. They comprise coarse-grained to pebbly, immature sandstones which are erosively based and planar and trough cross-stratified, with an abrupt upward transition into fine grained sediments and coal seams. The coal seams originated as peat swamps developed on broad, abandoned alluvial plains and less commonly in interfluves (backswamps). Most of the economically important coal seams occur in the fluvial succession. The rugged pre-

Karoo topography along the north-western margin of the basin provided sheltered environments for the development of coal swamps. The Vryheid Formation is of Permian age (Johnson et al., 2006).

The intrusive dolerite suite represents the shallow feeder system to the flood basaltic eruptions. It is best developed in the main Karoo Basin and occurs as an interconnected network of dykes, sills and saucer-shaped sheets, so that it is nearly impossible to single out any particular intrusive or tectonic event. The sills and inclined sheets range from a few metres to 200 metres or more in thickness, and typically form resistant caps of hills comprising softer sedimentary strata in the Karoo and elsewhere. The dykes are generally 2-10 m wide and 5-30 km long although some can be followed for 80 km. The Karoo dolerites are of Jurassic age in the Mesozoic Era (Duncan and Marsh, 2006).

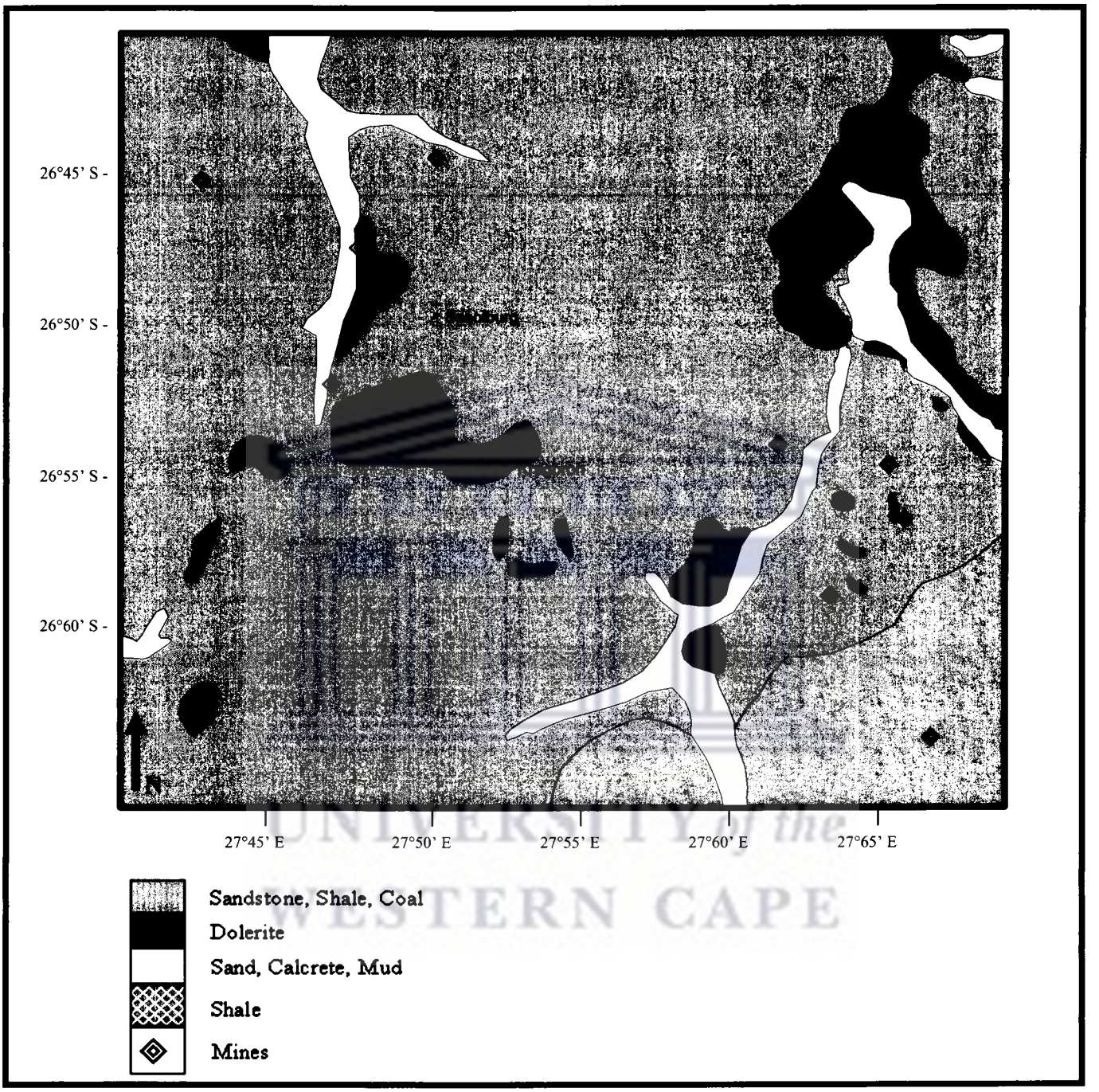

Fig 3.1: Map showing the geology of the study area (modified from Keyser, N., 1986)

3.3 Depositional Environment

Decreases in temperature during the mid-Carboniferous caused a global regression accompanied by the buildup of an extensive ice cover over the southern mountain chain fringing the paleo-Pacific margin and the cratonic highlands to the north and east of the Main Karoo Basin (Johnson et al., 2006). Initially, the deposition of the Dwyka Group took place largely from a grounded ice sheet, but the onset of slightly warmer conditions resulted in rain-out debris accumulating from a predominantly floating ice shelf which further led to the dissolution of the ice sheet during the Early Permian. Melting of the ice sheet resulted in a major regional transgression, producing the marine Ecca basin. Argillaceous material (Prince Albert and Whitehill Formations) was transported into the basin. Following the accumulation of the Whitehill Formation, volcanic activity in the magmatic arc which was forming in the subduction zone to the south of the basin resulted in the sub aqueous deposition of numerous thin ash layers that periodically interrupted the settling of mud from suspension in the overlying Collingham Formation. The subsequent sudden influx of coarser detritus from the magmatic arc provenance, which accompanied the downwarping of the Karoo Trough, led to the build up of sandy and silty submarine fans and basin plain turbidities of the Ripon, Laingsburg, Vischkuil and Skoorsteenberg Formations. Turbidity processes, in turn, gave way to suspension settling of rhythmically bedded prodelta mud (Fort Brown Formation) as the delta slope prograded across the turbidite fans at its foot. Deposition of mud (Tierberg Formation) took place in relatively shallow water towards the north of the Karoo Trough. In the northeastern part of the basin, the Ecca sea was initially starved of sediment due to glacial cover in the source areas and the shales of the Pietermaritzburg Formation reflect a major transgression (Johnson et al., 2006). As the climate warmed up, detritus was carried mainly from a granitic highland situated towards the northeast and, to a lesser extent, from the relatively low-lying quartzitic provenance to the north (Witwatersrand Arch) and deposited as a prominent fluvio-deltaic wedge (Vryheid Formation). The presence of the coal seams in the Vryheid Formation points to a luxuriant plant growth and also indicates that the organic-rich muds of the Whitehill Formation are probably a distal equivalent of this formation. A second major regional transgression due to epeiorogenic

subsidence shifted the locus of deltaic sedimentation landwards and gave rise to another thick mudrock succession (Volksrust Formation).

In the south, the transition from flysch to molasse is denoted by the progradation of delta-front sands of the Waterford Formation across prodelta Fort Brown Formation muds. Progradation of sandstone-rich delta-front and lower delta-plain sediments into the Ecca sea was followed by the subaerial deposition of upper delta-plain and fluvial mud and sand of the Adelaide Subgroup (Beaufort Group) during the Late Permian. In the northeast, the lower part of the Normandien Formation provides evidence that deltaic conditions persisted locally for some time after they had ceased elsewhere (Johnson et al., 2006). A strong uplift associated with major orogenic activity along the southern margin of the basin at the beginning of the Triassic led to the influx of medium grained, pebbly, bed load fluvial sandstones of the Katberg Formation. These sediments extended right across the basin, but with denudation of the provenance, a source-ward shift of facies occurred resulting in overstep of bed-load fluvial deposits by mixed-load and flood-basin deposits of the Burgersdorp Formation. A Middle Triassic hiatus, which increased northwards, was followed by a Late Triassic cycle consisting of a northward thinning, bed-load-dominated fluvial wedge (Molteno Formation). Denudation of the provenance again led to a source-ward shift of the facies with overstepping of the bed-load fluvial deposits by mixed-load fluvial and flood-basin/lacustrine deposits of the Elliot Formation. These deposits are overlain by the Late Triassic – Early Jurassic Clarens Formation, consisting largely of fine grained Aeolian sands derived from a western source. A progressive increase in aridity is evident in the Molteno-Elliot-Clarens depositional sequence. Sedimentation in the Main Karoo Basin was terminated during the Middle Jurassic with the outpouring of at least 1400 m of basaltic lavas (Drakensberg Group) (Johnson et al., 2006).

3.4 Relief/Topography

The area falls under the Northern Free State farmland and it is characterized by predominantly rolling and undulating landscape with fairly little topographical variations. Elevated topography noticeable is mostly isolated and rounded hills with concave side slopes, smoothing out into the surrounding plains. Land use in the area is strictly agriculture comprising of a combination of cultivated fields and grasslands utilized for grazing (Visual impact assessment, 2008).

3.5 Economic Resources

- **Coal** – The Karoo Supergroup hosts all the coal resource of South Africa. Most of the coal seams are found in Mpumalanga and some part of the Northern Province. The abundance of the low quality coal in these regions make coal combustion the most economical means of meeting the country's rising electricity demands. The coal seams are usually horizontal throughout the main basin. The distribution, lateral extent, thickness and maceral content of coal seams are primarily controlled by basin tectonics and differential subsidence. The wide range of depositional settings within which the peats accumulated, combined with variations in climate and plant communities as well as the Jurassic dolerite intrusions has impart to the coals' significant differences in grade, type and rank (Johnson et al., 2006).

- **Oil and Gas** – Numerous oil shows are known in the northern part of the Main Karoo Basin, but only two uneconomic accumulations have been found. The best oil shows encountered in the upper part of the Vryheid Formation were probably due to the shale sequence present. However, primary porosity and permeability of the sandstones in this formation are generally poor. Widespread intrusion of dolerites probably led to large-scale conversion of oil into gas and some escape along fractures. The economic potential of oil shales (torbanites) in the Vryheid Formation has been investigated, but existing deposits are not considered to be economically viable at present (Johnson et al., 2006).

- **Uranium and Molybdenum** – Uranium occurrences which are presently of subeconomic value are located in the western and central parts of the Main Karoo Basin within the Adelaide Subgroup and to a much lesser extent, the Molteno and Elliot Formations. The occurrences are epigenetic, tabular and sandstone hosted, forming discrete pods and lenses less than 10, 000 m^3 in volume. The dominant uranium mineral is coffinite but uranite may also occur. Molybdenum, in the form of molybdenite and jordisite, is present in the south western part of the basin (Johnson et al., 2006)

Chapter Four

Methodology

This chapter describes the sampling, experimental and analytical methods used in the study.

4.1 Sampling

A total of 33 samples were collected from one core drilled at Kragbron dump site (Fig. 4.1.1). The most recent emplacement of the ash as at the time of sampling was 2 years ago. No fresh ash sample was obtained.

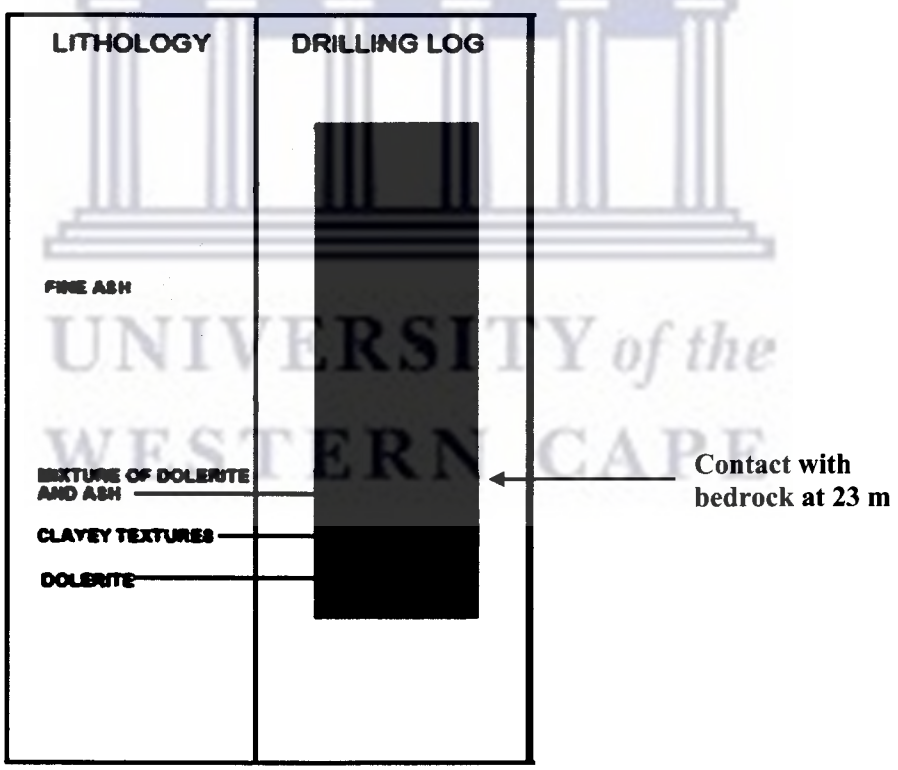

Fig. 4.1.1: Profile of drilled borehole at Kragbron

A single bore hole was drilled using air percussion drilling technique to 32 m depth. The core was drilled into a wet zone detected during the geophysical survey of the area

(Klerk, 2007). Sampling of the core was carried out at intervals of 1 m from the surface down the drilled column. No additional core was drilled due to financial constraints at the time.

4.1.1 Storage of Samples

The fly ash samples extracted from the drilled core were stored in sealed polyethylene sample bags. These sample bags were labeled accordingly and kept in a dark cool cupboard away from any source of heat, out of direct sunlight and away from fluctuating temperatures.

4.1.2 Storage of Leachates for Analysis

After leaching of drilled ash core samples as described in section 4.2.3, samples from the leachates of the fly ashes were taken after being filtered through a 0.45 μm membrane filter. Samples for cation analysis were acidified with dilute 1M HNO_3 to pH ±2 (to avoid precipitation of species) and kept in the refrigerator at 4 °C while the samples for anion analysis were kept in the refrigerator at 4 °C without adding dilute HNO_3. The samples were analyzed for anions and cations using ion chromatography (IC) and inductively coupled plasma atomic emission spectrometry – (ICP AES) respectively.

4.2 Standard Experimental Methods

The experimental methods employed in this study include the moisture content determination, pore water chemistry, total acid digestion, sequential extraction and the cation exchange capacity (CEC) of all the fly ash samples.

4.2.1 Moisture Content Determination

Moisture content is the quantity of water contained in a material such as soils and rocks. The moisture content influences the physical properties of a material such as weight, density, electrical conductivity and more. Two methods are usually employed in the determination of moisture content. They are the thermogravimetric and the loss on drying techniques. The loss on drying technique was employed in this study. The moisture content of the ash samples were determined by oven drying pre-weighed samples of each

of the samples taken at 1 m intervals down the ash column for 12 hours at 105 °C. The weight difference between the initial wet sample and the final dry sample was expressed as weight per cent of the initial wet sample and reported as moisture content per cent.

4.2.2 Loss On Ignition

The loss on ignition is the decrease in weight of a rock or an ore sample on heating at high temperatures, due to the expulsion of volatile components like chemically bound H_2O, CO_2, OH^-, F^-, SO.

Loss on ignition was determined by first weighing a porcelain crucible. Then 1 gram of each sample was weighed into the crucible. The sample was then dried in an oven for 30 minutes at a temperature of 120 °C.

The crucible plus sample was then placed in a pre-heated furnace at 1000 °C for approximately 45 minutes. The sample was allowed to cool in a dessicator after being removed from the furnace and then weighed again. The procedure was repeated until a constant weight was reached.

4.2.3 Pore Water Chemistry

The pore water chemistry of the ash samples was done to determine the likely cations and anions that are soluble after fly ash had been interacted with water. The alkalinity or acidity of the fly ash was also obtained from this experiment. Triplicate samples containing equal quantities of the collected fly ash and de-ionized water with corresponding liquid/solid ratio of 10:1 were stirred in polyethylene flasks with the aid of magnetic rods and magnetic stirrers at a contact time of 30 minutes. The solution was filtered through a 45 μm membrane filter paper after the pH, electrical conductivity and total dissolved solids measurements had been taken with a Hanna HI 991301 pH meter with portable pH/EC/TDS/Temperature probe. The measurements for pH, EC and TDS were taken before filtration because some species may become adsorbed unto the surface of the filter paper due to the cation exchange capacity of the filter paper, as CEC of filter paper increases with increased pH of solution. The removal of hydrogen or hydroxyl ions from the solution will reduce the pH. This also applies to the electrical conductivity of the

solution as filtration removes some of the species thus reducing the ionic strength or EC. The pH meter was calibrated before use with buffer solution of pH 4.01 and 7.01. 25 ml of the supernatant was collected and made up to 50 ml with de-ionized water in a standard volumetric flask. The samples to be analyzed for cations were acidified with drops of HNO_3 before storage. The filtrates were analyzed for anions and cations present using a Dionex DX-120 ion chromatograph (IC) with an Ion Pac AS14A column and AG14-4 mm guard column and inductively coupled plasma atomic emission spectrometry - ICP AES (Varian Liberty Radial) respectively.

4.2.4 Total Acid Digestion

Digestion of the fly ash with acid releases all the species present in the ash. The ash samples were digested with $HF/HClO_4/HNO_3$ according to USEPA SW3050 (SW-846, 1986). The method involved contacting fly ash with a mixture of the acids to determine the pseudo-total concentration of species in the samples. The various reagents used were of analytical grade. 7 ml of perchloric acid, hydrofluoric acid and nitric acid in the ratio 3:3:1 was reacted with 0.5 g of ash in a digestion vessel (Teflon inside a parr bomb) for 3 hrs at 180 °C inside an oven. The sample was allowed to cool after which it was leached with 25 ml of 1 % hydrochloric acid. The solution was then filtered through a 110 µm Whatman's membrane filter paper. 10 ml of the solution was extracted using a bulb pipette and made up to 100 ml with de-ionized water using a standard volumetric flask. This procedure was done in triplicates. Analysis of major elements was done with inductively coupled plasma atomic emission spectroscopy - ICP AES (Varian Liberty Radial) and the trace elements present in each solution analyzed with inductively coupled plasma mass spectroscopy - ICP MS (Agilent 7500ce).

4.2.5 Sequential Extraction

The ecological effects of metals in sediments are closely related to the distribution of species in the solid and liquid phases of the sediment (Lund, 1990). A comprehensive study of trace elements and their behaviour in the sediment is required to assess their environmental impacts. The behaviour of these elements (bioavailability, toxicity and distribution) cannot be reliably predicted on the basis of their total concentration (Petit

and Rucandio, 1999), hence the importance of chemical speciation. One of the popular methods of an operationally defined speciation is sequential extraction. Depending on their origin, trace metals exist in different mineral forms and chemical compounds, and in different combinations with minerals and organic components of the sediments which may vary according to various conditions. Parameters that could influence the forms of the metals in the environment include pH, redox conditions, oxidation states, temperature, the presence of organic matter and microbiological activity (Kot and Namiesnik, 2000). Sequential extraction involves subjecting a solid sample to successive attacks with reagents possessing different chemical properties (acidity, redox potential or complexing properties) in which each extract includes a part of the trace elements associated with the sample and multiple extracting agents are utilized (Kot and Namiesnik, 2000). These extractions form the basis for characterizing solid phases and associated trace elements in soils and sediments. In this study the sequential extraction provides an insight into the mineral phases holding the trace elements as the ash dump ages. This would be complimentary to the direct physical analysis of cored samples from the ash dumps. A major advantage of the sequential extraction procedure is that it simulates to an extent various environmental conditions to which the sediments may be subjected and from this, deductions can be made about the trace metal levels likely to be released under these conditions in the environment (Tessier et al, 1979).

The method used in this study is a hybrid of the sequential extraction sequence developed by Tessier et al (1979) but with the inclusion of a water soluble phase and a removal to the organic phase. The extraction procedure seeks to partition trace elements into: de-ionized water (soluble), ammonium acetate buffer solution at pH 7 (exchangeable), ammonium acetate buffer solution at pH 5 (carbonate), 0.25 M hydroxylamine hydrochloride in 0.025 M nitric acid at pH 2 (Iron and manganese) and the residual (silicate bound fraction). All the reagents used were of analytical grade.

- **Step 1 (Water soluble fraction)**: Triplicate samples of 0.5 g of oven dried ash was weighed into 100 ml clear, plastic bottles and 90 ml of de-ionized water added. The samples were shaken at room temperature for an hour with the aid of a

mechanical shaker. The solution was allowed to settle after which the supernatant was collected using a bulb pipette. 25 ml of the supernatant was collected into a standard volumetric flask with the aid of a measuring cylinder and the solution was made up to the 50 ml mark with de-ionized water. The solution was acidified with drops of HNO_3 prevent precipitation of species for pure metal analysis. Analysis of multi-elements on the samples was done using the ICP AES (major elements) and ICP-MS (trace elements).

- **Step 2 (Exchangeable fraction)**: 90 ml of 1 M ammonium acetate buffer solution (pH 7) was added to the residue recovered quantitatively from step 1. The solution was shaken for an hour at room temperature with the aid of a mechanical shaker. The solution was allowed to settle after which the supernatant was collected using a bulb pipette. 25 ml of the supernatant was collected into a standard volumetric flask using a measuring cylinder and the solution was made up to the 50 ml mark with de-ionized water. The procedure was done in triplicate. Multi-element analysis of the solution was done using ICP AES and ICP MS.

- **Step 3 (Carbonate fraction)**: 90 ml of 1 M ammonium acetate buffer solution (at pH 5) was added to the residue recovered quantitatively from Step 2. The solution was shaken for 1 hour at a room temperature using a mechanical shaker. The solution was allowed to settle after which the supernatant was collected using a bulb pipette. 25 ml of the supernatant was measured into a standard volumetric flask using a measuring cylinder and the solution was made up to the 50 ml mark with de-ionized water. The procedure was done in triplicate. Multi-element analysis of the solution was done using ICP AES and ICP MS for major and trace elements respectively.

- **Step 4 (Iron and manganese fraction)**: 90 ml of 0.25 M hydroxylamine hydrochloride (NH_2OHCl) prepared in 0.025 M nitric acid (HNO_3) at pH 2 was added to the residue recovered quantitatively from Step 3. The solution was shaken for 1 hour at a room temperature using a mechanical shaker. The solution

was allowed to settle after which the supernatant was collected using a bulb pipette. 25 ml of the supernatant was measured into a standard volumetric flask using a measuring cylinder and the solution was made up to the 50 ml mark with de-ionized water. The procedure was done in triplicate. Multi-element analysis was done using ICP AES and ICP MS for major and trace elements respectively.

- **Step 5 (Residual fraction)**: The residual phase (silicate bound fraction) was determined by the difference of sum of the four fractions for each target analyte with the total metal content from the digestion according to USEPA SW3050 (SW-846, 1986).

4.2.6 Cation Exchange Capacity (CEC)

Fly ash is predominantly composed of mineral phases formed initially at high temperatures. On exposure to an atmospheric environment many of these solids are metastable and will alter to form thermodynamically stable assemblages of minerals. The cation exchange capacity (CEC) of fly ash is therefore defined as the degree to which ash can adsorb and exchange cations. CEC is commonly measured in terms of moles of exchangeable cation per gram (or 100 grams) or in terms of equivalents of exchangeable cations per gram (or 100 grams). The method of cation exchange capacity by Chapman (1965) was employed. All reagents used were of analytical grade. 25 ml of ammonium acetate (pH 8.2) was added to 0.5 g of ash. The solution shaken for 15 minutes after which it was centrifuged for another 15 minutes at 4000 r.p.m before the supernatant was decanted. The procedure was repeated 4 times for each sample. The cumulative extract was brought to 100 ml. The concentrations of exchangeable cations (Na^+, Mg^{2+}, Ca^{2+} and K^+) in the final solution was determined using inductively coupled plasma atomic emission spectrometry - ICP AES (Varian Liberty Radial).

The concentration for each of cation obtained was converted to meq (milliequivalents) per g of sample as follows (Radojevic and Bashkin, 1999):

Mass (mg) of cation per gram of ash = Volume (L) $\times C_{ca}$ / weight of the sample used, where C_{ca} is the concentration of cationic specie in the sample extract in mg/l. Therefore,

meq of cation g-1 of sample = [Volume (L) × C_{ca} / (weight of ash sample used)] / (equivalent weight of the cation). The equivalent weight of the cation is the mass needed to provide 1 mole of charge or atomic weight divided by valence. Therefore:

meq of Ca per gram of sample = [0.1× C_{ca} / 0.5] / 20.0

meq of Mg per gram of sample = [0.1× C_{ca} / 0.5] / 12.2

meq of Na per gram of sample = [0.1× C_{ca} / 0.5] / 23.0

meq of K per gram of sample = [0.1× C_{ca} / 0.5] / 39.1

The calculated milliequivalents per g of each cation (Ca^{2+}, Mg^{2+}, Na^{+}, and K^{+}) was summed up to get the total cation exchange capacity of the ash samples per depth.

4.3 Analytical Techniques

The various analytical techniques employed in this study and their working principles are discussed below.

4.3.1 pH Measurement

The pH of a solution is a measure of the hydrogen ion [H^{+}] concentration in solution which defines the acidity or alkalinity of the solution. It is measured on a continuous scale from 0 - 14. The scale is logarithmic. The pH value of a given solution is a measure of the activity of the hydrogen ion (H^{+}) in that solution. pH measurement involves comparing the potential of solutions with unknown hydrogen ion [H^{+}] to a known reference potential. This is done when the indicating electrode, which is sensitive to the hydrogen ion, develops a potential directly related to the hydrogen concentration in the solution, and the reference electrode provides a stable potential against which the indicating electrode can be compared. The pH meter converts the potential (voltage) ratio between a reference half-cell and an indicating half-cell to pH values. In acidic or alkaline solutions, the voltage on the outer membrane surface changes proportionally to changes in [H^{+}]. The pH meter detects the change in potential and determines [H^{+}] of the unknown sample (Fatoba, 2007).

The pH of all the samples in this study was measured by using a Hanna HI 991301 pH meter with portable pH/EC/TDS/Temperature probe. The pH meter was calibrated before use with buffer solution of pH 4.01 and 7.01. Duplicate sample measurements were done at room temperature.

4.3.2 Electrical Conductivity (EC) Measurement

Electrical conductivity measurements focuses on salts - or their ions when dissolved in water - which are conductors of an electrical current. Conductivity is measured by a probe that applies voltage between two electrodes, spaced a known distance apart, and records the drop in voltage. This drop reflects the resistance of the water, which is then converted to conductivity. Thus, conductivity is the inverse of resistance and is measured as the amount of conductance over a certain distance. Electrical conductivity is normally measured in mS/cm or µS/cm, or in µmhos/cm (1mS/cm = 1000 µmhos/cm).

The electrical conductivity (EC) measurement of the samples was determined using a Hanna HI 991301 pH meter with portable pH/EC/TDS/Temperature probe. The meter was calibrated before use by using a standard of 12.88 mS/cm at room temperature. Duplicate samples measurements were taken at room temperature.

4.3.3 Total Dissolved Solids (TDS)

Total dissolved solids (TDS) is an expression of the combined content of all inorganic and organic substances contained in a liquid which are present in a molecular, ionized or micro-granular (colloidal sol) suspended form (Fatoba, 2007). Electrical conductivity of water is directly related to the concentration of dissolved ionized solids in the water. Ions from the dissolved solids in water create the ability for that water to conduct an electrical current, which can be measured using a conventional conductivity meter. When correlated with laboratory TDS measurements, electrical conductivity provides an approximate value for the TDS concentration, usually to within ten percent accuracy (Azzie, 2002).

The total dissolved solids (TDS) of all the samples in this study were estimated using a Hanna HI 991301 pH meter with portable pH/EC/TDS/Temperature probe. The pH meter was calibrated and duplicate samples measurements were taken at room temperature.

4.3.4 Ion Chromatography (IC)

Ion chromatography (IC) uses ion-exchange resins to separate atomic or molecular ions based on their interaction with the resin. Its greatest utility is for analysis of anions for which there are no other rapid analytical methods (Dionex, 1998). The instrument analyzes aqueous samples for quantities of common anions such as fluoride, chloride, nitrite, nitrate and sulphate in parts per millions (ppm) and parts per billions (ppb) for common cations like lithium, sodium and potassium using conductivity detectors. The leachates of the fly ashes were filtered through a 0.45 μm membrane filter with the aid of a vacuum pump to remove suspended solids. SO_4^{2-}, Cl^-, NO_3^- and PO_4^{3-} were analyzed in the leachates using a Dionex DX-120 ion chromatograph with an Ion Pac AS14A column and AG14-4 mm guard column.

Ion chromatography is a form of liquid chromatography where retention is predominantly controlled by ionic interactions between the ions of the solute and counter ions that are situated in, or on, the stationary phase. For example, to separate organic acids, it is the negatively charged acid ions that need to be selectively retained. It follows that the stationary phase must contain immobilized positively charged cations as counter ions to interact with the acid ions to retain them. Alternately, to separate cations, the stationary phase must contain immobilized anions as counter ions with which the cations can interact. Ion exchange stationary phases are available in mainly two forms. One form (probably the most popular) consists of cross-linked polystyrene polymer beads of an appropriate size which have been suitably treated to link ionic groups to the surface. The other form is obtained by chemically bonding ionic groups to silica gel by a process similar to that used to produce bonded phases. These materials are called ion exchange media, a term which has given rise to the term "ion exchange chromatography" as an alternative to ion chromatography. Ionic substances can also be adsorbed on the surface of a reverse phase media and act as an adsorbed ion exchanger. The mobile phase is made

to contain a small percentage of a soluble organic ionic material (e.g. tetrabutyl ammonium dihydrogen phosphate or n-octyl sulphonate). These substances are adsorbed onto the surface by dispersive interactions between the alkyl groups of the agent and those of the bonded phase and act as counter ions (Dionex 1998).

The Ion Chromatography (IC) unit was first calibrated with a certified reference standard solution and then recalibrated after every 10 samples. Reference value of standards are: F = 20.07 mg/L; Cl = 30.04 mg/L; Br = 100.3 mg/L; NO_3 = 100.2 mg/L; NO_2 = 99.9 mg/L; PO_4^{3-} = 150.2 mg/L; SO_4^{2-} = 150.1 mg/L. Average values are: F = 20.05 mg/L; Cl = 29.95 mg/L; Br = 100.6 mg/L; NO_3 = 100 mg/L; NO_2 = 100.35 mg/L; PO_4^{3-} = 149.15 mg/L: SO_4^{2-} = 150.15 mg/L.

4.3.5 Inductively Coupled Plasma Mass Spectroscopy (ICP MS)

The Inductively Coupled Plasma (ICP) with a mass spectrometer (MS) gives very high sensitivity for the determination of elements and even isotopes in solution. This technique has the ability to detect very low levels (parts per billion) of most elements in an aqueous sample. The dynamic range is typically ten orders of magnitude and data reduction is relatively simple. Rapid data acquisition and data reduction enables the measurement of large numbers of samples in a short period of time. ICP-MS is the technique of choice for trace element analysis of natural waters, and can be used in analyzing minerals and rocks after digestion.

In general, liquid samples are introduced by a peristaltic pump, to the nebulizer where the sample aerosol is formed. A double-pass spray chamber ensures that a consistent aerosol is introduced into the plasma. Argon (Ar) gas is introduced through a series of concentric quartz tubes which form the ICP. The torch is located in the center of an RF coil, through which RF energy is passed. The intense RF field causes collisions between the Ar atoms, generating high-energy plasma. The sample aerosol is instantaneously decomposed in the plasma (plasma temperature is in the order of 6000 - 10000 K) to form analyte atoms which are simultaneously ionized. The ions produced are extracted from the plasma into the mass spectrometer region which is held at high vacuum (typically 10-4 Pa). The

vacuum is maintained by differential pumping: the analyte ions are extracted through a pair of orifices known as sampling and skimmer cones. The analyte ions are then focused by a series of ion lenses into a quadrupole mass analyzer, which separates the ions based on their mass charge ration. Finally, the ions are measured using an electron multiplier, and are collected for each mass number (http://www.chem.agilent.com/en-us/products/instruments/icp-ms/pages/gp455.aspx).

In this study, samples to be analyzed were filtered with 45 μm membrane filter paper to remove suspended solids and refrigerated before analysis. Major, minor and trace elements were analyzed using ICP-AES (Varian Liberty) and ICP-MS (Agilent 7500ce). The instruments were calibrated twice daily using multi-element standards, with a calibration verification standard analyzed directly after the calibration and control standards for every 12 samples run by the ICP MS and every 20 samples for the ICP AES. Internal standards were used to correct for instrument drift in ICP-MS.

4.3.6 X-ray Fluorescence (XRF)

XRF spectroscopy is widely used for the qualitative and quantitative elemental analysis of solid environmental, geological, biological, industrial and other samples. XRF has the advantage of being non-destructive, multi-elemental, fast and cost-effective. Furthermore, it provides a fairly uniform detection limit across a large portion of the periodic table and is applicable to a wide range of concentrations, from a 100 % to few parts per million (ppm). Its main disadvantage is that analyses are generally restricted to elements heavier than fluorine and that a large sample is required (Kalnicky and Singhvi, 2001). Procedures for sample preparation vary considerably in the cases of in situ or intrusive measurements. Solid samples such as rock minerals must be polished to assure surface homogeneity, while powders are usually pressed into pellets.

Representative samples down the drilled core from the surface to 32 m were taken at 1 m intervals. The ash samples were oven-dried at 100 °C for 12 hrs to remove the adsorbed water and then crushed with a mortal and pestle to fine powder. 9 g of the dried powdered

sample was mixed with 2 g of binder (a mixture of Wax C and EMU powder). Binders are used to glue the individual grains of the samples together before making the mixture into pellets at a pressure of 15 kbar for a minute. A Phillips PW1480 sequential X-ray spectrometer was used to determine the bulk elemental composition of the fly ash samples. Elements reported as % oxides were converted as % elements using element conversion software downloaded at www.marscigrp.org/elconv.html.

4.3.7 X-ray Diffraction (XRD)

X-ray diffraction is an analytical technique which uses the diffraction pattern produced by bombarding a single crystal with X-rays to determine the crystal structure. The diffraction pattern is recorded and then analyzed or "solved" to reveal the nature of the crystal. This technique is widely used in chemistry and biochemistry to determine the structures of an immense variety of molecules, including inorganic compounds, DNA, and proteins. When single crystals are not available, related techniques such as powder diffraction or thin film x-ray diffraction coupled with lattice refinement algorithms such as Rietveld refinement may be used to extract similar, though less complete, information about the nature of the crystal. The spacing in the crystal lattice can be determined using Bragg's law ($n\lambda=2d\sin\theta$). The electrons that surround the atoms, rather than the atomic nuclei themselves, are the entities that physically interact with the incoming X-ray photons. If the angles of incidence (θ) and the wavelength (λ) are known, the spacing d of the reflecting atomic planes can be determined using the above equation. The lattice spacing is characteristic of the mineral, thus, the X-ray diffraction method can be used for the identification of minerals and for the analysis of mixtures of minerals and it was used for this purpose in the study.

Representative samples down the drilled core from the surface to 20 m at 4 m intervals and from 21 m to 28 m at interval of 1 m were analyzed for prominent mineral peak identification. The ash sample was oven-dried at 100 °C for 12 hours to remove the adsorbed water and then crushed with a mortal and pestle to a fine powder. A Phillips analytical instrument with a PW3830 X-ray generator operated at 40 kV and 25mA was used. The samples were pressed into rectangular aluminum sample holders using an

alcohol wiped spatula and then clipped into the instrument sample holder. The samples were step-scanned from 5 to 85 ° 2 θ at intervals of 0.02 ° 2 θ and counted for 0.5 seconds per step.

4.3.8 Scanning Electron Microscopy (SEM)

The scanning electron microscope (SEM) is a type of electron microscope capable of producing high-resolution images of a sample surface. SEM images have a characteristic three-dimensional appearance due to the manner in which the images are created. It is useful for judging the surface structure and morphology of samples.

The SEM used was a fully analytical Leica/Leo S440 Scanning Electron Microscope equipped with a Fissons Quantum EDS detector, using Sigma software. The samples were viewed at 20 KV at a working distance of about 25 mm and the EDS spectrum was collected over 60 seconds.

Specimen preparation involved drying of the samples in the oven at 105 °C for 12 hr. After this, the sample was crushed with mortar and pestle. Aluminum SEM stubs were covered with carbon graphite glue, and a small amount of each sample was sprinkled onto the stub. Once the glue had dried, the excess sample was tapped off the stub and the stubs were coated with carbon in an evaporation coater. The stubs were loaded onto a carousel and inserted into the SEM chamber.

Specimen beam interactions in the SEM produces a number of scattering events which may either be elastic or inelastic. For crystalline specimen, some of the elastically scattered electrons are diffracted and may be back scattered to form a pattern on the phosphor screen strategically placed within the specimen chamber. In order to obtain a significant yield of the diffracted electrons, the specimen is tilted at an high angle (usually 70 °) with respect to the horizontal axis. The video image of the electron back scattered diffraction is captured using a computer containing a MATROX IP8 framestore. Once the pattern of the image has been captured, the position of at least 3 zones is marked and the software is indexed by the software routine. The pattern is then replotted

and the results confirmed. The process allows for approximately 60 crystal orientations per hour (Wittridge et al., 2007).

4.3.9 Fourier Transform Infra Red Spectroscopy (FTIR)

Infrared spectrometry (IR) is a standard analytical tool that utilizes the fact that chemical bonds between unlike atoms can absorb IR light and cause vibrations of the bonds. Bond vibrations are of two main types; stretching vibrations in which the bond-length changes and bending (deformation) vibrations in which bond angles change. When IR radiation is passed through a sample, some of the infrared radiation is absorbed by the sample and some of it is passed through (transmitted). The resulting spectrum represents the molecular absorption and transmission, creating a molecular fingerprint of the sample. Like a fingerprint, no two unique molecular structures produce the same infrared spectrum. Most modern FT-IR instruments produce plots with wave number (units: cm^{-1}) on the abscissa and percent transmission (or absorbance) on the ordinate. The IR wavelength absorbed is characteristic of a particular bond in a particular molecule or mineral and can be measured by a FT-IR spectrometer. The different functional groups (SO_4^{2-}, OH^-, NO_3^- and O-Si-O) can be identified in an unknown material by comparison with published charts.

Samples to be analyzed were collected at 4 m intervals from the surface to 32 m depth. Samples were oven dried at a temperature of 100 °C and crushed with mortar and pestle. The FT-IR analysis of samples in this work was carried out on a Perkin Elmer 100 series, Universal ATR accessory spectrophotometer.

The solid samples are best analyzed on a single reflection ATR (attenuation total reflection) accessories; diamond being the preferred choice for most applications because of its robustness and durability. The ATR accessory operates by measuring the change that occur in a totally internally reflected infrared beam when the beam comes in contact with a sample. The infrared beam is directed unto an optically dense crystal with high refractive index at a certain angle. This internal reflectance creates an evanescent wave that extends beyond the surface of the crystal into the sample held in contact with the

crystal. The attenuated energy from each evanescent is passed back to the IR beam which exits the opposite end of the crystal and is passed into the detector of the IR spectrometer. The system then generates an infrared spectrum. The ATR crystal was cleaned using methanol soaked in tissue. After the crystal area had been cleaned and the background collected, the ash sample was placed unto the small crystal area. Milled sample just enough to cover the crystal area was required. The pressure arm of the equipment was positioned over the crystal/sample area and force was applied to the sample pushing it into the diamond surface (Perkin Elmer, 2005). The results obtained were compared with already published data for the purpose of identification of the functional groups.

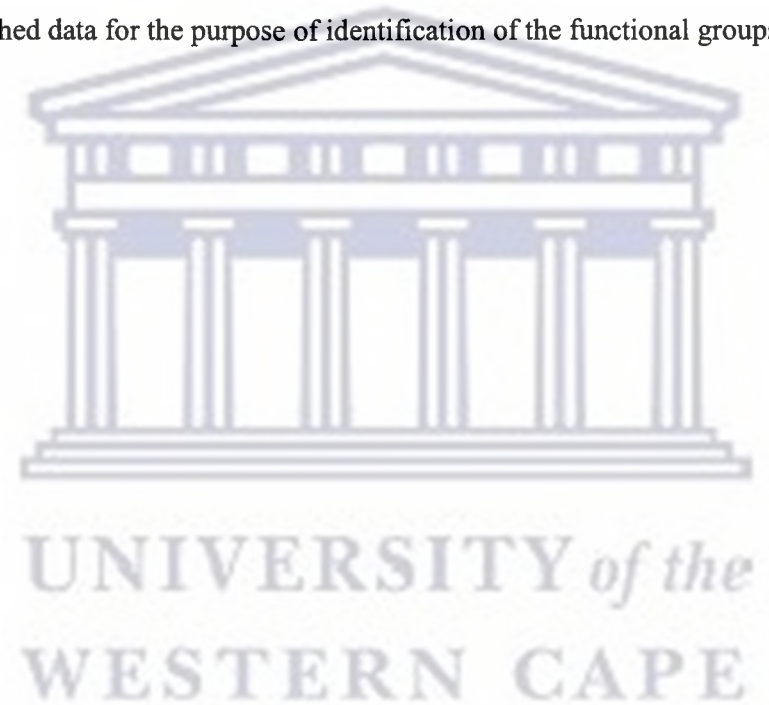

Chapter Five

Results and Discussion

The results obtained from the various experimental and analytical procedures reported in the previous chapter for the physical and chemical characterization of Kragbron ash core samples, mobility of the various species and their interpretations are presented in this chapter.

5.1 Description of Drilled Core Profile

The profile of the drilled core (Fig 4.1.1) shows that samples taken from the core from the surface (KS0) to 22 m in depth (KS22) (Table 4.1) was purely fly ash. The colour of these samples ranged from light grey to dark grey. There was a contact with the bedrock at 23 m depth (KS23) where, a mixture of fly ash, the bed rock and some clay was observed. A colour change from dark grey to greyish brown was also observed. The samples from 24 m (KS24) to 32 m (KS32) showed a similar orange brownish colour which was very different from the colour of samples from the surface to 22 m. The samples from 24 m (KS24) to 32 m (KS32) were from the bedrock as will be discussed in section 5.3 and 5.4 of this chapter.

The unburned carbon content in fly ashes is of importance because it corresponds to the loss on ignition values obtained from the fly ashes. Unburned carbon content ranging from 0.5 % to 10 or 12 % in some cases is responsible for the grey to black colour of fly ashes (Wesche, 1991). The light colour of some fly ashes is an indication of a low amount of unburned carbon in the ashes (Adriano et al., 1980). The colour of fly ash samples from the surface to 22 m depth varied from light to dark grey agreeing with the colour of ash reported in literature. Fly ash colour changes from grey to cream when treated at 1000 °C in order to make it a more marketable product (Landman, 2003).

Literature on the local geology of the Kragbron shows that the area is underlain by dolerite dyke of Jurassic age (Duncan and Marsh, 2006). Invariably, samples from 24 m

to 32 m depth in the drilled core are expected to be samples of dolerite as was determined by XRD (see section 4.3.7).

It was reported in literature that the major oxides found in fresh dolerite included: SiO_2 (51.5 %), Al_2O_3 (16.91 %), Fe_2O_3 (9.91 %), CaO (11.37 %), MgO (7.56 %), Na_2O (2.385 %) and TiO_2 (0.88 %). P_2O_5, MnO and K_2O were present in lower quantities. Trace elements reported included Ba (163 ppm), Sr (198 ppm), Cr (537 ppm) and V (214 ppm). Also present were Y, Zn, Cu, Ni, Co and Ce in concentrations ≤ 100 ppm (Marsh, 1991).

5.2 Morphology of Fly Ash

The morphology of a fly ash particle is usually controlled by the combustion temperature and cooling rate. During combustion, the heat causes the inorganic minerals to become fluid or volatile or to react with oxygen which may form crystalline solids, spherical amorphous particles or condense as coatings on particles during cooling (Kutchko and Kim, 2006).

The morphology of Kragbron fly ash was determined as described in section 4.3.8 of this study. The scanning electron microscopy (SEM) micrograph of the surface layer of the ash dump showed the typical spherical shape associated with fly ash particles (Fig. 5.2.1a). Some agglomerated and irregularly shaped particles were also observed. These were more prominent in deeper parts of the dump (16 m, 20 m, and 22 m) indicating some level of weathering (Fig. 5.2.1b and 5.2.1c). Energy dispersive spectroscopy spot analysis performed as described in section 4.3.8 showed that the spherical shaped particles were enriched with high amounts of Si, Al and the agglomerations were high in Ca and Fe (Fig. 5.2.1a).

The SEM micrograph obtained from samples at 23 m depth showed agglomerated and irregularly shaped particles (Fig. 5.2.1d).

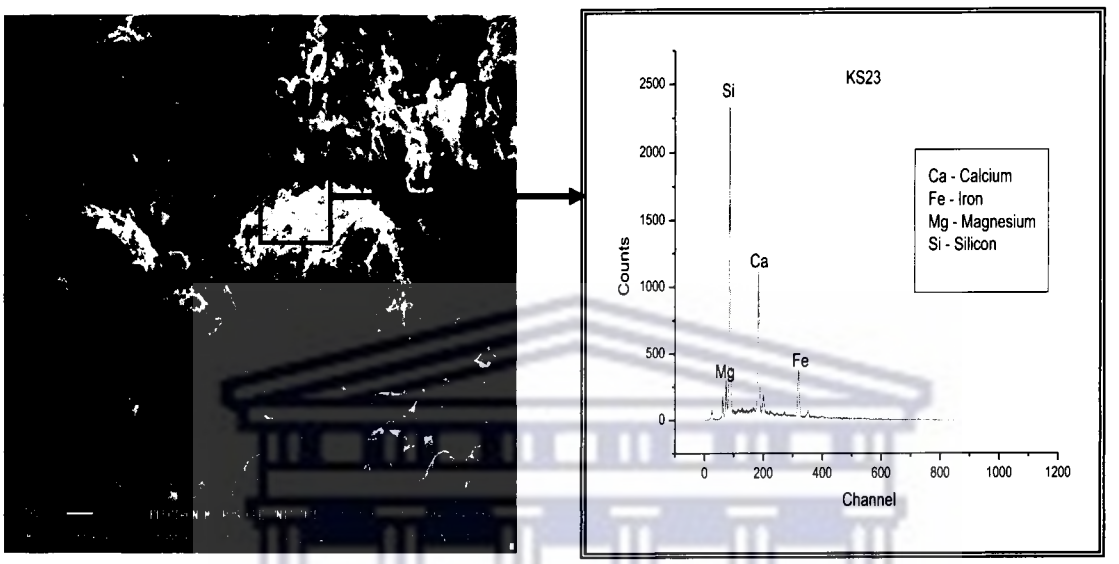

Fig. 5.2.1d: SEM micrograph and EDS of sample obtained at 23 m

At this depth, the bedrock which had a different composition compared to fly ash was sampled. EDS spot analysis showed high amounts of Si, Ca and Fe. It also showed Mg in a reasonable quantity. This agrees with the XRD result obtained for samples from 23 m depth (See section 5.5). Quartz (SiO_2), anorthite ($CaAl_2Si_2O_8$) and diopside ($CaMgSi_2O_6$) were the minerals found in KS23. Anorthite and quartz are known to be associated with fly ash (Russel et al., 2002; Erol et al., 2003). They are formed as secondary minerals during coal combustion (Vassilev and Vassileva, 2005). Diopside is a clinopyroxene mineral of the pyroxene group. It is rich in calcium, magnesium, silicon and oxygen. Dolerite of Jurassic age is composed mainly of plagioclase feldspars and clinopyroxenes (Jourdan et al., 2004).

SEM micrographs and EDS spot analysis of samples obtained between 25 and 32 m down the core profile showed the presence of Al, Si, Ca, Fe, Mg, Ti, and K in varying

amounts (Fig. 5.2.1e and 5.2.1f). This also supports the mineralogy of these samples as found by X-ray diffractometry (Also see section 5.5).

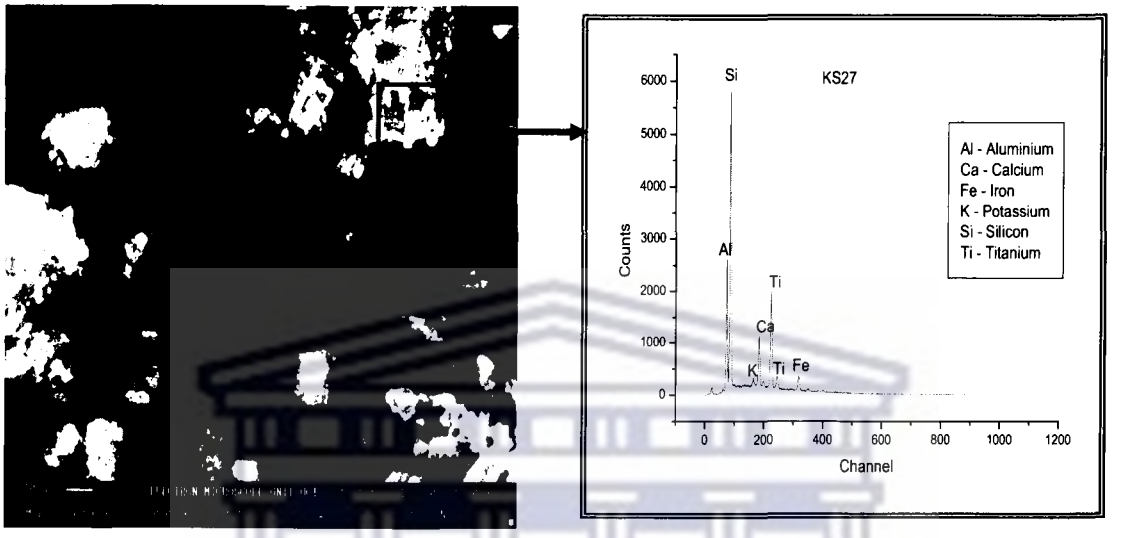

Fig. 5.2.1e: SEM micrograph and EDS of sample obtained at 27 m

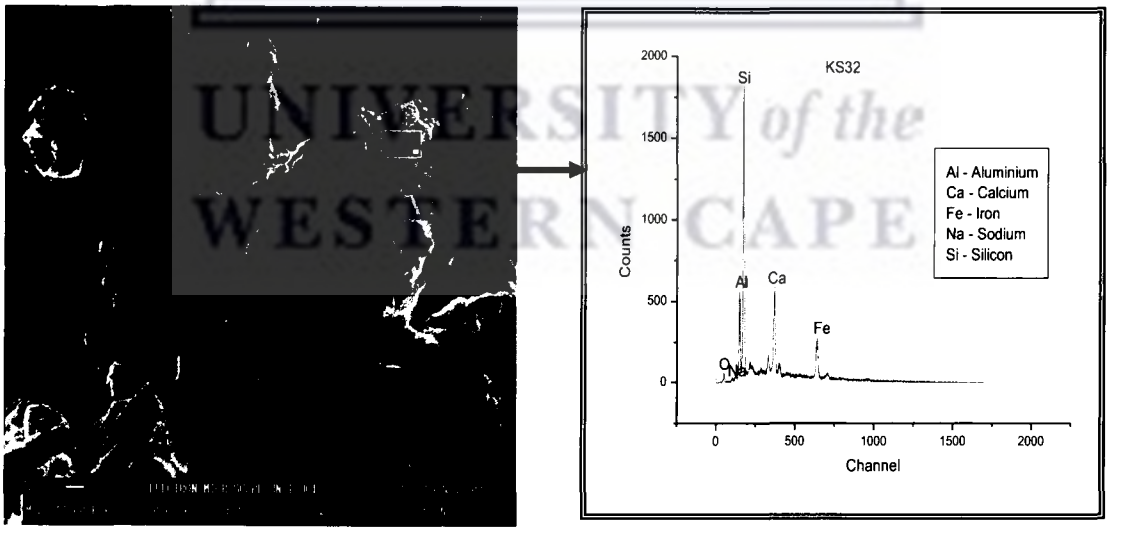

Fig. 5.2.1f: SEM micrograph and EDS of sample obtained at 32 m

5.3 Moisture Content Determination

The method of disposal of fly ash has a huge bearing on its moisture content. Fly ash transported as slurry will have a higher moisture content than that disposed of using the dry disposal method as described in section 2.6 of the literature review. The moisture content was determined to ascertain the quantity of water contained in the samples per depth as this plays an important part in the physical characteristics of the ash (see section 4.2.1).

The moisture content obtained from the samples ranged from 3.69 % to 15.97 % (Table 5.3.1 and Fig. 5.3.1) indicating a higher moisture content value in the ash column than in the bedrock.

Table 5.3.1: Moisture content of Kragbron ash core samples

Depth (m)	Sample Names	Moisture Content (g)	Moisture content %	Depth (m)	Sample Names	Moisture Content (g)	Moisture content %
0	KS0	0.24	8.82	17	KS17	0.40	13.79
1	KS1	0.17	6.25	18	KS18	0.46	15.97
2	KS2	0.18	6.59	19	KS19	0.43	15.09
3	KS3	0.21	7.72	20	KS20	0.45	15.41
4	KS4	0.20	7.35	21	KS21	0.48	15.89
5	KS5	0.16	5.88	22	KS22	0.39	13.68
6	KS6	0.18	6.64	23	KS23	0.27	9.22
7	KS7	0.17	6.23	24	KS24	0.24	8.28
8	KS8	0.17	6.25	25	KS25	0.29	10.03
9	KS9	0.21	7.69	26	KS26	0.19	6.57
10	KS10	0.21	7.72	27	KS27	0.28	9.66
11	KS11	0.22	8.06	28	KS28	0.26	9.00
12	KS12	0.15	5.54	29	KS29	0.17	6.12
13	KS13	0.16	5.90	30	KS30	0.17	6.12
14	KS14	0.19	7.04	31	KS31	0.13	4.71
15	KS15	0.20	7.38	32	KS32	0.10	3.69
16	KS16	0.33	12.81				

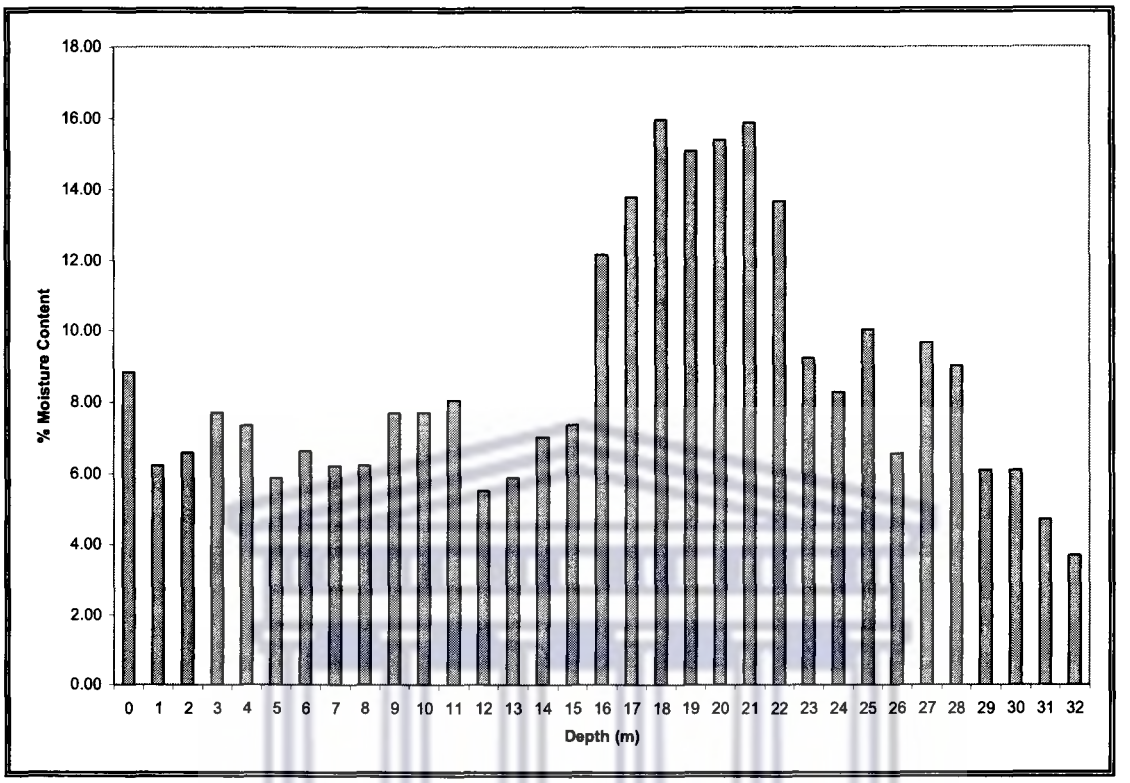

Fig. 5.3.1: Moisture content of Kragbron ash core samples as a function of depth profile

The ash layer extended from the surface to a depth of 22 m. A bimodal distribution in the moisture content values was noted, with the first 15 m having an average of 6.94 % moisture while samples at 16 m to 22 m of the Kragbron core showed elevated moisture content of above 14.57 %, where after the bedrock started. The inconsistent moisture content observed in the fly ash zone of the drilled core (surface to 22 m) could be attributed to a period of dumping followed by a period of inactivity allowing accumulation of water at certain depths of the profile due to contribution from rainfall. It could be said that there was vertical flow of water from the shallower depths to the deeper depths of the ash column. Accumulation of the water between 16 m and 22 m depth of the ash column is due to the nature of the material encountered at 23 m which considerably reduced the rate of flow down the bedrock.

Dolerite normally has a fine to medium grain sized texture but it weathers to give a reddish or chocolate clay loam soil, followed by a soapy yellowish clayey material (Beater and Frankel, 1965). Sample at 23 m was a greyish brown colour consisting of a mixture of fly ash, some clayey material and the bedrock. A yellowish brown clayey material was obtained from samples at 24 m down to 32 m. The fine texture of the clayey material makes it less porous. Hence, after saturation of the pores, dolerite is likely to prevent further ingress of water, causing an accumulation above 23 m (ash contact with the bedrock) as is evident from the elevated moisture content of samples from 16 m to 22 m depth.

5.4 Loss on Ignition (LOI)

ACI 16 (2000) defines loss on ignition as % loss in mass of a constant weight sample ignited at temperatures 900-1000 °C. Loss on ignition is a measurement of the amount of unburned carbon remaining in fly ash. It is one of the most important chemical properties of fly ash especially since it is an indicator of the fly ash's suitability for use as a cement replacement in concrete. The amount of unburned carbon in fly ashes is generally a function of the combustion temperature as well as the rank of coal utilized. A high temperature combustion unit and a low rank of coal will generate very low amount of unburned carbon while a low temperature unit and a high ranking coal decreases combustion efficiency thereby generating high amount of unburned carbon (Yinzhi et al., 2003). The loss on ignition was obtained using the procedure given in section 4.2.2. A dark grey colour was observed in the samples with higher LOI values. The % loss on ignition values obtained from Kragbron ash core samples is presented in Fig. 5.4.1.

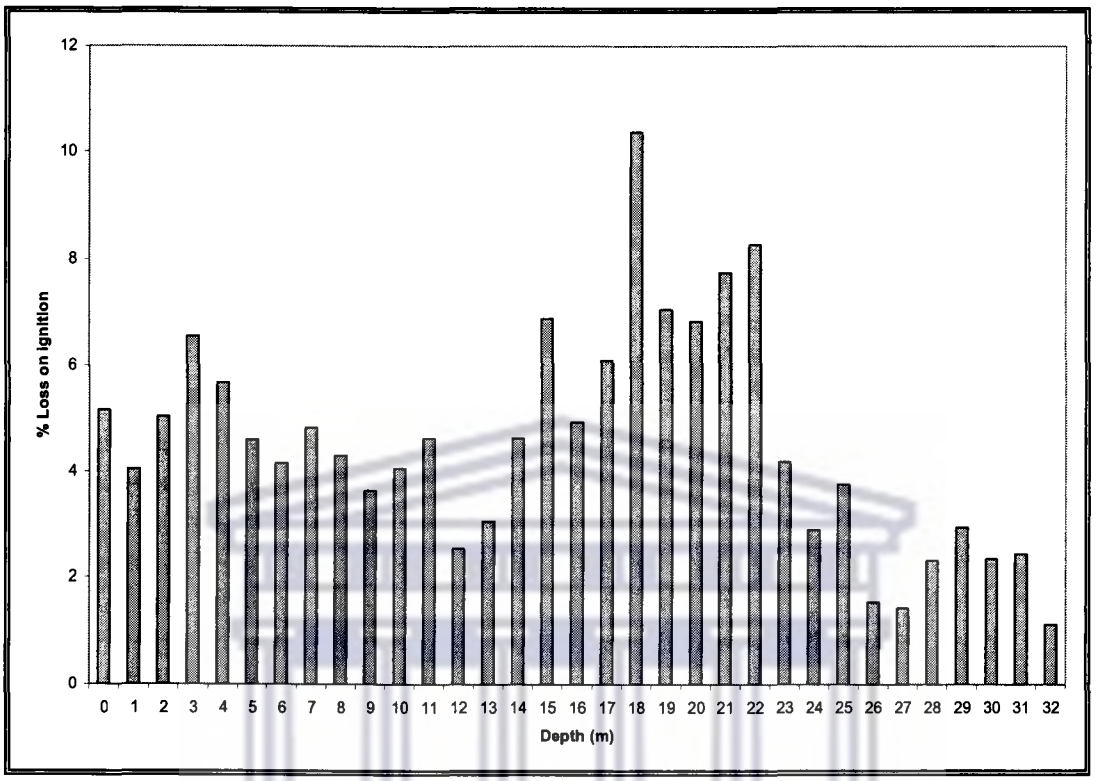

Fig. 5.4.1: % loss on ignition (LOI) of Kragbron core samples

The ash layer from surface to 11 m showed a bimodal distribution in the LOI values with an average of 4.73 % while an elevation was observed from 15 m to 22 m of depth, having an average of 7.28 %. Samples from 26 m to 32 m depth showed another bimodal distribution with an average of 2.01 %. The trend observed in the loss on ignition show a similarity to that observed in the moisture content of the samples. Samples obtained from 15 m to 22 m have higher loss on ignition values than samples at the shallower depths and after 23 m. The higher LOI values indicate higher porosity and thus, the higher moisture contents recorded at these depths (this is only applicable in undisturbed cores). The variations observed in the loss on ignition values could also be as a result of a change in the type of coal used in the combustion plants. Originally, coal supplied to Taaibos power station was from Coalbrook North Colliery of the Clydesdale collieries but after the close down of the colliery in 1960, the power station received coal from Coalbrook South Colliery which supplied coal to Highveld power station and also from Cornelia

Colliery in Vereeniging. ASTM C618, 2001 limits the LOI of pozzolanic fly ash materials to less than 6 % because higher level of LOI causes discoloration, poor air entrainment, segregation and low compressive strength of the mixed component. The LOI values obtained from 24 m to 32 m might therefore not necessarily be unburned carbon content but loss of waters of hydration in the dolerite layers.

Volatilization and the decomposition of inorganic species in the Kragbron ash samples may have an impact on the loss on ignition values obtained but majority of the volatile content can be attributed to the oxidation of partially combusted coal particles (Moreno et al., 2005).

5.5 Mineralogical Composition

The mineralogical composition of Kragbron ash was determined using the X-ray diffraction technique specified in section 4.3.7. The major minerals identified are quartz, mullite and calcite as seen in Fig. 5.5.1 and also in appendix B.

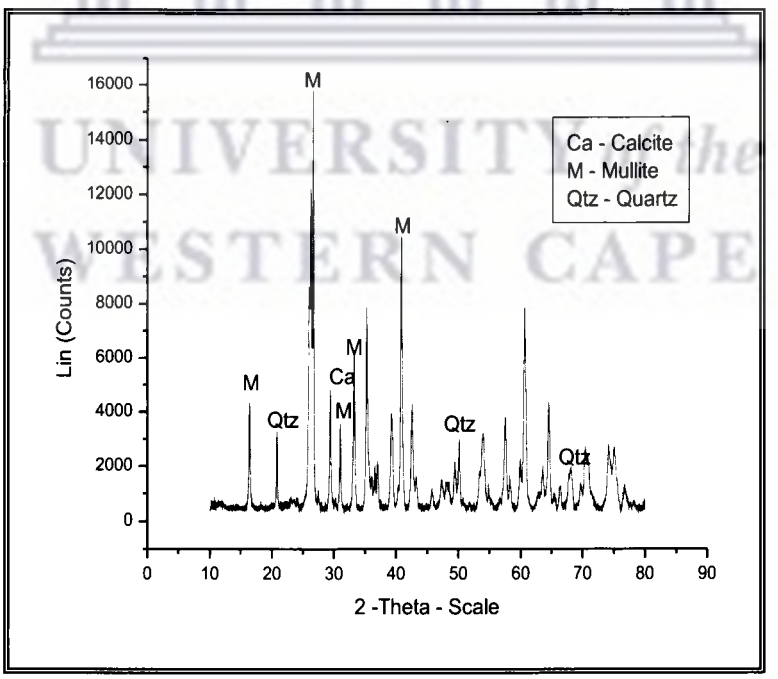

Fig. 5.5.1: Mineral peaks identified from the surface to 20 m depth at Kragbron

These mineral phases were consistent from the surface to a depth of 20 m in the Kragbron ash core samples.

In order to ascertain the extent of the ash into the bedrock (dolerite), the X-ray diffractometry of samples at 22 m and 23 m was included in the analysis (Fig. 5.5.2 and 5.5.3).

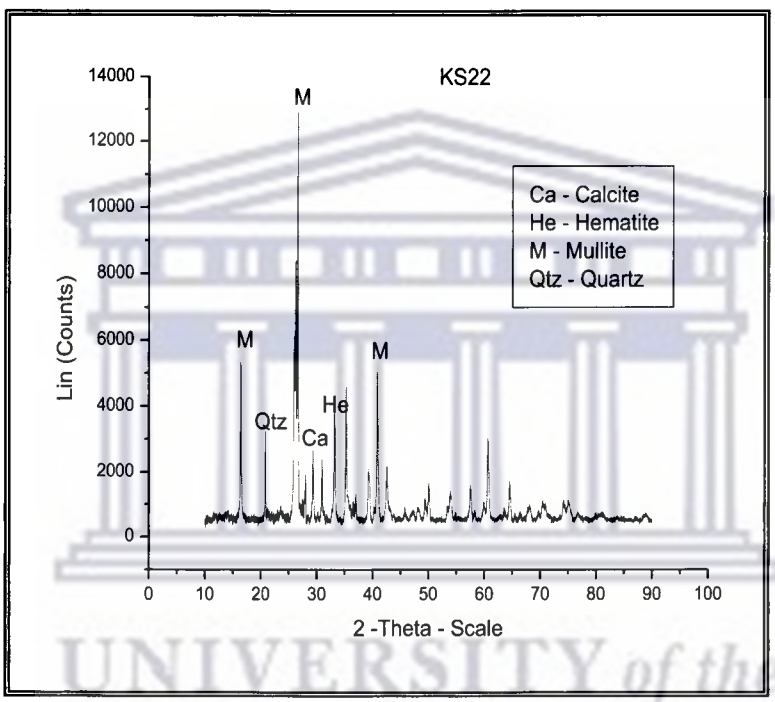

Fig. 5.5.2: Mineral peaks identified from 22 m at Kragbron

Quartz, mullite, calcite and a little bit of hematite were the minerals observed in at 22 m.

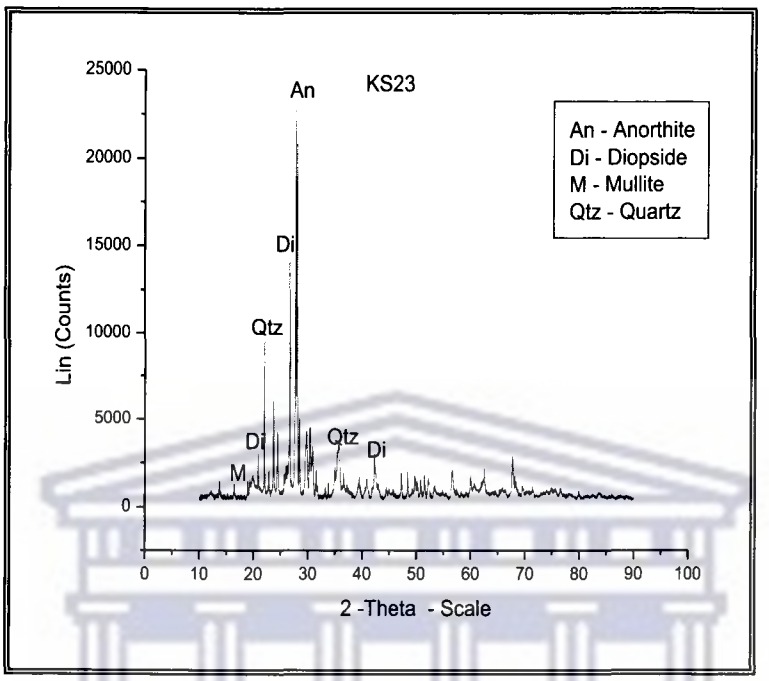

Fig. 5.5.3: Mineral peaks identified from 23 m at Kragbron

Quartz, a small percentage of mullite, anorthite and diopside were the minerals observed at 23 m. The presence of mullite at this depth indicates a mixture of the ash with the bedrock – dolerite.

The mineral phases observed dominating samples at 24 m to 32 m are presented in Fig. 5.5.4.

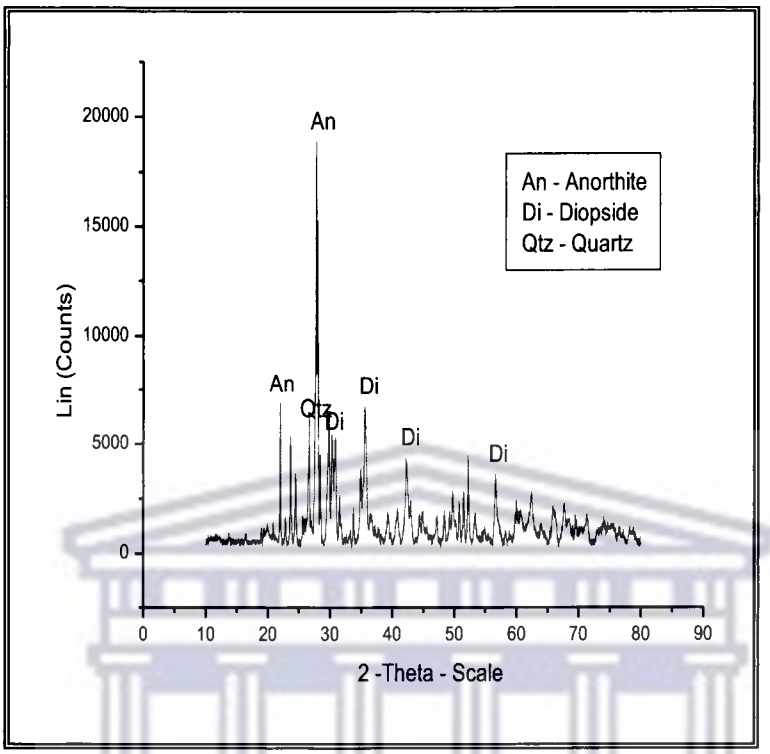

Fig. 5.5.4: Mineral peaks identified from 24 m to 32 m at Kragbron

The crystalline mineral phases typically present in fly ash consist of quartz (SiO_2), mica ($XY_{2-3}Z_4O_{10}(OH,F)_2$ with X = K, Na, Ba, Ca, Cs; Y = Al, Mg, Fe^{2+}, Li, Cr, Mn, V,Zn and Z = Si, Al, Fe^{3+}, Be, Ti, chlorite ($(Fe,Mg,Al)_6(Si,Al)_4O_{10}(OH)_8$), feldspars ($KalSi_3O_8$ – $NaAlSi_3O_8$ – $CaAl_2Si_2O_8$), mullite ($3Al_2O_3.2SiO_2$), spinel ($FeAl_2O_4$), hematite (Fe_2O_3) and magnetite (Fe_3O_4) depending on the mineralogy of the feed coal (Norton et al., 1986; Vassileva et al., 1997; Vassileva et al., 2005; Kutchko and Kim, 2006). Mineralogy of a class F South African coal fly ash revealed feldspars; mainly anorthite ($CaAl_2SiO_8$) as one of the secondary mineral phases found in minor quantities (Nathan et al., 1999).

Mullite ($3Al_2O_3.2SiO_2$), quartz (SiO_2) and calcite ($CaCO_3$) were predominant from the surface layer to a depth of 22 m at Kragbron. These show an alignment with the XRF results obtained in section 5.7 of this study. Anorthite and diopside peaks were identified at the contact with the bedrock (23 m). The mineralogical findings in this study agree with those reported in the literature for fly ash. Mullite present in fly ash forms from the

decomposition of kaolinite which is entrained in the coal during its genesis (White and Case, 1990).

South African dolerites are either tholeitic or olivine dolerites. The mineralogy consists mainly of plagioclase feldspars and pyroxenes (Bell and Jermy, 2000). Anorthite ($CaAl_2Si_2O_8$) – a calcium aluminium silicate member of the plagioclase feldspar group, diopside ($CaMgSi_2O_6$) – a calcium magnesium silicate member of the clinopyroxene group and quartz were the minerals dominant from 24 m to 32 m.

5.6 Changes in Molecular Vibrations

The different chemical bonding present in the fly ash was determined using the FTIR procedure described in section 4.3.9 of this study. The FTIR bands generated by quartz, mullite and the glassy phase of the ash overlap in the area between 900 and 1200 cm^{-1} as a result of the T-O-Si (T= Al and Si) stretching vibration (Criado et al., 2007). A medium asymmetrical stretching (Si-O-Si and Al-O-Si) band at 798 cm^{-1} is attributed to α-quartz and a strong band at 561 cm^{-1} is indicative of mullite (Vempati et al., 1994). The broad band located at 500 to 650 cm^{-1} is indicative of silicate and aluminosilicate glasses, which possess long-range structural order in the form of rings of tetrahedra or octahedra (Handke et al., 1994; Poe et al., 1992 and Sitarz et al., 1997). Most of the FTIR bands obtained for samples characterized in this study fall within these ranges (Fig. 5.6.1), agreeing with the literature. Figure 5.6.1 is a representative of the trends observed in the Kragbron ash core samples from the surface to 22 m depth.

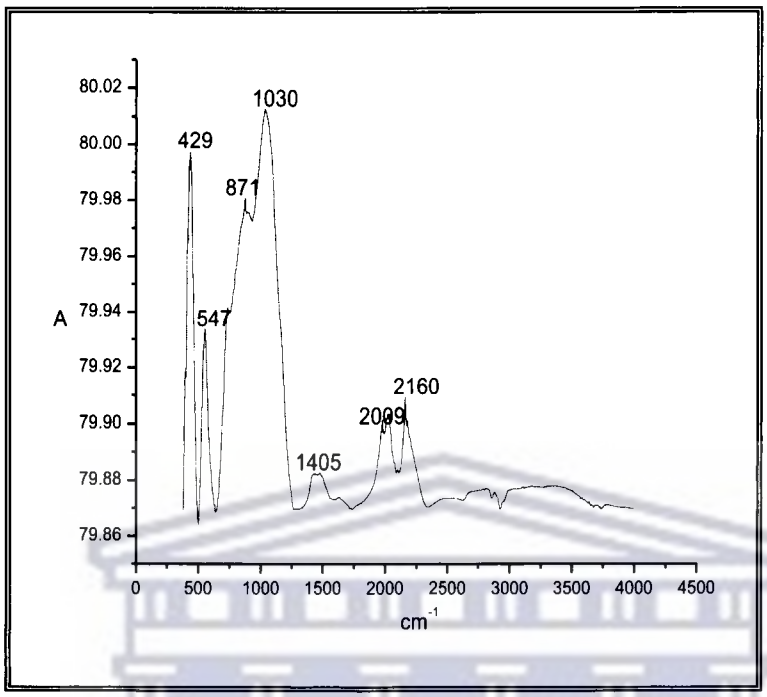

Fig.5.6.1: FTIR bands observed in Kragbron ash core sample at 4 m

5.7 Bulk Chemical Composition

The elemental composition of Kragbron ash core samples was determined by XRF as described in section 4.3.6. The chemical composition of the ash sample (KS0) obtained at the surface of Kragbron ash dump is presented in Table 5.7.1 below.

Table 5.7.1: Concentration of major and minor elements obtained from the surface of Kragbron ash dump using XRF

Major Elements	% w/w
Al_2O_3	33.00±0.43
CaO	5.40±0.12
Fe_2O_3	2.85±0.01
K_2O	0.51±0.02
MnO	0.03±0.01
MgO	1.31±0.01
Na_2O	1.00±0.03
P_2O_5	0.49±0.02
SiO_2	48.15±0.31
SO_3	0.02±0.02
TiO_2	2.03±0.05
LOI	5.18±1.01
Total	99.97±2.04

Trace Elements	ppm
As	29.29±1.28
Ba	51.48±0.40
Ce	279.66±0.07
Co	29.00±3.43
Cu	86.56±0.51
Mo	6.01±0.12
Nb	42.31±0.81
Ni	85.01±1.85
Pb	115.61±2.09
Rb	34.00±1.00
Sr	1006.37±22.02
V	434.41±4.59
Y	97.07±2.00
Zn	43.73±1.80
Zr	855.87±1.81

The table shows that the fly ash contains SiO_2, Al_2O_3, Fe_2O_3 and CaO as its major oxide constituents. According to the American Society for Testing and Materials - ASTM (ASTM C 618, 1993), Coal fly ashes have been classified into two types, based on the percentages of their aggregate alumina, silica and ferric oxide contents. These classes are F and C. Class F usually has a total of SiO_2, Al_2O_3 and Fe_2O_3 greater than 70 % while class C has a total of SiO_2, Al_2O_3 and Fe_2O_3 of between 50 % and 70 %. Kragbron ash can be classified as class F because the sum of the percentage composition of SiO_2, Al_2O_3 and Fe_2O_3 is greater than 70 % and the lime content is less than 10 % (Table 5.7.1). It can be inferred from this that the fly ash at Kragbron was derived from the burning of bituminous coal. The presence of oxides of Ca and Mg, which form hydroxides on exposure to water, is responsible for the alkaline nature of the fly ash (Furr et al., 1975).

5.7.1 Elemental Composition of Kragbron Ash Core Samples

The concentrations of major, minor and trace elements as determined by XRF in Kragbron ash dump as a function of depth are presented graphically below. Samples were collected from the surface down to 32 m depth of the ash horizon (see section 4.1). The data obtained for each element using X-ray fluorescence technique (see section 4.3.6) was converted from weight % to mg/kg and plotted against the depth profile on Microsoft excel. The elemental weight % of major and minor elements was obtained using software from www.marscigrp.org/elconv.html. The XRF data serves as a basis for the total concentration of the elements in each fly ash sample and all data obtained from other techniques is to be compared with it. The XRF data was left in mg/kg in order for comparison to be made.

5.7.1.1 Major Element Content

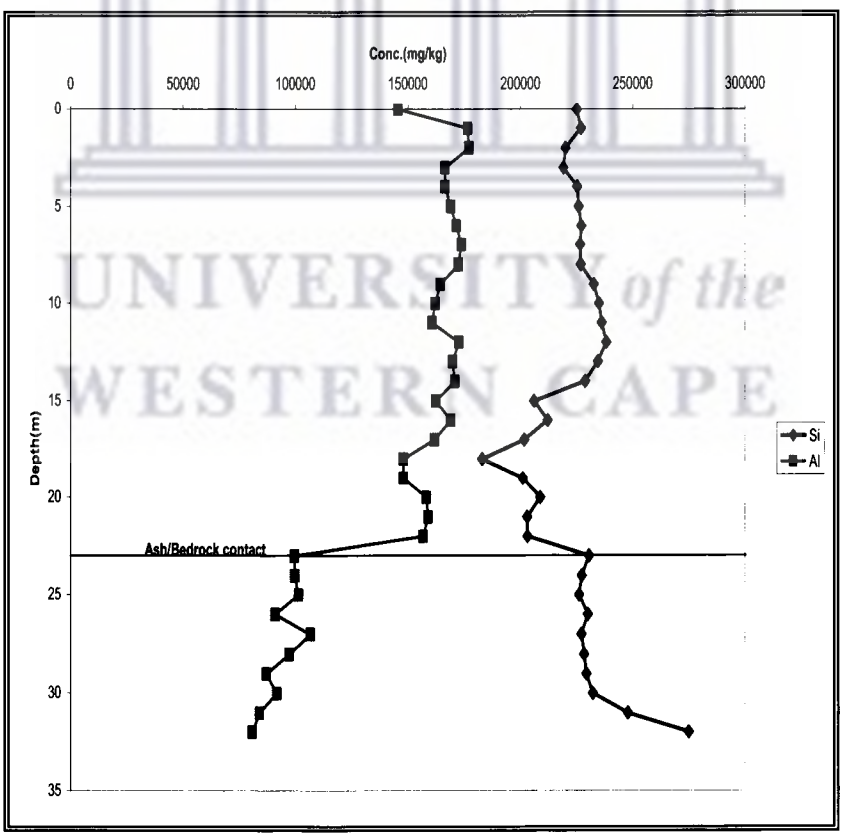

Fig.5.7.1: Trends (XRF) of Si and Al down the drilled Kragbron core

Si concentration as determined by XRF was relatively constant from the surface to 14 m into the dump (Fig. 5.7.1). From 16 m down to 22 m, Si levels showed a general decrease in concentration and a sudden increase at the ash/bedrock contact (23 m). The concentration of Si from 23 m was relatively constant until an increase was observed from 30 m. The Al trend as determined by XRF shows an initial decrease in concentration from depth of 1 m to 3 m. The concentration of Al then increased to its original concentration and thereafter maintained a relatively constant concentration at depths between 4 m to 8 m after which a variation was observed from 9 m to 22 m. A sharp decrease was observed from 22 m to the bedrock at 23 m. This lower concentration was observed to continue to deeper depths with some small fluctuations. The trends observed for the major elements Si and Al down the ash core horizon are consistent with weathering patterns in surface layers and a change in mineralogy at the point of contact with bedrock. Similar trends were observed in the case of Fe content in the ash horizon (Fig. 5.7.2 below).

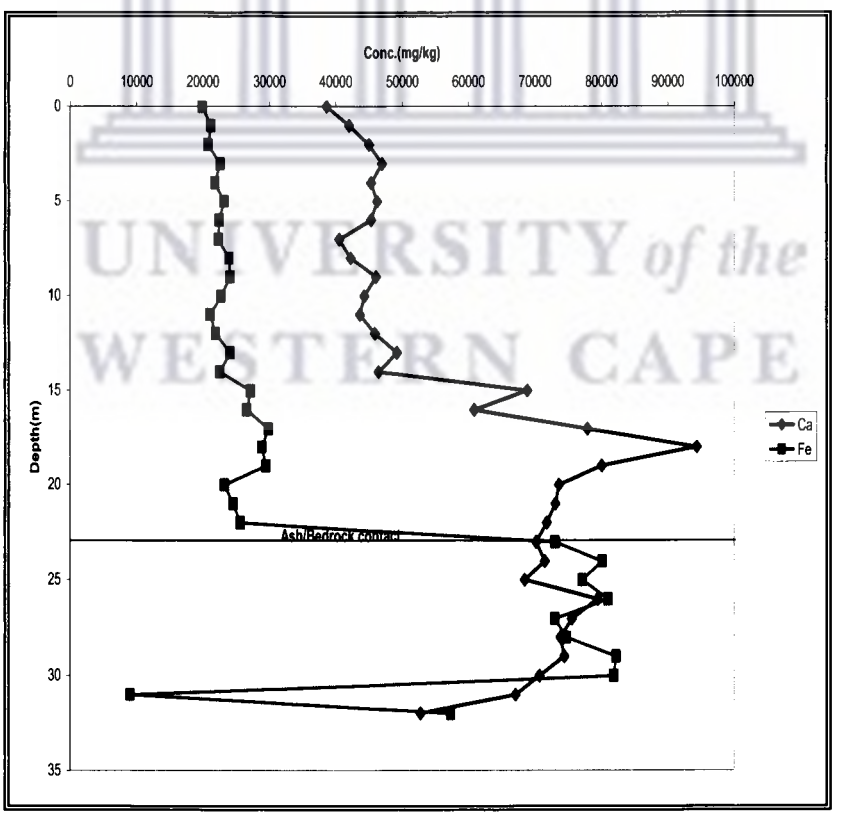

Fig. 5.7.2: Trends (XRF) of Ca and Fe down the drilled Kragbron core

The concentration of Fe in Fig. 5.7.2 is relatively constant from the surface to a depth of 13 m. A slight increase was observed at a depth of 14 m to 19 m. A very sharp increase was observed from 22 m to the contact at 23 m where after the levels of Fe showed fluctuations between 23 m and 30 m, then a sudden decrease at 31 m. The large increase in Fe content is consistent with a change in mineralogy observed after the contact with the bedrock.

The concentration of Ca (Fig. 5.7.2) shows some weathering in surface layers (between 1 and 4 m). Thereafter, levels fluctuated in a manner which is consistent with the mode of emplacement of the ash, in that the ash was placed in slurry form on top of previously hardened ash and allowed to dry, permitting the formation of calcite by the ingress of CO_2. A progressive increase from 14 m to 18 m was also observed which may indicate the dissolution of Ca bearing minerals due to long interaction with moisture at those depths or the use of coal with high Ca content at 18 m. This also would account for the decrease observed in the concentration of Al and Si at 18 m in figure 5.7.1. This section of the ash profile showed higher level of moistness than the surface layers (Fig. 5.3.1) after which a sharp decrease in concentration was observed between 18 m to 25 m. At the point of contact with the bedrock (23 m), some fluctuations in Ca levels are observed until a depth of 30 m where after levels decreased significantly.

The levels of Mg, Na, K and Ti in the ash core samples from Kragbron are shown in Fig. 5.7.3.

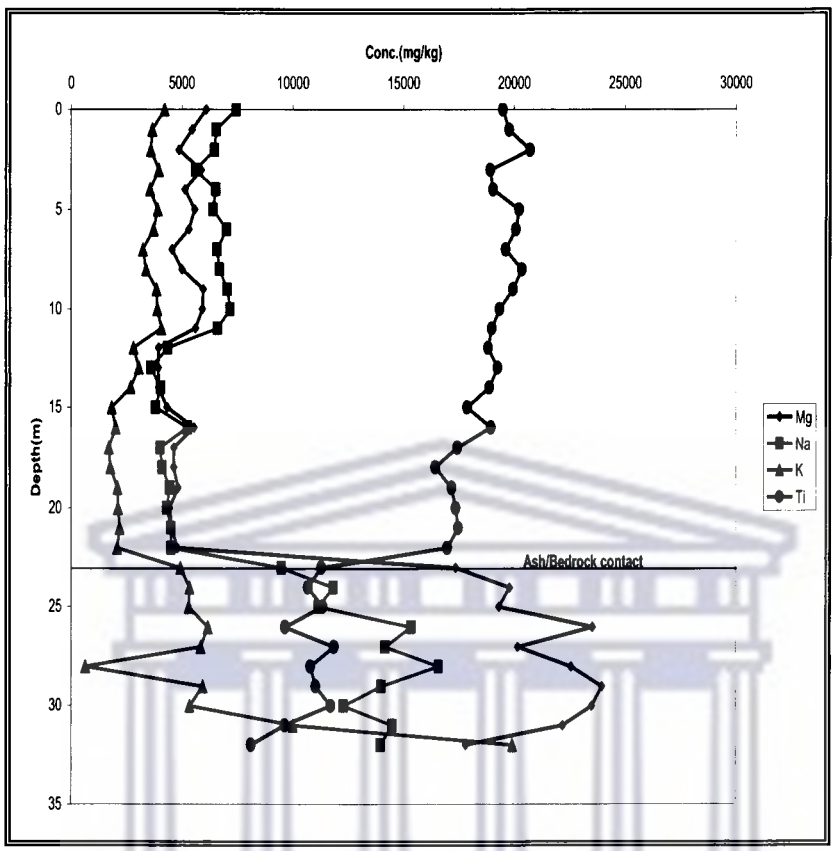

Fig. 5.7.3: Trends (XRF) of Mg, Na, K and Ti down the drilled Kragbron core

The concentration of Mg, Na, K and Ti showed similar trends from the surface layers to a depth of 23 m (Fig. 5.7.3). After 23 m, both Na and Mg increased significantly to higher concentrations whereas K levels increased somewhat. On the contrary, the concentration of Ti showed a decline from a depth of 23 m. The gradual decomposition of the aluminosilicate bearing phase of the fly ash causes a release of the elements trapped in them like Mg, Na and Ti, hence the trend observed for these elements within the ash profile. The change observed at 12 m for Na, K and Mg could be as a result of the use of a different kind of coal.

These trends for Na, Mg and K are similar to the Fe trends and indicate that Na, Mg, K and Fe are major components of the bedrock layer whereas Ti and Al are depleted in the bedrock layer compared to the ash. These trends also show the significant difference in

the composition of the ash horizon and that of the bedrock strata. The significant increase in the concentration of K from 28 m to 32 m could be as a result of the dissolution of its host mineral due to the presence of moisture at those depths. The fairly constant concentration of Ti within the ash profile (0 – 22 m) could be as a result of the similar concentration of titanium dioxide in the various coals used at the power stations.

A similar depletion in the bedrock layer compared to the ash is observed in the case of P and S as can be seen in Fig. 5.7.4.

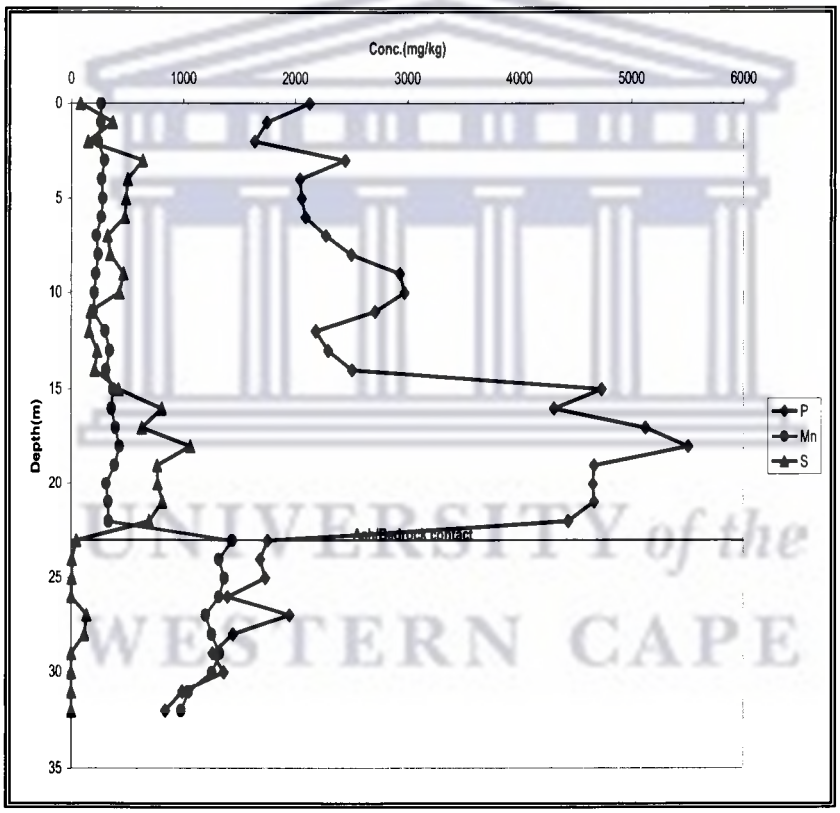

Fig. 5.7.4: Trends (XRF) of P, Mn and S down the Kragbron drilled core

The concentration of P and S showed a similar trend down the drilled core. Variation in the concentrations of both elements was observed from the surface to a depth of 15 m where after both elements increased in concentration until the bedrock layer where the levels decreased significantly. S was below detection limit from 23 m with a small

concentration at 27 m and 28 m. P showed a sharp decrease from 23 m onward with a small increase in concentration at 27 m. Similar trend observed for P and S at 4 m and 18 m could be as result of the dissolution of their host minerals causing release of the elements in these regions. It could also be that the type of coal from which the ash at these regions was got had higher concentrations of phosphate and sulphate bearing minerals. The concentration of Mn was relatively constant from the surface to a depth of 22 m (Fig. 5.7.4). A sharp increase was thereafter observed at the bedrock layer at 23 m. This shows that apart from Na, Mg, K and Fe, Mn was also present in the bedrock layers to a significant extent compared to the ash horizon. XRF analysis of fresh and weathered dolerite of the Karoo showed that the rock is rich in Fe, Mg, Na, K and Mn (Marsh, 1991). This therefore explains the higher concentration observed for the elements within the bedrock profile (23 m to 24 m). The accumulation of P in the deeper ash layers is consistent with the trends observed for Ca (Fig. 5.7.2) and show that P and Ca may be correlated or associated with an increase in moisture content of the ash. It also indicates the depth of weathering in this very old dump. Over time, these elements may have migrated down the ash horizon to accumulate above the bedrock layer.

It is possible that the depletion observed for Al, P, S, Ti in the bedrock layers could be due to leaching caused by a lateral flow in the bedrock layer; however the moisture content in the bedrock samples is much lower than that of the ash in the deeper horizons, thus a change in the mineralogy between the ash and the bedrock is a more consistent interpretation of the data.

5.7.1.2 Minor and Trace Element Content

In Fig. 5.7.5 to 5.7.8, the minor and trace element trends of the ash and bedrock horizon of the Kragbron core are graphed. Fig. 5.7.5 shows the trends observed for Pb, Ce, Y, As and Nb.

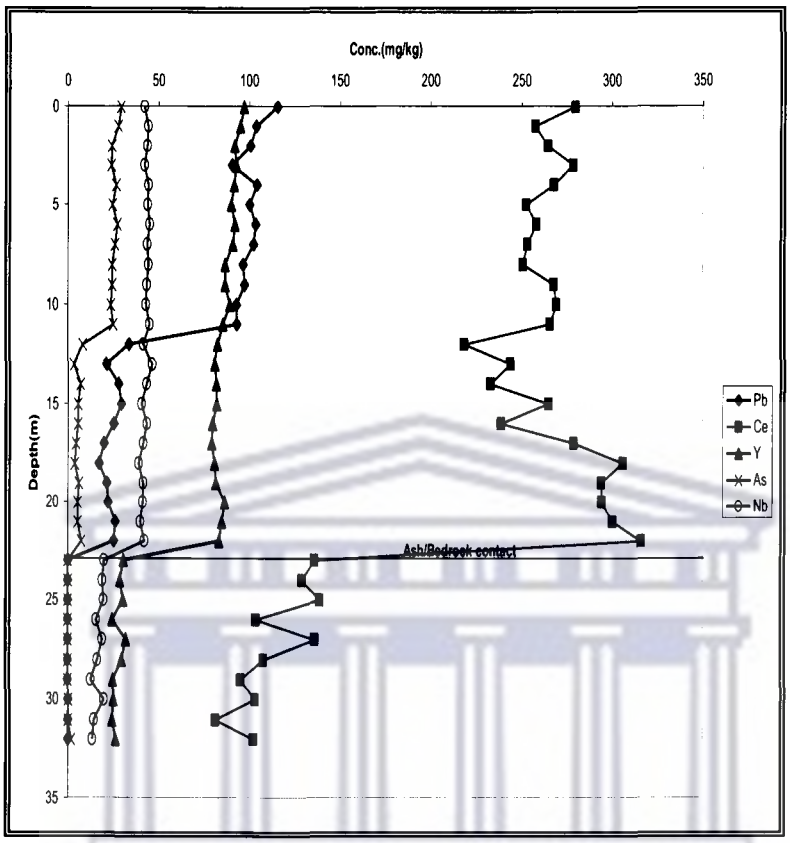

Fig. 5.7.5: Trends (XRF) of Pb, Ce, Y, As and Nb down the Kragbron drilled core

Nb and Y showed relatively constant concentrations throughout the horizon. A decrease was observed in both elements at the bedrock layer at 23 m after which levels remained at the lower concentrations (Fig. 5.7.5). This could be attributed to the presence of the elements in lower concentrations in the bedrock layers (Marsh, 1991). Pb and As showed similar trends from the surface throughout the horizon. Both elements were below detection limit at the point of contact with the bedrock (23 m) and showed a sudden decrease in concentration at about 11 m down the ash profile. This decrease is also consistent with the deep weathering observed in this old ash dump because as the other major elements such as Ca, P and S are weathered. Trace elements are known to be associated with the surface of fly ash particles. The release of Pb and As from the surface to 11 m could be as a result of the dissolution of their host minerals in the presence of moisture or their abundance in the type of coal used. Ce showed a higher concentration

from the surface to 22 m and a much lower concentration from the bedrock layer (Figure 5.7.5). Similar trends as Ce were observed in the case of Sr, Zr and V (Fig. 5.7.6).

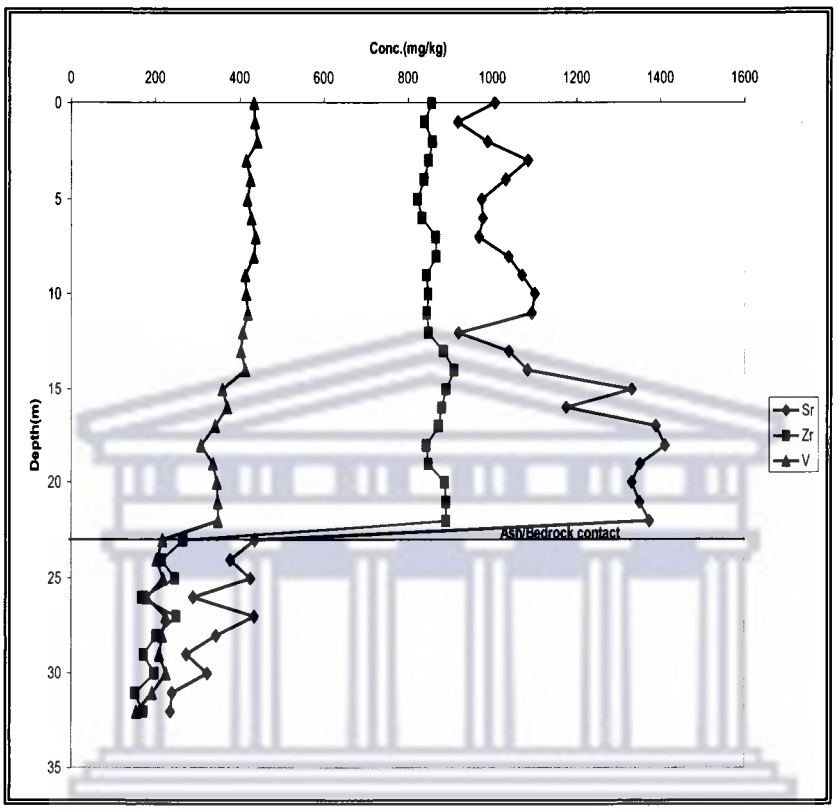

Fig. 5.7.6: Trends (XRF) of Sr, Zr and V down the drilled Kragbron core

Zr and V showed the same trend from the surface to a depth of 32 m (Fig. 5.7.6). Thereafter their concentration was much lower from the point of contact with the bedrock. Concentration of Sr showed the same trend from 23 m but inconsistent fluctuations were observed from 0 to 22 m. The concentration of Sr was highest at 18 m depth.

Sr and Ce show very similar trends to the elements P, S and Ca which indicates that these five elements maybe associated with soluble components in the ash that are more readily weathered and migrate to accumulate in the deeper ash horizon between 13 m and 22 m where a higher moisture content was also observed (Fig. 5.3.1).

Fig. 5.7.7 shows the trends of trace elements Cu, Ni, Zn and Co concentration in the ash horizon at Kragbron.

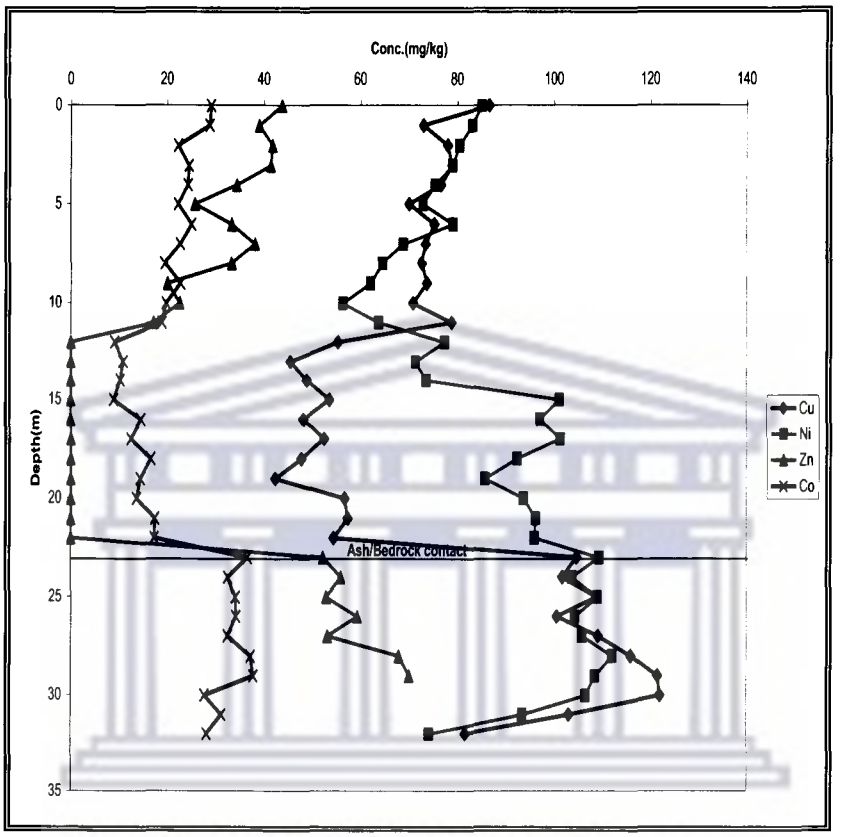

Fig. 5.7.7: Trends (XRF) of Cu, Ni, Zn and Co down the drilled Kragbron core

Co, Zn and Cu showed a similar trend in the ash profile as was observed in the case of Pb and As, where these elements appear enriched in the first 10 m of the ash horizon due to leaching and also their abundance in the coal type utilized at the power stations. A considerable increase from the point of contact with the bedrock was also observed with the elements. Zinc was below detection limit from 12 m to 22 m. Zn, Cu, Ni, Co are enriched in dolerites (Marsh, 1991), hence the higher concentrations observed for the elements in the dolerite layers.

Fig. 5.7.8 shows the trends of Rb and Mo concentration in the ash horizon at Kragbron.

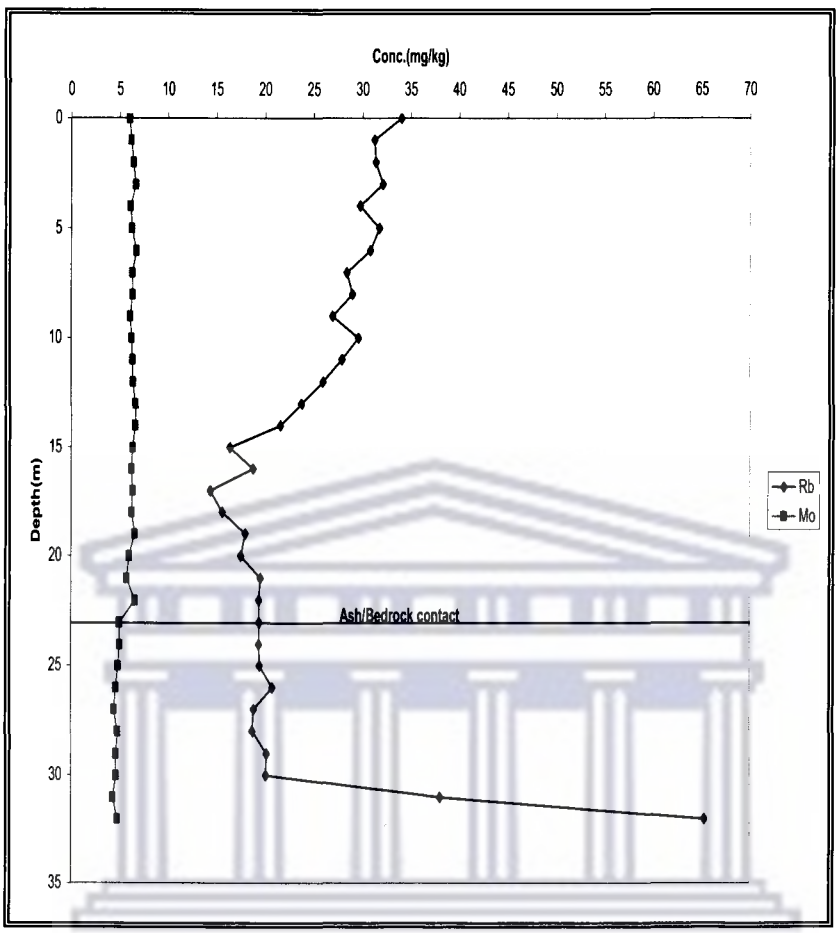

Fig. 5.7.8: Trends (XRF) of Rb and Mo down the drilled Kragbron core

Mo showed a constant concentration from the surface of the ash and throughout the profile (Fig. 5.7.8). Rb on the other hand showed a decreasing trend from the surface to a depth of 17 m (Fig. 5.7.8) where after levels were fairly constant from 21 m to 30 m depth. The concentration of Rb increased suddenly beyond 30 m. The only other element showing their sudden increase in the lower bedrock layer was K and to a lesser extent Si.

Varying concentrations of elements typically present in fly ash were observed in the ash profile. The initial low concentrations observed for Ca (Fig. 5.7.2) could be due to the formation of less soluble hydroxide and carbonate minerals ($Ca(OH)_2$ and $CaCO_3$) as a result of rain water infiltration and CO_2 ingress at the time of deposition at those depths e.g. calcite. The availability of Ca as CaO and Mg as MgO is responsible for the alkaline

pH of the ash samples. Major and minor elements present in the ash profile at Kragbron dump included Si, Al, Ca, Fe, Ti, Mg, Na, K, P, Sr, Zr and S while Pb, As, Ce, Y, Nb, V, Cu, Ni, Zn, Co, Rb and Mo were the present trace elements. The behaviour exhibited by the elements was as a result of their release from their host minerals in the presence of moisture over time and changes in the coal type during the life span of the power stations. This is evident from 11 m as elements like Mg, Na, K, Pb, As, Co, Zn and Cu showed depletions.

Samples taken between 23 to 32 m depth are observed to have a high concentration of Fe, Mg, Si, Na, K, Mn, Ni, Cu, Zn, Co and a lower concentration of Al, Ti, P, S, Ce, Y, Nb, Pb, As, Sr, Zr, V and Rb. XRD results revealed a different mineralogy at these depths from that which was observed in the fly ash column. Literature revealed that the ash dump site is underlain by Karoo dolerites (see section 3.2). XRF revealed low TiO_2, P_2O_5 and Zr values with a relatively high SiO_2 value. This makes the dolerite a low-Ti dolerite as characterized by Jourdan et al, (2004). Elements such as Ca, Sr, Ba and V are reported to show high level of depletion in weathered dolerite (Marsh, 1991). This explains the lower concentration of the elements after the 23 m depth. The presence of the elements common to fly ash in lower concentrations after the ash/ bedrock contact (KS23) does not indicate the migration of species downward. This is most likely as a result of the impervious nature of the dolerite encountered from a depth of 23 m onward. The secondary minerals formed as a result of weathering could also prevent the leaching of metals through adsorption, co-precipitation and physical encapsulation. Trace metals such as Cu, Co, Mo, Nb, Pb, Zn, Mn and Ni are co-precipitated with hydroxides of Fe and Al as well as clay minerals formed as a result of weathering (Zevenbergen et al., 1999).

5.8 Pore Water Chemistry

This involved contacting fly ash with de-ionized water for 30 min to determine the water soluble species of the fly ash, the pH, electrical conductivity and the total dissolved solids in the leachate obtained. The procedure was carried out as described in section 4.2.3 after

which the leachates were analyzed using the ICP AES/MS and IC for soluble cations and anions present respectively.

5.8.1 pH

pH values were obtained using the procedure described in section 4.3.1. This was done to determine the acidity or alkalinity of the fly ash samples obtained from Kragbron ash dump. The trend of pH values obtained from the leachates of Kragbron ash core samples is shown in Fig. 5.8.1.

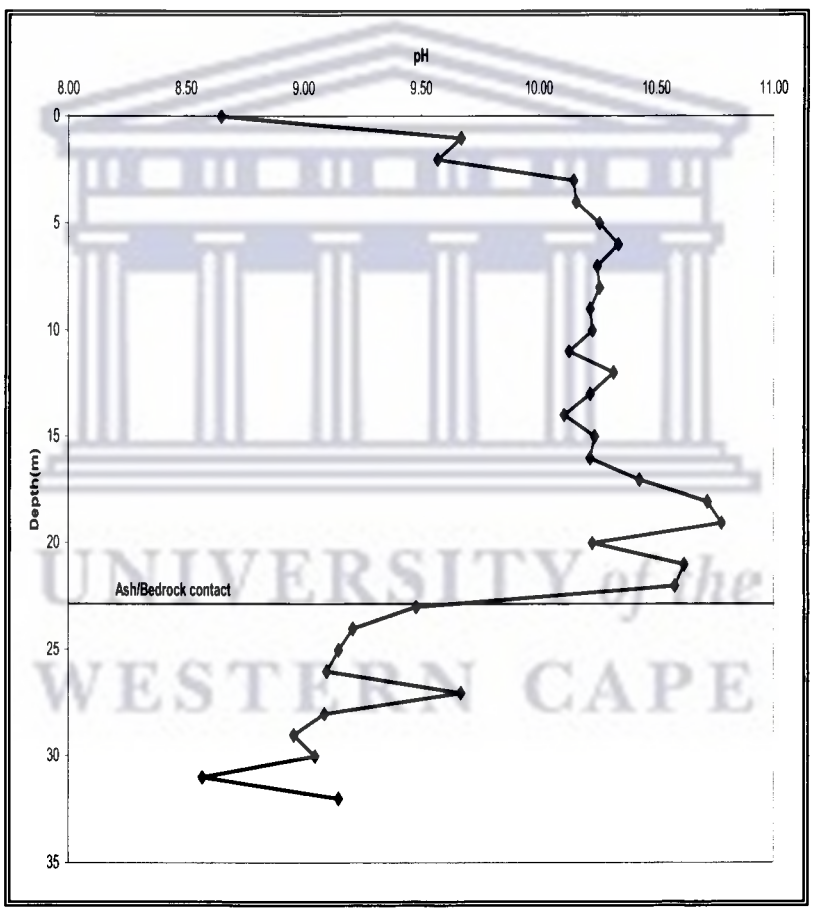

Fig. 5.8.1: pH variation down the drilled Kragbron core

The pH values obtained from the leachates ranged from 8.65 to 10.78. A progressive increase was observed from the surface to about 19 m while a progressive decrease was observed from 23 m to 32 m (9.48 to 8.57). The increased pH observed from 16 m to 22

m most likely resulted from the dissolution of MgO or CaO present in the ash samples while in contact with water. When CaO, a major contributor to the alkalinity of fly ash is exposed to air, it reacts with CO_2 to form $CaCO_3$. Also, when rain falls on fly ash, free lime CaO is hydrated to Ca $(OH)_2$ which reacts with CO_2 to form calcite ($CaCO_3$), a sparing soluble mineral. The formation of calcite reduces the pH of fly ash and this explains the lower pH (8.65) obtained at the surface of the ash dump site at Kragbron. The pH values obtained from 16 m to 22 m showed that the ash retained its alkalinity over many years, seeing that the dump is about 44 yrs old. The high pH values obtained in deeper layers of the ash agree with those from previous studies (Choi et al., 2002).

Killingley et al (2000) suggested that the pH of the ash-water system depends on the balance between the concentration of alkaline-earth elements; Ca and Mg in the ashes on one hand and the proportion of potentially acid-generating SO_3 on the other hand. Reardon et al (1995) also reported that the dissolution and hydrolysis of oxides of calcium and magnesium tend to contribute to the high pH values of water extracted ash leachates.

The pH is highest at 19 m because of the long interaction between the insoluble and soluble compounds of alkaline and alkali earth elements in the presence of moisture over time.

5.8.2 Electrical Conductivity (EC)

The electrical conductivity value was obtained using the procedure described in section 4.3.2. This was done to determine the amount of salts and their ions dissolved in solution. The trend of electrical conductivity as a function of the depth of the drilled core at Kragbron is shown in Fig. 5.8.2. The electrical conductivity (EC) values of the leachates of samples from the Kragbron core ranged from 0.08 to 0.46 mS/cm. The value was highest at 16 m depth. This indicates the accumulation of soluble species in the ash at this depth.

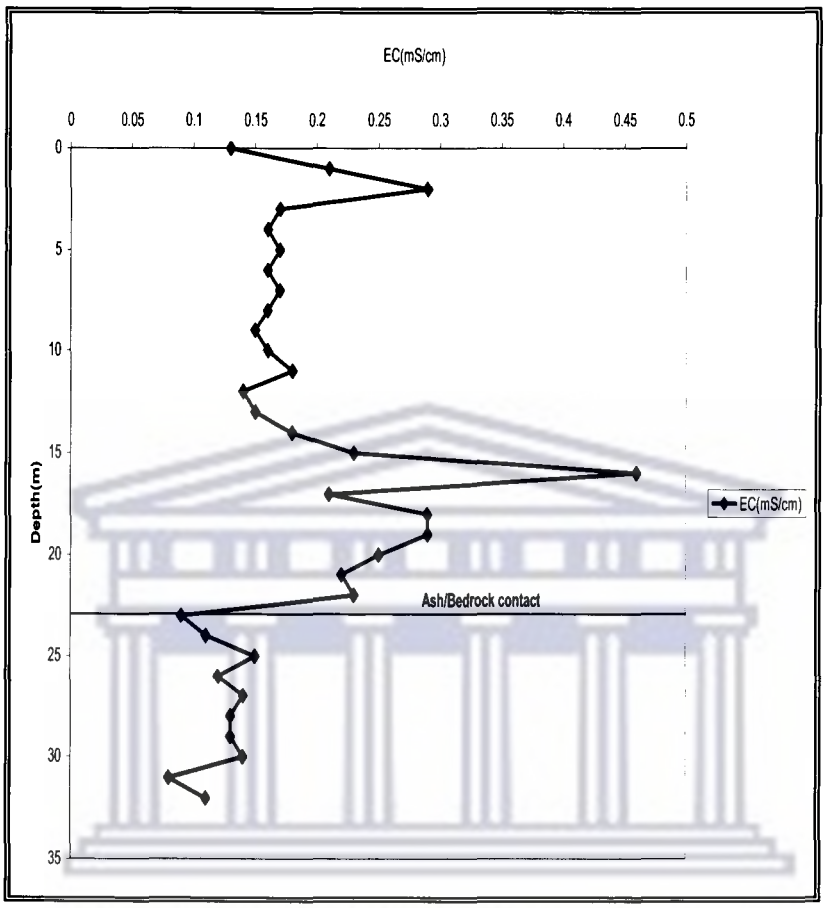

Fig. 5.8.2: Plot of EC as a function of depth

The wet method was used during the disposal of the ash where it was conveyed as slurry via pipes to the dump. Each ash layer is overlain by another so that it resembles a stack of pancakes. Movement of the soluble elements from the top layers and accumulation at 16 m most likely was enhanced by weathering and the vertical flow of water down the dump. Hence, the high electrical conductivity (EC) recorded at this depth. The trend observed for the electrical conductivity from 16 m to 22 m is the same as that observed with the pH at these depths. It indicates the accumulation of soluble species of the ash at these depths.

5.8.3 Major and Minor Elements

The elements that are adsorbed on the surface of the fly ash particles are much more easily mobilized into solution during fly ash water interaction than elements incorporated into the glassy phases of the ash. Their mobility depends on the phases with which they are associated in the ash as well as the pH of the leaching solution (Jankowski et al., 2006). The levels in concentration of major elements in pore water samples from Kragbron drilled core are shown in Fig. 5.8.3a to 5.8.3c.

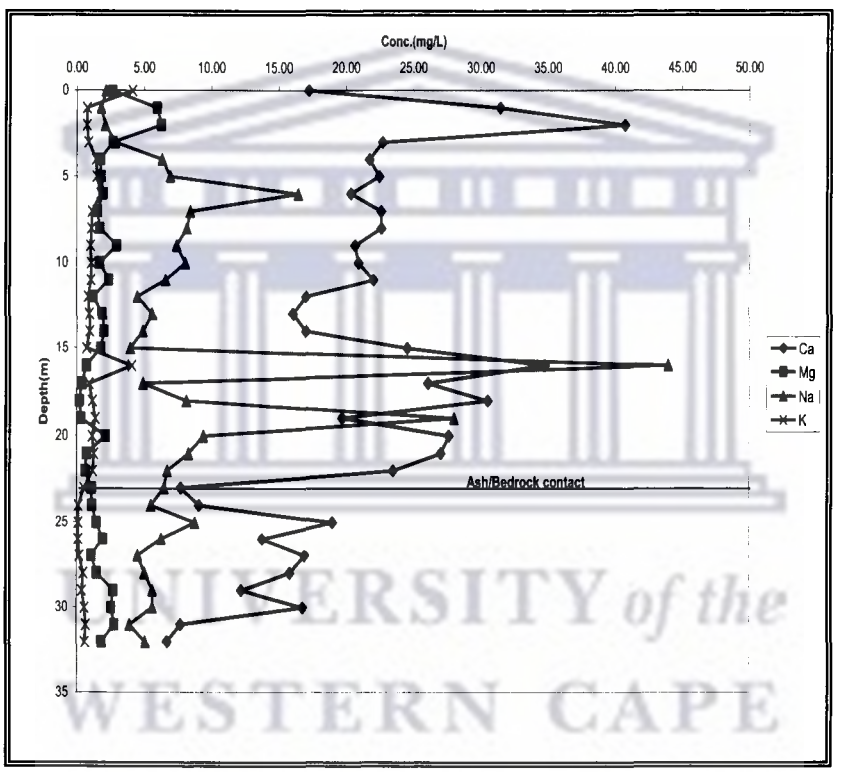

Fig. 5.8.3a: Trends of Ca, Mg, Na and K concentration in pore water samples from Kragbron

Ca is known to be associated with the surface of fly ash particles, as well as forming part of the main components of the aluminosilicate glass fractions, along with other major elements like K and Al (Choi et al., 2002). An initial high concentration of Ca (Fig. 5.8.3a) was observed for samples between 1 and 2 m at a pH of 8.65 and 9.57. The Ca concentration is much lower and showed slight fluctuations from 3 m to about 15 m. This was followed by a sharp increase at 16 m (Fig. 5.8.3a) which is correlative to EC and

5.8.3 Major and Minor Elements

The elements that are adsorbed on the surface of the fly ash particles are much more easily mobilized into solution during fly ash water interaction than elements incorporated into the glassy phases of the ash. Their mobility depends on the phases with which they are associated in the ash as well as the pH of the leaching solution (Jankowski et al., 2006). The levels in concentration of major elements in pore water samples from Kragbron drilled core are shown in Fig. 5.8.3a to 5.8.3c.

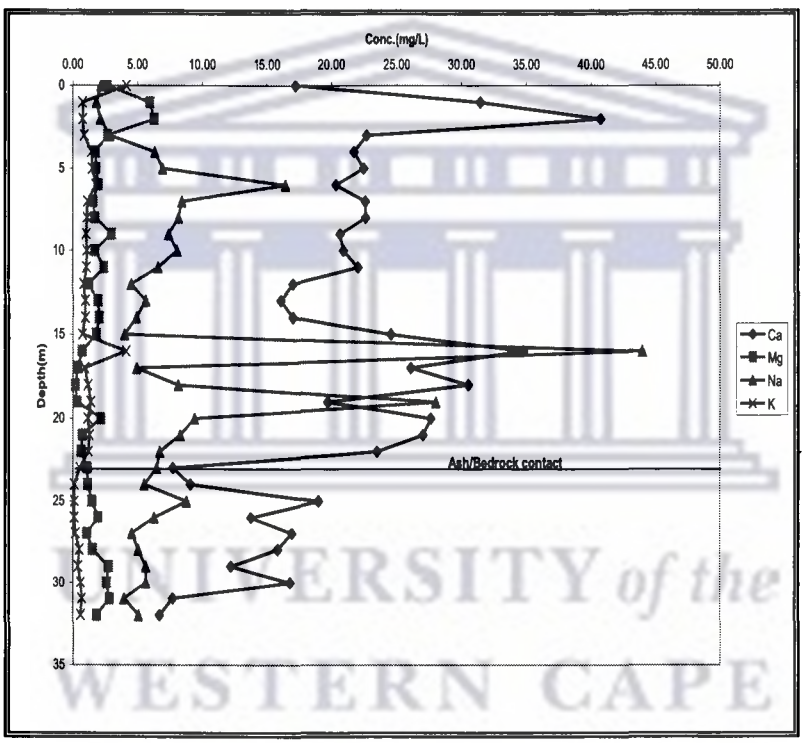

Fig. 5.8.3a: Trends of Ca, Mg, Na and K concentration in pore water samples from Kragbron

Ca is known to be associated with the surface of fly ash particles, as well as forming part of the main components of the aluminosilicate glass fractions, along with other major elements like K and Al (Choi et al., 2002). An initial high concentration of Ca (Fig. 5.8.3a) was observed for samples between 1 and 2 m at a pH of 8.65 and 9.57. The Ca concentration is much lower and showed slight fluctuations from 3 m to about 15 m. This was followed by a sharp increase at 16 m (Fig. 5.8.3a) which is correlative to EC and

re-precipitated to form secondary solids that are more stable during ash-water interactions (Jankowski et al., 2006). This was observed in the case of Mg (Fig. 5.8.3a).

The levels of Al and Si in pore water samples from Kragbron are shown in Fig. 5.8.3b.

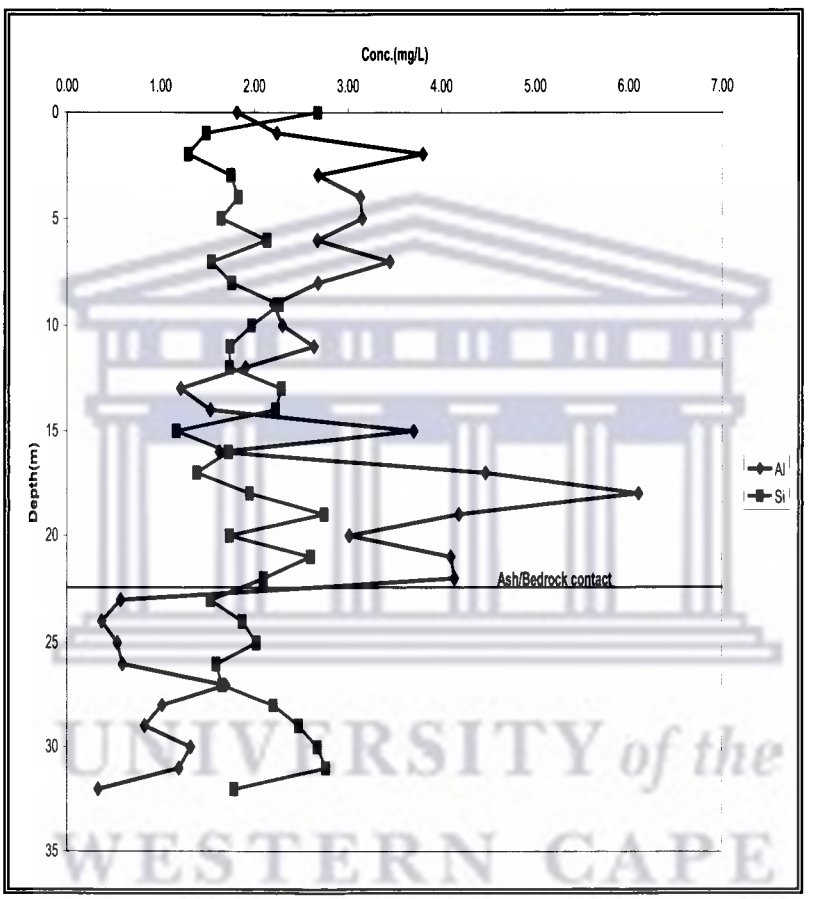

Fig.5.8.3b: Trends of Al and Si concentration in pore water samples from Kragbron

Normally, most compounds of Si and Al are insoluble in water because their mineral compounds form centre matrices of fly ash particles making them almost water insoluble (Jiang et al., 2009). Al may be associated with a silicate complex such as mullite but its release in neutral to alkaline solutions is strongly correlated to a non silicate association in the ash. Its presence in the pore water extract which is predominantly an alkaline solution reflects the solubility of aluminium oxide or hydroxide in high pH fluids (Kim and Kazonich, 2004). However, the release of Si and Al in the leachate obtained after the

interaction of fly ash with water was highest at 18 m and 19 m depths respectively. XRF showed a high concentration of Al and Si at these depths. The release of Al between 16 and 20 m indicates its presence in soluble phases in this region of the dump compared to the lower levels observed at the surface and in the bedrock. The Al profile is similar to the Na profile at 16 m to 18 m, so both elements may be associated with similar soluble phases and become mobile during water infiltration of the ash dump. It was reported by Roy and Griffin, (1984), Fruchter et al., (1990), Garavaglia and Caramuscio, (1994) that the leaching of Al is controlled by amorphous $Al(OH)_3$ for a pH ranging between 6 and 9, and by gibbsite for pH higher than 9.The release of Si is said to be governed by the solubility of quartz at pH lower than 10 and by the solubility of wairakite ($CaAl_2Si_4O_{12}.2H_2O$) at a higher pH (Tiruta –Barna et al., 2006).

Ca, Na and K were found accumulating at 16 m due to the high quantity of moisture locked within this depth. The vertical flow of water down the dump mostly likely facilitated this occurrence. But unfortunately, understanding the infiltration rate of rain water over the life time of the facility could not be achieved because the rainfall data collected during the period was out of reach as at the time of this research.

The levels of Mn, Fe and B in pore water samples from Kragbron are shown in Fig. 5.8.3c.

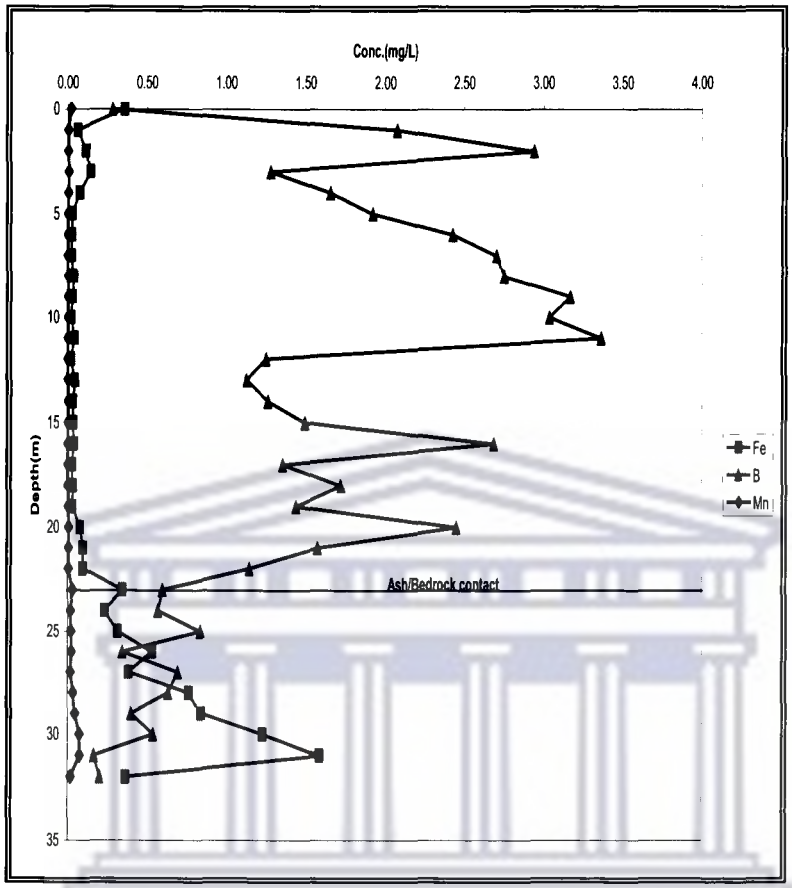

Fig.5.8.3c: Trends of Fe, B and Mn concentration in pore water samples from Kragbron

The concentrations of Fe and Mn were generally low in the pore water leachates of Kragbron core samples (Fig. 5.8.3c). Only a slight increase was observed at a depth of 31 m for Fe where the pH of the pore water extract was 8.57. The low concentrations could be due to the sorptive capacities of the Fe and Mn oxides as well as the high pH of the fly ash solution (Theis and Wirth, 1977). Fe and Mn in alkaline solution form hydrous iron and manganese oxides (oxy-hydroxides), which occur as coatings around the silicate grains of fly ash and as discrete grains of oxide mineral. At high pH, Fe and Mn oxy-hydroxides are negatively charged and have a cation exchange capacity that increases with increasing pH (Drever, 1997). At low pH, reduction of the oxy-hydroxides leads to the dissolution of their oxides, hence the slight increase in concentration for Fe at 31 m.

The concentration of B in the pore water leachates of Kragbron varied from 0.10 to 3.37 mg/L in a periodic fashion. B content in the Kragbron samples showed strong weathering trends. The first weathering profile (as taken from the surface of the dump- namely the most recently placed ash) extends from the surface to 2 m depth, the second from 3 m to 11 m, the third weathering profile extends from 12 m to 16 m depth from the surface and the fourth from 17 m to 22 m depth. This is consistent with the layering of the ash slurry during ash disposal and periods of inactivity where the ash would have been exposed to infiltration by rain as well as percolation through the profile of the ash which may explain the periodic variability of the B content. B is very often found associated with the surface particles of ash and in water soluble fractions, and therefore has high leachability rates (Querol et al, 1995 and Elseewi et al., 1980). B, because of its presence in solution in anionic form, is readily soluble in alkaline environment (Jankowski et al., 2006). Se and As levels are shown in Fig.5.8.3d for pore water extracts from Kragbron core.

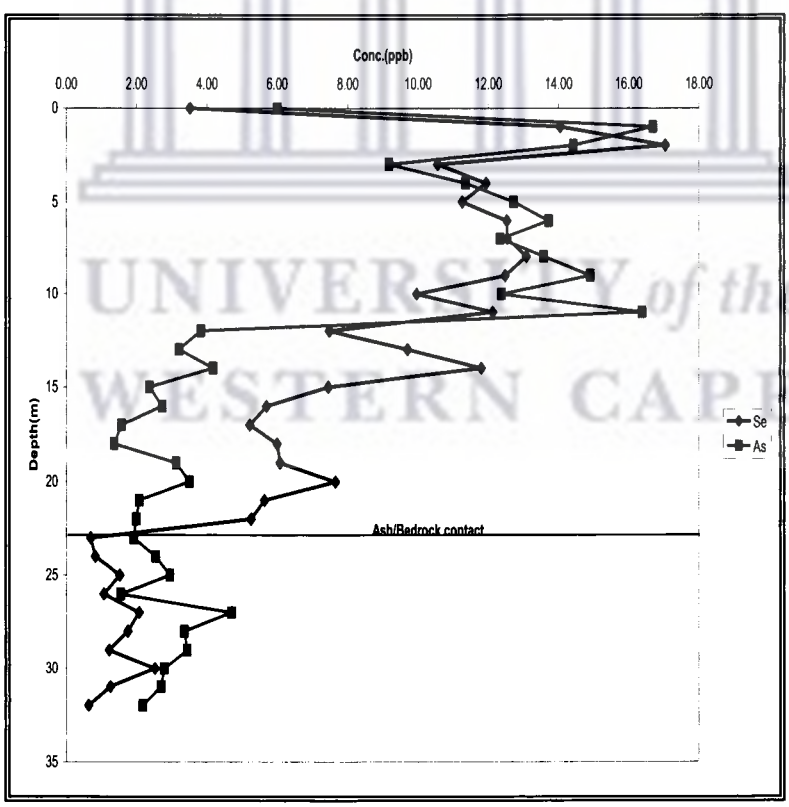

Fig.5.8.3d: Trends of Se and As concentration in pore water samples from Kragbron

Values of Se concentration in pore water extract recorded varied from 0.63 to 17.05 µg/L. The availability of Se in solution at high pH could be due to its enrichment on the surface of the ash particles. Depending on the oxidation state of Se, it can be in solution at both alkaline and neutral pH. The decrease in the concentrations of Se released at low pH could be due to adsorption and formation of insoluble mineral phases (Fatoba, 2007). Se showed similar trends of weathering as B. The enrichment of As has been observed on smaller particles of the ash and enrichment was correlated with increased surface area (Martinez-Tarazona and Spears, 1996; Hower et al, 1999) and could have caused an initial rapid mobilization of As in the leachates. The ash dump pH shows weathering trends but EC as well as other elements show accumulation at point where As appears to be depleted from 12 m. So, these elements may actually be more abundant making As appear less. Cr, Mo and Ba levels are shown in Fig.5.8.3e for pore water extracts from Kragbron core.

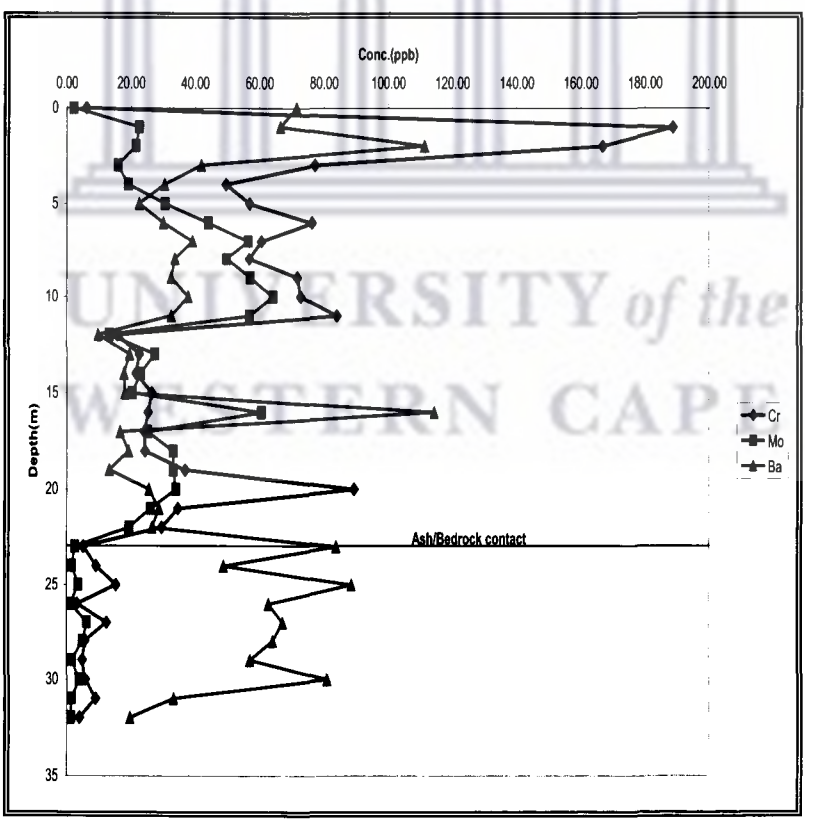

Fig.5.8.3e: Trends of Cr, Mo and Ba concentration in pore water samples from Kragbron

Cr and Mo displayed a similar pattern of release in the leachates but Cr concentration was a little bit much higher than that of Mo (Fig. 5.8.3e). The concentration of Cr was highest at depth of 1 m where the pH was 9.67 and a lower concentration was observed at a higher pH. Drever (1997) reported that the release of Cr with respect to pH of the leachate depends on the oxidation state of Cr present in the fly ash and the amount of Cr-bearing mineral phases in the ash. Although, the oxidation state of Cr was not determined in this study, its leaching behavior indicates its presence in different oxidation states in the fly ash. Cr^{3+} is known to be insoluble and usually have a strong tendency to adsorb at a low pH while Cr^{4+} is found to be easily available in solution (Drever 1997; Tiruta-Barna et al., 2006). Mo is very mobile under alkaline conditions and also precipitates as MoO_3 at high pH (Jankowski et al., 2006). This was observed in the concentration Mo released into solution in this study. The slow release of Mo from alkaline fly ashes can be attributed to its presence in the amorphous glassy phase of the ash and not on the surface. Molybdenum concentration can be controlled by Fe and Al in solution which reduces the leaching of Mo substantially at low pH by adsorbing the oxyanion (MoO_4^{2-}) (Comans et al., 2000; Kukier et al., 2003).

Ba trend showed weathering from the upper layers of the ash column before an accumulation at 16 m depth. This trend was also observed in Na and Al. The trend indicates the association of Ba with some soluble salts on the surface of the ash. The initial increase in concentration of Ba could be due to the dissolution of its oxide in the fly ash. It has been observed that the oxide of Ba when in contact with water is readily soluble leading to high concentration of the specie in solution (Reardon et al, 1995).

Co, Ni, Cu and Pb levels are shown in Fig.5.8.3f for pore water extracts from Kragbron core.

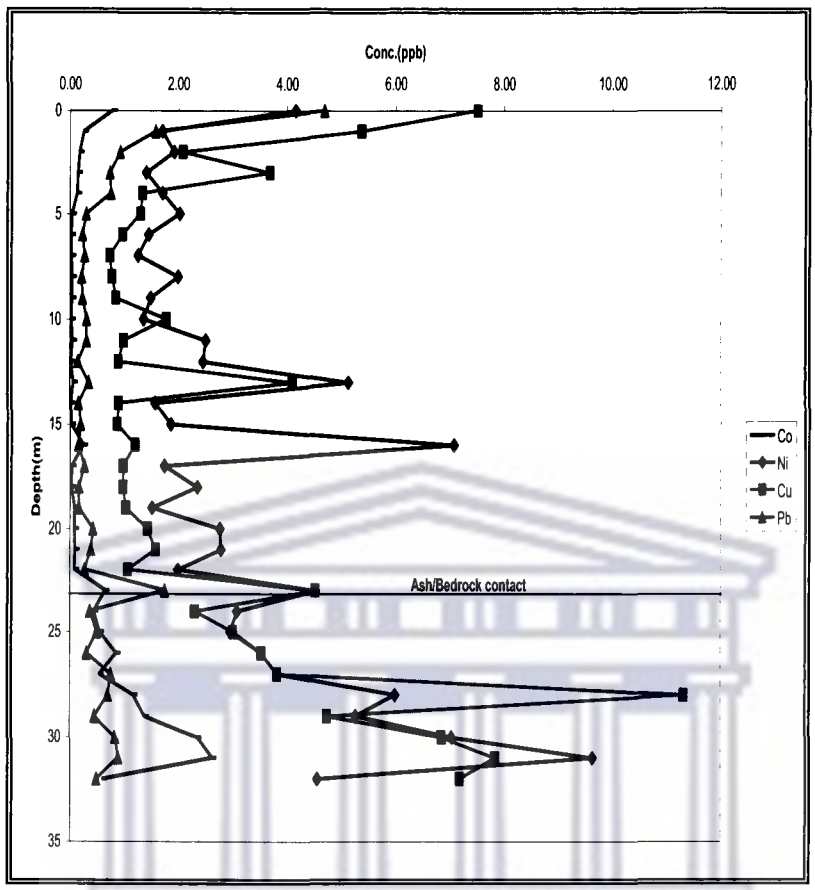

Fig.5.8.3f: Trends of Co, Ni, Cu and Pb concentration in pore water samples from Kragbron

The concentrations for some of the heavy metals present in this study are as follows: Co varied from 0.015 to 2.62 µg/L, Ni from 1.25 to 9.63 µg/L, Cu from 0.73 to 11.3 µg/L, Pb from 0.147 to 1.748 µg/L, Zn from 3.26 to 255.625 µg/L, Ti from 1.31 to 153.05 µg/L and V from 12.1 to 73.71 µg/L. The concentration of Cd was mostly < 0.01 µg/L.

Cu and Ni showed enrichment at depths 13 m and 16 m as a result of the leaching of other elements caused by weathering in the ash profile. A higher level of Cu and Ni was observed after the contact with the bedrock. Elements like Fe, Ti, Zr, Zn, Cu, Co and Ni are associated with the behaviour of Al during weathering (Marsh, 1991). The mobility of Al by weathering processes causes either a depletion or enrichment in these elements to exactly same degree. Al was observed to be in lower concentrations after 23 m depth

(Fig. 5.8.3b) while Cu, Ni, Co and Fe were observed in higher levels in the bedrock (dolerite). The release of these elements is likely to be from the weathering of Al in the dolerite layers. Zn, Ti and V levels are shown in Fig.5.8.3g for pore water extracts from Kragbron core.

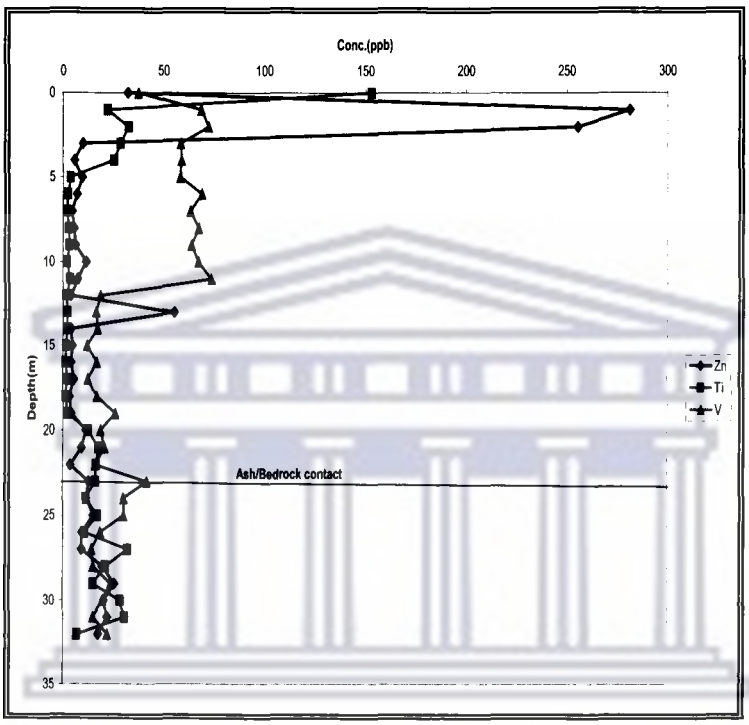

Fig.5.8.3g: Trends of Zn, Ti and V concentration in pore water samples from Kragbron

Zn and Ti showed elevated levels from the surface to 3 m while the elevated levels observed for V continued to 11 m. These elevations observed are as a result of the intense flushing of soluble components from the upper layers of the ash column due to weathering. The depletion made Zn, Ti and V look enriched at those depths.

The low concentrations and below-detection-limit values recorded for the heavy metals in this study could be as a result of their insolubility at highly alkaline pH, their low concentration in the fly ashes, and their presence in the glass phases, or could be due to the adsorption of these metals on the oxy-hydroxide species in the fly ash solution. At high pH, the surface of fly ash in solution becomes negatively charged and the positively

charged heavy metals are attracted to the fly ash surface due to electrostatic forces of attraction (Ugurlu, 2004), thus making the elements not readily soluble.

5.8.4 Anions

The anions observed to be released into solution during the fly ash/water interaction were SO_4^{2-} and Cl^-. The trends they exhibited down the drilled core at Kragbron are shown in Fig. 5.8.4.

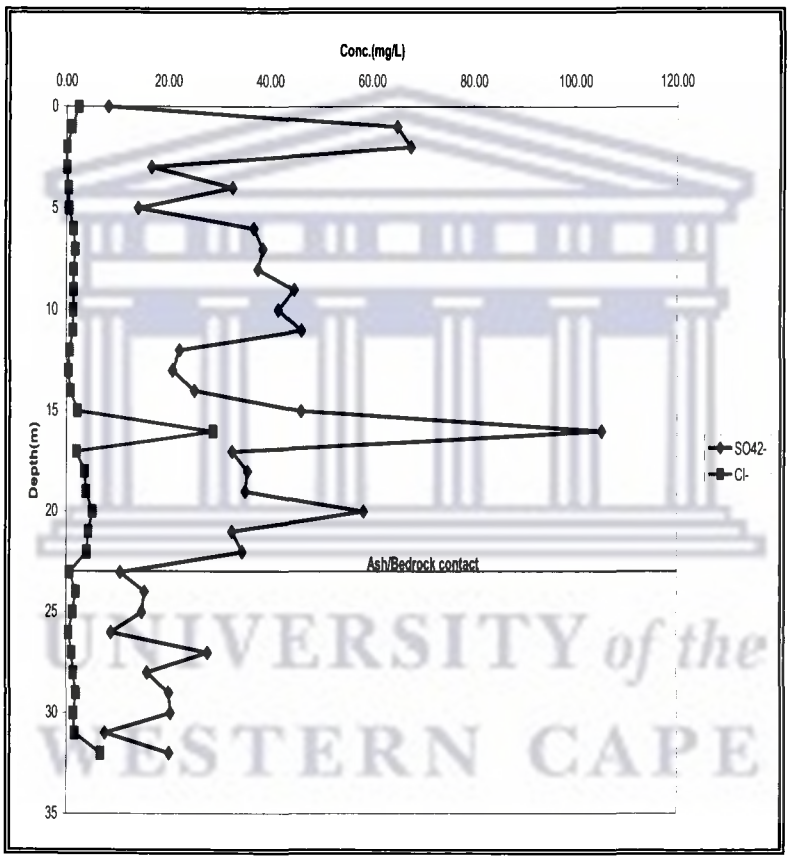

Fig. 5.8.4: Trends of SO_4^{2-} and Cl^- in pore water samples from Kragbron

Concentration of SO_4^{2-} ranged from 7.6 to 105.2 mg/L (Fig. 5.8.4). It was highest at 16 m depth. This trend was also observed in Na, Al and Ba indicating the high level of SO_4^{2-} to be from the dissolution of Na_2SO_4 since $BaSO_4$ is insoluble in water. Dissolved soap from municipal sewage run offs could also have contributed to the concentration of SO_4^{2-} through infiltration processes down the dump. Cl^- concentrations ranged from 0.05 to

28.8 mg/L (Fig. 5.8.4). It is also observed to be highest at 16 m. Dissolution and migration of Cl^- bearing compounds from the upper layers could be responsible for its accumulation at 16 m depth. Treatment of the Vaal river water with chlorine could be another contributing factor to the high concentration of Cl^- present, especially at 16 m. The high concentration of these anions at 16 m is mostly likely responsible for the high EC obtained at that depth.

5.9 Total Acid Digestion

The total acid digestion experiment was carried out as reported in section 4.2.4. The digestates obtained were analyzed using the ICP MS (see section 4.3.5). This was done to determine the total metal concentration of the Kragbron ash core samples and it could also be used in calculating the available species when the ash is in contact with an acidic medium. Figures 5.9.1 to 5.9.4 shows the concentration of the major elements in mg/L per depth of the borehole at Kragbron.

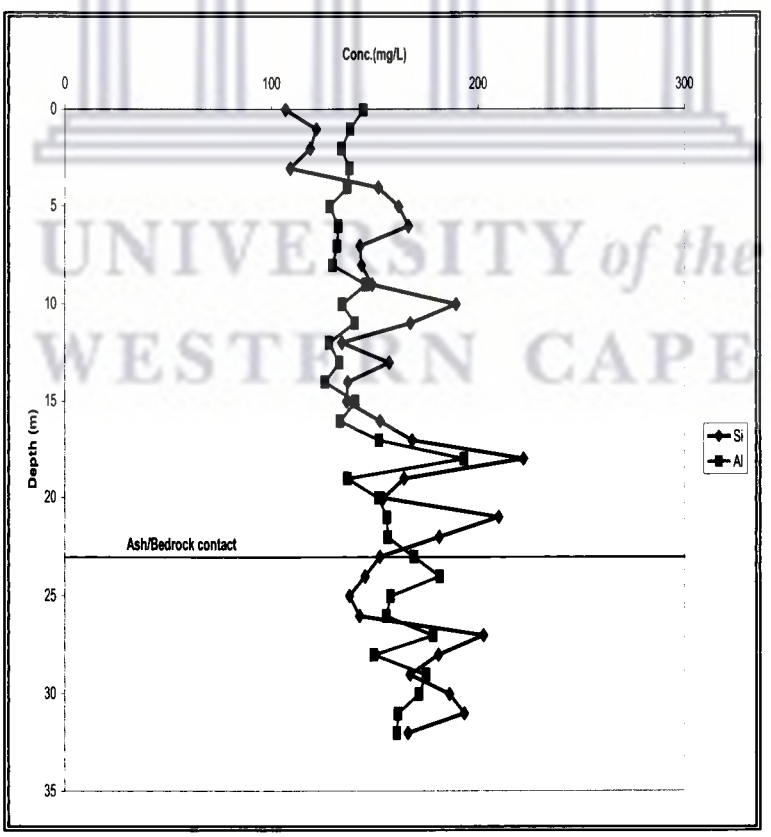

Fig. 5.9.1: Concentration of Si and Al in mg/L (ICP-AES)

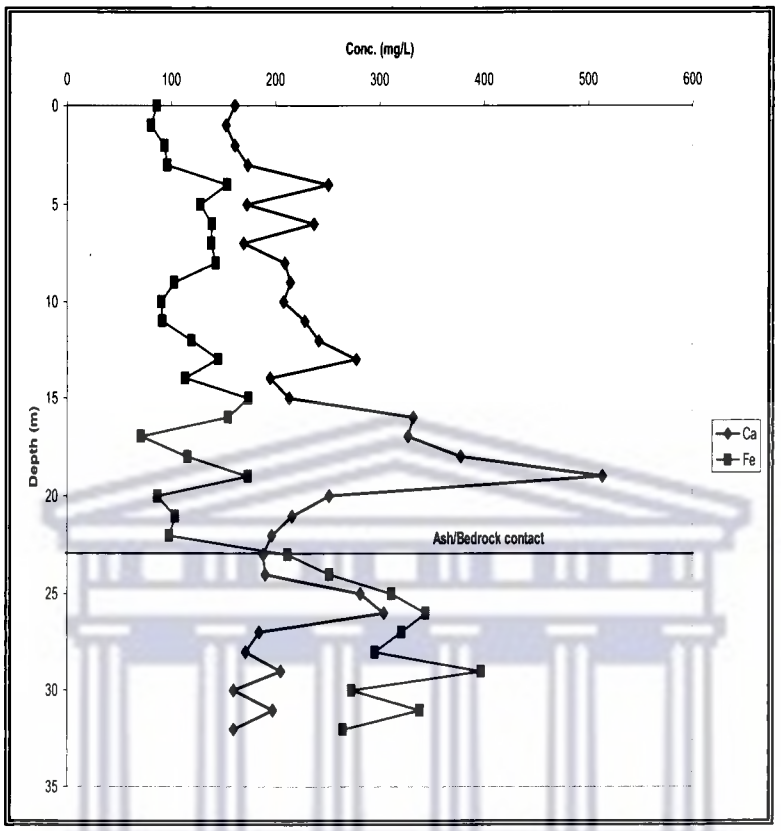

Fig. 5.9.2: Concentration of Fe and Ca in mg/L (ICP-AES)

The concentrations for Al, Ca and Fe obtained were moderately high from the surface to 22 m depth of the ash column. The high Si and Al concentrations recorded in some depths confirm the aluminosilicate property of fly ashes. The leaching of the top layers account for the lower concentrations of Si recorded at those depths. A noticeable change was observed for the elements at point of contact with the bedrock (23 m). Fe showed an appreciable increase from 23 m depth of the Kragbron ash core. Ca concentration was at its peak at 19 m while a much lower concentration was observed after contact with the bedrock. This trend is similar to that observed for Ca in the pore water chemistry result (Fig. 5.8.3a). Ca is seen to be associated with the water soluble phase of the ash. The increased level observed from 17 m to 19 m depth is as result of weathering in the upper layers of the ash profile causing the migration of Ca to deeper depths. The lower levels observed between 20 m and 24 m could be attributed to remineralization at these depths

due to the formation of calcite. Al and Si concentration alternated from moderate to high after the contact with the bedrock.

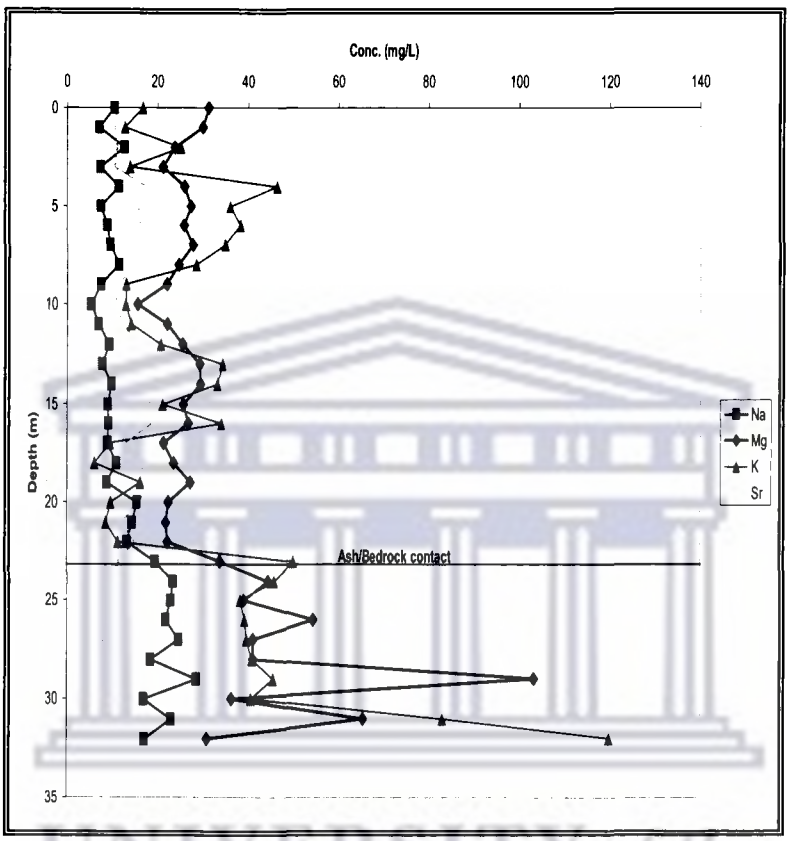

Fig. 5.9.3: Concentration of Na, Mg, K and Sr in mg/L (ICP-AES)

The concentrations of K and Mg were much higher after the contact with the bedrock at 23 m. The concentration of Na showed only a slight increase in the deeper depths of the Kragbron ash column. Sr showed a decrease in concentration after the contact at 23 m.

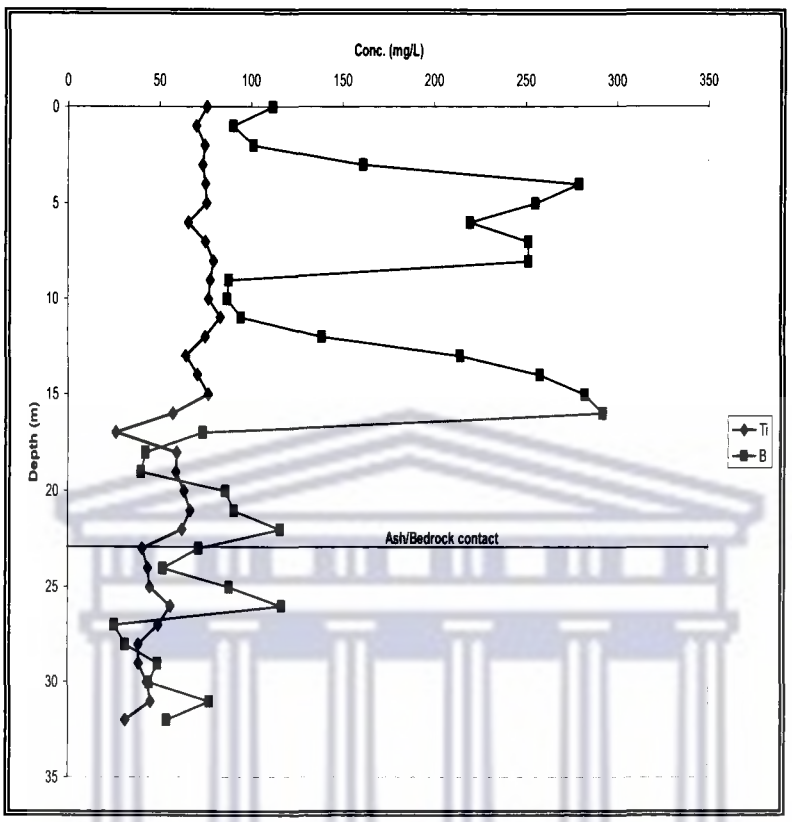

Fig. 5.9.4: Concentration of Ti and B in mg/L (ICP-AES)

B showed an increase from 2 m to 4 m, an accumulation between 7 m and 8 m and another sharp increase from 10 m to 16 m in the ash profile. A considerable decrease was observed from the contact with the bed rock at 23 m. The trend for B is similar to that observed in the pore water result for B (Fig. 5.8.3c). B is easily released into solution because it is usually associated with the surface of fly ash particles. The trend observed indicates weathering from the surface and at certain depths thereby causing accumulations at other depths in the ash column. Ti concentration was lower in the deeper depths (23 m to 32 m) as compared to its concentration in the ash column (surface to 22 m).

Elements found in fly ash have association with either the silicate bearing, non silicate bearing or both phases of the ash. Si is mostly associated with the silicate bearing portion of fly ash. Most of the Al is found with the aluminosilicate compounds e.g mullite in the

Moderate to slight variations was observed in the concentrations obtained from both techniques for Mo, Cu, Co, As, Pb, Ti, Ca, Mg and Fe in the surface sample of the ash core. Si, Al and Na concentrations were higher in XRF than in the total acid digestion for the chosen depths. Concentration for Ca, Fe, Mg, Ti and K was higher in the total acid digestion data for the depths than was recorded in XRF. This could be as a result of errors in the instrumentation or contamination during the sample preparation for both procedures.

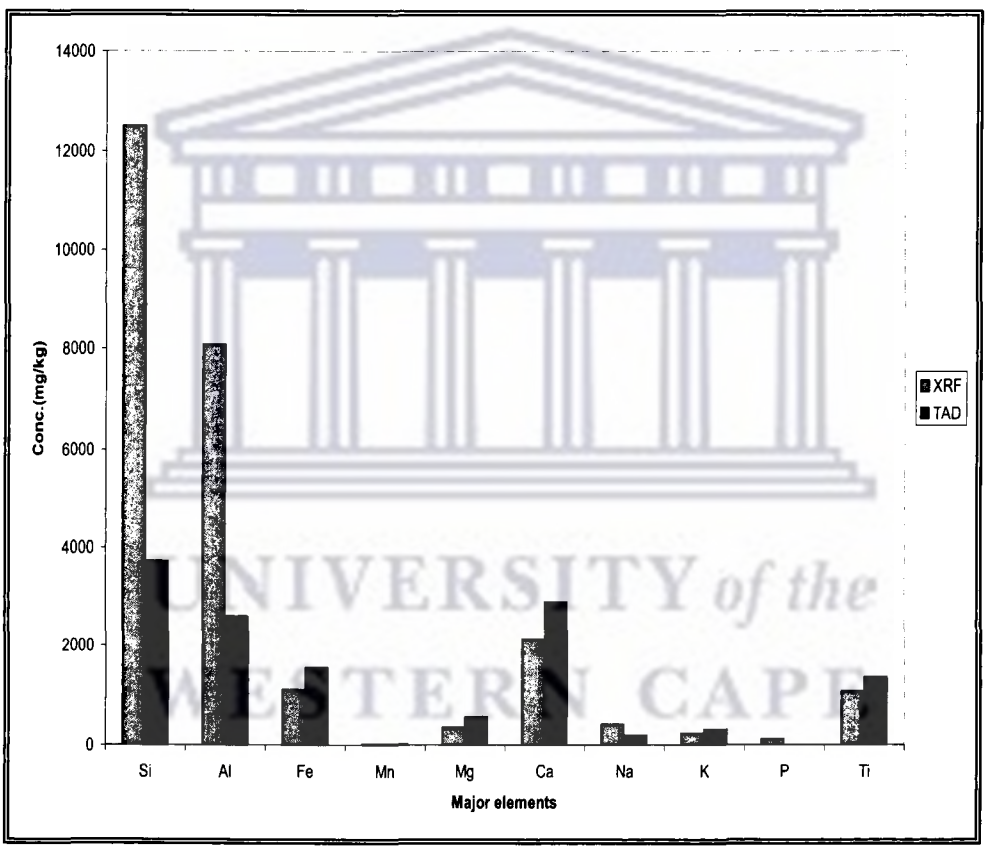

Fig. 5.9.5: Distribution pattern of some major elements in XRF and total acid digestion for sample obtained at the surface from Kragbron ash dump

Ordinarily, the concentration of analytes present in significant levels in the ash is expected to be higher in XRF than in total acid digestion because the former is a relatively non- destructive procedure. However, analytes present at very low levels (< 1

Table 5.9.1: Comparison of total acid digestion and XRF data obtained from Kragbron ash core samples in ppm

Elements	Surface (XRF)	Surface (TAD)	16 m (XRF)	16 m (TAD)	32 m (XRF)	32 m (TAD)
Si	12506.57	3722.91	11782.95	2747.92	15267.70	2990.71
Al	8079.69	2600.75	9399.90	2398.48	4484.14	2893.97
Fe	1105.87	1551.64	1476.87	2784.63	3184.71	4768.07
Mn	14.64	28.61	19.86	42.11	54.55	119.17
Mg	338.85	562.53	308.17	482.84	990.74	556.35
Ca	2145.71	2897.22	3380.67	5984.33	2930.30	2883.07
Na	414.00	188.35	291.74	164.58	776.41	308.07
K	234.65	301.08	112.17	614.26	1107.34	2156.75
P	118.24	-	239.46	-	46.70	-
Ti	1082.61	1364.83	1053.81	1031.33	451.47	564.77
S	4.51	-	44.90	-	ND	-
Pb	6.4230	8.8697	1.4046	3.3689	ND	1.8038
As	1.6270	1.8180	0.3110	0.3905	0.1015	0.4283
Ba	2.8597	66.2796	ND	134.6530	19.7137	133.2486
Ce	15.5366	-	13.2621	-	5.6912	-
Co	1.6115	3.0117	0.8113	1.4489	1.5639	4.2303
Cu	4.8088	5.9849	2.6802	2.8214	4.5427	5.1830
Mo	0.3337	0.5072	0.3448	0.8163	0.2648	0.4683
Nb	2.3509	-	2.4192	-	0.7453	-
Ni	4.7230	7.5212	5.3990	8.1008	4.1257	7.0928
Rb	1.8889	-	1.0414	-	3.6286	-
Sr	55.9096	195.9838	65.3277	334.9690	13.0982	190.9766
V	24.1339	17.9127	20.5807	11.1141	8.6354	23.6142
Y	5.3927	-	4.4373	-	1.4710	-
Zn	2.4296	17.4051	ND	6.9795	2.9010	17.2989
Zr	47.5484	-	48.9122	-	9.5535	-

*** TAD – Total Acid Digestion**
*** ND- Not Detected**

Moderate to slight variations was observed in the concentrations obtained from both techniques for Mo, Cu, Co, As, Pb, Ti, Ca, Mg and Fe in the surface sample of the ash core. Si, Al and Na concentrations were higher in XRF than in the total acid digestion for the chosen depths. Concentration for Ca, Fe, Mg, Ti and K was higher in the total acid digestion data for the depths than was recorded in XRF. This could be as a result of errors in the instrumentation or contamination during the sample preparation for both procedures.

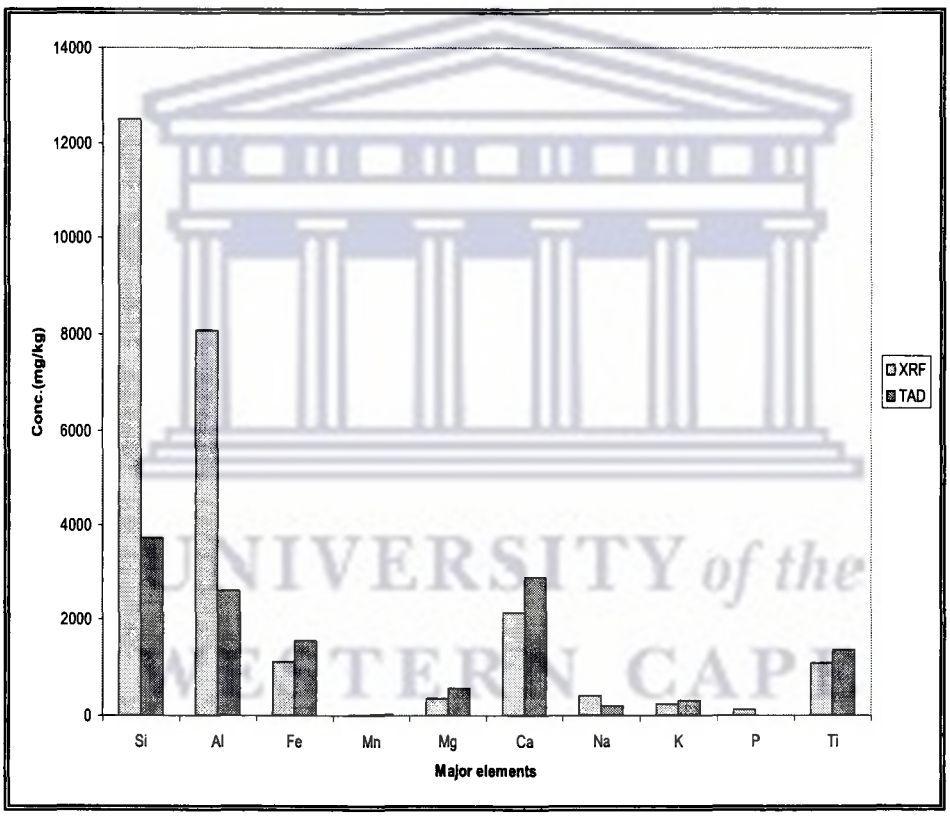

Fig. 5.9.5: Distribution pattern of some major elements in XRF and total acid digestion for sample obtained at the surface from Kragbron ash dump

Ordinarily, the concentration of analytes present in significant levels in the ash is expected to be higher in XRF than in total acid digestion because the former is a relatively non- destructive procedure. However, analytes present at very low levels (< 1

ppm) in the ash will be detected by the ICP-MS. Bulk chemical analysis of samples using XRF is more reliable than total acid digestion with ICP-MS analysis because of the relative ease and low cost of sample preparation and the stability of X ray spectrometers.

Cr was not included in the elements analyzed for in XRF due to likely interference from the Cr tube used by the machine. Other trace elements like Cd, Se, and B were not included in the standards used in calibrating the equipment; hence they could not be analyzed for. The concentration in ppm of Cr and B in the total acid digestion data was high in the compared samples. The release of Cr, Mn, Ni and Zn in the digestate is due to the acid attack on the iron oxide and spinel group minerals with which they are associated. Cd is found to be associated with the silicate phase in fly ash while As and Se are associated predominantly with the non-silicates (Kim and Kazonich, 2004). Hence, their release although in smaller concentrations, is due to the acid attack on these phases bearing the elements.

5.10 Cation Exchange Capacity (CEC)

The cation exchange capacity is the ability of a material to attract and exchange cations and is a measure of the exchangeable cations Al^{3+} and Si^{4+} by other cations like Na^{+}, K^{+} Ca^{2+} and Fe^{2+} (Singh and Kolay, 2002). Thus, the CEC of ash is a measure of the quantity of sites on its surface that can retain cations by electrostatic forces. The CEC of the ash samples from the surface to 32 m was determined using the method described in section 4.2.6 of this study. The trend observed is shown in Fig. 5.10.1.

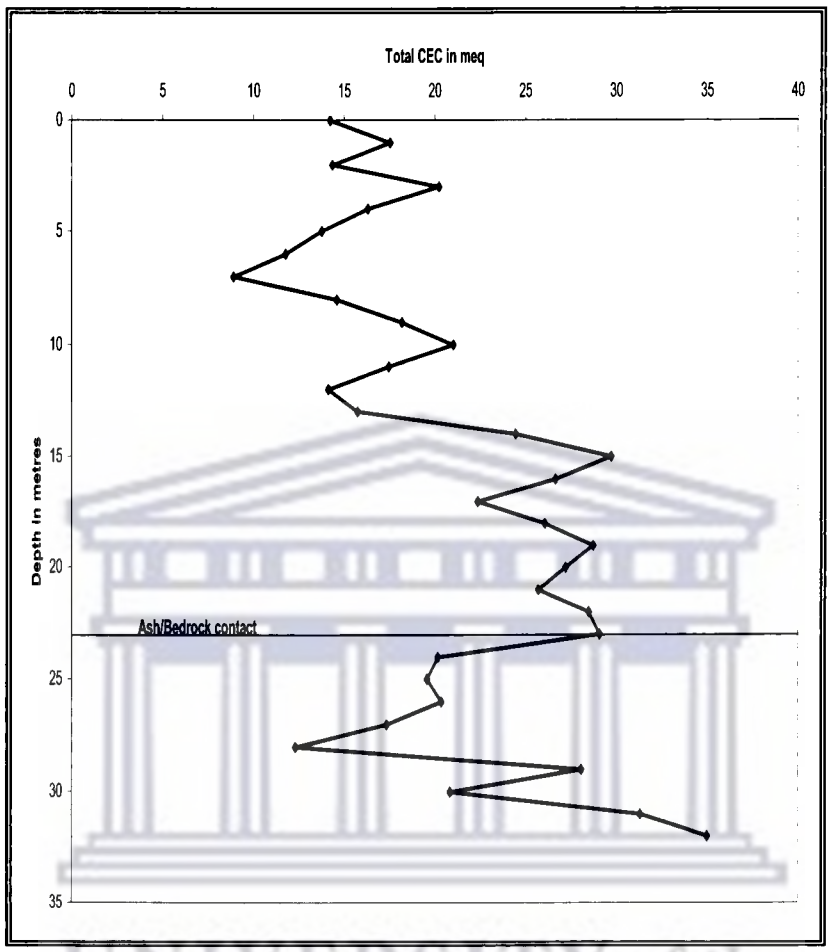

Fig. 5.10.1: Total CEC in meq of Ca, Na, K and Mg with respect to depth

The result obtained show similar trend to that obtained from the per cent moisture content. CEC and per cent moisture content were highest at 18 m at a pH of 10.72. It also showed a similar trend to the weathering pattern observed in B (Fig. 5.8.3c). The trend observed between 14 m and 22 m was peculiar to Ca (Fig. 5.8.3a), Na (Fig.5.8.3a), Al (Fig.5.8.3b) and SO_4^{2-} (Fig.5.8.4). This is a clear indication that transient mineral phases in this region in the dump can trap cations and anions due to surface adsorption or exchange processes.

During initial weathering, solutions in contact with coal fly ash generally develop very high pH values by reaction with the alkaline earth oxide components (Mattigod et al., 1990), leading to glass dissolution. Carbonation due to CO_2 uptake from the atmosphere and microbial respiration reduces and stabilizes the pH at about 8.3 (Schramke, 1992). This decreases the solubility of Si and Al (Wada and Wada, 1980) thereby promoting their precipitation from fly ash pore water, abundantly yielding non crystalline aluminosilicate with low Al/Si molar ratio (Zevenbergen et al., 1999).

A drop in CEC value was observed from 22 m (Fig.5.10.1). Per cent moisture content and pH also dropped from this depth (Fig. 5.2.1 and 5.8.1). In an aqueous solution of high pH (above 10), dissolution of the glass components of fly ash takes place releasing a considerable amount of Al and Si into solution, making available room for exchange of the Al or Si with other cations like Na^+, Ca^{2+}, K^+ e.t.c. Thus a high CEC value was obtained. But at lower pH, precipitation of the Al and Si occurs making them unavailable for any exchange.

5.11 Sequential Extraction

The results for the 5 step sequential extraction procedure carried out as described in section 4.2.5 are presented below. The supernatant for each sample obtained was analyzed for various analytes using ICP MS. Solutions of different pH were used as leachants to target the different mineral association phases in the ash samples. No leachant was added in the last extraction step as this represents the residual fraction present in the ash matrix.

5.11.1 Water Soluble Fraction

This step was done to determine what percent of the total concentration of each element was associated with the water soluble species in the supernatant after subjecting the ash samples to the procedure described in section 4.2.5.

Fig. 5.11.1a to 5.11.1h shows the trends observed for the various elements in the water soluble fraction phase down the profile of the Kragbron drilled ash core.

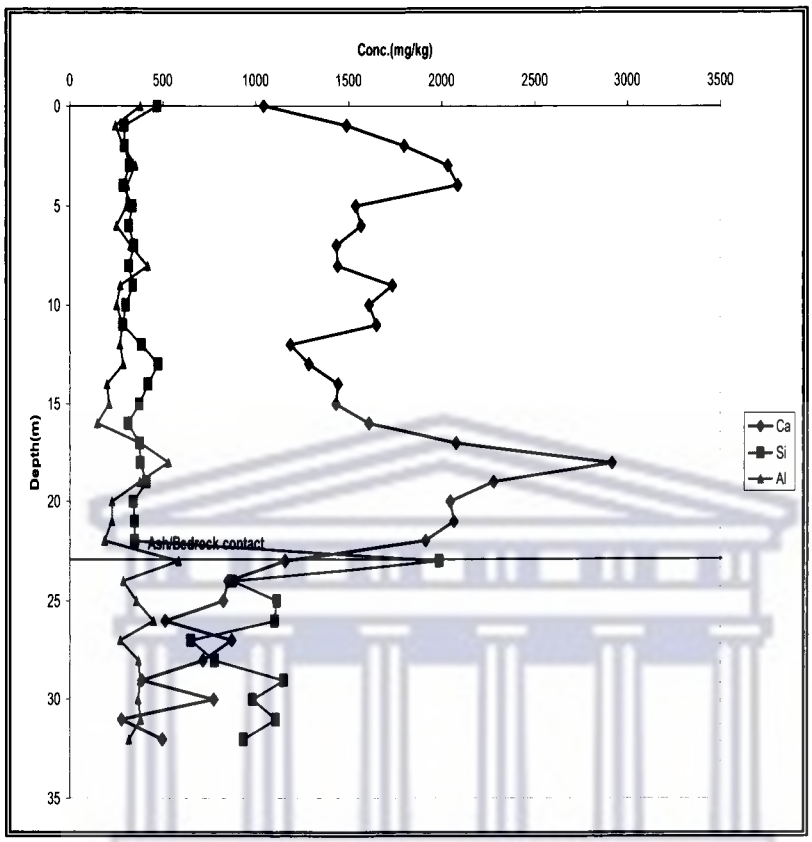

Fig. 5.11.1a: Trends of water soluble fraction Ca, Si and Al down the drilled ash core at Kragbron

Water soluble Ca showed weathering at the surface layer and an accumulation between 16 m and 22 m in the ash profile. This could be due to weathering from the surface and upper layers of the ash column causing dissolution of Ca bearing compounds such as calcite, mobilizing this element and allowing its movement to lower depths. A higher release of the element was probably due to a longer contact time with water (30 min in pore water and 1 hr in the water soluble phase). A lower level of Ca was observed from 23 m due to the change in mineralogy after the ash contacted the bedrock as Ca is present as an aluminosilicate (anorthite) which is not readily soluble in water.

The water soluble fractions of Si and Al (Fig. 5.11.1a) showed a somewhat similar trend in the ash column (from the surface to 22 m depth). It could be as a result of the

association of the elements with the residual glass phase of the fly ash particles making them available in lower concentrations (Dudas and Warren, 1987).

The accumulation of the water soluble fraction Al at depths 16 m to 22 m indicates the dissolution of its soluble oxides or hydroxides from the surface and shallower depths of the profile due to weathering and its association with the high moisture level recorded at these depths (Fig. 5.2.1). Si concentration was higher after the contact with the bedrock at 23 m indicating its presence in the bedrock composition while Al maintained a similar trend to that observed above the contact (surface to 22 m depth).

The water soluble fractions of Mg, Na, Fe and K in the profile of the drilled ash core at Kragbron are shown in Fig. 5.11.1b below.

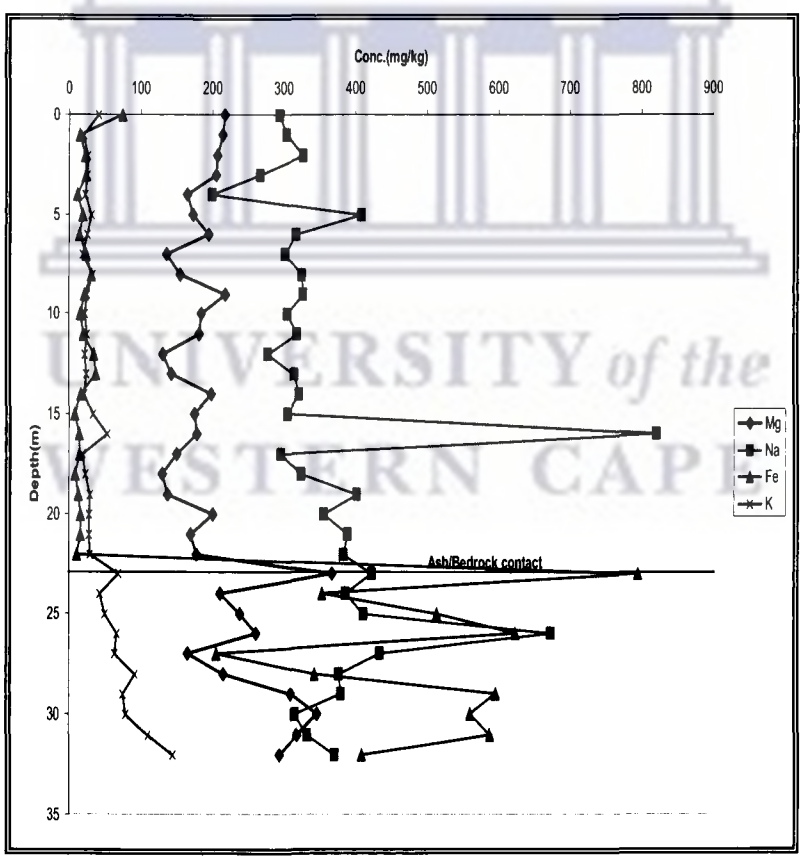

Fig. 5.11.1b: Trends of water soluble fraction Mg, Na, Fe and K down the drilled ash core at Kragbron

The concentration of the water soluble fraction Fe was relatively constant from 1 m to 22 m (Fig. 5.11.1b) after a reduction from the surface indicating weathering. Fe showed a similar trend to that observed in Si from 22 m to 32 m depth of the drilled core.

The water soluble fraction Na trend observed is similar to that which was observed for it in the pore water extract at 16 m depth (Fig. 5.8.3a). The trend shows its association with the highly soluble phase of the fly ash particles, hence the high levels released into solution. The release of Na after the contact at 23 m could be as a result of the weathering and dissolution of Na bearing components of the bedrock.

The water soluble fraction of Mg showed a near constant concentration from the surface to 3 m after which reasonable fluctuations was observed. The trend shows weathering and dissolution of the easily soluble sublimates on the ash particle surface, forming accumulations at certain depths in the ash horizon. The high level observed at the contact at 23 m is due to its presence as a component of the bedrock (Marsh, 1991). The drop in concentration after this layer could be due to weathering within the dolerite bedrock from lateral flow of groundwater.

The water soluble fraction of K showed a relatively constant level through out the ash column (surface to 22 m depth) with only a slight increase at 16 m and 22 m depth. This is probably due to its presence in glass fractions of the fly ash samples rather than on the surface. The trend exhibited can therefore be attributed to the gradual dissolution of the glassy phase of the fly ash bearing the element.

The water soluble fraction of Si, Fe, Mg, Na and K observed to be higher at 23 m and beyond is due to their presence in the bedrock itself (Marsh, 1991).

The water soluble fractions of B and Sr in the profile of the drilled ash core samples at Kragbron are shown in Fig. 5.11.1c below.

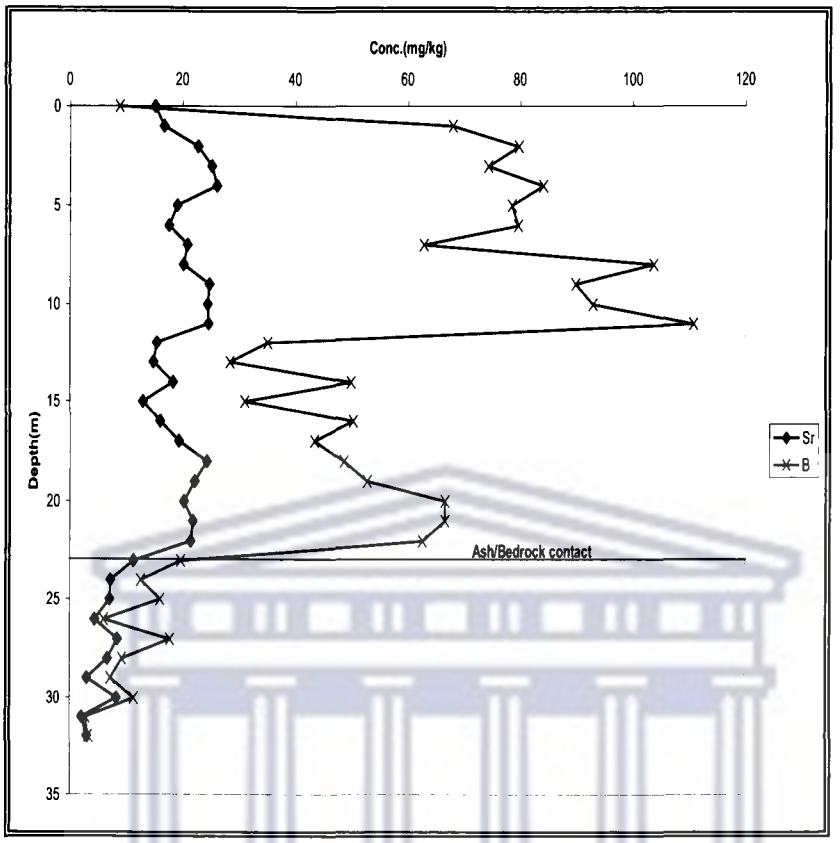

Fig. 5.11.1c: Trends of water soluble fraction Sr and B down the drilled ash core at Kragbron

The water soluble fraction Sr exhibited somewhat similar water soluble trend to that observed in the case of B but at lower concentrations. Fluctuations of high and low concentration down the ash horizon were observed. This also is an indication of weathering resulting in the accumulation at certain depths in the ash profile. Sr shows preferential association with the soluble phases on the surface of fly ash particles (Dudas and Warren, 1987), hence the ease with which it is released in layers having higher moisture content levels in the ash column. Sr levels observed from 23 m (contact with the bedrock) downwards was much lower indicating the impervious nature of the bedrock as Sr is also a composition of the bedrock (Marsh, 1991).

The water soluble fraction of B (Fig. 5.11.1c) showed an initial increase from the surface of the drilled core and accumulations between 7 m and 12 m and 18 m and 22 m.

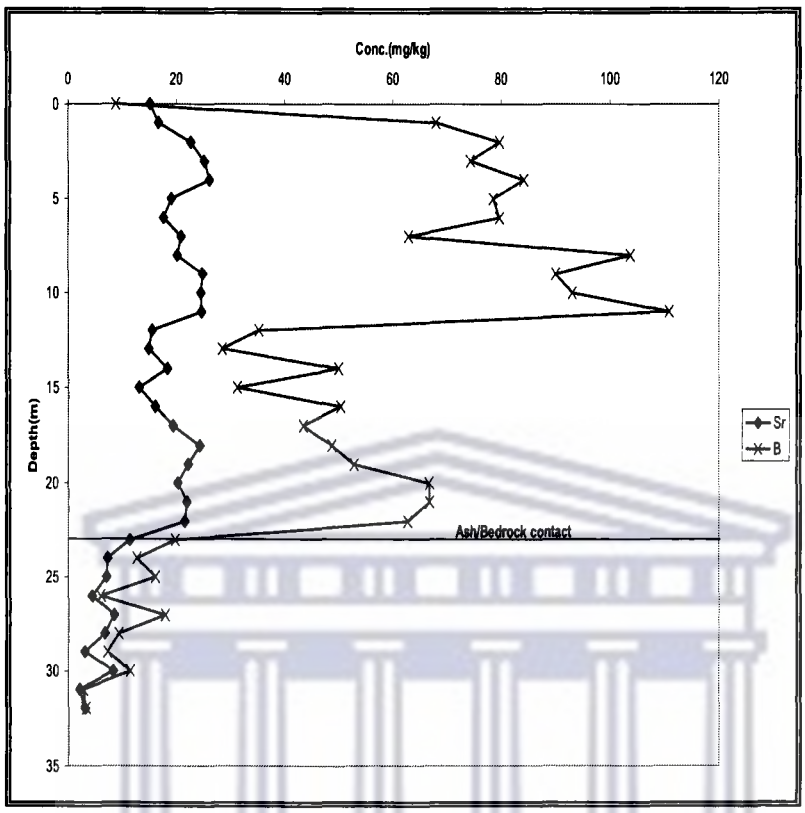

Fig. 5.11.1c: Trends of water soluble fraction Sr and B down the drilled ash core at Kragbron

The water soluble fraction Sr exhibited somewhat similar water soluble trend to that observed in the case of B but at lower concentrations. Fluctuations of high and low concentration down the ash horizon were observed. This also is an indication of weathering resulting in the accumulation at certain depths in the ash profile. Sr shows preferential association with the soluble phases on the surface of fly ash particles (Dudas and Warren, 1987), hence the ease with which it is released in layers having higher moisture content levels in the ash column. Sr levels observed from 23 m (contact with the bedrock) downwards was much lower indicating the impervious nature of the bedrock as Sr is also a composition of the bedrock (Marsh, 1991).

The water soluble fraction of B (Fig. 5.11.1c) showed an initial increase from the surface of the drilled core and accumulations between 7 m and 12 m and 18 m and 22 m.

Leaching due to rain water infiltration over time from the surface of the drilled core explains this trend observed in B. Disposal water that accompanied the overlying top layers could have aided dissolution of B bearing compounds in the layers beneath causing more of the element to be released. The element is associated with the smallest particles and the water soluble bearing phases of fly ash. The trend observed for B coincides with the moisture content trend in the Kragbron drilled ash core (Fig. 5.3.1). A lower level of B was observed from 23 m to the deeper layers of the drilled core indicating low levels in the bedrock.

The water soluble fractions of Mn, Ba and Ti in the profile of the drilled ash core at Kragbron are shown in Fig. 5.11.1d.

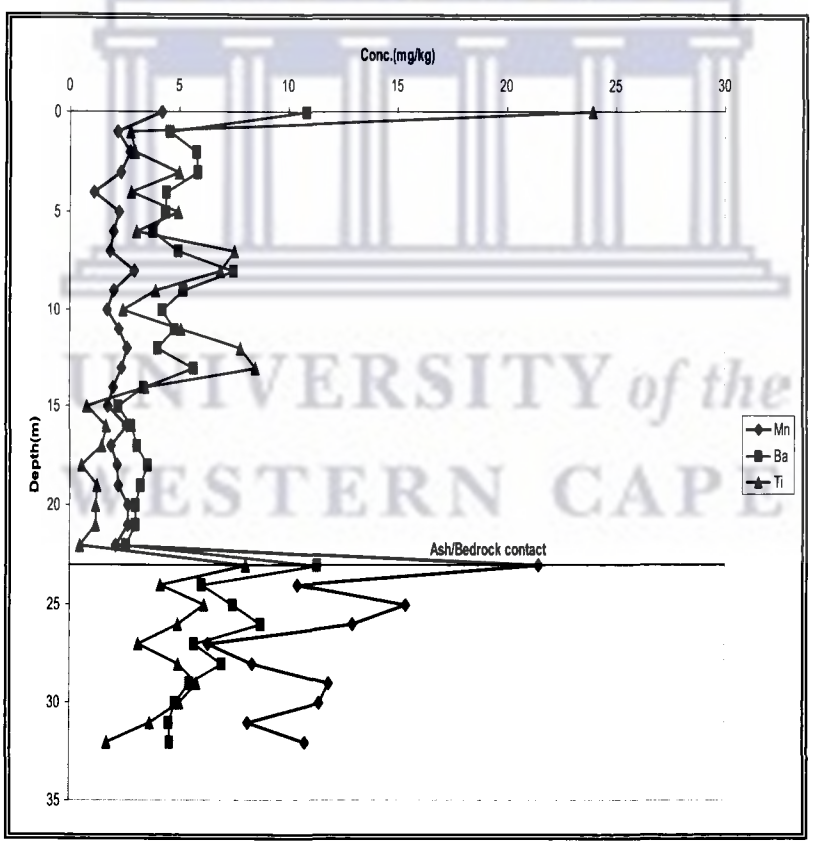

Fig. 5.11.1d: Trends of water soluble fraction Mn, Ba and Ti down the drilled ash core at Kragbron

The water soluble fraction of Mn, Ba and Ti (Fig.5.11.1d) showed similar trends from the surface of the ash column to 32 m depth. In the very top layers, these elements are enriched probably due to the vegetation found growing at the surface of the dump. Levels of these elements after the contact with the bedrock at 23 m were higher than the levels observed from the surface to 22 m. The sharp increase in the concentration of the elements at 23 m could be as a result of weathering and migration from shallower depths causing an accumulation at the contact with the bedrock (Fig. 5.11.1d). And the slightly lower concentration observed from 24 m could be attributed to a change in composition of material (from ash to dolerite-bedrock) or the impervious nature of the bedrock, preventing the migration of these elements downwards. The Mn trend is similar to that observed in the XRF results (Fig. 5.7.4).

Similar trends as those for water soluble fraction of Al and Si (Fig. 5.11.1a) was observed for Mn, Ba and Ti. Ti usually substitutes Si in the crystals of clay minerals (Kabata-Pendias and Pendias, 1984). Similarity in the trend observed for Ba in which case it could be due to its association with SO_4^{2-} released in considerable amounts in the pore water analysis from the surface to 22 m depth of the Kragbron drilled ash core. Thus, the release of Ba was probably as a result of the dissolution of $BaSO_4$ at these depths.

The water soluble fractions of V, Cr, Cu and Zn in the profile of the drilled ash core at Kragbron are shown in Fig. 5.11.1e and Fig. 5.11.1f below.

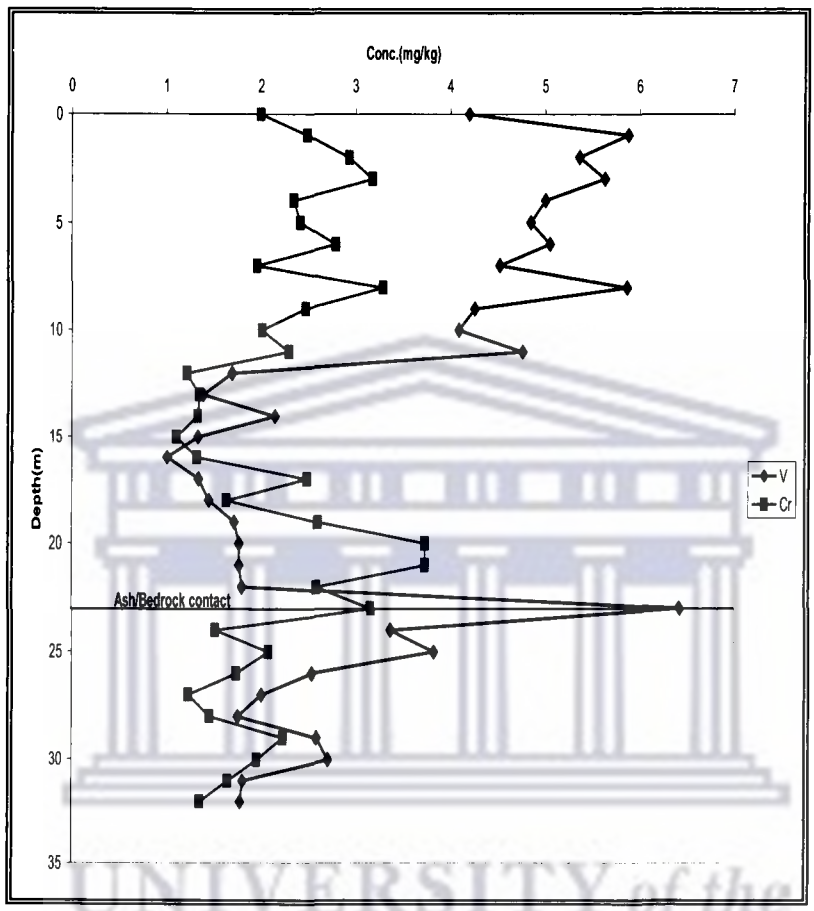

Fig. 5.11.1e: Trends of water soluble fraction V and Cr down the drilled core at Kragbron

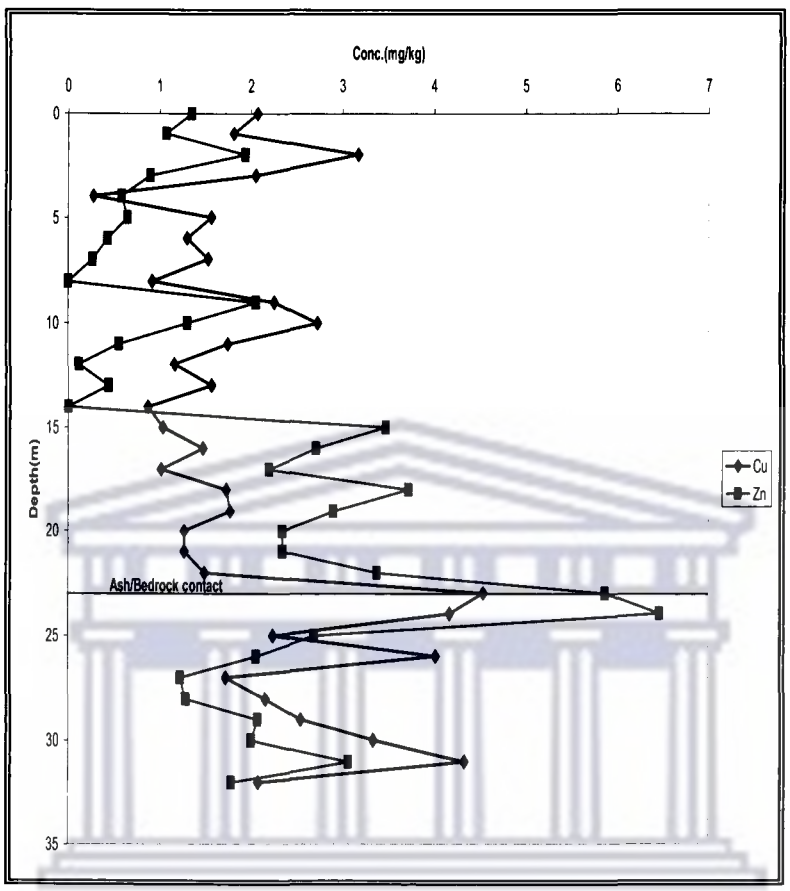

Fig. 5.11.1f: Trends of water soluble fraction Cu and Zn down the drilled core at Kragbron

The water soluble fraction of V and Cr (Fig.5.11.1e) exhibited similar trends from the surface to 32 m as well as Cu and Zn (Fig. 5.11.1f). All of these elements except Zn showed a continuous increase to 24 m before dropping in concentration. The element showed signs of deep weathering in the lower layers of the dump.

The release of the water soluble fraction of these elements in lower concentrations in the ash column is only due to the gradual dissolution of the mineral phase bearing the elements. Hulett et al, (1980) reported the preferential distribution of Cr, Mn, Cu, Ni, V and Zn on magnetic fractions of fly ash such as magnetite and ferrite and on iron oxides

such as hematite. The release of these elements can only be as fast as the dissolution of the solids bearing them (see section 2.9).

The water soluble fraction of As and Se concentration in the profile of the drilled core at Kragbron are shown in Fig. 5.11.1g.

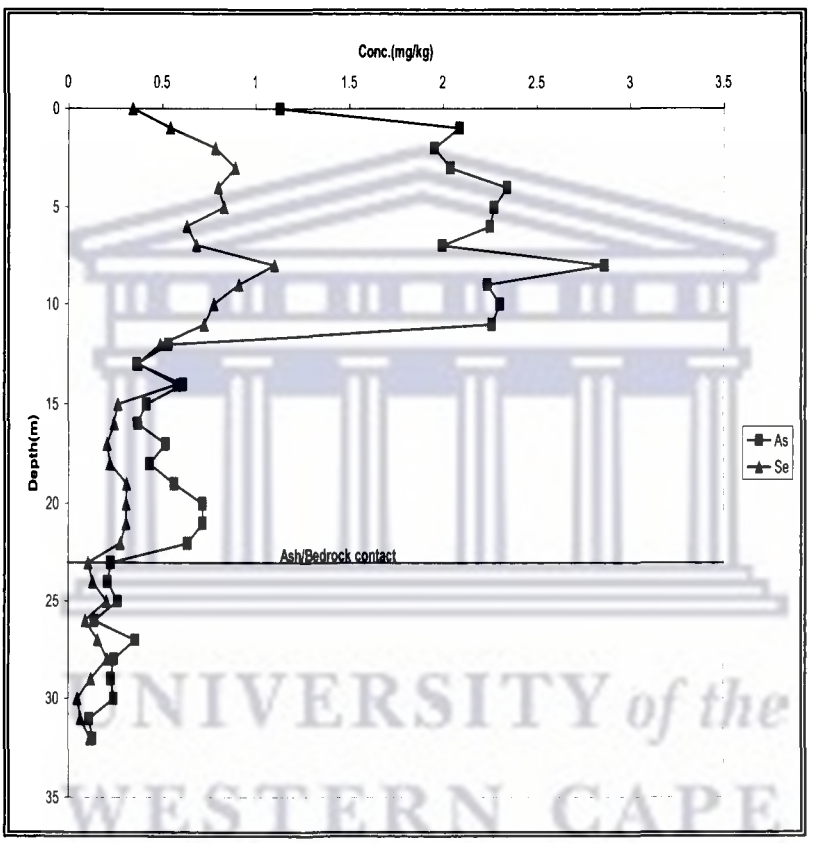

Fig. 5.11.1g: Trends of water soluble fractions of As and Se down the drilled ash core at Kragbron

The water soluble fractions of As and Se (Fig. 5.11.1g) showed a similar trend from the surface to 32 m depth of the drilled profile although As was present in higher concentrations than Se. The trend observed for As and Se at depths 1 m to 11 m could be due to enrichment as a result of the depletion of other more soluble elements leaving these elements behind. The lower levels observed from 12 m could be precipitation

and/or sorption of As back into the less soluble matrix of the solid phase (Jankowski et al., 2006).

The water soluble fraction of Se is enriched on the surface of fly ashes (Martinez-Tarazona and Spears, 1996) and it is also present in silicates and oxyanions (Senior et al., 2000; Kim et al., 2003). Hence, the release pattern of Se is most likely to be due in part to its presence in the water soluble silicate bearing phases of the ash samples as the trend for this water soluble fraction is similar to that of water soluble Si (Fig. 5.11.1a).

The water soluble fractions of Co, Pb and Mo in the profile of the drilled ash core at Kragbron are shown in Fig. 5.11.1h.

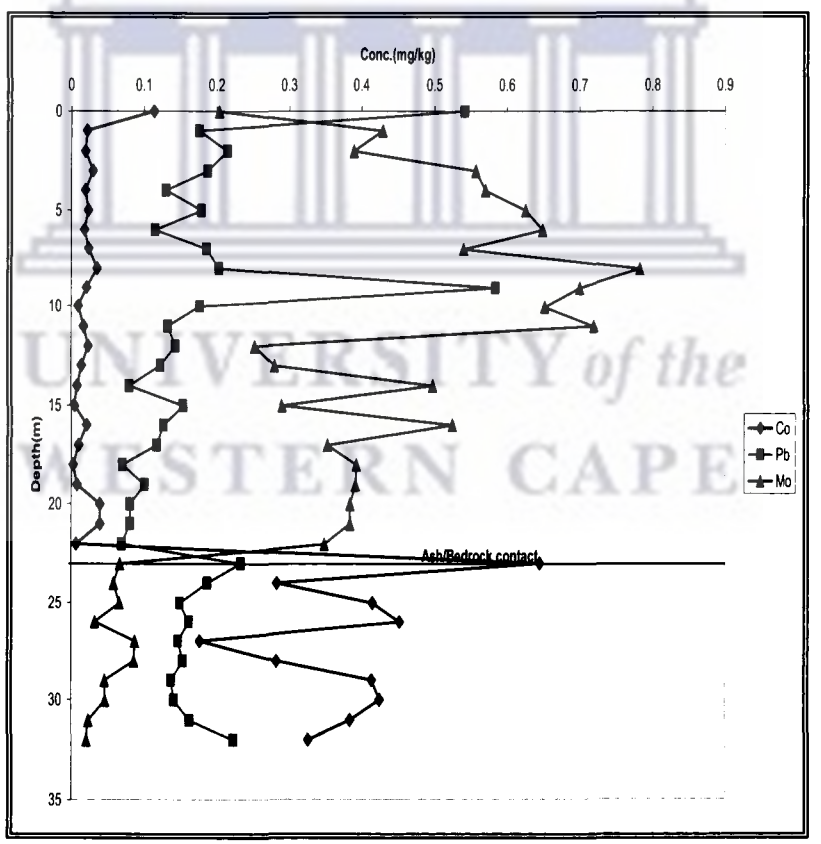

Fig. 5.11.1h: Trends of water soluble fraction Co, Pb and Mo down the drilled core at Kragbron

The water soluble fraction of Co (Fig. 5.11.1h) was relatively constant from 1 m to 22 m depth after an initial decrease from the surface where it may be part of a soil cover used for amendment to lower concentrations or could be indicative of weathering and dissolution of mineral phases bearing the element just below the surface of the dump. A similar pattern is observed for Pb. An accumulation of both elements is observed at the contact with the bedrock at 23 m probably due to the impervious nature of the bedrock material. Levels of water soluble Co after the contact with the bedrock was more than that observed within the ash profile (surface to 22 m depth). The trend observed for the water soluble Co is similar to that exhibited by water soluble Fe from the surface to 32 m depth (Fig. 5.11.1b). Co is normally strongly adsorbed into Fe oxyhydroxides (Kabata-Pendias and Pendias, 1984). This could explain the similar trends exhibited by both elements.

The trend observed for water soluble Mo is similar to that observed in As (Fig. 5.11.1g). Both elements weather more slowly than the other water soluble major elements, resulting in the relative enrichment of Mo and As in the first 12 m of the dump. Mo has a relatively high potential for mobility into solution due to its association with the finer particles of fly ash but when its concentration is low in solution, association with the amorphous glass phase is likely to be the case (Jankowski et al., 2006). Although, water soluble Mo was released into solution from the surface to 22 m depth, its concentration in mg/kg was generally low indicating that the release is from the dissolution of the glass phase of the fly ash particles.

The water soluble fraction of Pb within the ash profile was generally low with only an increase at 9 m and from 22 m to 23 m depth. Significant portions of Pb are incorporated into the glass matrix of the fly ash with lesser portions existing as surface precipitates (Hulett et al., 1980). Thus, the release of Pb in low concentrations may be associated with the gradual dissolution of the glass fractions phase present in fly ash due to weathering.

5.11.2 Exchangeable Fraction Phase

Determination of the exchangeable fraction of the Kragbron ash core samples was carried out as described in section 4.2.5 using 1 M ammonium acetate solution at pH 7. This procedure was performed on the residues remaining after the water extraction and was done to determine the fraction of each species associated with the exchangeable phase of the ash.

Fig. 5.11.2a to 5.11.2h shows the trends observed for the release of various elements in the exchangeable fraction phase down the profile of the Kragbron drilled ash core.

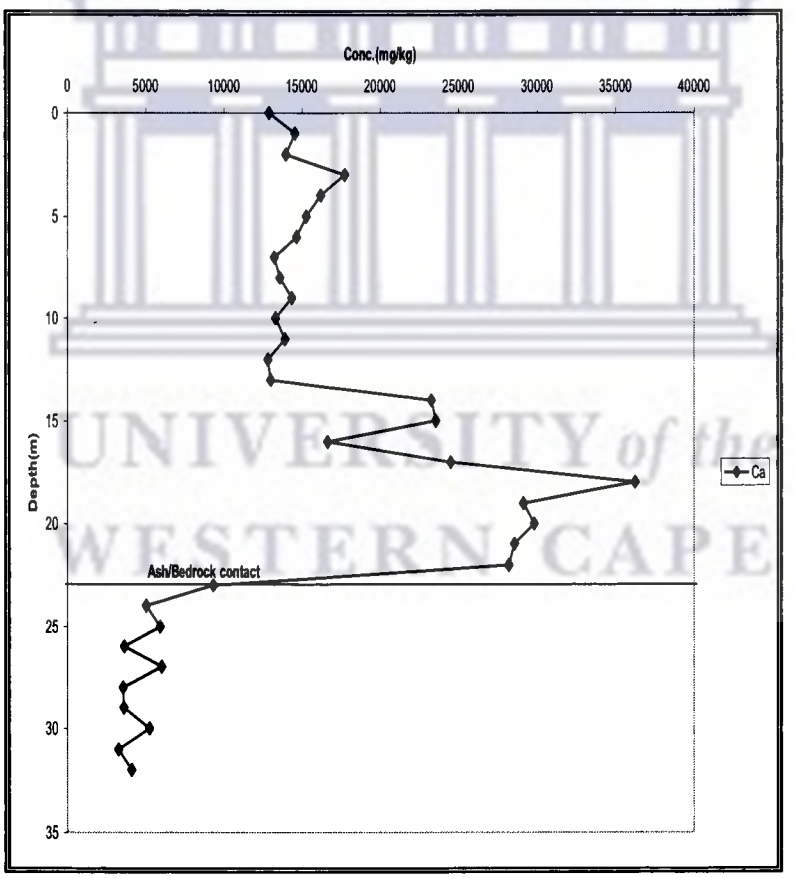

Fig. 5.11.2a: Trend of exchangeable fraction Ca down the drilled core at Kragbron

The exchangeable fraction Ca (Fig. 5.11.2b) exhibited the same trend as that observed in the water soluble fraction extraction phase. Much more of the Ca was observed to be associated with the exchangeable fraction phase. The accumulation of the element at 15 m to 23 m indicates possible mineralization due to concentration build up after the deep weathering observed in the ash horizon between 0 to 12 m.

The exchangeable fractions of Mg, Si and Na in the profile of the drilled ash core at Kragbron are shown in Fig. 5.11.2b.

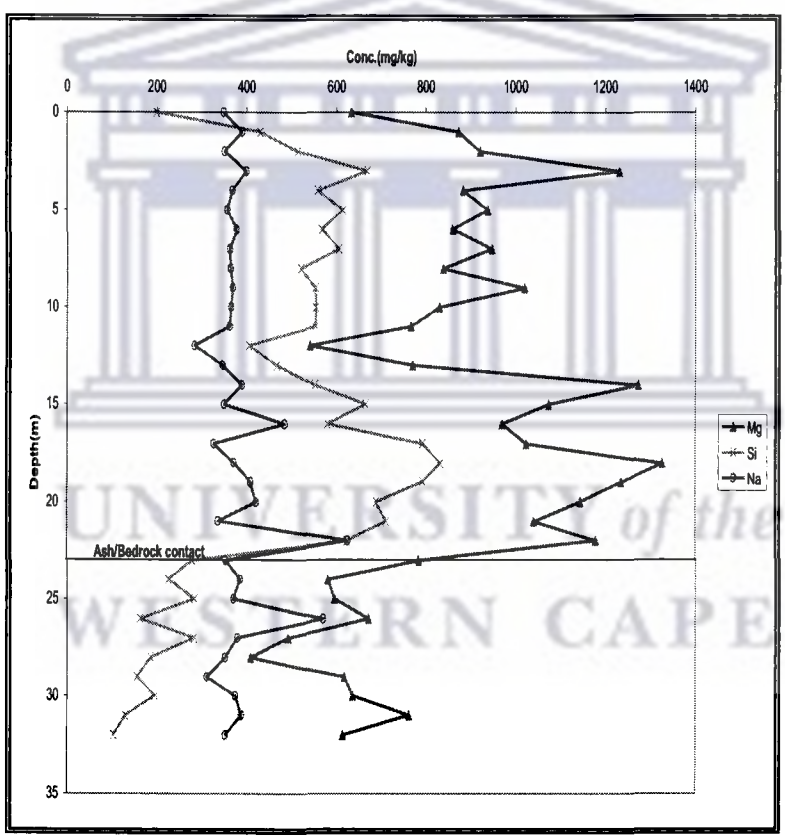

Fig. 5.11.2b: Trends of exchangeable fraction Mg, Si and Na down the drilled core at Kragbron

A higher level of the exchangeable fraction of Mg and Si was released into the solution (Fig. 5.11.2b) than that observed in the water soluble fraction. Mg and Si showed

accumulation in the deeper layers of the dump indicative of deep weathering and association with phases involved in remineralization such as Ca and K (Fig. 5.11.2a and Fig. 5.11.2c). A decrease was observed for both elements after the contact with the bedrock at 23 m depth showing that these elements were not associated to a great degree with the exchangeable fraction in the doleritic bedrock layer. The exchangeable fraction of Na followed a similar trend to that observed in the water soluble fraction (Fig. 5.11.1b) but the concentration in solution was lower in the ash column.

The exchangeable fraction of K in the profile of the drilled ash core at Kragbron is shown in Fig. 5.11.2c.

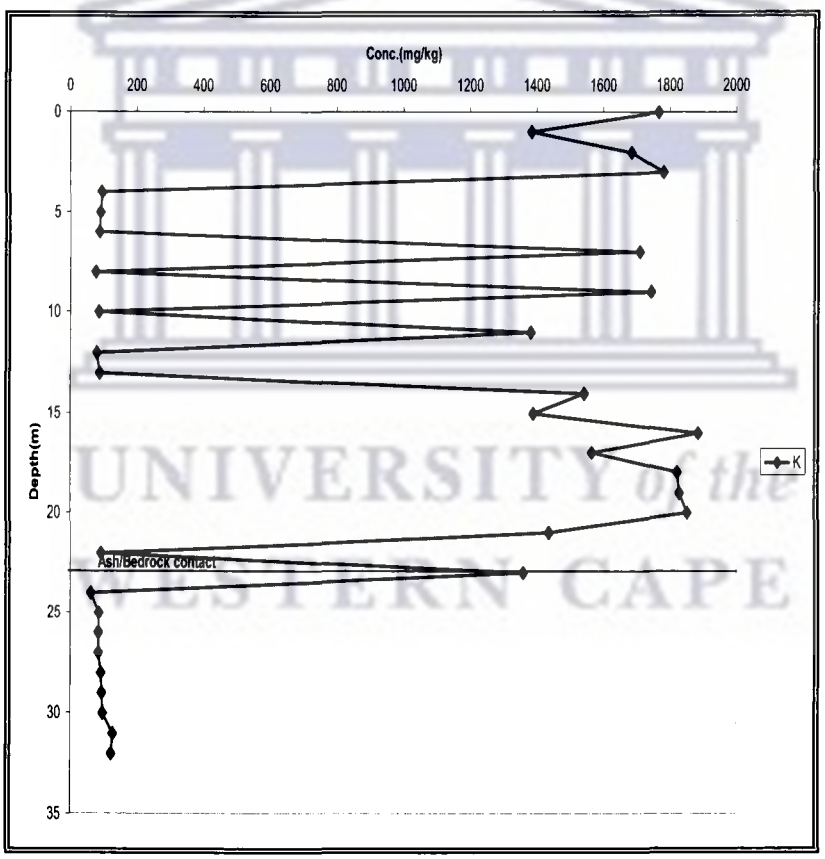

Fig. 5.11.2c: Trend of exchangeable fraction K down the drilled core at Kragbron

The trend of the exchangeable fraction of K (Fig. 5.11.2c) was different from that which was observed in the water soluble fraction extraction phase. Great variability in its concentration in this fraction was observed in the upper 12 m of the dump with

weathering from the surface and upper layers and accumulation at 7 m, 9 m, 11 m and between 14 m and 21 m was observed. The deep weathering pattern between 15 and 23 m observed for Ca (Fig. 5.11.2a) is also associated with this element indicating remineralization in this region due to concentration build up. The same trend as seen in the water soluble phase was exhibited after the contact with the bedrock at 23 m.

The exchangeable fractions of Al and Fe in the profile of the drilled ash core at Kragbron are shown in Fig. 5.11.2d.

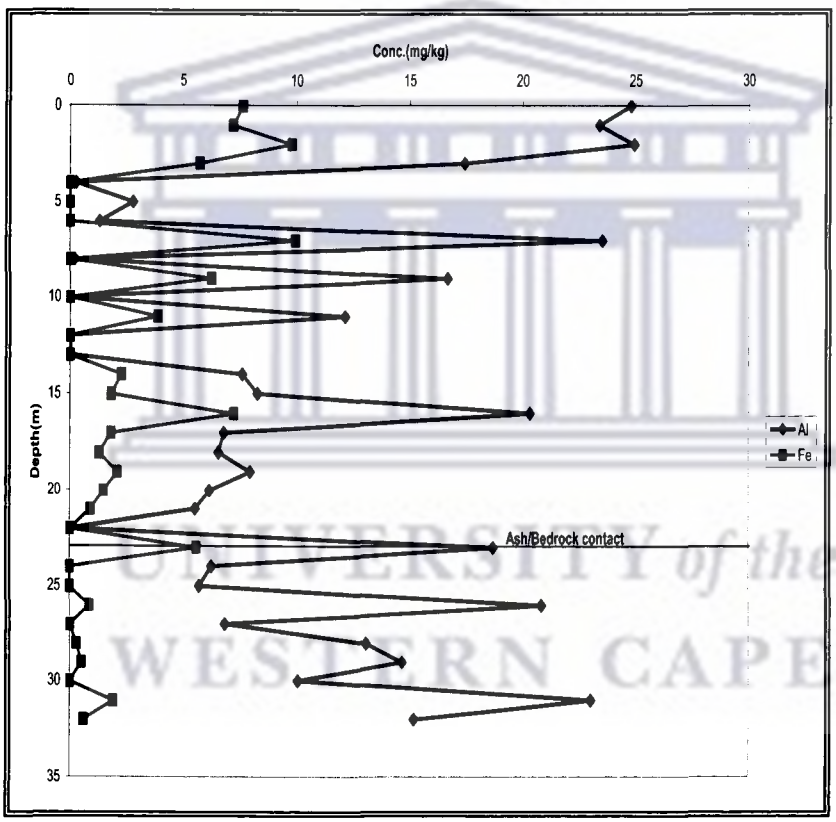

Fig. 5.11.2d: Trends of exchangeable fraction Al and Fe down the drilled core at Kragbron

The exchangeable fractions of Fe and Al showed similar trends to K in the first section of the dump between 0 to 12 m of the Kragbron ash column. The overall concentration for both elements was much lower than that observed in the water soluble extraction phase. The fluctuations observed in the upper layers continued in the deeper depths to 32 m

contrary to the accumulation observed for K and Ca, Si and Mg indicating that the major elements associated with remineralization did not include the exchangeable fractions of Fe whereas Al may have some role in the remineralization.

The exchangeable fractions of Sr, B, Mn and Ba in the profile of the drilled ash core are shown in Fig. 5.11.2e.

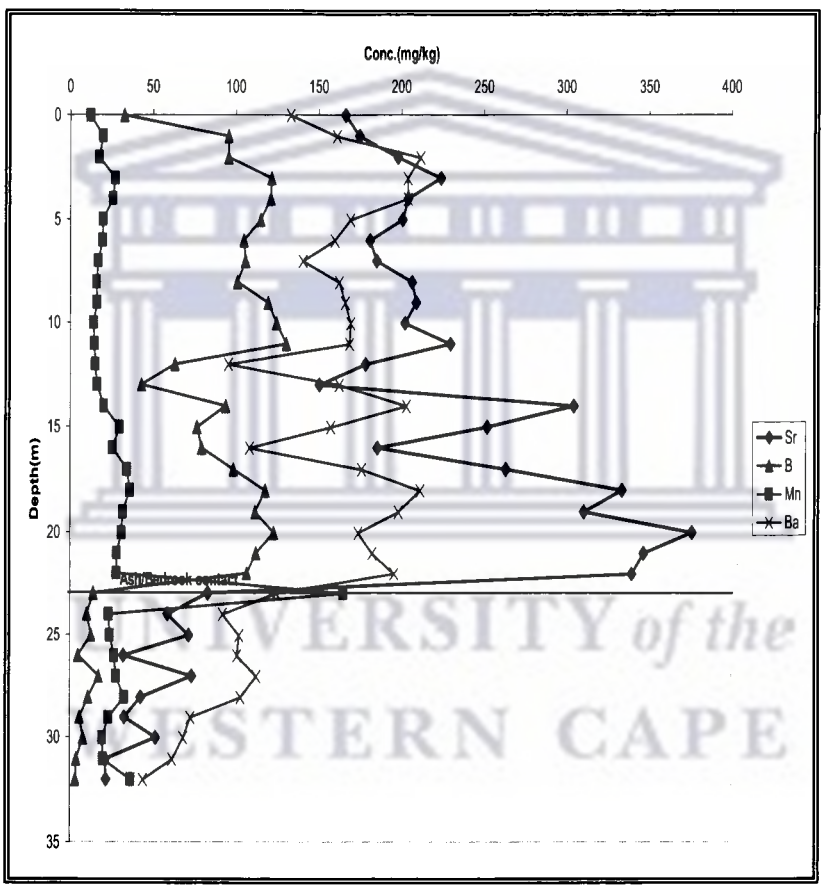

Fig. 5.11.2e: Trends of exchangeable fraction Sr, B, Mn and Ba down the drilled core at Kragbron

The exchangeable fractions of Sr, Ba and B exhibited similar trends to those like observed in the case of the water soluble fractions but the concentrations of these elements were higher in the exchangeable fraction phase. Sr in particular was strongly associated with deep weathering profile as was observed in Ca (Fig. 5.11.2a). A similar

trend to that observed in the water soluble extraction phase was also seen in Mn but in slightly higher levels.

Higher availability of Mn compared to Fe (Fig. 5.11.2d) in this extraction fraction is due to the redox condition of the fly ash in this phase. Under low redox conditions, Mn is more available than Fe as the release of the latter into solution is controlled by pH (Schoer et al., 1993).

The exchangeable fractions of As, V, Cr and Se in the profile of the drilled ash core at Kragbron are shown in Fig. 5.11.2f.

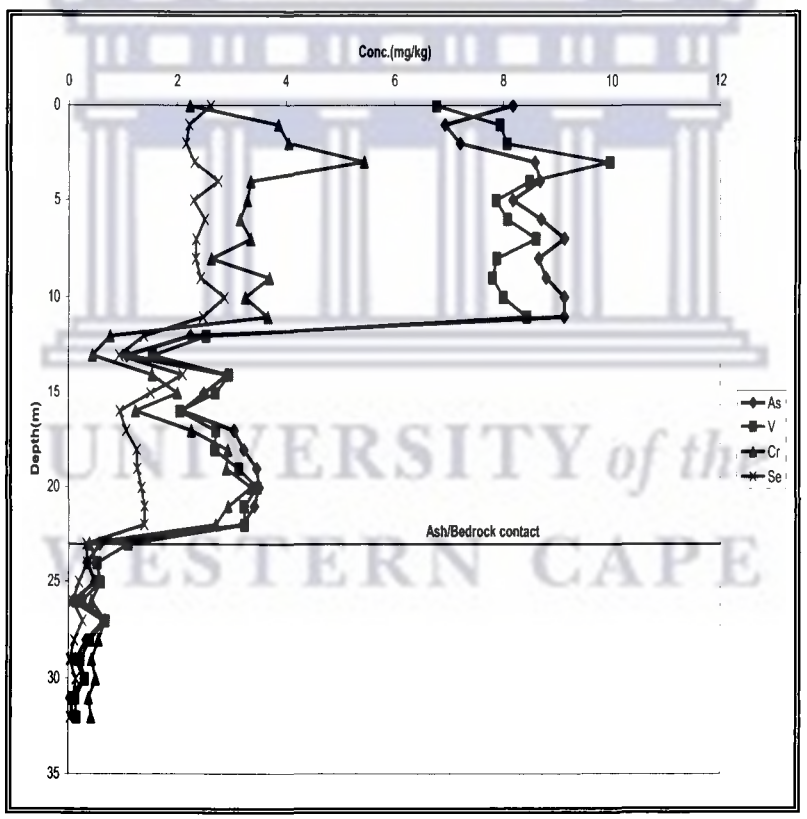

Fig. 5.11.2f: Trends of exchangeable fraction As, V, Cr and Se down the drilled core at Kragbron

The exchangeable fraction of Se (Fig. 5.11.2e) showed the same trend in the ash horizon as observed in the case of the water soluble fraction and much lower levels after the

contact with the bedrock at 23 m depth. As and V showed a similar trend to the water soluble fraction as well with slightly higher concentrations being released from the exchangeable fraction than what was observed in the water soluble extraction phase. The trend of As and V shows a strong indication of the exchangeable fraction of As and V being resistant to weathering and thus left behind as other more mobile species leach out of the surface layers. More Cr was associated with the exchangeable fraction than with the water soluble phase and it followed a similar pattern of weathering as the exchangeable V fraction. All these elements were of very negligible concentration in the bedrock layers.

The exchangeable fractions of Ni, Cu and Zn in the profile of the drilled ash core at Kragbron are shown in Fig. 5.11.2g.

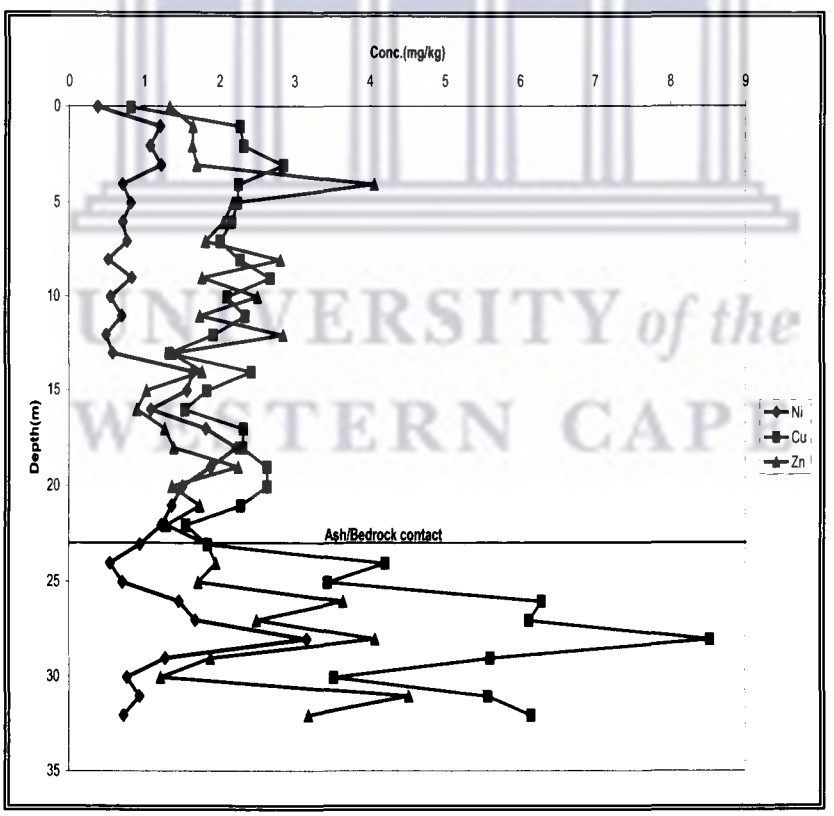

Fig. 5.11.2g: Trends of exchangeable fractions Ni, Cu and Zn down the drilled core at Kragbron

5.11.2 Exchangeable Fraction Phase

Determination of the exchangeable fraction of the Kragbron ash core samples was carried out as described in section 4.2.5 using 1 M ammonium acetate solution at pH 7. This procedure was performed on the residues remaining after the water extraction and was done to determine the fraction of each species associated with the exchangeable phase of the ash.

Fig. 5.11.2a to 5.11.2h shows the trends observed for the release of various elements in the exchangeable fraction phase down the profile of the Kragbron drilled ash core.

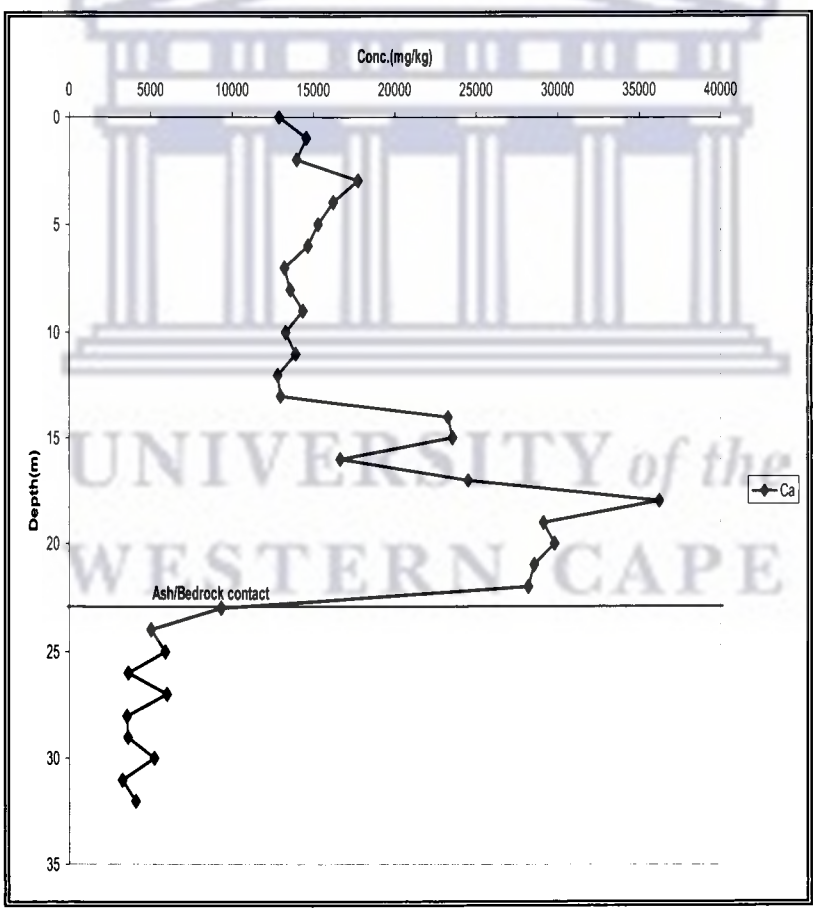

Fig. 5.11.2a: Trend of exchangeable fraction Ca down the drilled core at Kragbron

The exchangeable fraction Ca (Fig. 5.11.2b) exhibited the same trend as that observed in the water soluble fraction extraction phase. Much more of the Ca was observed to be associated with the exchangeable fraction phase. The accumulation of the element at 15 m to 23 m indicates possible mineralization due to concentration build up after the deep weathering observed in the ash horizon between 0 to 12 m.

The exchangeable fractions of Mg, Si and Na in the profile of the drilled ash core at Kragbron are shown in Fig. 5.11.2b.

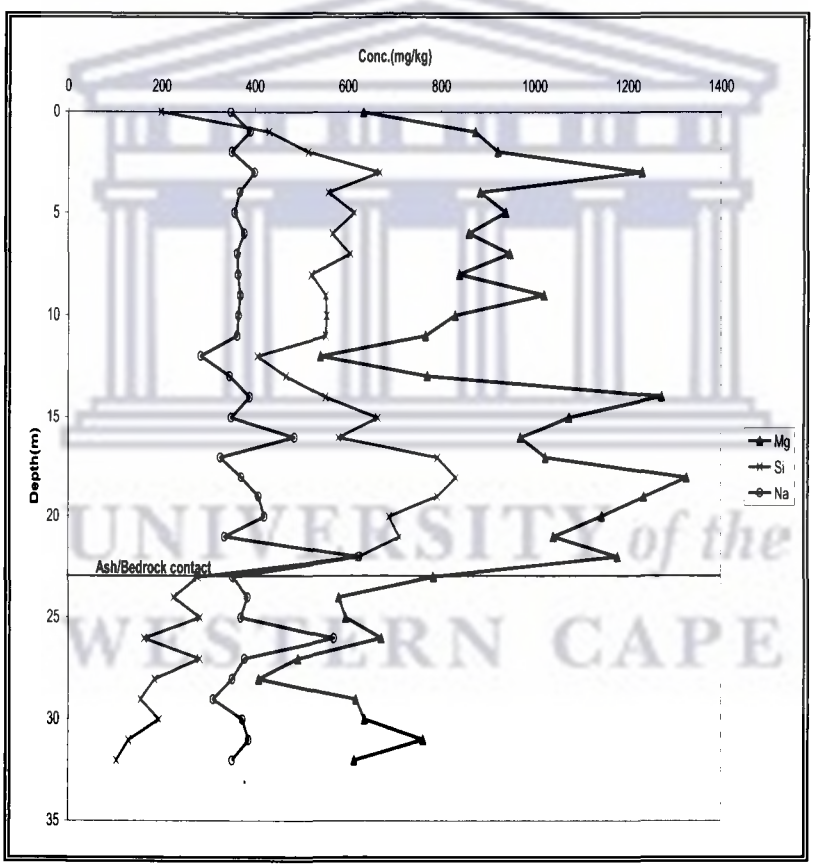

Fig. 5.11.2b: Trends of exchangeable fraction Mg, Si and Na down the drilled core at Kragbron

A higher level of the exchangeable fraction of Mg and Si was released into the solution (Fig. 5.11.2b) than that observed in the water soluble fraction. Mg and Si showed

accumulation in the deeper layers of the dump indicative of deep weathering and association with phases involved in remineralization such as Ca and K (Fig. 5.11.2a and Fig. 5.11.2c). A decrease was observed for both elements after the contact with the bedrock at 23 m depth showing that these elements were not associated to a great degree with the exchangeable fraction in the doleritic bedrock layer. The exchangeable fraction of Na followed a similar trend to that observed in the water soluble fraction (Fig. 5.11.1b) but the concentration in solution was lower in the ash column.

The exchangeable fraction of K in the profile of the drilled ash core at Kragbron is shown in Fig. 5.11.2c.

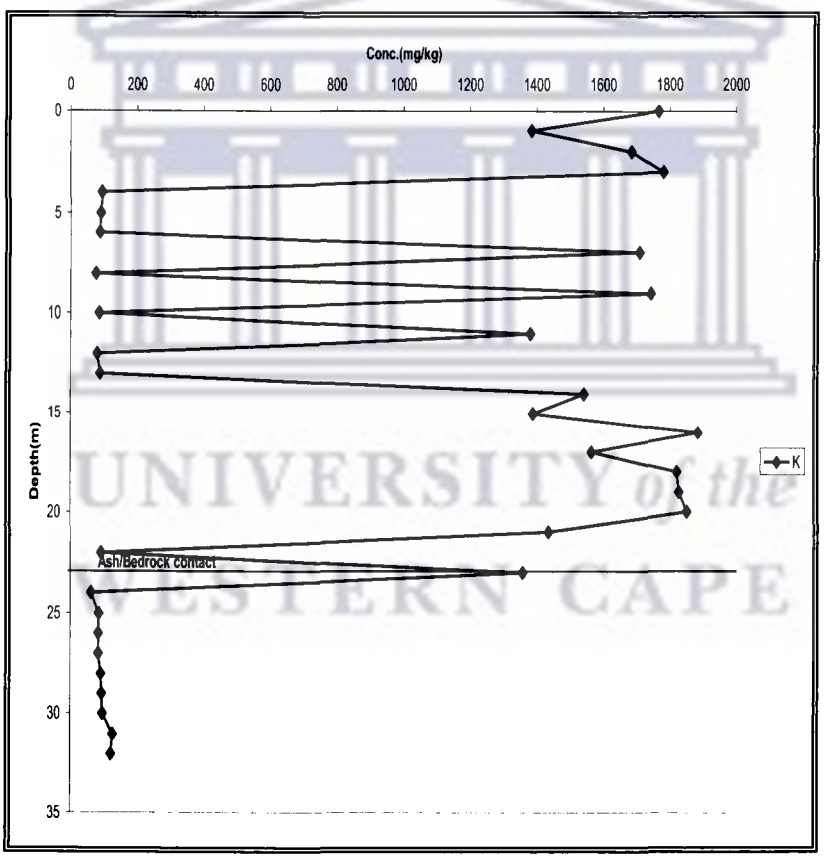

Fig. 5.11.2c: Trend of exchangeable fraction K down the drilled core at Kragbron

The trend of the exchangeable fraction of K (Fig. 5.11.2c) was different from that which was observed in the water soluble fraction extraction phase. Great variability in its concentration in this fraction was observed in the upper 12 m of the dump with

weathering from the surface and upper layers and accumulation at 7 m, 9 m, 11 m and between 14 m and 21 m was observed. The deep weathering pattern between 15 and 23 m observed for Ca (Fig. 5.11.2a) is also associated with this element indicating remineralization in this region due to concentration build up. The same trend as seen in the water soluble phase was exhibited after the contact with the bedrock at 23 m.

The exchangeable fractions of Al and Fe in the profile of the drilled ash core at Kragbron are shown in Fig. 5.11.2d.

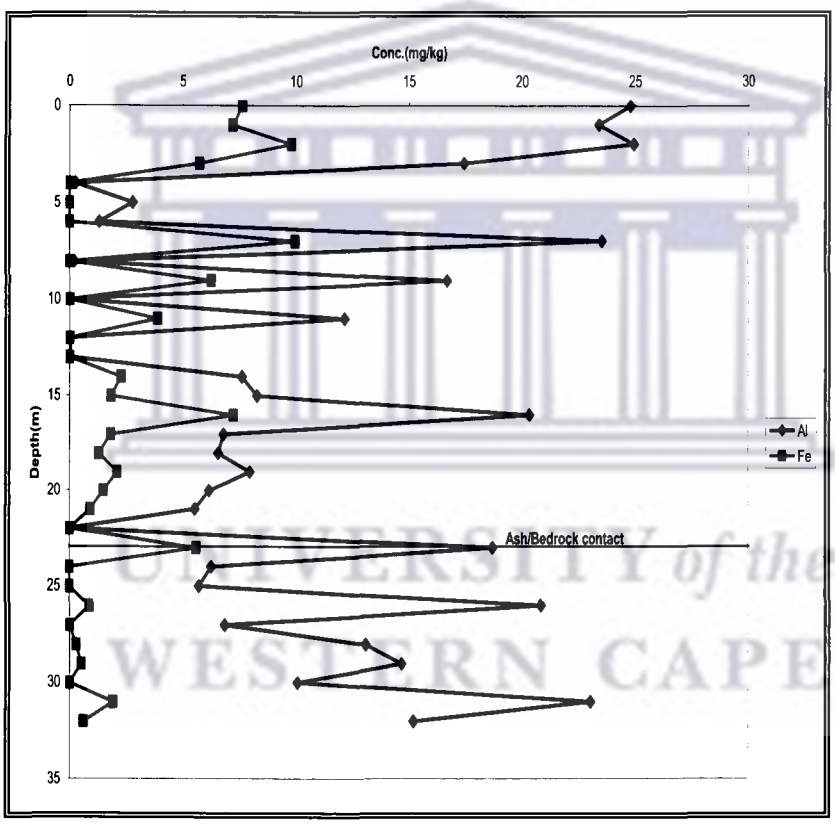

Fig. 5.11.2d: Trends of exchangeable fraction Al and Fe down the drilled core at Kragbron

The exchangeable fractions of Fe and Al showed similar trends to K in the first section of the dump between 0 to 12 m of the Kragbron ash column. The overall concentration for both elements was much lower than that observed in the water soluble extraction phase. The fluctuations observed in the upper layers continued in the deeper depths to 32 m

contrary to the accumulation observed for K and Ca, Si and Mg indicating that the major elements associated with remineralization did not include the exchangeable fractions of Fe whereas Al may have some role in the remineralization.

The exchangeable fractions of Sr, B, Mn and Ba in the profile of the drilled ash core are shown in Fig. 5.11.2e.

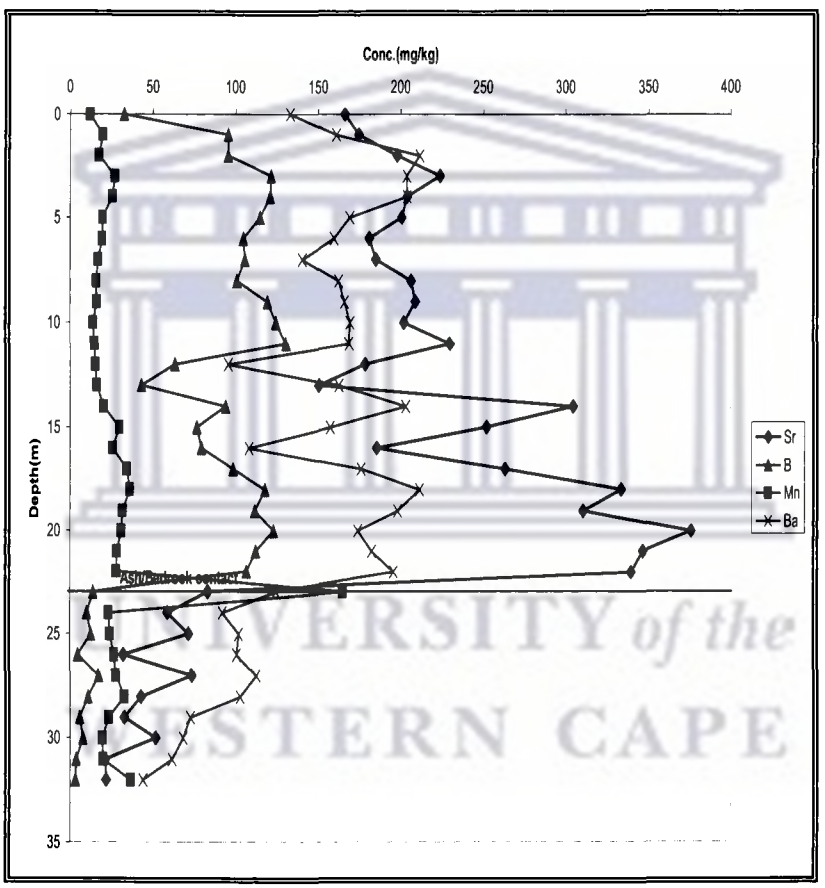

Fig. 5.11.2e: Trends of exchangeable fraction Sr, B, Mn and Ba down the drilled core at Kragbron

The exchangeable fractions of Sr, Ba and B exhibited similar trends to those like observed in the case of the water soluble fractions but the concentrations of these elements were higher in the exchangeable fraction phase. Sr in particular was strongly associated with deep weathering profile as was observed in Ca (Fig. 5.11.2a). A similar

trend to that observed in the water soluble extraction phase was also seen in Mn but in slightly higher levels.

Higher availability of Mn compared to Fe (Fig. 5.11.2d) in this extraction fraction is due to the redox condition of the fly ash in this phase. Under low redox conditions, Mn is more available than Fe as the release of the latter into solution is controlled by pH (Schoer et al., 1993).

The exchangeable fractions of As, V, Cr and Se in the profile of the drilled ash core at Kragbron are shown in Fig. 5.11.2f.

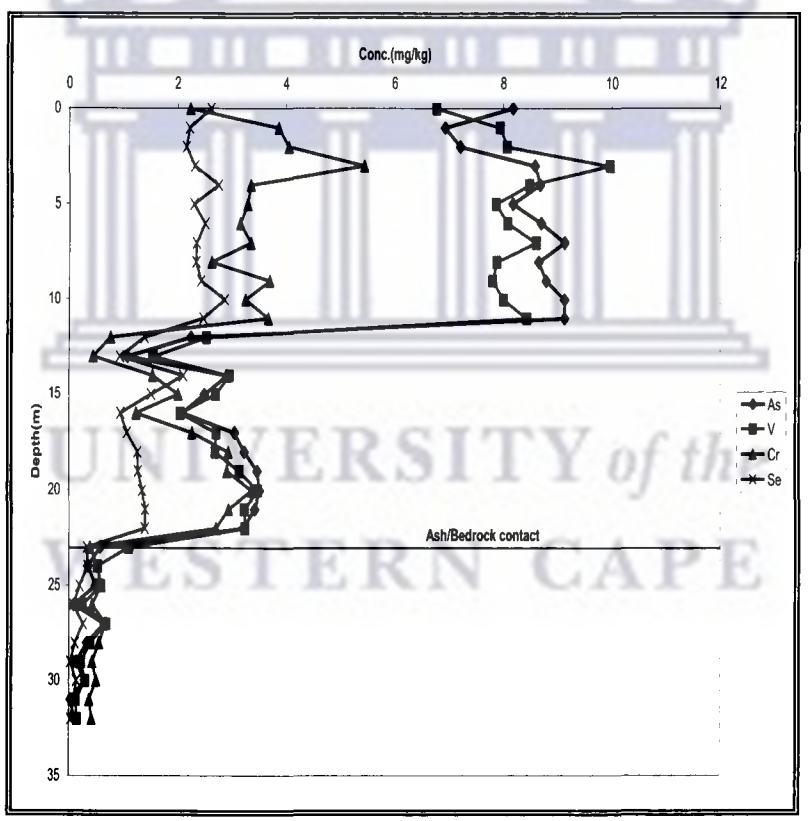

Fig. 5.11.2f: Trends of exchangeable fraction As, V, Cr and Se down the drilled core at Kragbron

The exchangeable fraction of Se (Fig. 5.11.2e) showed the same trend in the ash horizon as observed in the case of the water soluble fraction and much lower levels after the

contact with the bedrock at 23 m depth. As and V showed a similar trend to the water soluble fraction as well with slightly higher concentrations being released from the exchangeable fraction than what was observed in the water soluble extraction phase. The trend of As and V shows a strong indication of the exchangeable fraction of As and V being resistant to weathering and thus left behind as other more mobile species leach out of the surface layers. More Cr was associated with the exchangeable fraction than with the water soluble phase and it followed a similar pattern of weathering as the exchangeable V fraction. All these elements were of very negligible concentration in the bedrock layers.

The exchangeable fractions of Ni, Cu and Zn in the profile of the drilled ash core at Kragbron are shown in Fig. 5.11.2g.

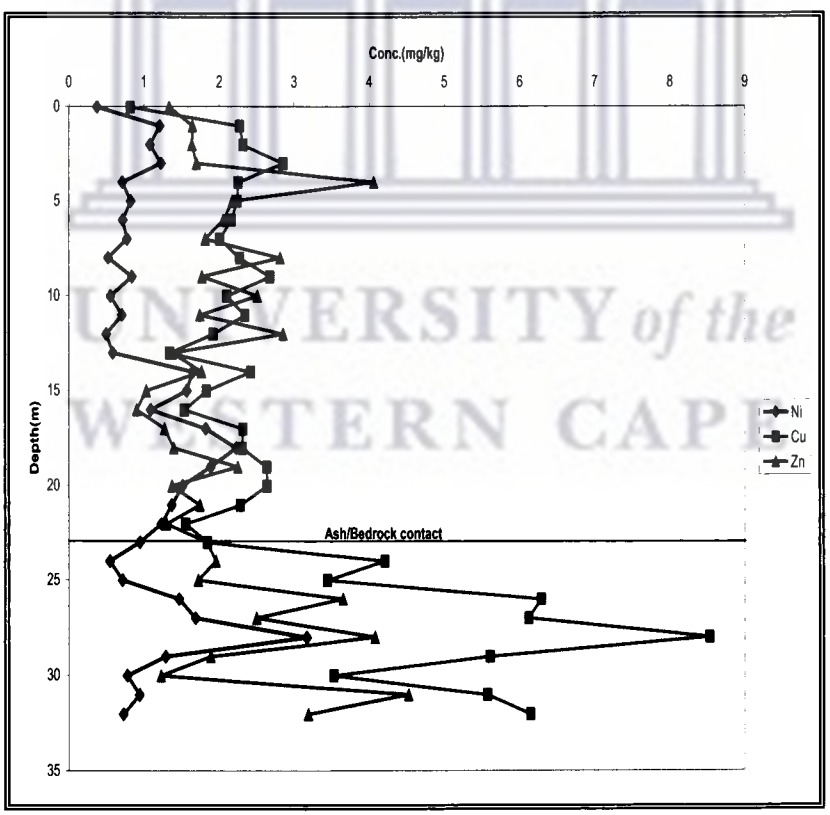

Fig. 5.11.2g: Trends of exchangeable fractions Ni, Cu and Zn down the drilled core at Kragbron

Fig. 5.11.2g shows the same trend for Cu and Zn in the exchangeable fraction as was observed in the water soluble fraction. A higher concentration was seen at deeper depths (24 m to 32 m). Ni also showed a similar trend to Cu and Zn. It was barely above detection limit in the water soluble fraction phase. Cu was observed to be very strongly associated with the bedrock layer as was also apparent in the water soluble fraction.

The exchangeable fractions of Ti, Co, Mo and Pb in the profile of the drilled ash core at Kragbron are shown in Fig. 5.11.2h.

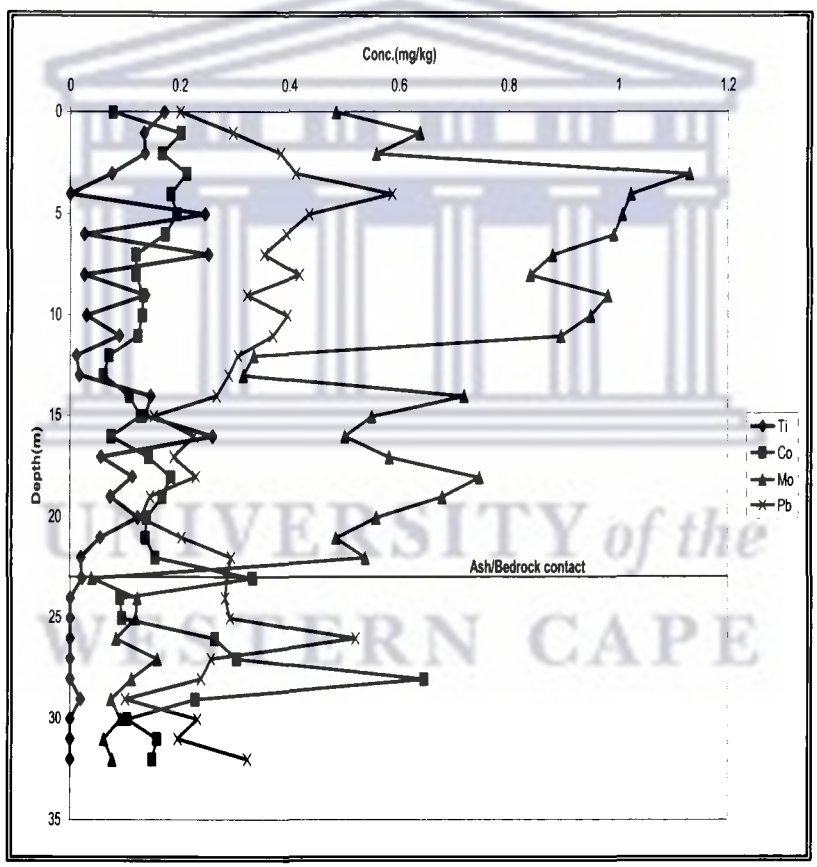

Fig. 5.11.2h: Trends of exchangeable fraction Ti, Co, Mo and Pb down the drilled core at Kragbron

The exchangeable fractions of Co, Mo and Pb (Fig. 5.11.2h) showed similar trends in the ash profile (surface to 22 m) as in the case of the water soluble extraction phase but the concentration of the elements was much lower (below 1.2 mg/kg). Ti also exhibited a

similar trend to that observed in the water soluble fraction and its concentration was < 0.4 mg/kg. After the contact at 23 m, it was below detection limit except at 29 m.

The low concentration of some of the metal ions in the exchangeable fraction suggests poor solubility and availability of the metals in the ash residue used for the exchangeable fraction which can be attributed to high pH (Rath et al., 2008).

5.11.3 Carbonate Fraction Phase

The determination of the carbonate fraction was carried out as described in section 4.2.5 using 1 M ammonium acetate solution at pH 5. This procedure was performed on the residues remaining after the extraction of pore water and exchangeable fractions and it was done to determine the species associated with the carbonate fraction phase of the ash.

Fig. 5.11.3a to 5.11.3i shows the trends observed for the various elements in the carbonate fraction phase down the horizon of the Kragbron drilled ash core.

Fig. 5.11.3a below shows the trends of carbonate fractions of Al, Si and Ca.

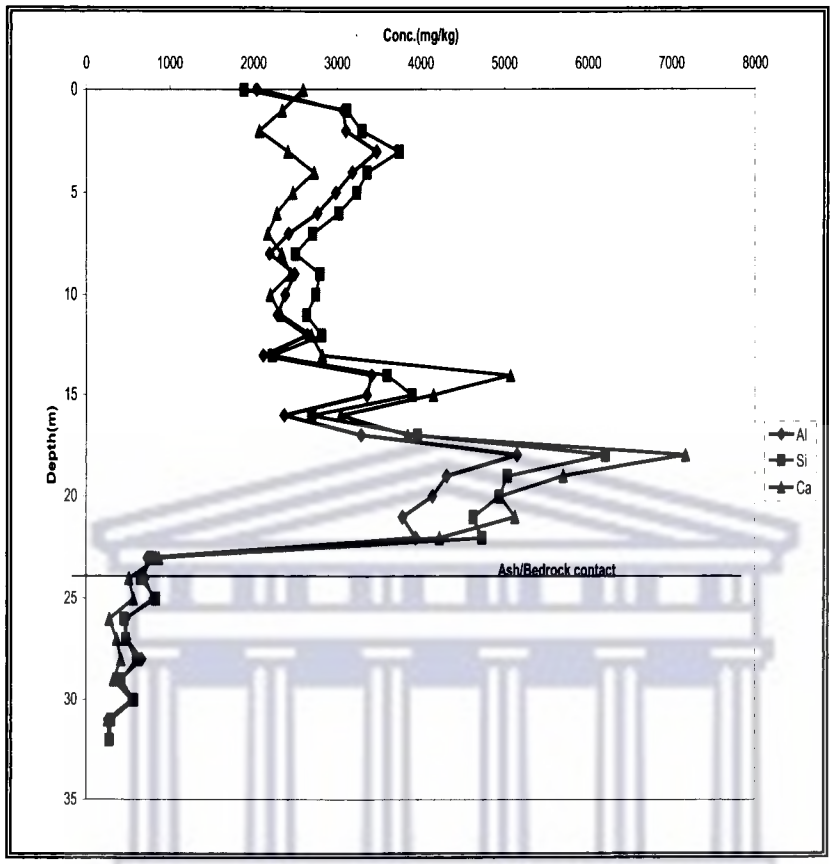

Fig. 5.11.3a: Trends of carbonate fraction Al, Si and Ca down the drilled core at Kragbron

The carbonate fractions of Al, Si and Ca showed similar trend of high concentrations from the surface to 32 m depth of the drilled ash core at Kragbron. These elements show deep weathering, accumulation and remineralization between 14 m and 23 m. Dissolution of the carbonate compounds bearing these elements could be responsible for their accumulation at 14 m and from18 m to 22 m depth. A sharp decrease was observed from 23 m depth.

The carbonate fractions of Mg and Fe in the drilled ash core at Kragbron are shown in Fig. 5.11.3b.

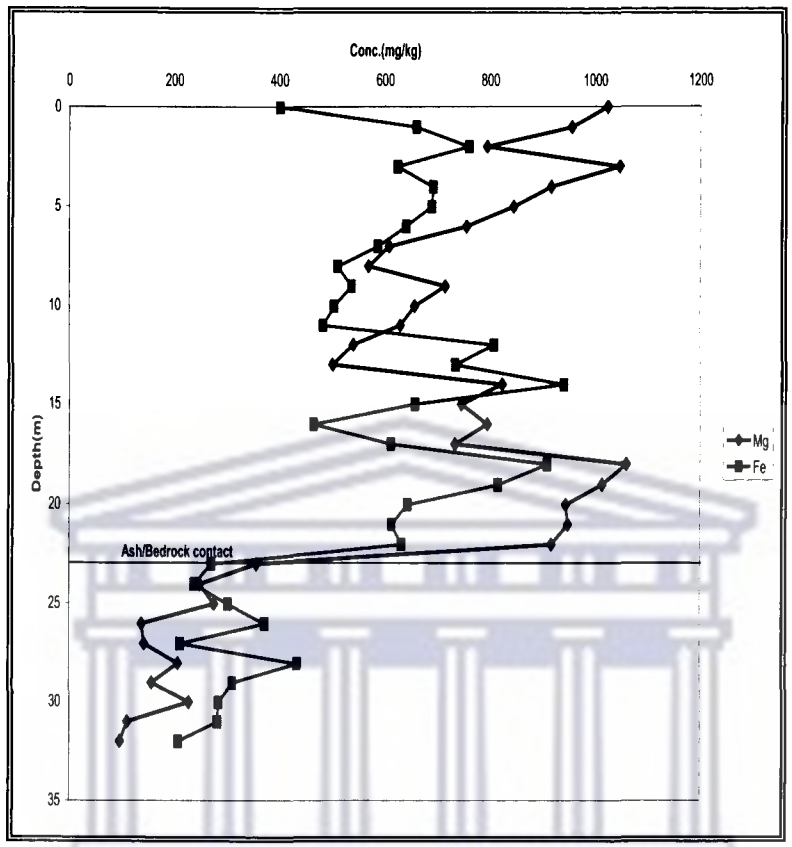

Fig. 5.11.3b: Trends of carbonate fraction Mg and Fe down the drilled core at Kragbron

The carbonate fractions of Mg and Fe showed similar trends from 2 m down to 32 m. The trend is characterized by weathering which led to migration, accumulation and remineralization between 14m and 23 m depths as observed in the case of Al, Si and Ca (Fig.5.11.3a). This could be attributed to the association of the elements with the carbonate bearing phases of the ash. Lower levels were observed in the concentration of the elements after the contact at 23 m.

The carbonate fraction of K in the profile of the drilled ash core at Kragbron is shown in Fig. 5.11.3c.

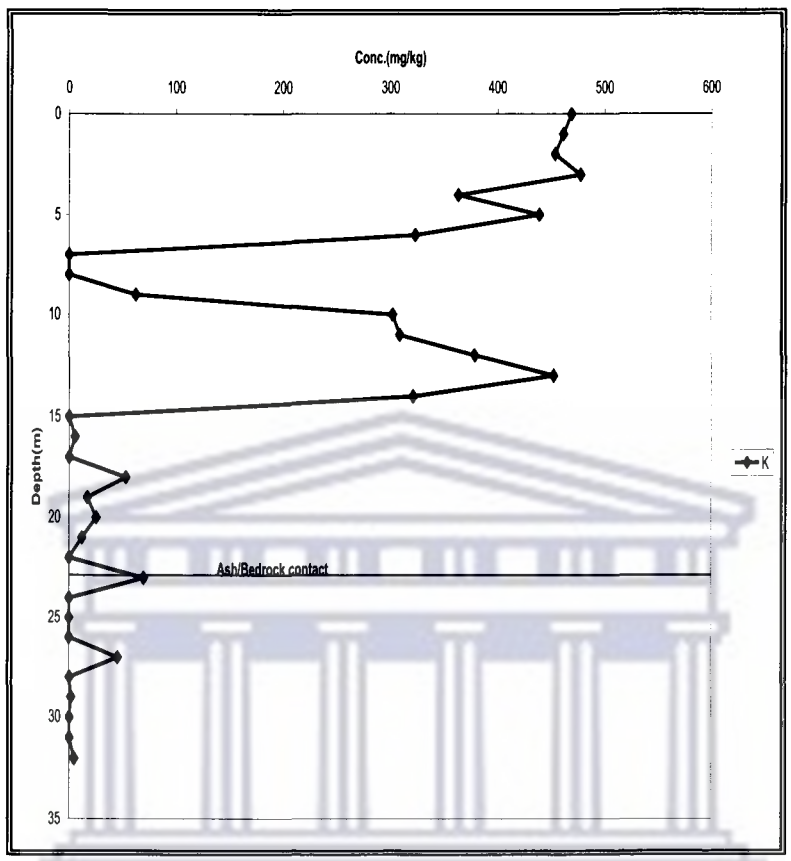

Fig. 5.11.3c: Trend of carbonate fraction K down the drilled core at Kragbron

Intense weathering and dissolution of K bearing compounds associated with the carbonate fraction of the ash accounts for the flushing and accumulation of the element between 0 and 6 m and also 10 m and 14 m depth of the ash column. Depths having lower concentration of K could be lacking in soluble carbonate bearing compounds of K.

The carbonate fractions of Sr and Ba in the drilled ash core at Kragbron are shown in Fig. 5.11.3d.

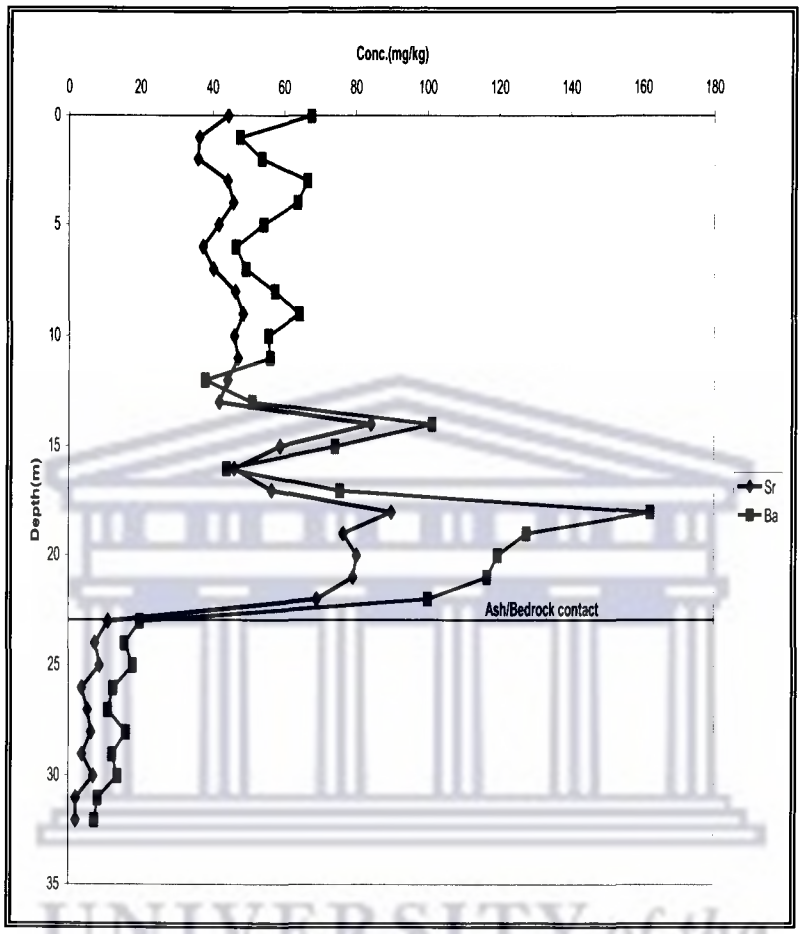

Fig. 5.11.3d: Trends of carbonate fraction Sr and Ba down the drilled core at Kragbron

The carbonate fractions of Sr and Ba showed similar trends from the surface to 32 m depth of the drilled core. Concentration observed in this extraction phase was lower than what was observed in the exchangeable fraction phase. Deep weathering and leaching from the upper layers was observed resulting in the accumulation of these elements at depth 14 m, and between 18 and 22 m. Lower levels for Sr and Ba was observed after the contact with the bedrock at 23 m indicating less association of the elements with the carbonate fractions within the bedrock layers.

The carbonate fractions of Na and Mn in the profile of the drilled ash core at Kragbron are shown in Fig. 5.11.3e.

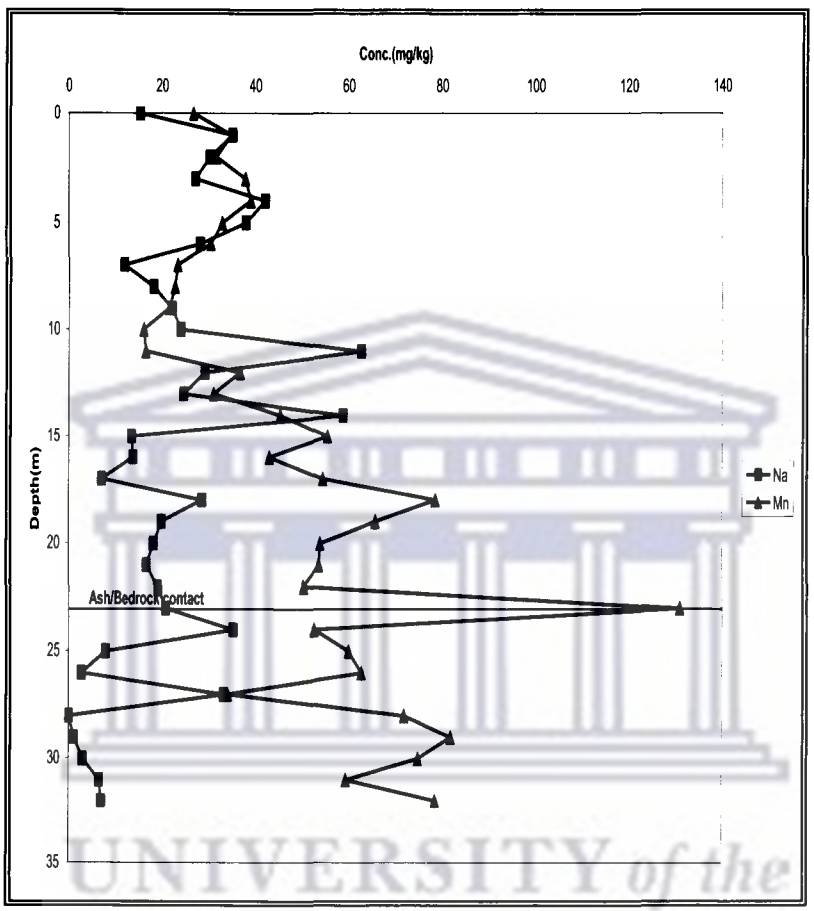

Fig. 5.11.3e: Trends of carbonate fraction Na and Mn down the drilled core at Kragbron

The carbonate fractions of Na and Mn exhibited similar trends from the surface to 22 m depth of the ash column. Accumulations at 12 m, 14 m and 18 m was observed in the carbonate fraction of Na due to weathering and migration of species from the upper layers of the ash column. Mn showed an accumulation at 18 m and 23 m as a result of similar processes as in the case of Na.

The carbonate fractions of Se, Mo and Pb in the profile of the drilled ash core at Kragbron are shown in Fig. 5.11.3f.

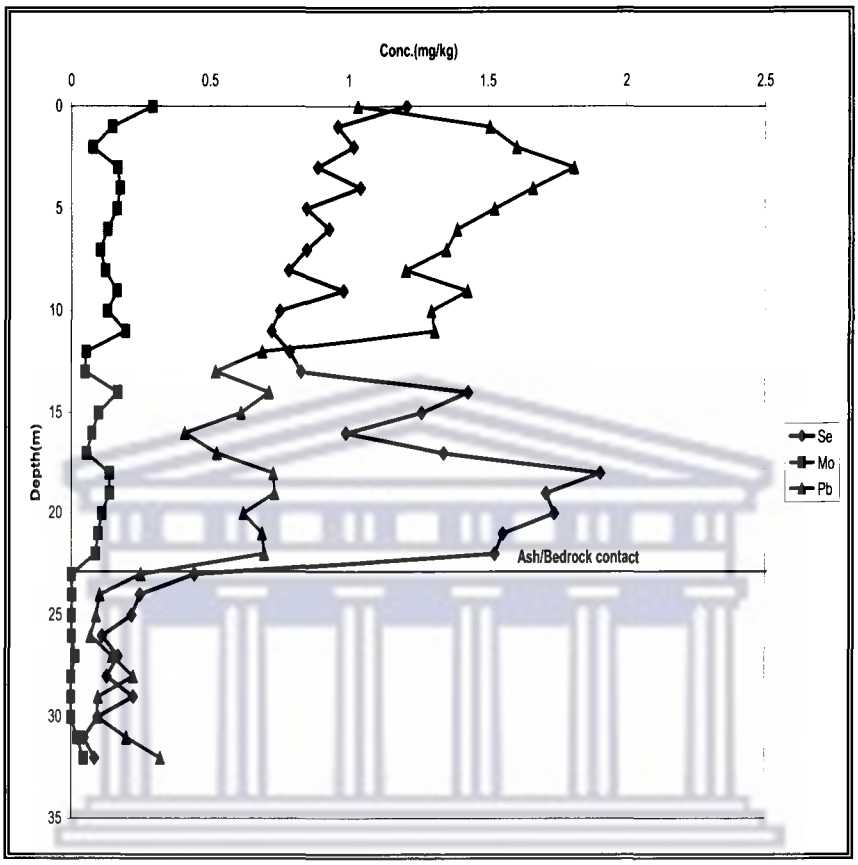

Fig. 5.11.3f: Trends of carbonate fraction Se, Mo and Pb down the drilled core at Kragbron

The carbonate fraction of Se showed similar trends to the carbonate fractions of Al, Si, Ca, Fe, Mg, Sr and Ba between 14 m and 23 m. This trend is indicative of intense weathering from the upper layers leading to the accumulation of the element and possible remineralization at these depths. The trend observed in carbonate fraction Mo is similar to what was observed in the exchangeable fraction phase in the Kragbron drilled ash column although in lower concentrations. The trend of carbonate fraction Pb from the surface to 32 m and carbonate fraction Se from 23 m could be attributed to the gradual dissolution of the glassy fraction of the fly ash because significant portions of the elements are incorporated in the glass matrix of fly ash particles (Huletts et al., 1980).

The carbonate fractions of V, Cr and As in the profile of the drilled ash core at Kragbron are shown in Fig. 5.11.3g.

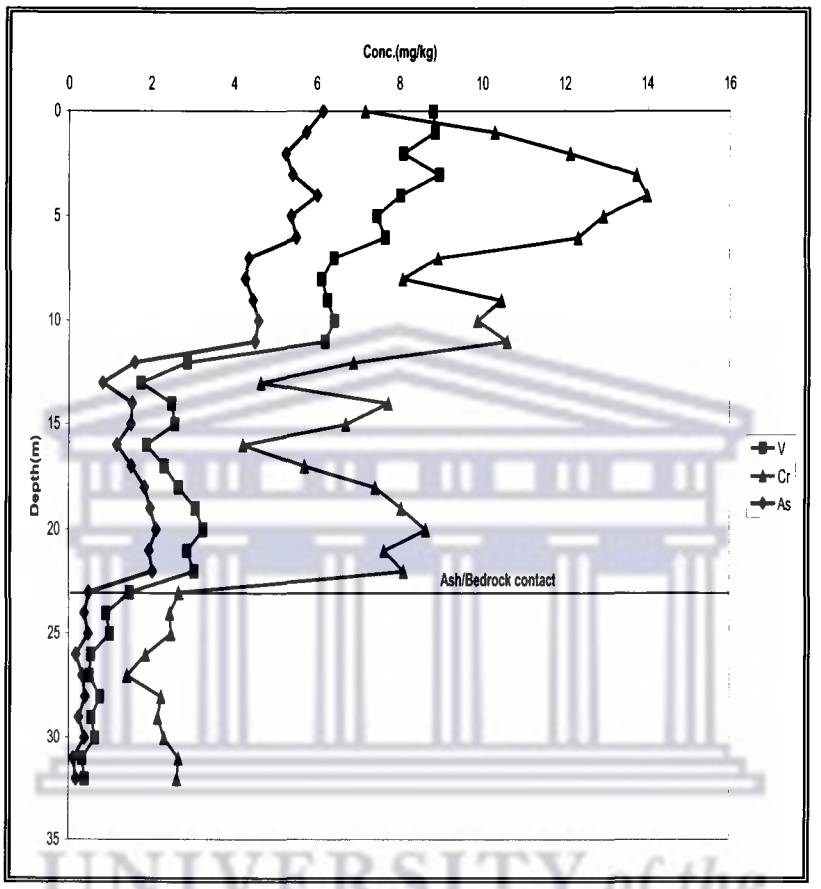

Fig. 5.11.3g: Trends of carbonate fraction V, Cr and As down the drilled core at Kragbron

Fig. 5.11.3g shows an appreciable release in the carbonate fractions of V, Cr and As from the surface to 22 m depth of the ash column. These elements appear to be enriched from the surface to 12 m because of the leaching of more soluble species associated with the carbonate fraction of the ash within the column. The concentration of the carbonate fraction of the elements was seen to be lower after the contact with the bedrock at 23 m indicating less association with the carbonate fraction in deeper layers of the bedrock.

The carbonate fractions of Ti and B in the profile of the drilled ash core at Kragbron are shown in Fig. 5.11.3h.

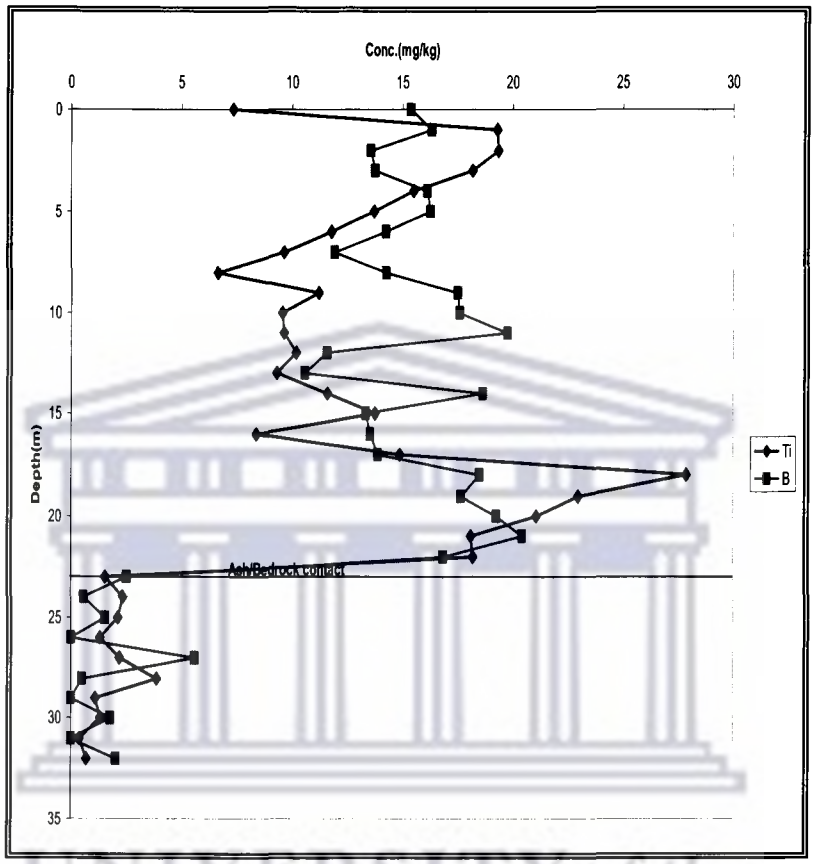

Fig. 5.11.3h: Trends of carbonate fraction Ti and B down the drilled core at Kragbron

The trend observed in the carbonate fraction of Ti could be attributed to the dissolution of the silicate matrix with which the element is incorporated, causing leaching and accumulation at 18 m depth of the ash profile. The trend was similar to the trend observed in the exchangeable fraction for Ti. The carbonate fraction of B maintained a similar trend to what was observed in the exchangeable fraction phase from the surface to 32 m depth of the profile, indicative of weathering and accumulation at deeper layers within the ash column. Both elements had lower concentrations after the contact with the bedrock.

The carbonate fractions of Zn, Cu, Ni and Co in the profile of the drilled ash core at Kragbron are shown in Fig. 5.11.3i.

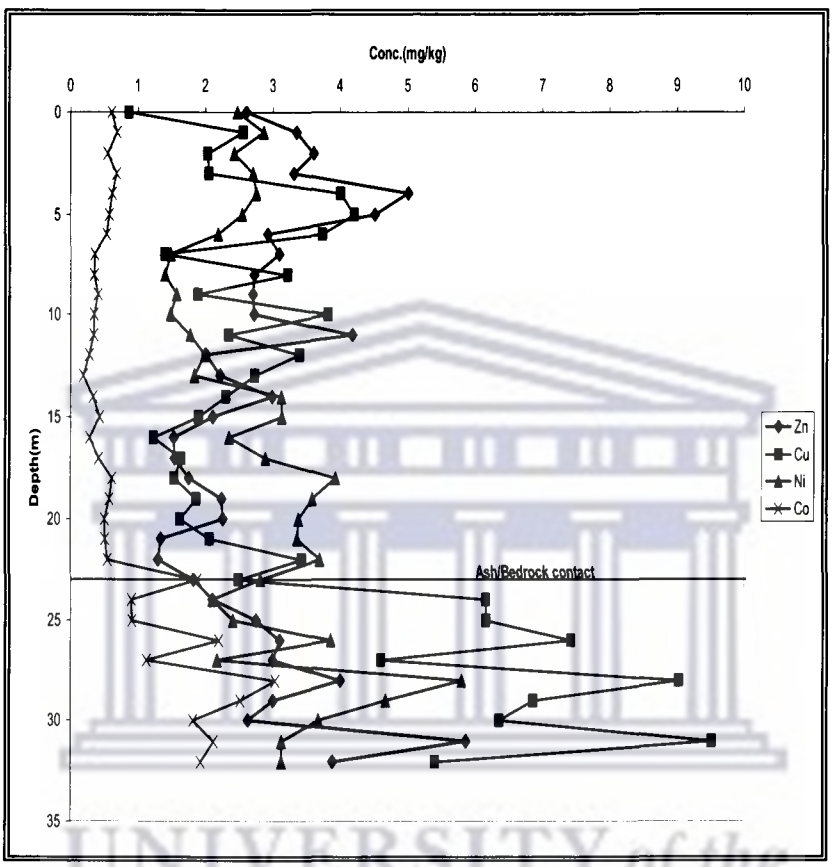

Fig. 5.11.3i: Trends of carbonate fraction Zn, Cu, Ni and Co down the drilled core at Kragbron

The trend pattern observed for the carbonate fractions of Zn, Cu and Ni showed various degrees of weathering and accumulations at certain depths down the ash profile as a result of the dissolution of solids bearing them in the ash. Co showed a relatively constant concentration from the surface to 22 m depth. The carbonate fractions of these elements were observed to be higher after the contact with the bedrock at 23 m. This could probably be due to the availability and dissolution of solids bearing them in carbonate forms within the bedrock.

5.11.4 Iron and Manganese Fraction Phase

The determination of the iron and manganese fraction of the Kragbron ash core samples was carried out as described in section 4.2.5 using 0.25 M hydroxylamine hydrochloride prepared in 0.025 M nitric acid at pH of 2. This procedure was performed on the residues remaining after the carbonate fraction extraction and it was done to determine the fraction of each species associated with the iron and manganese fraction phase of the ash.

Fig. 5.11.4a to 5.11.4h shows the trends observed for the various elements associated with the iron and manganese fraction phase down the Kragbron drilled ash core.

Fig. 5.11.4a shows the trend of iron and manganese fractions of Si, Al, and Ca down the profile of the drilled ash core at Kragbron.

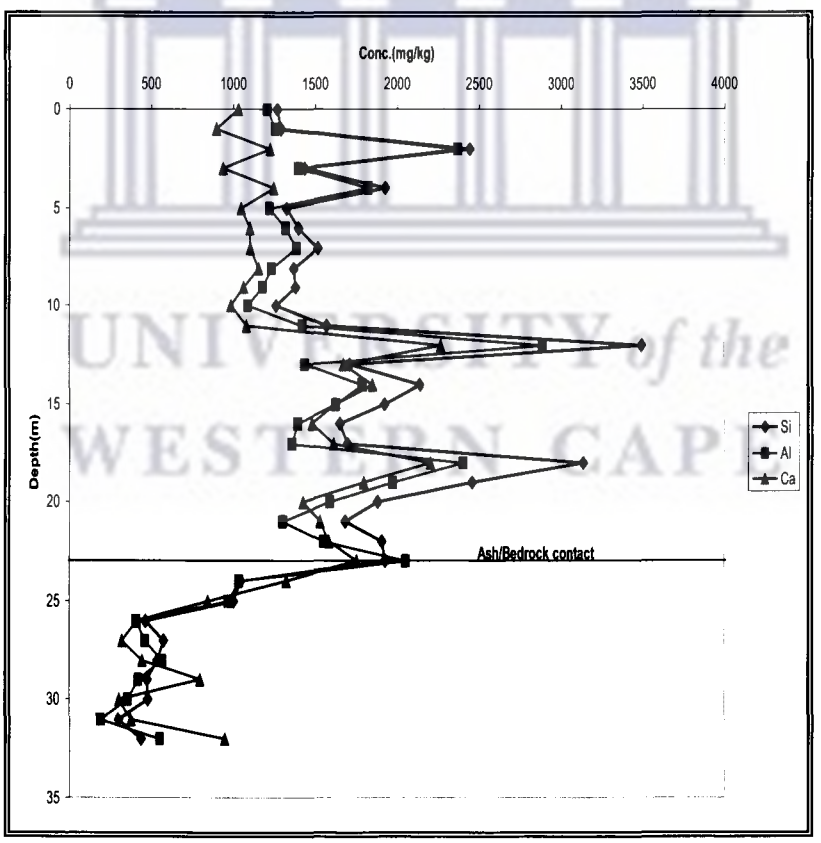

Fig. 5.11.4a: Trends of iron and manganese fraction Si, Al and Ca down the drilled core at Kragbron

The iron and manganese fraction trends of Si, Al and Ca were similar from the surface of the dump to 32 m depth. Accumulations of the iron and manganese fraction of the elements were observed at 2 m, 4 m, 12 m and 18 m depths indicating the weathering, dissolution and leaching of the aluminosilicate phase of the fly ash causing migration and accumulation at the observed depths. The iron and manganese fraction of the elements observed after the contact at 23 m was much lower probably due to less association of the elements with solids soluble in this phase within the bedrock.

The iron and manganese fractions of Mg, Fe and Mn in the profile of the drilled ash core at Kragbron are shown in Fig. 5.11.4b.

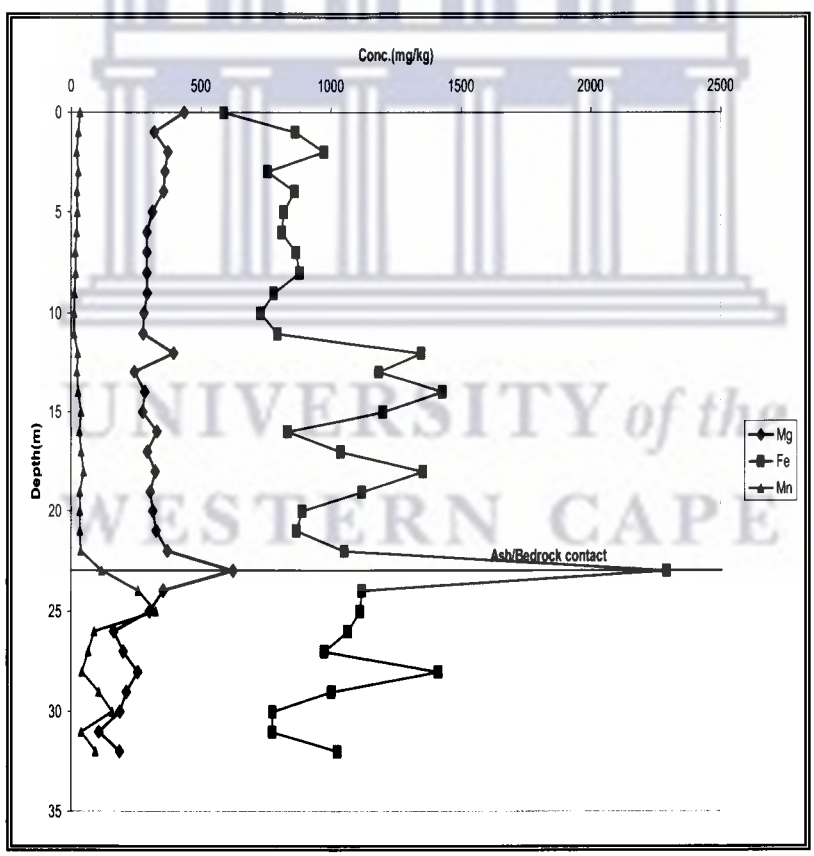

Fig. 5.11.4b: Trends of iron and manganese fraction Mg, Fe and Mn in the drilled core at Kragbron

The iron and manganese fraction of Mg showed a relatively constant concentration from the surface of the dump to 22 m depth except at 12 m and 23 m where slight increases were observed. The iron and manganese fraction of Mg was observed to be lower after 23 m depth. A considerable amount of the iron and manganese Fe was observed within the ash column. The weathering and dissolution of spinel minerals of the ash such as magnetite and ferrite could be responsible for the release of the element in the iron and manganese fraction extraction phase. A similar trend was observed after 23 m depth for the element. Mn showed a relatively constant low concentration from the surface of the dump to 22 m, after which an increase was seen beyond 23 m due to its presence in considerable amounts in the bedrock.

The iron and manganese fractions of K and Na in the profile of the drilled ash core at Kragbron are shown in Fig. 5.11.4c.

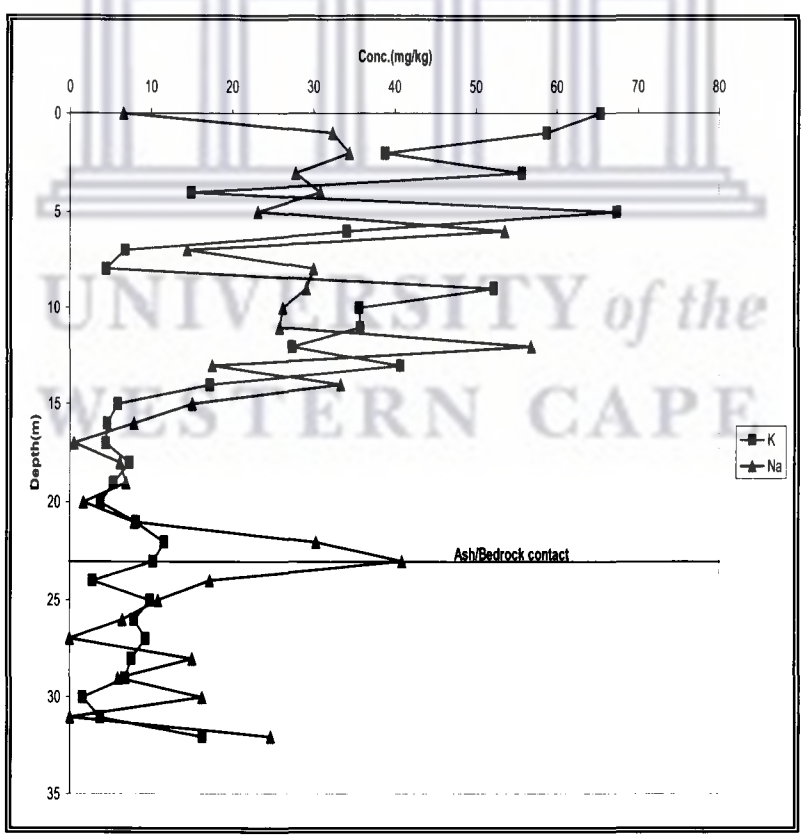

Fig. 5.11.4c: Trends of iron and manganese fractions K and Na in the drilled core at Kragbron

The trend observed in the iron and manganese fraction of K was similar to that which was observed in the carbonate fraction phase but in lower concentrations. The dissolution and possible remineralization at 5 m, 9 m and 13 m of K bearing components of the ash could be responsible for this trend. The iron and manganese fraction of Na showed a highly weathered trend having accumulations at 6 m, 12 m, 14 m and 23 m due to remineralization as a result of concentration build up at those depths. The trend continued down to 32 m depth.

The iron and manganese fractions of Ba and Sr in the profile of the drilled ash core at Kragbron are shown in Fig. 5.11.4d.

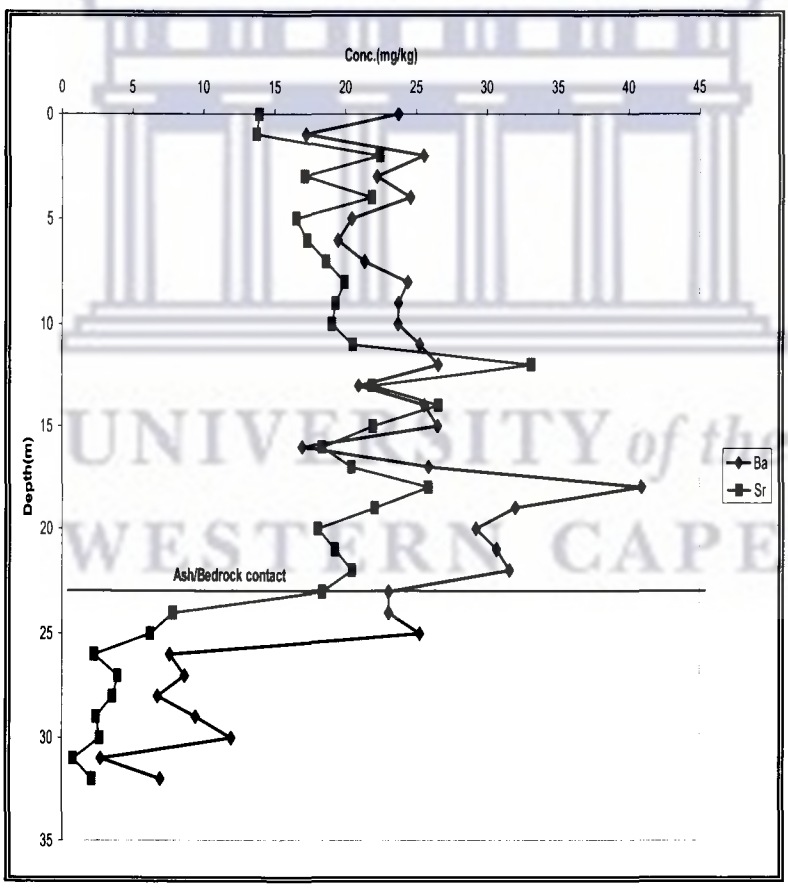

Fig. 5.11.4d: Trends of iron and manganese fraction Ba and Sr in the drilled core at Kragbron

The iron and manganese fractions of Ba and Sr showed a similar trend to what was observed in the carbonate fraction but their concentration in the iron and manganese extraction phase was lower. Accumulations as a result of weathering and remineralization were observed at 12 m, 14 m and between 18 and 22 m depths of the ash column.

The iron and manganese fractions of Mo, Se, Pb and As in the profile of the drilled ash core at Kragbron are shown in Fig. 5.11.4e.

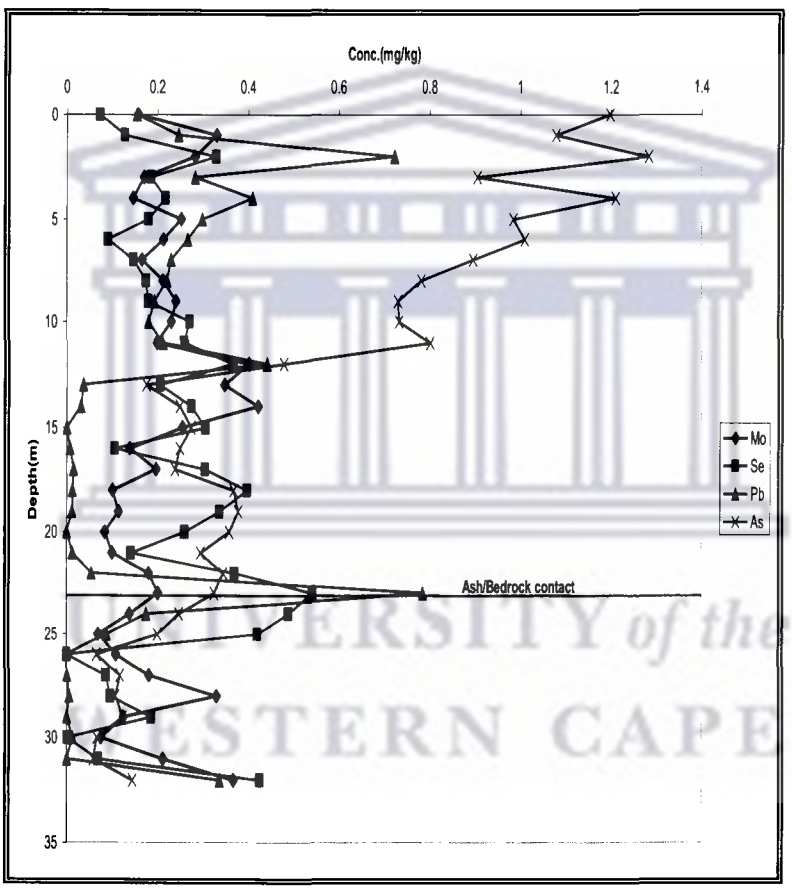

Fig. 5.11.4e: Trends of iron and manganese fraction Mo, Se, Pb and As in the drilled core at Kragbron

Intense leaching was observed in the trend of iron and manganese fractions of Mo, As and Pb between 12 m and 22 m depth of the ash profile. Iron and manganese fraction Pb showed almost depletion between 13 m and 22 m and an accumulation at 23 m. Iron and

manganese fraction Se appeared to be enriched from the surface to 11 m due to the depletion of more soluble components of the ash at those depths. The presence of iron and manganese fraction As, Se and Pb at certain depths in the profile could be from the dissolution of the silicate matrix of the fly ash with which some portions of the elements are associated. The lower concentration of Mo observed in the iron and manganese fraction could be as a result of the low pH of the leaching medium. Mo concentration in leaching solution is controlled by acidity and alkalinity. It has been observed to have a higher solubility under alkaline pH conditions (Kukier et al., 2003; Querol et al., 2001). Its solubility is significantly reduced under acidic conditions.

The iron and manganese fractions of Ni and Co in the profile of the drilled ash core at Kragbron are shown in Fig. 5.11.4f.

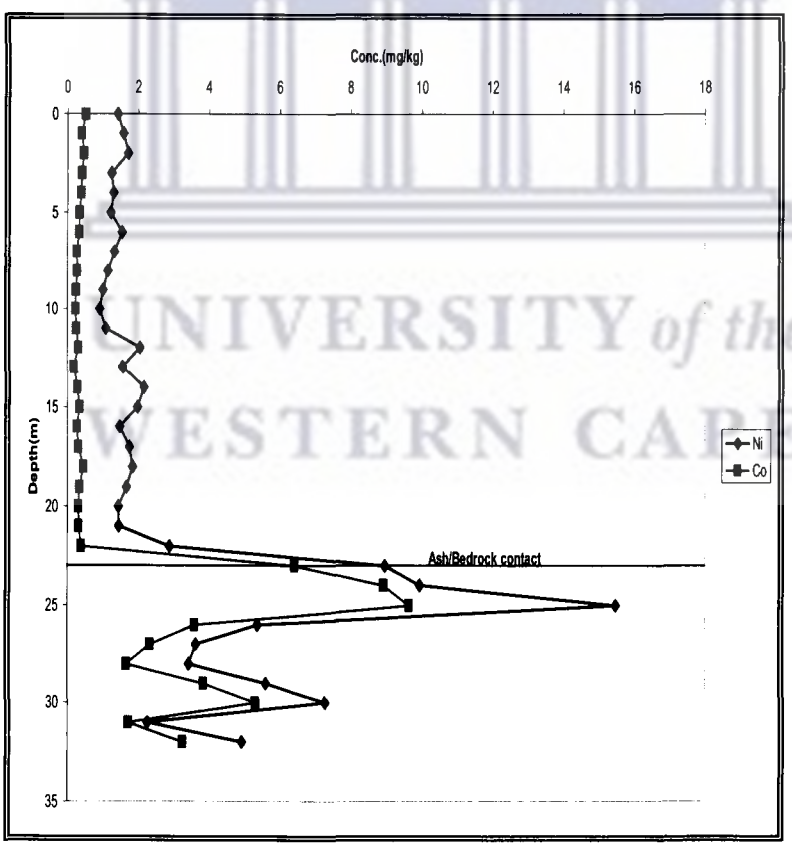

Fig. 5.11.4f: Trends of iron and manganese fraction Co and Ni down the drilled core at Kragbron

The iron and manganese fraction of Co exhibited a relatively low constant trend from the surface to 22 m depth. An increase was observed from 23 m depth which was followed by a sharp decrease at 28 m. Iron and manganese fraction Ni showed a similar trend to iron and manganese fraction Co from the surface to 32 m depth. The trend observed in iron and manganese fraction of Co and Ni after 23 m could be an indication of weathering due to lateral flow of ground water within the bedrock layers.

The iron and manganese fractions of Cr, V, B and Ti in the profile of the drilled ash core at Kragbron are shown in Fig. 5.11.4g.

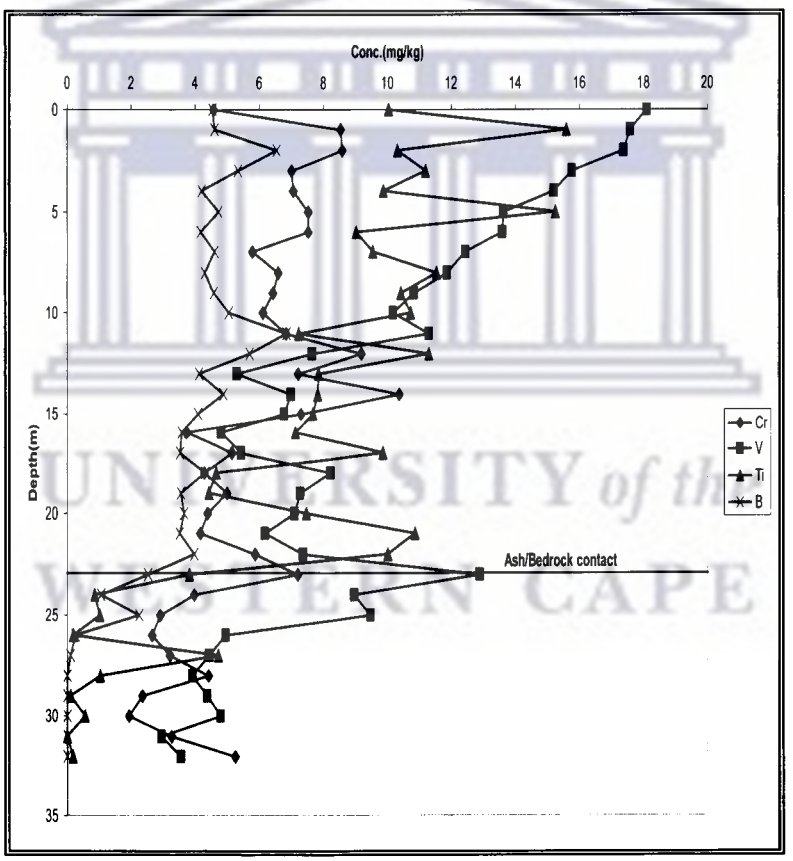

Fig. 5.11.4g: Trends of iron and manganese fraction Cr, V, Ti and B down the drilled core at Kragbron

The trend observed in the iron and manganese fraction of V showed gradual dissolution and migration from the surface of the dump to deeper layers. A highly leached trend was observed between 11 m and 21 m, accumulation at the contact with the bedrock was observed at 23 m after which the concentration of the iron and manganese fraction V showed a sharp drop and the leaching trend continued into the bedrock. The trend observed in Cr and Ti is similar to that in V. The release of Cr and V was most likely due to their association with the magnetic fractions of fly ashes. The dissolution of these fractions in fly ash in acidic medium made the elements available in higher concentrations. B is known to be highly soluble in an alkaline environment due to its presence in solution in anionic form (Jankowski et al., 2006). However, some studies have shown that greater leaching rates for B occur in acidic environment (Elseewi et al., 1980; Cox et al., 1978). The trend observed in iron and manganese B could be attributed to the dissolution of the B left behind from the previous extraction phases. The iron and manganese fractions of Zn and Cu in the profile of the drilled ash core at Kragbron are shown in Fig. 5.11.4h.

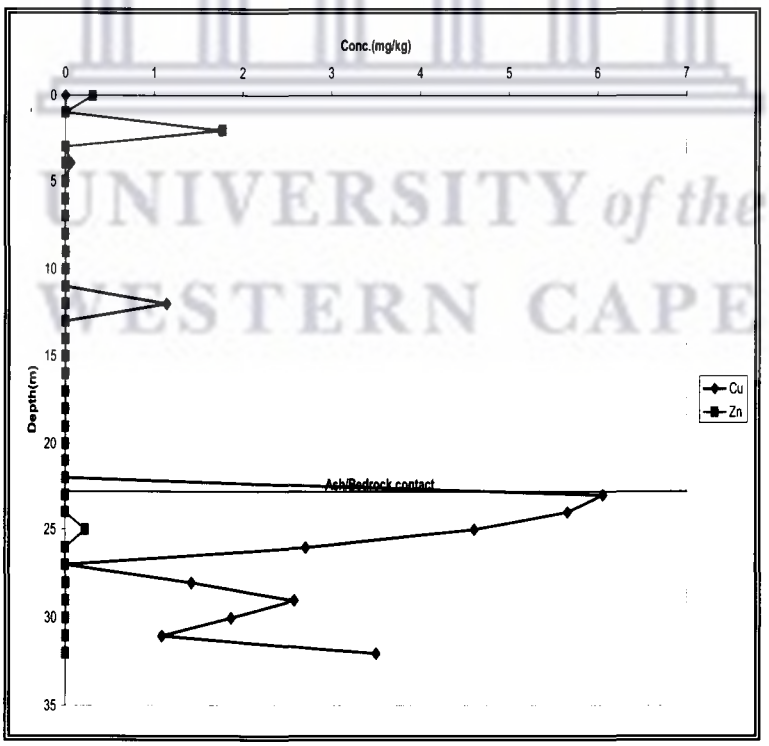

Fig. 5.11.4h: Trends of iron and manganese fraction Zn and Cu in the drilled core at Kragbron

The iron and manganese fraction trend of Zn only showed an increase at 2 m and 25 m depth. Most of the iron and manganese fraction of Cu was observed in the bedrock beyond 23 m and at 12 m depth of the ash column. The trends observed in the iron and manganese fractions of these elements could mean the non availability of the elements in iron and manganese soluble phase of the fly ash residue or their presence in very low amounts.

It was observed that the level of trace elements such as V, Cr, Co, Pb and Ni obtained was higher in the carbonate and iron and manganese extraction phases. This was probably due to the low pH of the leaching media, causing the gradual dissolution of the fly ash silicates and magnetic fractions with which the elements are incorporated. The availability of the elements in the water soluble and exchangeable fractions could be attributed to their presence on the surface of fly ash particles and also their association with the soluble oxides and hydroxide components in the fly ash.

5.11.5 Residual Fraction Phase

The residual fraction constitutes mainly the silicate bound fractions in the fly ash. It was determined by subtracting the sum of the four fractions for each analyte from the total metal content obtained from the total acid digestion (section 5.9).

The estimated residual fractions of the elements in the profile of the drilled ash core at Kragbron are shown in Fig. 5.11.5a to Fig. 5.11.5h.

Fig. 5.11.5a shows the residual fractions of Al, Si and Ca.

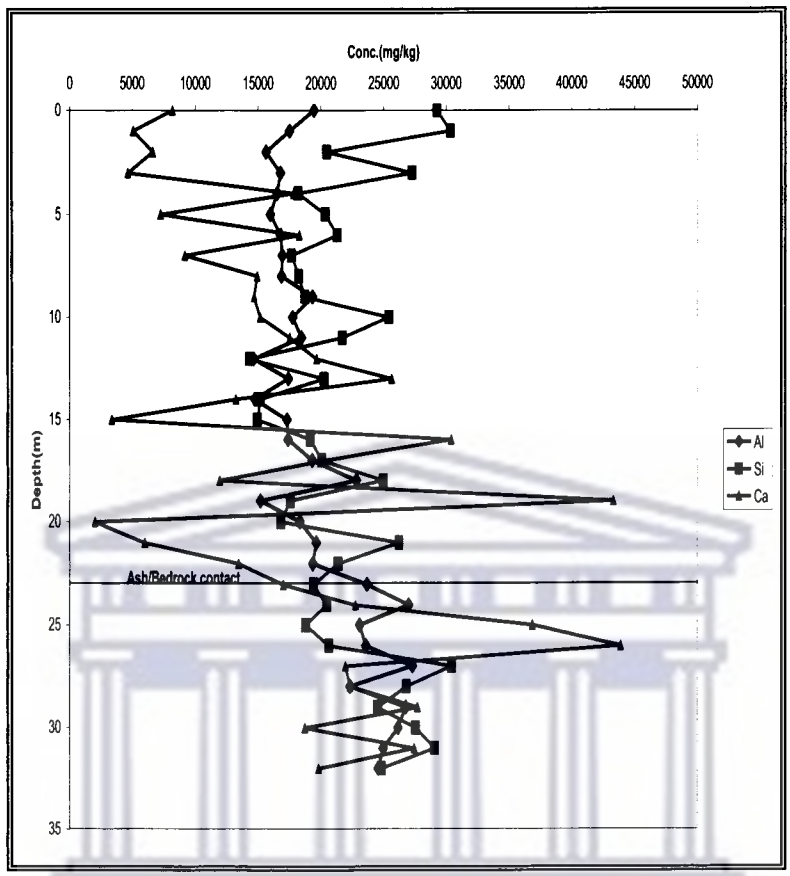

Fig. 5.11.5a: Trends of residual fraction Al, Si and Ca in the drilled core at Kragbron

The residual fractions of Al and Si were observed in very high concentrations (15000 mg/kg and 31000 mg/kg). This is an estimate of the residual fraction of the elements locked up in the silicate matrix of the fly ash particles. The dissolution of the solids bearing the elements can only take place under aggressive weathering conditions over time. The residual fraction of Ca was as high as 44000 mg/kg at some depths and showed depletion at other depths. The irregular trend observed in Ca could be attributed to the intervals experienced between the dumping of the various layers of ash. Layers with low residual Ca indicate intense weathering and dissolution of Ca bearing compounds in the silicate matrix of the ash. Layers with high residual Ca show that after the layer had been

dumped, there was enough time for the lime present in the ash to react with CO_2 from the atmosphere, thereby forming calcite an insoluble mineral.

Fig. 5.11.5b shows the residual fractions of Mg, K and Na in the profile of the drilled ash core at Kragbron.

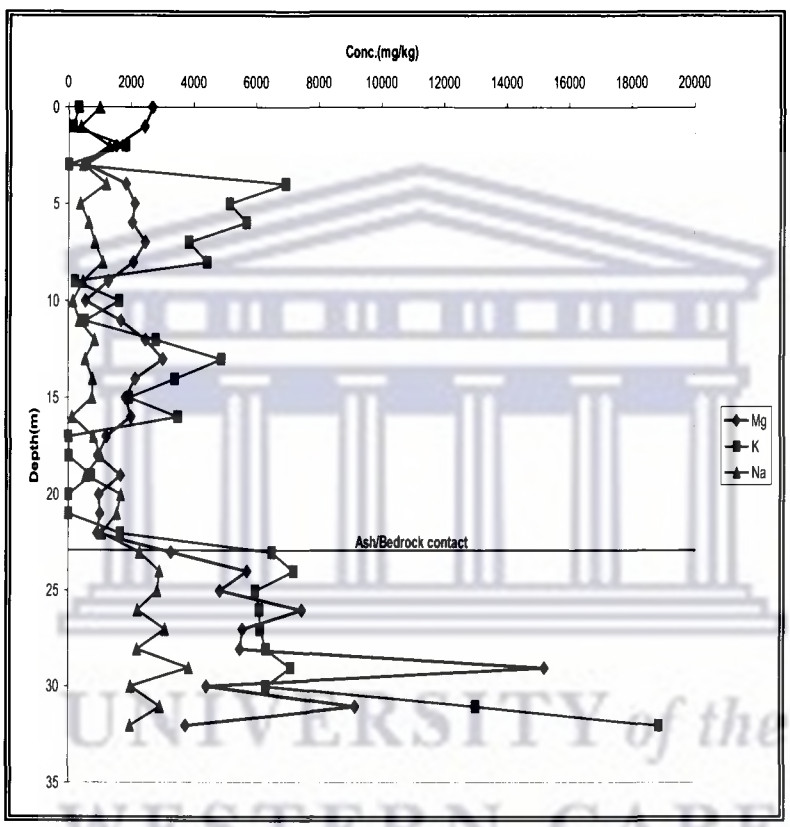

Fig. 5.11.5b: Trends of residual fraction Mg, K and Na in the drilled core at Kragbron

The residual fractions of Mg and Na showed a similar trend from the surface to 32 m depth of the drilled core. The residual fraction of Mg was as high as 3200 mg/kg and that of Na as high as 2000 mg/kg within the ash profile. The residual fractions of these elements were observed to be much higher within the bedrock layers (as high as 16000 mg/kg for Mg and 5000 mg/kg for Na). These trends observed in the residual fractions of Mg and Na shows the estimate of the elements still locked up in the silicate matrix of the

fly ash particles and in the bedrock. The residual fraction of K was also observed to be very high at some depths. It was as high as 7000 mg/kg within the ash profile and as high as 19000 mg/kg within the bedrock. Although it showed depletion at certain depths owing to the intense weathering patterns observed at those depths in the previous extraction phases (Fig. 5.11.2c, Fig. 5.11.3c and Fig. 5.11.4c). The very high level of the residual fraction K within the ash profile and the bedrock is an indication of its association with silicate bearing phases in fly ash and also in the bedrock.

Fig. 5.11.5c shows the residual fractions of B, Sr and Ti in the profile of the drilled ash core at Kragbron.

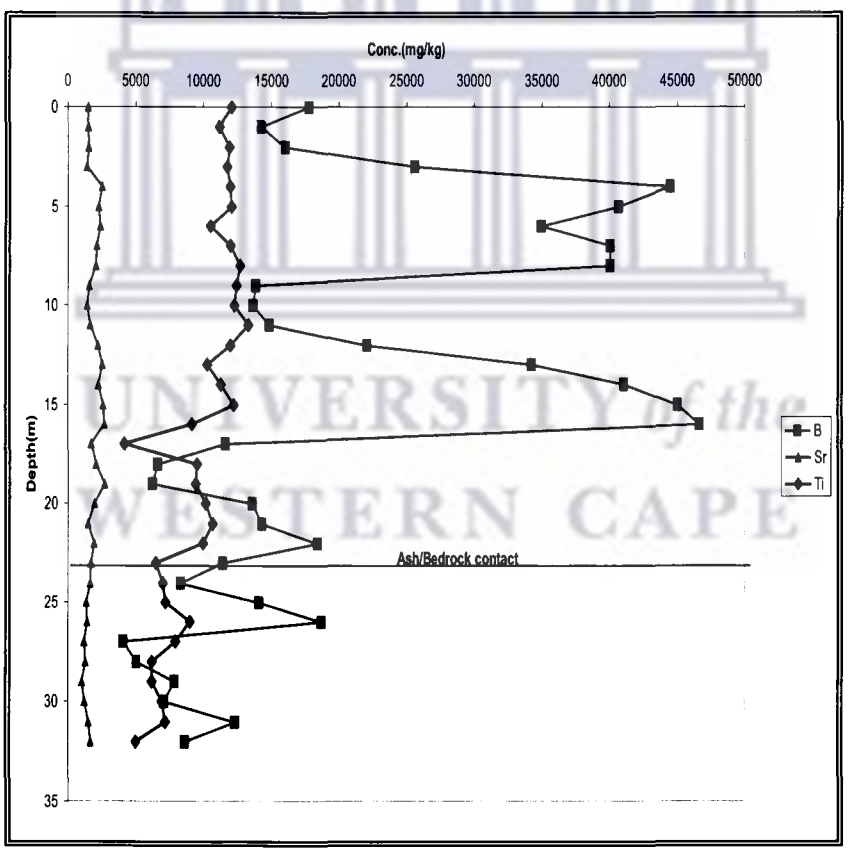

Fig. 5.11.5c: Trends of residual fraction B, Sr and Ti in the drilled core at Kragbron

The residual fraction of Sr showed a relatively constant trend from the surface to 32 m. The level of the residual fraction of Sr however was very much higher than the levels observed in the previous fractions (Fig. 5.11.2e, 5.11.3d and 5.11.4d). This showed the strong association of the element with the silicate bearing phases of the ash. The residual fraction level of B showed a huge portion of it associated with the glassy and silicate phase of the fly ash particles. Its concentration in the residual fraction was as high as 45000 mg/kg at some depths in the ash profile. The residual fraction of Ti showed values as high as 12000 mg/kg, also indicative of its association with the silicates present in the fly ash and the bedrock.

Fig. 5.11.5d shows the residual fractions of Mn and Ba in the profile of the drilled ash core at Kragbron.

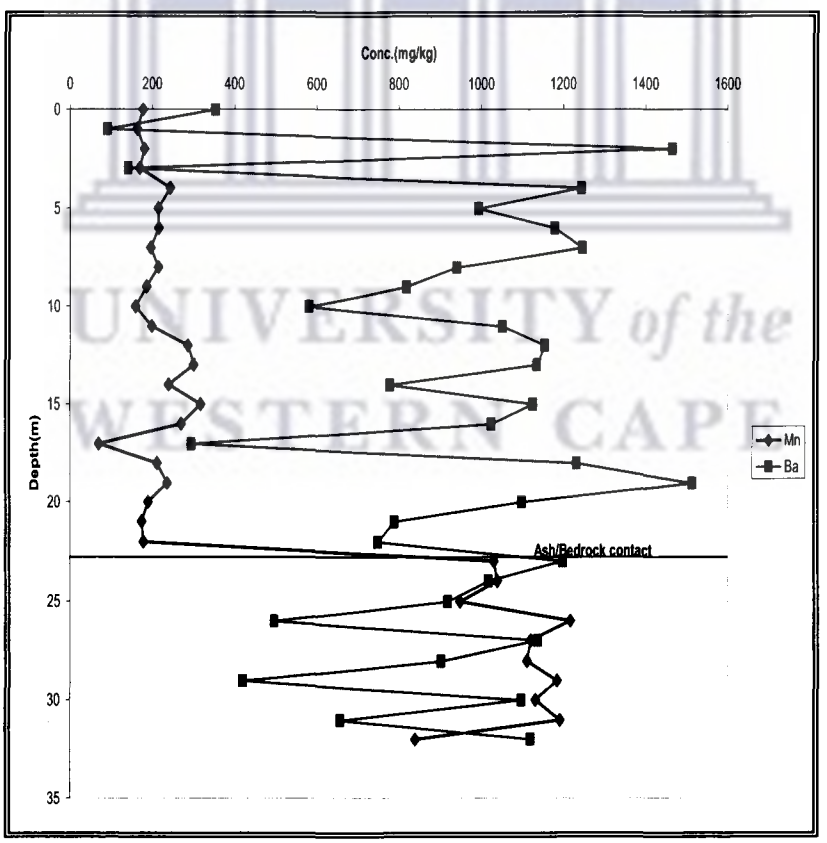

Fig. 5.11.5d: Trends of residual fraction Mn and Ba in the drilled core at Kragbron

The residual fractions of Mn and Ba showed higher values recorded for the elements down the ash profile than observed in the previous extraction phases. The residual fraction of both elements showed a lower value at 17 m depth (where it appeared enriched in the exchangeable fraction) (Fig. 5.11.2e). Higher values were observed for the residual fraction of Mn in the bedrock. The pattern of trend observed in Ba within the ash profile continued into the bedrock. The observation in the residual fractions of the elements indicates their incorporation into silicate minerals present in fly ash and the bedrock.

Fig. 5.11.5e shows the residual fractions of Cr and V in the profile of the drilled ash core at Kragbron.

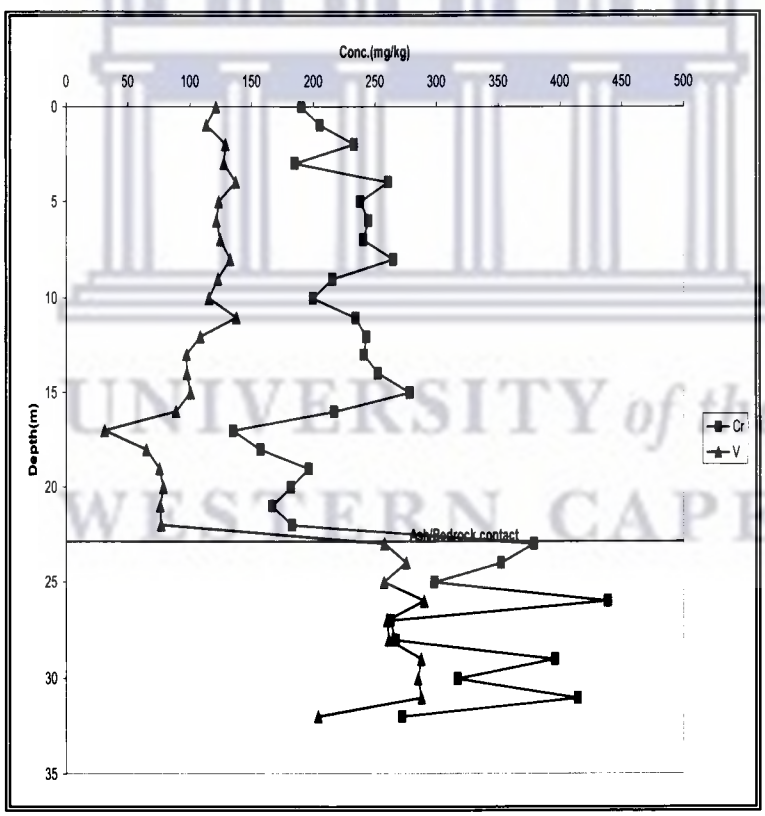

Fig. 5.11.5e: Trends of residual fraction Cr and V in the drilled core at Kragbron

The residual fraction of Cr and V was observed to be very high when compared to the values recorded in the previous extraction phases (Fig. 5.11.1e, Fig. 5.11.2f, Fig. 5.11.3g and Fig. 5.11.4g).

Fig. 5.11.5f shows the residual fractions of Cu, Ni and Zn in the profile of the drilled ash core at Kragbron.

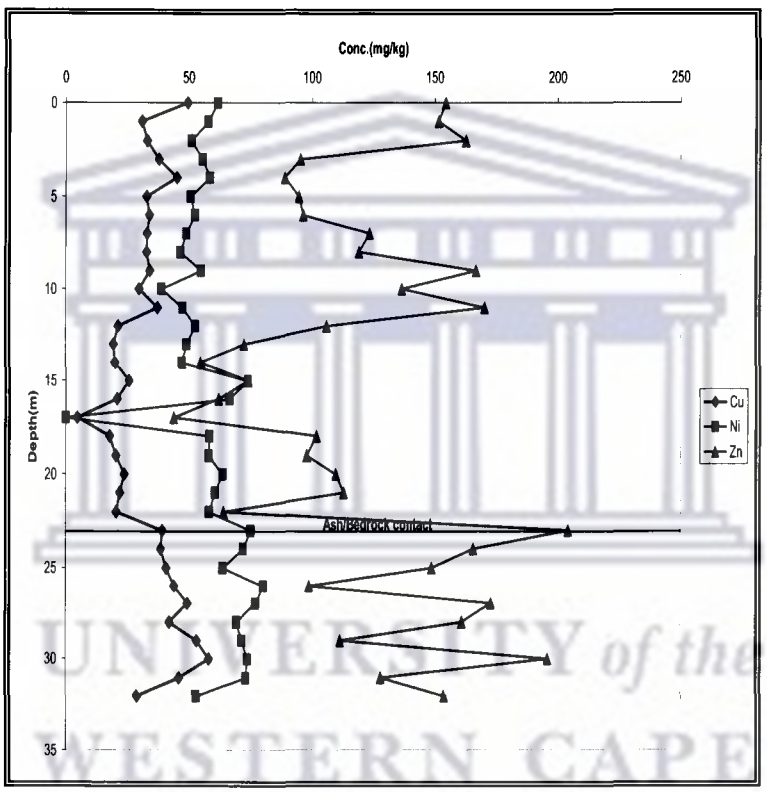

Fig. 5.11.5f: Trends of residual fraction Cu, Ni and Zn in the drilled core at Kragbron

The residual fractions of Cu, Ni and Zn were observed in higher concentrations than what was obtained in the previous extraction fractions (Fig. 5.11.1f, Fig. 5.11.2g, Fig. 5.11.3i, Fig. 5.11.4h and Fig. 5.11.4f). This could be attributed to the strong association of these elements with the silicate matrix of fly ash particles. High values were also observed for the residual fraction of these elements in the bedrock.

Fig. 5.11.5g shows the residual fractions of Mo, Cd, Co and Pb in the profile of the drilled ash core at Kragbron.

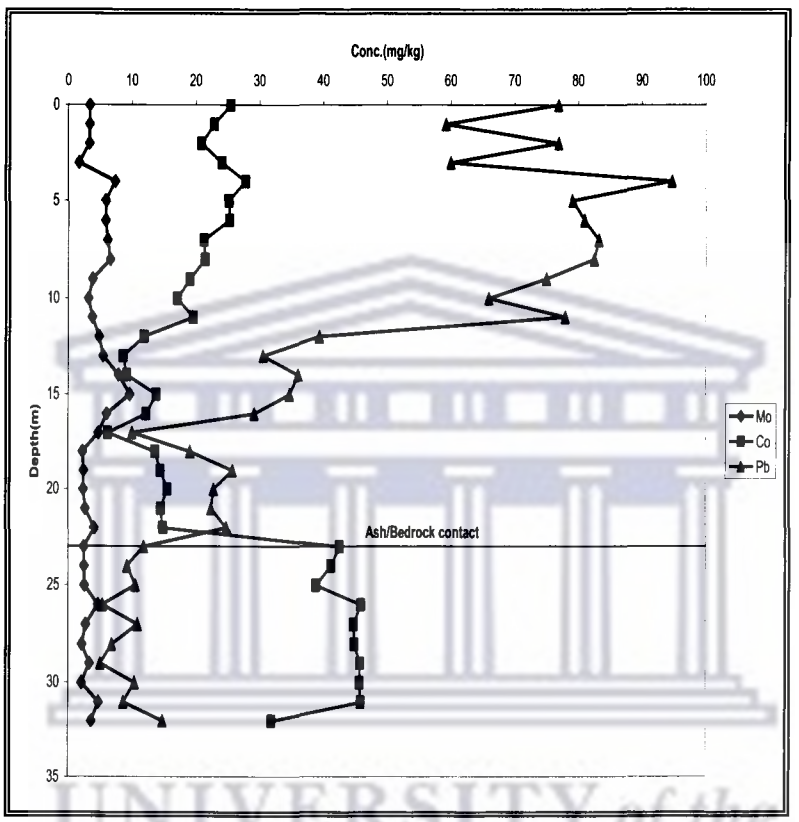

Fig. 5.11.5g: Trends of residual fraction Mo, Co and Pb in the drilled core at Kragbron

The residual fractions of Mo, Co and Pb were observed to be higher than the values obtained in the previous extraction phases (Fig. 5.11.1h, Fig. 5.11.2h, Fig.5.11.3f, Fig. 5.11.4e and Fig. 5.11.4f). The trend is indicative of their association with the silicate phases present in the fly ash and in the bedrock.

Fig. 5.11.5h shows the residual fractions of As and Se in the profile of the drilled ash core at Kragbron.

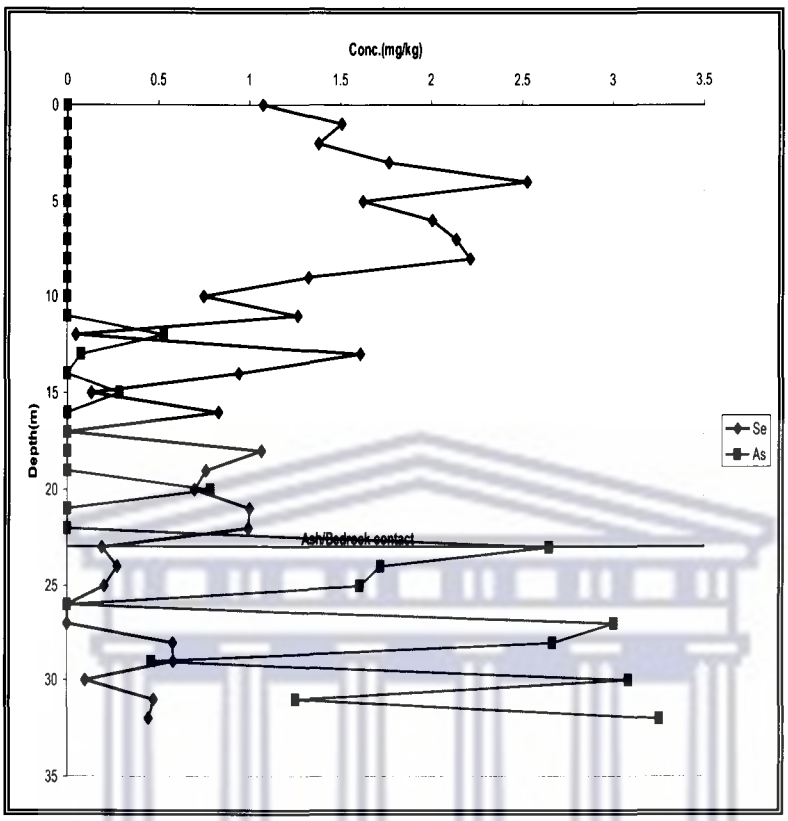

Fig. 5.11.5h: Trends of residual fraction As and Se in the drilled core at Kragbron

The trend observed in the residual fractions of As and Se shows that a large portion of these elements was associated with the non silicate phase of fly ash hence, the low values obtained within the ash profile (from the surface to 22 m). However, the trend observed for the residual fraction of As in the bedrock could be due to some components of the bedrock.

The mineralogy of Kragbron fly ash showed quartz, mullite and calcite as the major mineral phases present. A small amount of hematite was also observed at deeper depths (section 5.5). The high values obtained for the various elements especially trace and minor elements such as Zn, Cr, Pb, Cu, Co, Ni and B indicate a strong association of the elements with the silicate minerals present in Kragbron ash.

5.11.6 Percentage Distribution of Major and Trace Elements across the Various Fractions

The percentage of each element released per leaching phase was calculated as a fraction of the total amount and is shown below. Only the surface sample and the sample taken at 18 m were considered. The surface sample represents the most recent sample at the dump although it is between 15 to 20 yrs old. The moisture content was seen to be highest at 18 m, hence the sample was also considered as the release of the soluble components of fly ash was expected to be more at this depth.

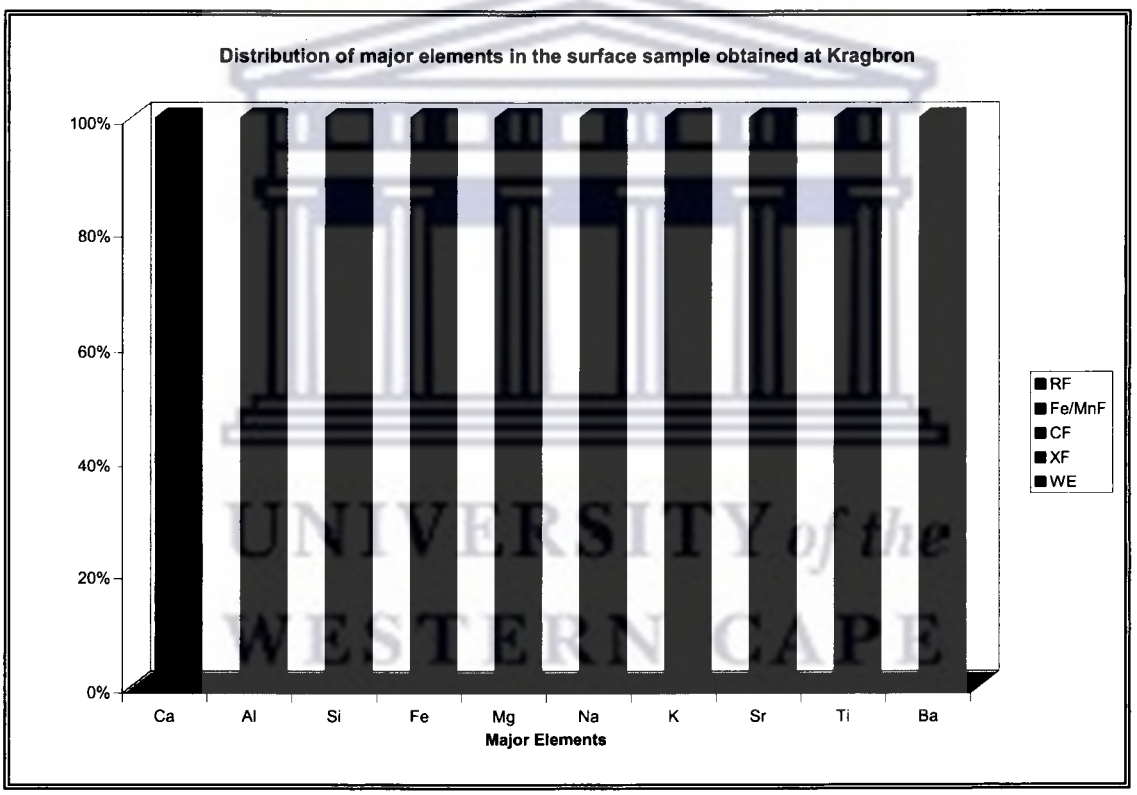

Fig.5.11.6a: Distribution of major elements in the surface sample obtained at Kragbron

In the above figure, about 50 % of Ca, 12.7 % of Mg, 20.8 % of Na, 66 % of K, 9.5 % of Sr and 22 % of Ba was released in the exchangeable fraction phase. The bulk of Si, Al, Fe and Ti were released in the residual fraction phase of the fly ash particles. The bulk of

Ca and K were in the exchangeable fraction while Na is the only element having appreciable release in the water soluble fraction phase (17.55 %).

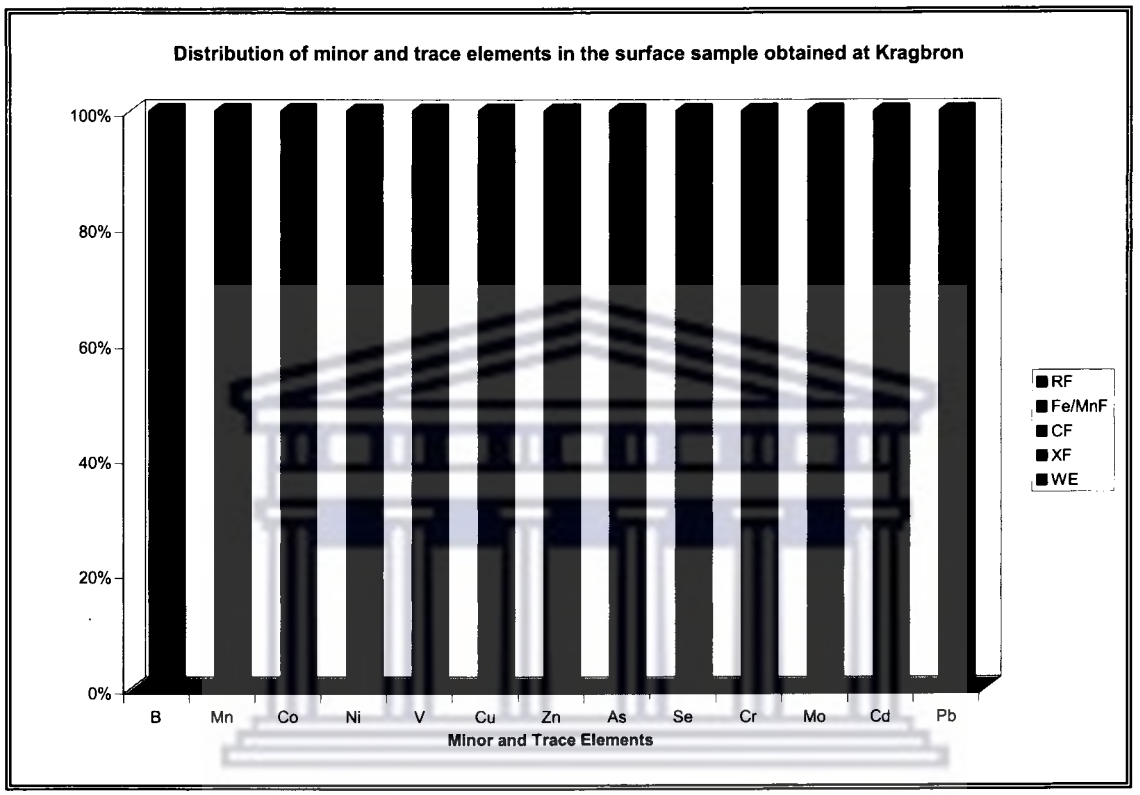

Fig.5.11.6b: Distribution of minor and trace elements in the surface sample obtained at Kragbron

Elements such as B, Ni, Co, Cu, Zn, Cr, Cd, Pb had their highest release in the residual fraction phase while As and Se showed their highest concentration in the exchangeable fraction phase (49 and 61.7 % respectively). Most trace elements are mobile under strongly alkaline or acidic pH with lower solubilities observed at neutral pH (Jankowski et al., 2006). The release of As and Se in the water soluble and exchangeable fraction phases is most likely due to their presence in oxyanions that are soluble in alkaline pH.

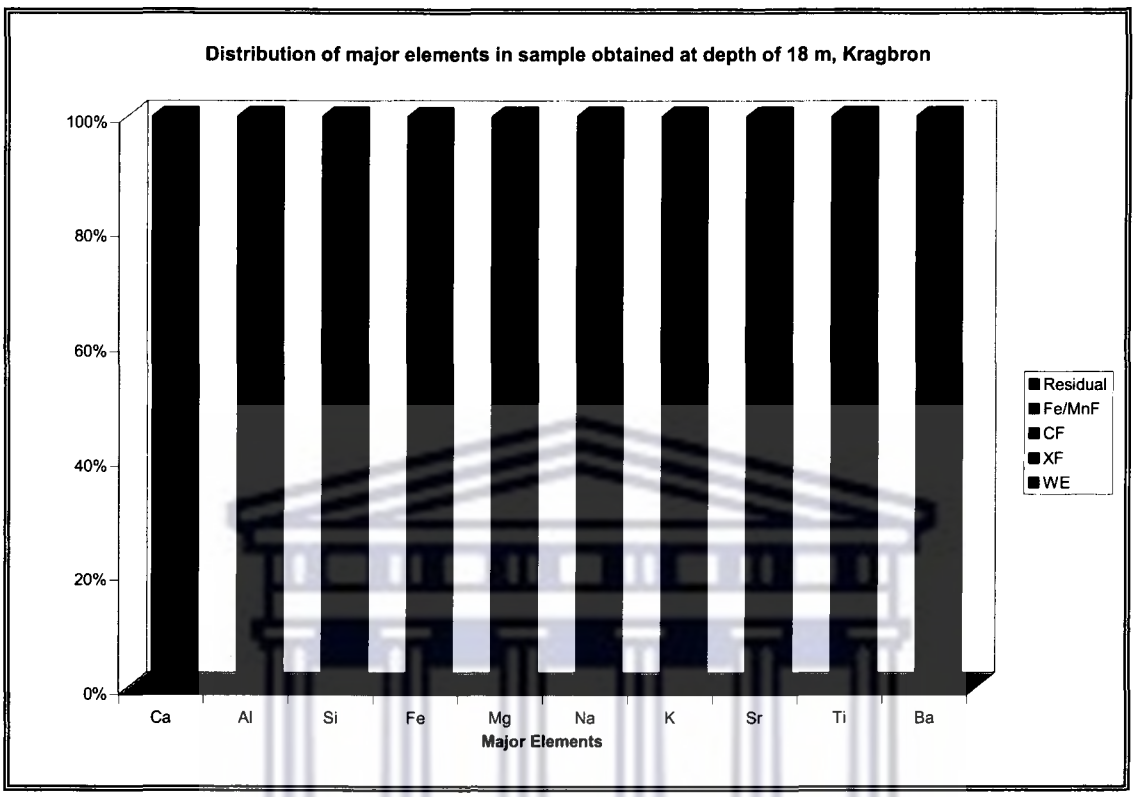

Fig.5.11.6c: Distribution of major elements in sample obtained at 18 m, Kragbron

Ca, K and Mg had the bulk of their concentration in the exchangeable fraction. The concentration of elements like Al, Si, Fe, Na, Sr, Ti and Ba was more in the residual fraction due to their association with the silicate matrix of the fly ash particles. The release of the elements were in slightly acidic (carbonate fraction, pH 5) to strongly acidic (iron and manganese fraction, pH 2) medium.

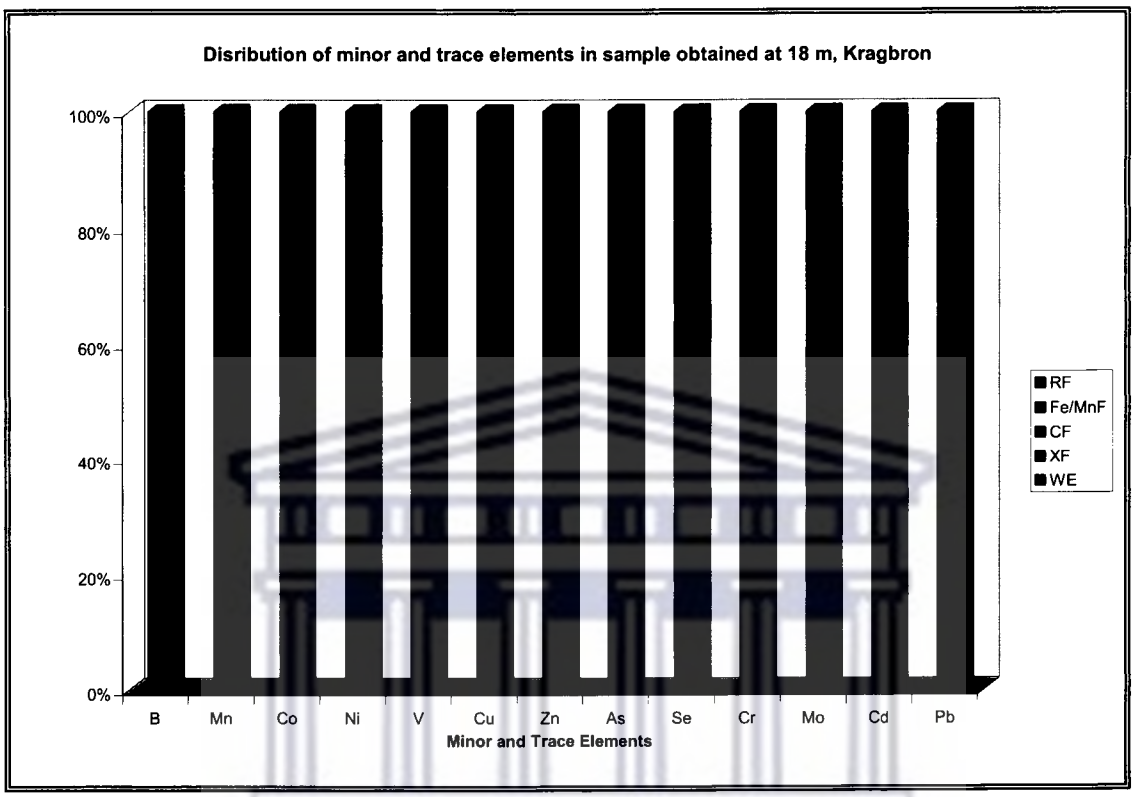

Fig.5.11.6d: Distribution of minor and trace elements in sample obtained at 18 m, Kragbron

As and Se are the elements likely to pose a threat to ground water due to their solubility in alkaline pH. The release of Mn, Co, Ni, V, Cu, Mo in the exchangeable fraction could be due to the long interaction of the fly ash particles with water at this depth because ordinarily the mobility of Cu and Ni ought to be lower in an alkaline medium. Cd is only available in the residual fraction phase of the fly ash particles which removes it as a threat to the ground water beneath the dump.

The tables for the above bar graphs can be found in Appendix T.

Chapter Six

Conclusions and Recommendations

This chapter gives a summary of the results presented in the previous chapter and also highlights significant findings in the study. Recommendations on some aspects are also made.

6.1 Overview

The aim of the study was to characterize Kragbron, the location of an old ash dump site in terms of its chemistry and mineralogy; to understand the elemental composition and leaching patterns when fly ash is interacted with de-ionized water; the various mineral phases with which metals are associated and finally draw conclusions about the long term effect of weathering at the dump site.

6.2 Borehole Profile

Analysis of the borehole profile revealed that the fly ash had a contact with the bedrock at 23 m. The total depth of the borehole was 32 m. It showed that the fly ash column ranged from the surface to 22 m and the bedrock from 24 m to 32 m. A mixture of ash, some clay and the bedrock was observed at a depth of 23 m. Literature study revealed the dump site to be underlain by Jurassic dolerite of the Karoo Supergroup.

6.3 Moisture content, Loss on ignition, pH and Electrical Conductivity

The wet method of disposal employed at the dump accounts for the high moisture content observed in the ash samples but the accumulation of water between 16 m and 22 m could be attributed to high infiltration rates and the impermeable dolerite layer at 23 m, preventing the vertical flow of water deeper into the drilled core.

The high carbon content observed in the deeper depths of the ash column (15 m to 22 m) shows that different burner conditions were employed during the life span of the power stations.

The Kragbron ash samples exhibited alkaline pH down the profile of the drilled core due to the lime content of the ash. pH was above 10 from 3 m to 22 m depth of the ash column. The formation of calcite at the surface of the dump accounts for the lower pH recorded.

The electrical conductivity of the samples ranged from 0.08 to 0.46 mS/cm. EC value was highest at 16 m. Moisture level was also high at this depth thus, aiding the release of water soluble species.

6.4 Fly Ash Interaction with De-ionized Water

Ca and B in the fly ash pore water leachates showed same pattern with the electrical conductivity at 2 m and 16 m. The oxides of these elements are readily soluble in water, hence their release. Other elements with similar trends at 16 m are Na, Ba, Mo, Ni and anions such as SO_4^{2-} and Cl^- . Al was observed in high concentrations at 15 m and 18 m due to its presence in soluble hydroxide form. Se, As, Cr, Zn, Cu and V showed a considerable release in the fly ash pore water leachates. Ti, Pb, Co, Fe, Mn and Mg were present in water insoluble phases in the fly ash samples.

The solubility of the major and minor elements in water was due to either their association with the surface of the fly ash particles or their presence in the soluble phase of their hydroxide or oxide forms. Some of the elements were also available in soluble sulphate and chloride bearing compounds such as $CaSO_4.2H_2O$, Na_2SO_4 and KCl (owing to the moderately high level of K at 16 m). The very low concentrations recorded for some of the trace elements in this study are as a result of their insolubility at alkaline pH and their association with the relatively insoluble silicate bearing phases of the fly ash samples. The presence of these metals in water therefore indicates a gradual weathering of the silicate minerals in the ash. The release of Si and Al is fairly constant down the drilled core at Kragbron except in the wet zone (16 m -20 m) where higher concentrations are seen. This shows the disintegration of the silicate bearing phases of the ash due to long contact with water.

6.5. Chemical Composition

XRF revealed the main constituents of the ash samples to be SiO_2, Fe_2O_3 and Al_2O_3. Lime content of < 10 per cent was also observed. The sum of the silicon, ferric and aluminum oxide content present in the Kragbron ash was > 70 % making the ash a class F fly ash according to ASTM C 618, 1993.

XRF analysis also showed that samples from the bedrock profile contained certain elements at much higher concentration as compared to fly ash and also other elements much lower than typical fly ash. Levels of Fe, Mg, Na, K and Mn were observed to be higher from 24 m to 32 m. Literature study confirms this as a normal occurrence in dolerite owing to its richness in ferromagnesian minerals. Dolerite weathers into clayey materials as observed at 23 m depth of the profile of the drilled borehole at Kragbron. The presence of clayey materials in the bedrock makes it impervious and thus prevents the migration of species from the ash column into the bedrock profile. The lack of migration of the species from the ash profile into the bedrock could also be the result of adsorption and co-precipitation of the species into secondary minerals formed within the ash profile over time.

6.6 Morphology and Mineralogy

The morphology of the ash samples showed spherical rounded particles and some agglomerations at the surface of the ash dump indicating a degree of weathering due to exposure to air and rainwater. Irregularly shaped ash particles and some agglomeration due to progressive weathering dominated the rest of the micrographs. Quantitatively, the elements in the fly ashes are predominantly Si, Al, Fe, Ca and O as determined by XRF and EDS. Agglomerated and irregularly shaped particles dominated the samples from 23 m to 32 m. EDS spot analysis of sample at 27 m revealed the presence of Al, Ca, Si, Ti, K and Fe in varying amounts confirming the presence of minerals anorthite, diopside and quartz in the bedrock material as observed in XRD.

XRD revealed the primary minerals present in the fly ash samples to be quartz and mullite. The ingress of CO_2 in the ash overtime upon disposal led to the formation of calcite. Hematite observed at 22 m is most likely due to a mix up of the ash and bedrock at 23 m during the original construction of the disposal site. The major minerals revealed to be present in dolerite (bedrock) are quartz, anorthite and diopside.

6.7 Acid Digestion of Kragbron Ash Samples

Digestion of the fly ash samples from Kragbron in acid released Al, Si, Ca, Fe and B in high concentrations from the samples of fly ash profile (surface to 22 m depth). The concentration of Mg, Na, Fe and K was higher beyond 23 m due to the presence of clino-pyroxenes such as diopside, feldspars such as anorthite and some dendritic iron oxide in the bedrock.

The results obtained from the ICP-MS analysis of the surface sample digestate was compared with the result obtained using XRF on same sample. Both results showed similar trends for Al, Si and Na although concentration was lower with the ICP-MS. The levels of Ca, Fe, Mg and K were higher in the ICP-MS than in XRF. This ought not to be since these elements are found available in reasonable quantities in fly ashes. This elevated concentrations observed with the ICP-MS is likely due to interference and matrix effects. Generally, the results obtained using XRF are more reliable because the technique gives the composition of the solid sample and also the chances of sample contamination are minimal.

6.8 Cation Exchange Capacity

The CEC values obtained was observed to be high between 14 m and 22 m of the ash column. This indicates a region where transient mineral phases in the ash dump can trap available cations and anions in solution due to surface adsorption or exchange processes. B, Na, Ca, Al and SO_4^{2-} in the pore water extracts exhibited the same trend as seen in the CEC. The highest release of these species coincided with the region of high CEC, making them active participants in the remineralization process taking place between 14 m and 22 m.

6.9 Sequential Extraction

Most of the major elements were found to be associated with the carbonate, iron and manganese and residual fraction phases. The trend observed for Ca, Mg, K, Sr and Si in the exchangeable fraction phase and Al, Si, Ca, Mg, Ba and Sr in the carbonate fraction phase showed a similarity with the trend observed in the CEC between 14 m and 22 m, thus making these elements a part of the remineralization process due to surface adsorption and exchange processes. Ca, Al, Si, Mg and Na were also found to be associated with the water soluble fraction phase showing their presence in readily soluble forms. As and V showed appreciable release in the exchangeable fraction and carbonate fraction, Cr, Zn, Cu, B and Ti levels were a little bit high in the carbonate fraction and a higher release was observed for Cr, V, Ti and B in the iron and manganese fraction. This shows that the release of trace elements is mostly governed by the dissolution of the mineral phase with which they are associated. Minor and trace elements such as B, Sr, V, Cr, Zn, Cu, Se and As were available in considerable amounts in the water soluble fraction of the ash samples. This is an indication that under normal conditions these elements could be released into solution causing them to migrate deeper into the dump. The potentially harmful element Cd was not found available in the water soluble fraction but was only present in the residual fraction phase. As and Se were both available in appreciable quantities in all the fractions except in the residual fraction phase. The concern at the disposal site would be the placement of the ash materials under aggressive environments (pH 2 and 5), which would result in As mobilization due to dissolution at low pH.

Findings from this study showed that weathering due to infiltration of rainwater and water from the ash slurry play a huge role in the dissolution of solids and the migration of species down the ash dump. The high cation exchange capacity observed between 14 m and 22 m serves as a trap for mobile cations and anions released into solution in the ash column. The mobile species are adsorbed through the process of remineralization, thereby making them immobile. The contact with the bedrock at 23 m also acts as a lining beneath the ash dump due to its impervious nature and it has prevented the movement of mobile species deeper into the ground. The sequential extraction procedure

was very useful in the study as it showed the various mineral phases with which the elements found in fly ashes are associated, making possible the understanding of their mobility tendencies.

6.10 Significance of the study

The study shows that there is mobility and movement of species present in the ash down the dump. It was observed that elements were leached out of the ash at both alkaline and acidic pH and their movement down the dump hampered, by the formation of secondary minerals (remineralization process) at certain depths within the dump. But over time, with high moisture and a low pH, these mineralized zones experienced dissolution causing the trapped elements to be mobile again. The geology of the area showed that Kragbron is underlain with dolerite. The contact point between the ash profile and the bedrock (dolerite) was at 23 m. The results obtained from the study did not show the migration of the mobile elements past 23 m due to the impermeable nature of the dolerite but migration into subsurface waters and soils cannot be ruled out.

6.11 Recommendations

The lining of ash dumps and regular monitoring exercises at the site of disposal are recommended to industry. The lining will serve as an effective measure in retaining the potentially harmful species within the ash dump as it has been observed in this study and the latter would serve as a check for leakages or runoffs into subsurface streams and rivers.

Also, combustion systems that would completely burn coal are advised as this will reduce the amount of residual carbon in fly ash and improve its quality.

Due to limitation in funds, only the XRD analysis of some selected samples from the ash dump was done. It is recommended that the XRD analysis on all the samples including a fresh sample of the bedrock be carried out as it would aid the proper understanding of the mineralogy at each depth of the drilled core.

Modeling is also recommended to know the various minerals formed due to remineralization as a result of the high cation exchange capacity observed between 14 m and 22 m of the ash column.

Future research to understand the adsorption and co-precipitation of species into secondary minerals resulting in the lack of migration into the bedrock is also recommended.

REFERENCES

ACI Committee 116, ACI 116R – 00, 2000. Cement and Concrete terminology. American Concrete Institute; 73.

Adriano, D.C., Page, A.L., Elseewi, A.A., Chang, A.C., Straugan, I., 1980. Utilization and disposal of fly ash and other coal residues in terrestrial ecosystems; a review. *Journal of Environmental Quality* 9: 333-344

Álvarez-Ayuso, E. and Querol, X., 2007. Stabilization of FGD gypsum for its disposal in landfills using amorphous aluminium oxide as a fluoride retention additive. *Chemosphere* 69: 295-302

Álvarez-Ayuso, E. and Querol, X., 2008. Study of the use of coal of fly ash as an additive to minimize fluoride leaching from FGD gypsum for its disposal. *Chemosphere* 71: 140-146.

American Society for Testing and Materials 1993: ASTM C 618: Standard speciation for fly ash and raw or calcined natural pozzolan for use as a mineral admixture in Portland cement concrete. In: Annual Book of ASTM Standards. ASTM, Philadelphia, PA.

ASTM C 618, 2001. Standard specification for coal fly ash and raw calcined natural pozzolan for use as a mineral admixture in concrete. ASTM C 618 – 2001. In: Annual book of ASTM Standard 4: 2.

American Coal Ash Association (ACAA) 1996. Coal Combustion By-products Survey, Virginia: ACAA; 1997.

Ainsworth, C.C., Mattigod, S.V., Rai, D., Amonette, J.E., 1993. Detailed Physical, chemical and mineralogical analyses of selected coal and oil combustion ashes. Electric Power Research Institute, Palo Alto, CA.

Asokan, P., Saxena, M., Asolekar, S.R., 2005. Coal combustion residues- environmental implications and recycling potentials. *Resources, Conservation and Recycling* 43: 239-262.

Azzie, B. A-M. 2002: Coal mine waters in South Africa: Their geochemistry, quality and classification. *PhD Thesis*, University of Cape Town, South Africa.

Beater, B.E and Frankel, E., 1965. Alterations in chemical composition during the progressive weathering of Dwyka Tillite and dolerite in Natal, Proceeding Symposium. African Sugar Technologists Association. 1-4.

Bell, F.G and Jermy, C.A., 2000. The geotechnical characters of some South African dolerites especially their strength and durability. *Quarterly Journal of Engineering Geology and Hydrogeology.* Part 1 33: 59-76

Bhattacharyya, S., Donahoe, R.J and Patel, D., 2009. Experimental study of chemical treatment of coal fly ash to reduce the mobility of priority trace elements. *Fuel* 88: 1173-1184.

Bilski, J.J., Alva, A.K., Sajwan, K.S., 1995. Fly ash. In. Reckcigl, J.E (Ed.), "Soil Amendments and Environmental Quality". CRC Press Inc., Boca Raton, Fl, 327-363.

Chapman, H.D., 1965. Cation exchange capacity. In: C.A Black (ed.) "Methods of soil analysis" – Chemical and microbiological properties. *Agronomy* 9: 891-901.

Choi, S.K., Lee, S., Song, Y.K., Moon, H.S., 2002. Leaching characteristics of selected Korean fly ashes and its implications for the ground water composition near the ash disposal mound. *Fuel* 81: 1083-1090.

Coal. Available online at http://www.dme.gov.za/energy/coal.stm . Last accessed on the 10th of February, 2010.

Coal, origin of coal, composition of coal, properties and reactions, environmental problems associated with the burning of coal. Available online at http://science.jrank.org/pages/1533/coal-combustion-coal.html . Last accessed on the 10th of February, 2010.

Comans, R.N.J., Meima J.A., Geelhoed, P.A., 2000: Reduction of contaminant leaching from MSWI bottom ash by addition of sorbing components, *Waste Management* 20: 125–133.

Cox, J.A., Lundquist, G.L., Przyjazvy, A., Schmulbach, C.D., 1978. Leaching of boron from coal ash. *Environmental Science Technology* 12: 722-723.

Criado, M., Fernandez-Jimenez, A., Palomo, A., 2007. Alkali activation of fly ash: Effect of the SiO_2/Na_2O ratio, Part 1: FTIR study. *Microporous and Mesoporous Materials* 106: 180-191.

Dabrowski, J.M, Ashton, P.J., Murray, K., Leaner, J.J., Mason, R.P., 2008. Anthropogenic mercury emissions in South Africa: coal combustion in power plants. *Atmospheric Environment* 42: 6620-6626.

Davison, R.L., Natusch, D.F.S., Wallace, J.R., Evans, C.A., 1974. Trace elements in fly ash: dependence of concentration on particle size. *Environmental Science and Technology* 8: 1107-1113.

Dionex 1998: Application notes on conductivity detection. Dionex DX-120 Ion Chromatography Operator's Manual, Dionex. Overview of principles behind conductivity and concentration relation of ionic solutions, as well as description of auto self-regenerating suppression module, and eluent composition for anion analysis.

(DME) Department: Minerals and Energy, South Africa Mineral Economics Directorate (Minerals Bureau), 2004. Operating and developing coal mines in the Republic of South Africa 2003. Directory D2/2004.

Drever I. James 1997: "The geochemistry of natural waters: surface and groundwater environments". 3rd Edition. Published by Prentice Hall, Inc. New Jersey 436.

Dudas, M.J and Warren, C.J., 1987. Submicroscopic model of fly ash particles. *Geoderma* 40: 101-114.

Duncan, A.R. and Marsh, J.S., 2006. The Karoo Igneous Province. In: Johnson, M.R., Anhaeusser, C.R., Thomas, R.J (Eds.), "The Geology of South Africa". Geological Society of South Africa, Johannesburg/Council for Geoscience, Pretoria, 501-520.

Durgun, D. and Genc. A, 2009. Effects of caol properties on the production rate of combustion solid residue. *Energy* 34: 1976-1979.

Eary, L.E., Rai, D., Mattigod, S.V., Ainsworth, C.C., 1990. Geochemical factors controlling the mobilization of inorganic constituents from fossil fuel combustion residues: II. Review of the minor elements. *Journal of Environmental Quality* 19: 202-214.

Elseewi, A.A., Page, A.L., Grimm, S.B., 1980. Chemical characterization of fly ash aqueous systems. *Journal of Environmental Quality* 9: 424-428

Erol, M., Genç, A., Oveçoglu, M.L., Yucelen, E., 2000. Characterization of a glass-ceramic produced from thermal power plant fly ashes. *Journal of European Ceramic Society,* 20: 2209-2214.

Erol, M., Demirler, U., Kuçukbayrak, S., Ersoy-Meriçboyu, A., Oveçoglu, M.L. 2003. Characterization investigations of glass – ceramics developed from Seyitomer thermal power ash plant. *Journal of the European Ceramic Society* 23: 757-763.

Eskom: Understanding electricity, 2006. Available online at http://www.eskom.co.za/live/content.php?CatergoryID=96 . Last accessed on the 20th of February, 2010.

Eskom Heritage: Taaibos power station. Available online at http://heritage.eskom.co.za/heritage/taaibos.htm. Last accessed on the 20th of February, 2010.

Fatoba, O.O., 2007. Chemical compositions and leaching behaviour of some South African fly ashes. Unpublished MSc thesis, Department of Chemistry, University of the Western Cape, South Africa.

Fishman, N.S., Rice, C.A., Breit, G.N., Johnson, R.D., 1999. Sulphur-bearing coatings on fly ash from a coal fired power plant: Composition, origin and influence on ash alteration. *Fuel* 78: 187-196.

Fruchter, J.S., Rai, D., Zacchara, J.M. 1990: Identification of solubility-controlling solid phases in a large fly ash field lysimeter, *Environmental Science Technology* 24: 1173-1179.

Fulekar, M. H and Dave, J.M., 1986. An environmental problem. *International Journal of Environmental Studies 26*: 191-215.

Furr, A.K., Stoewsand, G.S., Bathe, C.A., Gutenmann, W.H., Lisk, D.J., 1975. Multi-element residues in tissues of guinea pigs fed sweet clover grown on fly ash. *Arch Environment Health* 30: 244-248.

Furr, A.K., Parkinson, T.F., Hinrichs, R.A., D.R. Van Campen, C.A. Bache, W.H. Gutenmann, L.E. St. John, Jr., I.S. Pakkala, and D.J. Lisk. 1977: National survey of elements and radioactivity in fly ashes: absorption of elements by cabbage grown in fly ash-soil mixtures. *Environment Science Technol*ogy 11: 1104-1112.

Fytianos, K and Shroder, H., 1997. Determination of polychlorinated dibenzodioxins and dibenzofurans in fly ash. *Chromatographia* 46: 280-284.

Fytianos, K., Tsaniklidi, B., Voudrias, E., 1998. Leachability of heavy metals in Greek fly ash from coal combustion. *Environment International* 24: 477-486.

Garavaglia, R and Caramuscio, P. 1994: Coal fly-ash leaching behaviour and solubility controlling solids, in: Environmental Aspect of Construction with Waste Materials. Wascon, Elsevier, Amsterdam, 87-102.

Gurupira, T., Jones, C.L., Howard, A., Lockert, C., Wandell, T., Stencel, J.M., 2001. New products from coal combustion ash: Selective extraction of particles with density < 2. In 2001 International Ash Utilization Symposium, Center for Applied Energy Research – University of Kentucky, Paper # 44

Handke, M., Mozgawa, W., Nocun, M., 1994. Specific features of IR spectra of silicate glasses. *Journal of molecular structure* 325: 129-136

Hajarnavis, M.R and Bhide. A. D., 1999. Leacheability and toxicity of heavy metals from fly ash. *Indian Journal of Environmental Health* 41: 326-332.

Halstead, W.J., 1986: Use of fly ash in concrete. National Highway Research Program Synthesis of Highway Practice #127. Washington, DC; Transportation Research Board.

Harvey, R.D and Ruch, R.R., 1986. Mineral matter in Illinois and other US coal. In: Vorres, K.S. (eds) 'Mineral matter and ash in coal'. American Chemical Society Symposium Series, 301, Washington D.C

Haw, M. and Hughes, A., 2007. Clean energy and development for South Africa. Background data Report 1/3. Energy Research Centre, University of Cape Town. Available online at http://www.erc.uct.ac.za/Research/publications/07Haw-Hughes%20Clean%20energy%20&% 20development%20-%201.pdf

Haynes, R.J., 2009. Reclamation and revegetation of fly ash disposal sites- Challenges and research needs. *Journal of Environmental Management 90*: 43-53.

Heemun, J. and Etsell, T.H., 2005. Morphological and mineralogical characterization of oil sands fly ash. *Energy and Fuels* 19: 2121-2128.

Helmuth, R., 1987. Fly ash in Cement and Concrete. Portland Cement Association, Skokie, IL.

Hessley, R.K., Reasoner, J.W., Riley, J.T., 1986. "Coal Science: An introduction to chemistry technology and utilization". John Wiley & Sons, New York. NY.

Hower, C.J., Robi, T.L., Thomas, G.A., 1999. Changes in the quality of coal combustion by-products produced by Kentucky power plants, 1978-1997: *Consequences of clean air act directives* 78: 701-712.

Hubbard, F.H., McGill, R.J., Dhir, R.K., Ellis, M.S., 1984. Clay and pyrite transformations during ignition of pulverized coal. Mineralogical Magazine 48: 251-256.

Hulett, L.D., Weinberger, A.L., Northcut, K.J., Ferguson, M., 1980. Chemical species in fly ash from coal-burning power plants. *Science* 210: 1356-1358.

International energy agency (IEA) 2005. Profiles: Cement and concrete- benefits and barriers in coal fly ash utilization. PF05-01.
http://www.greenspec.co.uk/documents/materials/cementsub/flyash.pdf

International energy outlook (IEO) 2009. DOE/EIA- 0484 2009. www.eia.doe.gov/oiaf/ieo/index.html

Iyer, R., 2002. The surface chemistry of leaching coal fly ash. *Journal of Hazardous Materials* 93: 321-329.

Jala, S and Goyal, D., 2006. Fly ash as a soil ameliorant for improving crop production- a review. *Bioresource Technology* 97: 1136-1147.

Jambhulkar, H.P and Juwarkar, A.A., 2009. Assessment of bioaccumulation of heavy metals by different plant species grown on fly ash dump. *Ecotoxicology and Environmental Safety 72*: 1122-1128.

Jankowski, J., Ward, C.R., French, D., Groves, S., 2006. Mobility of trace elements from selected Australian fly ashes and its potential impact on aquatic ecosystems. *Fuel* 85: 243-256.

Jiang, J., Zhang, C., Chan, M., Zhang, Y., 2009. Assessing the chemical behaviour of metals in municipal solid waste incineration fly ash using an enhanced CO_2 absorption. Environmental Engineering Science 26: 1615-1621.

Jianjun, C and Yuncong, L., 2006. Coal fly ash as an amendment to container substrate for *Spathiphyllum* production. *Bioresource Technology* 97: 1920-1926.

Johnson, M.R., van Vuuren, C.J., Visser, J.N.J, Cole, D.I., Wickens, H. de V., Christie, A.D.M., Roberts, D.L, Brandl, G., 2006. Sedimentary rocks of the Karoo Supergroup. In: Johnson, M.R., Anhaeusser, C.R., Thomas, R.J (Eds.), "The Geology of South Africa".

Geological Society of South Africa, Johannesburg/Council for Geoscience, Pretoria, 461-499.

Jourdan, F., Feraud, G., Bertrand, H., Kampunzu, A.B., Tshoso, G., Le Gall, B., Tiercelin, J.J., Capiez, P., 2004. The Karoo triple junction questioned: evidence from Jurassic and Proterozoic $^{40}Ar/^{39}Ar$ ages and geochemistry of the giant Okavango dyke swarm (Botswana). *Earth and Planetary Science Letters* 222: 989-1006

Kabata-Pendias, A. and Pendias, H., 1984. Trace elements in soils and plants. 2nd Edition. CRC Press, Boca Raton, Florida. 315

Kalnicky D.J and Singhvi R. 2001: Field portable XRF analysis for environmental samples. *Journal of Hazardous Materials* 83: 93-122. Khan M.R and Khan, M.W., 1996. Effect of fly ash on growth and yield of tomato. *Environmental Pollution* 92: 105-111.

Khan, M.R and Khan, M.W., 1996. The effect of fly ash on plant growth and yield of tomato. *Environmental Pollution* 92:105-111

Kim, A.G., 2002. Physical and chemical CCB characteristics Coal combustion by-products and western coal mines: A technical interactive forum. Denver, CO: US DOI, Office of Surface Mining; 2002

Kim, A.G., Kazonich, G., Dahlberg, M., 2003. Relative solubility of cations in class F fly ash. *Environmental Science Technology* 37: 4507-4511.

Kim, A.G and Kazonich, G., 2004. The silicate/non silicate distribution of metals in fly ash and its effect on solubility. *Fuel* 83: 2285-2292.

Killingley, J., McEvoy, S, Dokumcu, C., Stauber, J., Dale, L., 2000. Trace element leaching from fly ash from Australian power stations. End of grant report, Australian coal

association research program, project C8051, CSIRO division of energy technology pp. 98.

Kirby, C.S. and Rimstidt, J. D. 1994: Interaction of municipal solid waste ash with water. *Environmental Science Technology* 28: 443 – 451.

Kirby, J., Maher, W., Krikowa, F., 2001. Selenium, cadmium, copper, and zinc concentrations in sediments and mullet (*Mugil cephalus*) from the Southern Basin of Lake Macquarie, NSW, Australia. *Archives of Environmental Science and Toxicology* 40: 246-256.

Klerk de M, 2007. Resistivity Imaging Survey. Kragbron Power Plant. July 2007. martindeklerk@whalemail.co.za.

Kot, A. and Namiesnik, J., 2000. The role of speciation in analytical chemistry. *Trends in analytical chemistry* 19: 69-79.

Kruger, R.A and Kreuger, J.E., 2005. Historical development of coal ash utilization in South Africa. http://www.flyash.info/2005/204kru.pdf. [last accessed on October 8, 2009]

Kukier, U., Ishak, C.F, Summer, M.E and Miller, W.P., 2003. Composition and element solubility of magnetic and non magnetic fly ash fractions. *Environmental Pollution* 123: 255-266.

Kutchko, B.G and Kim, A.G., 2006. Fly ash characterization by SEM-EDS. *Fuel* 85: 2537-2544.

Landman, A.A., 2003. Aspects of solid-state chemistry of fly ash and ultramarine pigments. University of Pretoria etd.

Laursen, K., 1997. Characterisation of minerals in caol and interpretations of ash formation and deposition in pulverized coal fired boilers. Ph.D. Thesis. Geological Survey of Denmark and Greenland. Report 1997/65

Lin, Y.K: Compressibility, strength and frost susceptibility of compacted fly ash (PhD Thesis). Michigan: University of Michigan; 1971.

Lothia, R.P and Joshi, R.C., 1995: Mineral admixtures. In Concrete Admixtures Handbook-Properties, Science, and Technology, edn 2. Edited by Ramachandran, V.S. Parkridge, NJ: Noyes Publications; 657-739.

Lund, W., 1990. Speciation analysis – why and how? *Fresenius' Journal of analytical chemistry 337*: 557-564.

Marsh, J.S., 1991. REE fractionation and Ce anomalies in weathered Karoo dolerite. *Chemical Geology* 90: 189-194.

Martinez-Tarazona M.R and Spears D.A. 1996: The fate of trace elements and bulk minerals in pulverized coal combustion in power stations. *Fuel Processing Technology* 47: 79-92.

Matsi, T and Keramidas, V.Z., 1999. Fly ash application on two acid soils and its effect on soil salinity, Ph, B, P and on ryegrass growth and composition. *Environmental Pollution* 104: 107-112.

Matsunaga, T., Kim, J.K., Hardcastle, S, Rohatgi, P.K., 2002. Crystallinity and selected properties of fly ash particles. *Material Science and Engineering* A325: 333-343.

Mattigod, S.V., Rai, D., Eary, L.E., Ainsworth, C.C., 1990. Geochemical factors controlling the mobilization of inorganic constituents from fossil fuel combustion

residues: I. Review of the major elements. *Journal of Environmental Quality* 19: 187-201.

McCarthy, G.J., Solem, J.K., Manz, O.E., Hassett, D.J., 1990. Use of a database of chemical, mineralogical and physical properties of North American fly ash to study the nature of fly ash and its utilization as a mineral admixture in concrete. Material Research Society Symposium Proceedings 178: 3-34.

Meyers, J.J., Pichumani, R., Kapples, B.S., Fly ash – a highway construction material. Monroeville, PA: Prepared for the Federal Highway Administration by GAI Consultants; 1976.

Miller, B.G., 2005. "Coal Energy Systems", Elsevier Inc. 374.

Mills, W.B., Loh, J. Y., Bate M.C., Johnson, K.M., 1999. Evaluation of potential risks from ash disposal site leachate. *Journal of Environment Engineering* 125: 306-313.

Moreno, N., Querol, X., Andres, J.M., Stanton, K., Towler, M., Nugteren, H., Janssen-Jurkovicova, M., Jones, R., 2005. Physico-chemical characteristics of European pulverized coal combustion fly ashes. *Fuel* 84: 1351-1363.

Nathan, Y., Dvorachek, M., Pelly, I., Mimran, U., 1999. Characterization of coal fly ash from Israel. *Fuel* 78: 205-213

Norton, G.A., Markuzewski, R., Shankls, H.R., 1986. Morphological and chemical characterization of iron rich fly ash fractions. *Environmental Science and Technology* 20: 409-413.

Page, A.L., Elseewi, A.A., Straughan, I.R., 1979. Physical and chemical properties of 40 fly ash from coal-fired power plants with reference to environmental impacts. *Residue Reviews 71*: 83-120.

Petit, M.D and Rucandio, M.I., 1999. Sequential extractions for determination of cadmium distribution in coal fly ash, soil and sediment samples. *Analytica Chimica Acta* 401: 283-291.

Petrik, L., White, R., Klink, M., Somerset, V., Key, D., Iwuoha, E., Burgers, C., Fey, M.V., 2005. Utilization of fly ash for Acid Mine Drainage remediation. WRC Report No. 1242/1/05

Petrik, L.F., White, R.A., Klink, M.J., Somerset, V.S., Burgers, C.L., Fey, M.V., 2003. Utilization of South African Ash to treat Acid Coal Mine Drainage and production of high quality zeolites from the residual solids. 2003 International Ash Utilization Symposium, Center for Applied Energy Research, University of Kentucky, Paper #61

Perkin Elmer, 2005. FTIR Spectroscopy technical notes. Attenuated Total Reflectance (ATR). Perkin Elmer, Inc.

Plummer, C.C., McGeary, D., Carlson, D.H., 1999. 'Physical geology' 8th Edition. WCB/McGraw-Hill, 550

Poe, B.T., McMillan, P.F., Cote, B., Massiot, D., Coutures, J.P., 1992. Silica-alumina liquids: in-situ study by high temperature aluminium 27 NMR spectroscopy and molecular dynamics simulation. *Journal of physical Chemistry* 96: 8220-8224.

Praharaj, T., Swain, S.P., Powell, M.A., Hart, B.R., Tripathy, S., 2002. Delineation of ground water contamination around an ash pond. Geochemical and GIS approach. *Environment International* 27: 631-638.

Querol, X., Fernández-Turiel, J.L. and López-Soler, A. 1995: Trace elements in coal and their behaviour during combustion in a large power station. *Fuel* 74: 331-343.

Querol, X., Juan, R., Lopez-Soler, A., Fernandez-Turiel, J.L., Ruiz, C.R., 1996. Mobility of trace elements from coal and combustion wastes. *Fuel* 75: 821-838.

Querol, X., Umana, J.C., Alastuey, A., Ayora, C., Lopez-Soler, A., Plana, F., 2001. Extraction of soluble major and trace elements from fly ash in open and closed leaching systems. *Fuel* 80: 801-813.

Radojević Miroslav and Bashkin N. Vladimir, 1999. "Practical environmental analysis". The Royal Society of Chemistry, 353-355.

Ramesh, A and Kozinski, J.A., 2001. Investigations of ash topography/morphology and their relationship with heavy metals leachabilty. *Environmental Pollution* 111: 255-262.

Rath, P., Panda, U.C., Bhatta, D., Sahu, K.C., 2008. Use of sequential leaching, mineralogy, morphology and multivariate technique for quantifying metal pollution in highly polluted aquatic sediments- A case study: Brahmani and Nandira Rivers, India, *Journal of Hazardous Materials* 163: 632-644.

Reardon E.J., Czank C.A., Warren C.J., Dayal R., and Johnston H.M., 1995: Determining controls on element concentrations in fly ash leachate. *Waste Management & Research* 13: 435-450.

Reynolds, K.A., Kruger, R.A., Rethman, N.F.G., 1999. The manufacture of and evaluation of an artificial soil prepared from fly ash and sewage slugde. Proc. 1999 International Ash Utilization Symposium, Lexington, Kentucky, U.S.A. 387-397.

Roy, W. R. and Griffin, R.A. 1984: Illinois basin coal fly ashes. 2. Equilibria relationships and quantitative modelling of ash-water reactions. *Environment Science Technology* 18: 739-742.

Russell, N.V., Wigley, F., Williamson, J., 2002. The roles of lime and iron oxide on the formation of ash and deposits in PF combustion. Fuel 81: 673-681.

Saikia, N., Kato, S., Kojima, T., 2006. Compositions and leaching behaviors of combustion residues. *Fuel* 85: 264-271.

Sakorafa, V., Michailidis, K., Burragato, F., 1996. Mineralogy, geochemistry and physical properties of fly ash from the Megalopolis lignite fields, Peloponnese, Southern Greece, *Fuel* 75: 419-423.

Sale, L.Y., Naeth, M.A., Chansyk, D.S., 1996. Growth response of barley on unweathered fly ash-amended soil. *Journal of Environmental Quality* 25: 684-691.

Senior, C.L., Bool, L.E, Morency, J.R., 2000. Laboratory study of trace element vaporization from combustion of pulverized coal. *Fuel processing Technology* 63: 109-124.

Scheetz, B.E, Schueck, J., Silsbee, M.R.:1995. Field applications of cementitious grouts to address the formation of acid mine drainage. A paper presented at Sudbury'95, Conference on Mining and the Environment: 1995 May 28- June 1; Sudbury, Ontario. Salt Lake City, Utah. Abandoned Mine Reclamation Program, Division of Oil, Gas and Mining; 1995.

Scheetz, B.E., 2004. "Chemistry and mineralogy of coal fly ash: Basis for beneficial use". Office of Surface Mining Mid Continent Region. (http://www.mcrcc.osmre.gov/PDF/Forums/CCB5/1.4.pdf)

Scheetz, B.E and Earle, R., 1998. Utilization of fly ash. *Current Opinion in Solid State and Materials Science* 3: 510-520.

Schoer, J.U., Hong, Y.T, Forstner, U., 1983. Variation of chemical forms of Fe, Mn and Zn in suspended sediments from Elbe and Weser rivers during estuarine mixing, *Environmental Technology Letters* 4: 277-282.

Schramke, J.A., 1992. Neutralization of alkaline coal fly ash leachates by CO_2 (g). *Applied Geochemistry* 7: 481-492.

Sikka, R and Kansal, B.D., 1995. Effect of fly ash application on yield and nutrient composition of rice, wheat and on pH and available nutrient status of the soils. *Bioresource Technology* 51: 199-203.

Simsimam, G.V., Chesters, G.A., Anders, W., 1987. Effect of fly ash disposal ponds on groundwater quality at coal fired power plant. Water Research, 21: 417-426.

Singh, D.N and Kolay, P.K., 2002. Simulation of ash water interaction and its influence on ash characteristics. *Progress in Energy and Combustion Science* 28: 267-299.

Sinha, K.S and Basu, K., 1998. Mounting fly ash problems in growing coal based power stations – few pragmatic approaches towards a solution. In: Verma, C.V.J., Lal, P.K., Kumar, V., Lal, R., Krishnamurthy, R. (Eds.), Proceedings of the International Conference on Fly ash Disposal and Utilization, vol.1. Central Board of Irrigation and Power, New Delhi, India, 15-27.

Sitarz, M., Mozgawa, W., Handke, M., 1997. Vibrational spectra of complex ring silicate anions-method of recognition. *Journal of Molecular Structure* 404: 193-197.

Smith, R.D., 1980. The trace element chemistry of coal during combustion and the emissions from coal-fired plants. *Progress in Energy Combustion Science* 6: 53-119.

Solem, J. K and McCarthy, G. J., 1992: Hydration reactions and ettringite formation in selected cementitious coal conversion by-products, in Advanced Cementitious Systems:

Mechanisms and Properties. *Material Research Society Symposium Proceedings* 245: 71-79.

Spears, D.A., 2000. Role of clay minerals in UK coal combustion. *Applied Clay Science* 16: 87-95.

Swamy, R.N., 1992. "The alkali-silica reaction in concrete". Blackie and Son Ltd. 34-35.

SW-846: 1986, 'Method 3050, Acid digestion of sludges', Test methods for evaluating solid waste, Vol. 1A: Laboratory manual, physical and chemical methods, USEPA.

Tessier, A., Campbell, P.G.C., Bisson, M., 1979. Sequential extraction procedure for the speciation of particulate trace metals. *Analytical Chemistry* 51: 844-851.

Theis, T.L and Gardener, K.H., 1990. Environmental assessment of ash disposal. *Critical Review on Environmental Control* 20: 21-42.

Theis, T.L and Richter, R, O., 1979. Chemical speciation of heavy metals in power plant pond ash leachate. *Environment Science Technology* 13: 219-224.

Theis, T.L and Wirth, J.L. 1977: Sorptive behavior of trace metals on fly ash in aqueous systems. *Environment Science Technology* 11: 1096-1100.

Tiruta-Barna, L., Rakotoarisca, Z., Mehu, J., 2006. Assessment of multi-scale leaching behaviour of compacted coal fly ash. *Journal of Hazardous Materials* 137: 1466-1478.

Tishmack, J.K and Burns, P.E, 2004. The chemistry and mineralogy of coal and coal combustion products. In: Giere, R and Stile, P., (eds) "Energy, Waste and the Environment: A Geochemical Perspective", Geological Society, London, Special publications. 236: 223-246.

Tishmack, J.K., Olek, J., Diamond, S., 1999. Characterization of high-calcium fly ashes and their potential influence on ettringite formation in cementious systems. *Cement, Concrete and Aggregations*, 21: 82-92.

Tsadilas, C., Tsantilas, E., Stramatiadis, S., Antoniadis, V., Samaras, V., 2006. Influence of fly ash application on heavy metal forms and their availability. In: Presad, M.N.V., Sajwan, K.S and Naidu, R, Editors, "Trace Elements in the Environment, Biotechnology and Bioremediation", CRC Press, Boca Raton, 63-75.

Twin Cities Testing and Engineering Laboratory, Inc: 'Investigation of Fly Ash for Use as Compacted Fill', 1970 October; St. Paul, MN. In Fly Ash A Highway Constuction Material. SW Washington, DC; US Department of Transportation, Federal Highway Administration; 1970.

Ugurlu, A. 2004: Leaching characteristics of fly ash. *Environmental Geology* 46: 890-895.

Using coal to generate electricity. Available online at http://www.eskom.co.za/content/ESK0000114Coal%20Poster.pdf . Last accessed on the 15th of February, 2010.

Vaal Triangle History: A surge of post-war development. Available online at www.vaaltriangleinfo.co.za/history/vereeniging/chapter14/57.htm . Last accessed on the 15th of February, 2010.

Van der Hoek, E.E., Bonouvrie, P.A., Comans, R.N.J., 1994. Sorption of As and Se on mineral components of fly ash: Relevance for leaching processes. *Applied Geochemistry* 9: 403-412.

Vassilev, S.V., Vassileva, C.G., Karayigit, A.I., Bulut, Y., Alastuey, A, Querol, X., 2005. Phase-mineral and chemical composition of composite samples from feed coals, bottom

ashes and fly ashes at the Soma power station, Turkey. *International Journal of Coal Geology* 61: 35-63.

Vassilev, S., Menendez, R., Alvarez, D., Diaz-Somoano, M., Martinez-Tarazona, M.R., 2003. Phase-mineral and chemical composition of coal fly ashes as a basis for their multi-component utilization: 1. Characterization of feed coals and fly ashes. *Fuel* 82: 1793-1811.

Vassilev, S.V and Vassileva, C.G., 1997. Geochemistry of coal, coal ashes and combustion wastes from coal-fired power stations. *Fuel Processing Technology* 51: 19-45.

Vassilev, S.V and Vassileva, C.G. 1996. Occurrence, abundance and origins of minerals in coals and coal ashes. *Fuel Processing Technology* 48: 85-106.

Vempati, R.K., Rao, A., Hess, T.R., Cocke, D. L., Lauer Jr., H.V., 1994. Fractionation and characterization of Texas lignite class "F" fly ash by XRD, TGA, FTIR and SFM. *Cement and Concrete Research* 24: 1153-1164.

Vidya, S.B and Snigdha S., 2006. Analysis of fly ash heavy metal content and disposal in three thermal power plants in India, *Fuel* 85: 2676-2679.

Visual Impact Assessment, 2008. Proposed coal-fired power station in the Northern Free State. Visual Impact Assessment. Eskom Holdings Limited, Generation Division. Prepared by Strategic Environmental Focus. SEF REF: 501430

Valkovic, V., 1983. "Trace Elements in Coal: Volume I and II". CRC Press, INC. Boca Raton, FL

Wada, S.I and Wada, K., 1980. Formation, composition and structure of hydroxy-aluminosilicate ions. *Journal of Soil Science* 31: 457.

Wesche, K., 1991. "Fly ash in concrete – Properties and performance". Edited by Wesche, K. RILEM Report 7. RILEM, 22.

White, S.C and Case, E.D., 1990. Characterization of fly ash from coal-fired power plants. *Journal of material science* 25: 5215-5219.

Wigley, F and Williamson, J., 1998. Modelling fly ash generation for pulverized coal combustion. *Progress in Energy Combustion Science* 24: 337-343.

Wittridge, N.J., Knutsen, R.D., Gerneke, D.A., Sewell, B.T., 2007. Application notes for the Leica S440 Scanning Electron Microscope at the Electron Microscope Unit, University of Cape Town, South Africa.

World Coal Institute, 2005. "The coal resource - A comprehensive overview of coal". World Coal Institute.31-32.

Xu, A: Fly ash in concrete. "In Waste Materials Used in Concrete Manufacturing". Edited by Chandra S. Westwood, NJ: Noyes Publications; 1997: 142-183.

Yazici, H., 2001. Utilization of coal combustion byproducts in building blocks. *Fuel* 86: 929-937.

Yinzhi, Z., Zhe Lu, M., Maroto-Valer, M., Andresen, J.M., Schobert, H.H., 2003. Comparison of high unburned carbon fly ashes from different combustor types and their steam activated products. *Energy Fuels*, 17: 369-377.

Zevenbergen, C., Bradley, J.P., Reeuwijk, L.P.V., Shyam, A.K., Hjelmar, O., Comans, R.N.J., 1999. Clay formation and metal fixing during weathering of coal fly ash. *Environment Science Technology* 33: 3405.

Zevenbergen, C. and Comans, R.N.J. 1994. Geochemical factors controlling the mobilization of major elements during weathering of MSWI bottom ash. *Environmental Aspects of Construction with Waste Materials*, Goumans J.J.J.M., van der Sloot H.A. and Aalbers Th.G. (Editors), Elsevier Science B.V. 179-194.

APPENDIX A

FTIR bands observed from the surface layer to 32 m at Kragbron

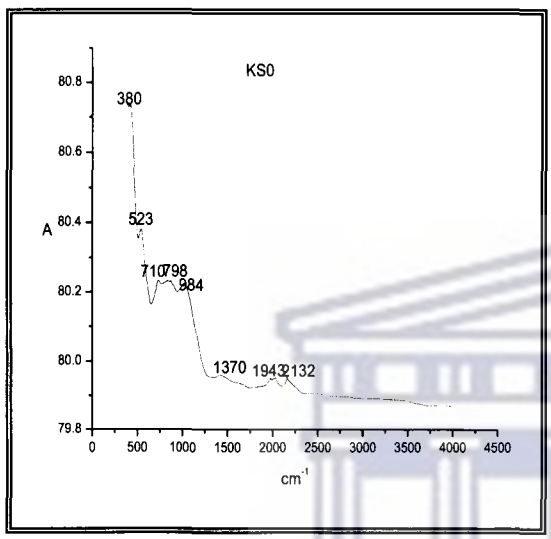

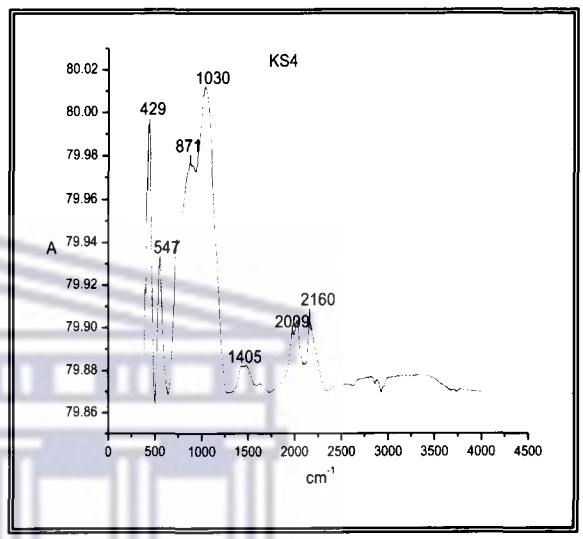

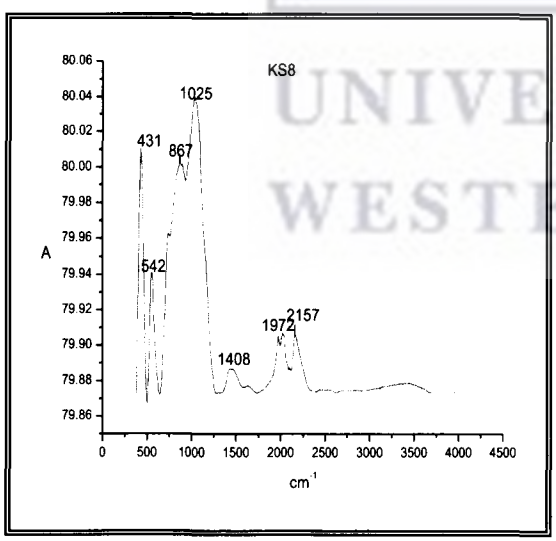

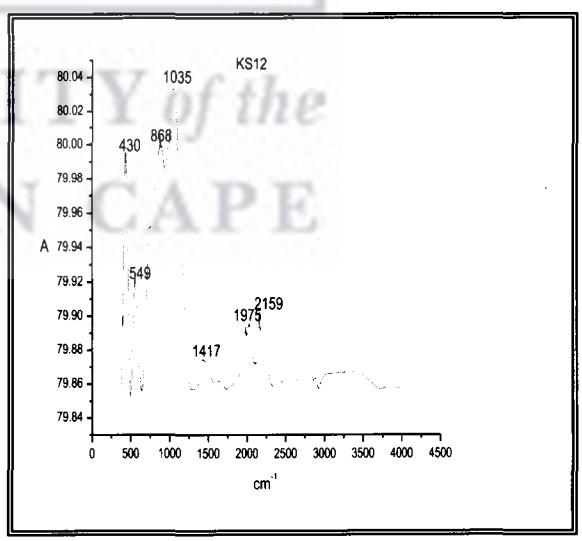

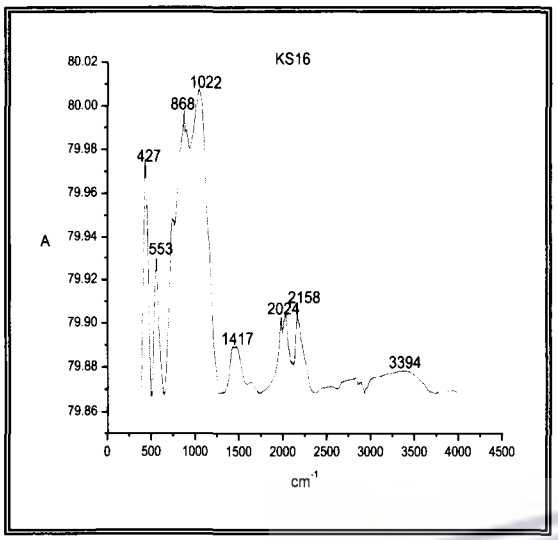

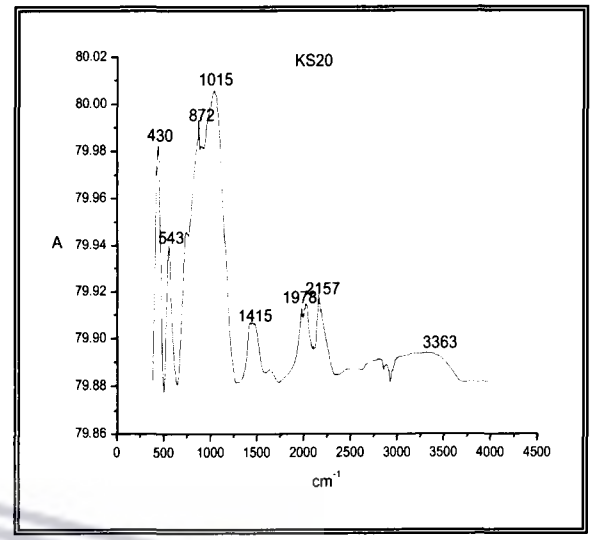

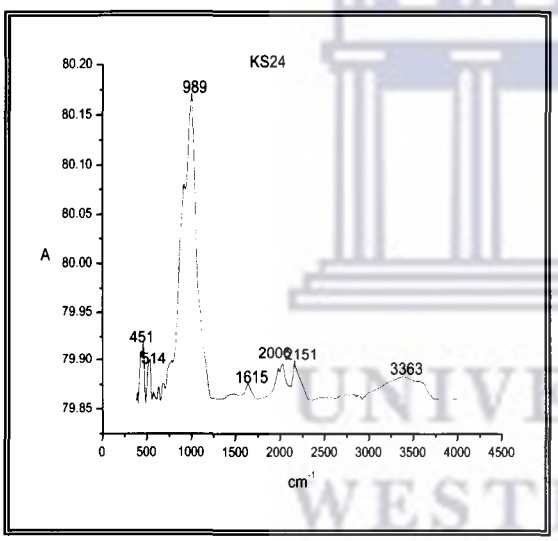

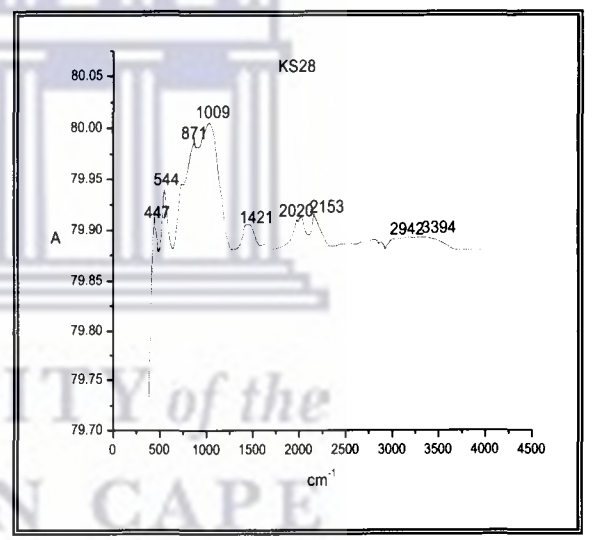

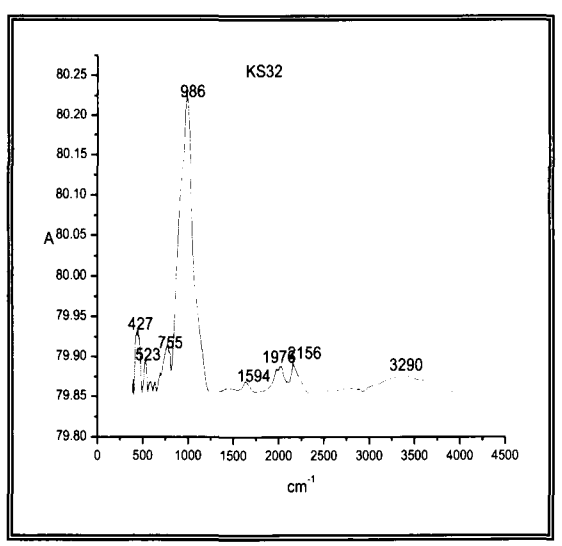

APPENDIX B

XRD spectra of samples obtained from Kragbron drilled core

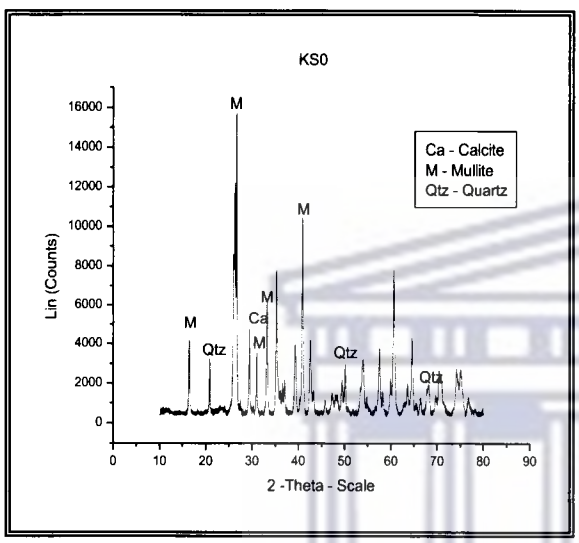

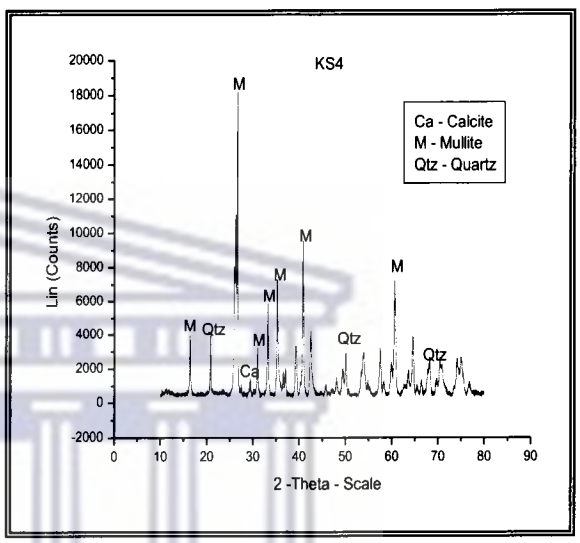

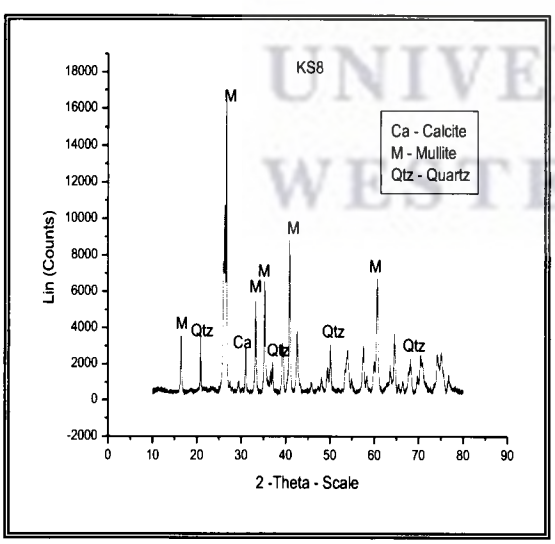

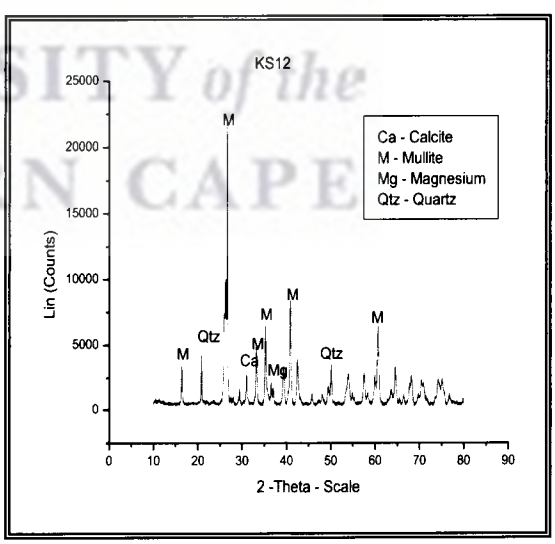

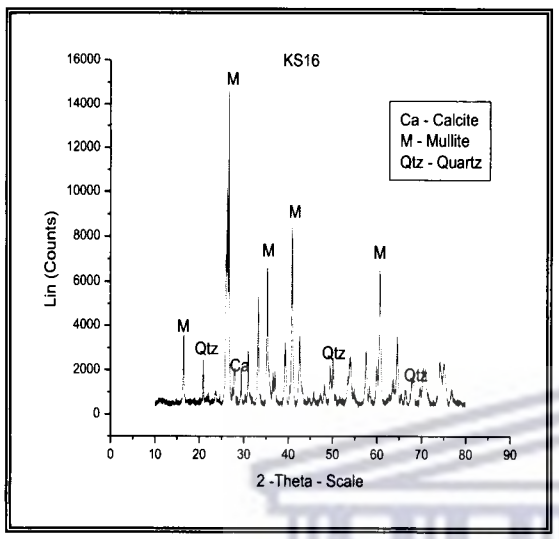

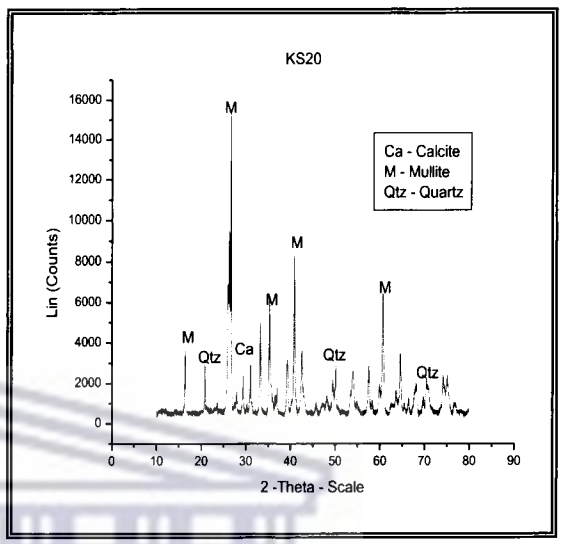

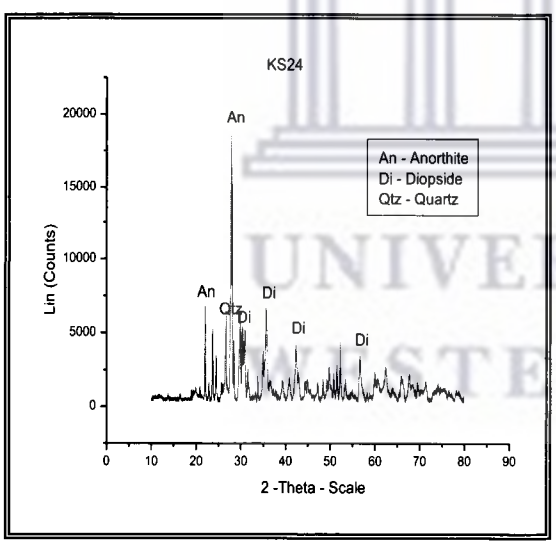

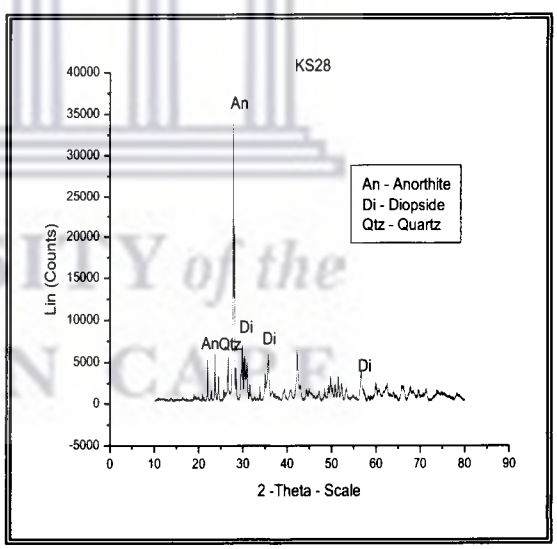

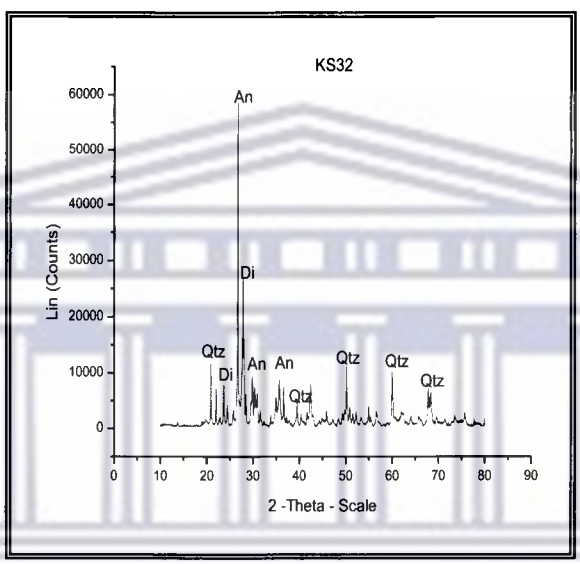

APPENDIX C – CEC data

Sample Names	Depth (m)	meq of Ca	meq of Na	meq of K	meq of Mg	Total
KS0	0	0.105	0.001	0.002	0.013	0.120
KS1	1	0.162	0.001	0.001	0.017	0.180
KS2	2	0.160	0.001	0.001	0.014	0.176
KS3	3	0.231	0.002	0.001	0.019	0.252
KS4	4	0.226	0.002	0.001	0.015	0.244
KS5	5	0.184	0.002	0.001	0.013	0.120
KS6	6	0.134	0.002	0.001	0.011	0.148
KS7	7	0.120	0.002	0.001	0.008	0.131
KS8	8	0.183	0.002	0.001	0.014	0.199
KS9	9	0.193	0.002	0.001	0.017	0.213
KS10	10	0.168	0.002	0.001	0.020	0.191
KS11	11	0.156	0.002	0.001	0.016	0.176
KS12	12	0.147	0.002	0.001	0.013	0.163
KS13	13	0.145	0.002	0.001	0.014	0.162
KS14	14	0.201	0.002	0.002	0.023	0.227
KS15	15	0.320	0.002	0.001	0.028	0.351
KS16	16	0.247	0.012	0.003	0.023	0.286
KS17	17	0.305	0.002	0.001	0.021	0.330
KS18	18	0.395	0.003	0.001	0.024	0.423
KS19	19	0.345	0.002	0.001	0.027	0.376
KS20	20	0.359	0.002	0.001	0.026	0.389
KS21	21	0.360	0.002	0.001	0.024	0.388
KS22	22	0.331	0.002	0.001	0.027	0.361
KS23	23	0.138	0.003	0.002	0.028	0.169
KS24	24	0.074	0.002	0.001	0.020	0.096
KS25	25	0.088	0.003	0.002	0.018	0.120
KS26	26	0.047	0.002	0.002	0.019	0.069
KS27	27	0.126	0.003	0.002	0.015	0.146
KS28	28	0.059	0.002	0.002	0.011	0.073
KS29	29	0.059	0.002	0.002	0.026	0.089
KS30	30	0.075	0.002	0.002	0.019	0.099
KS31	31	0.044	0.002	0.003	0.029	0.078
KS32	32	0.074	0.003	0.004	0.031	0.112

APPENDIX D – Trace element plots obtained from total acid digestion

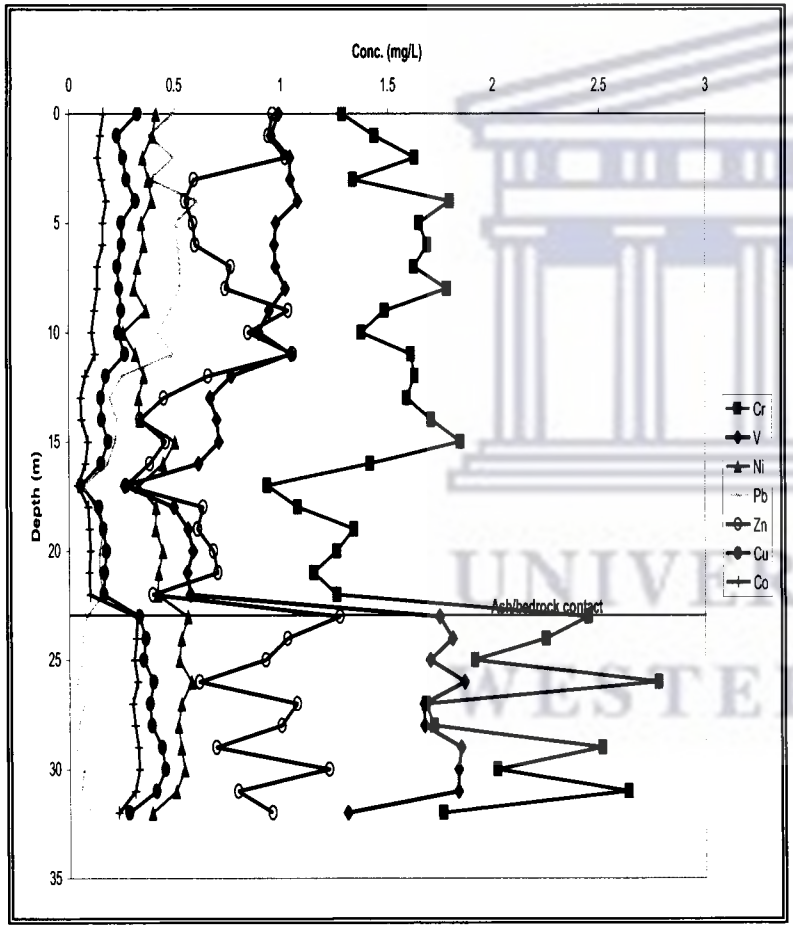

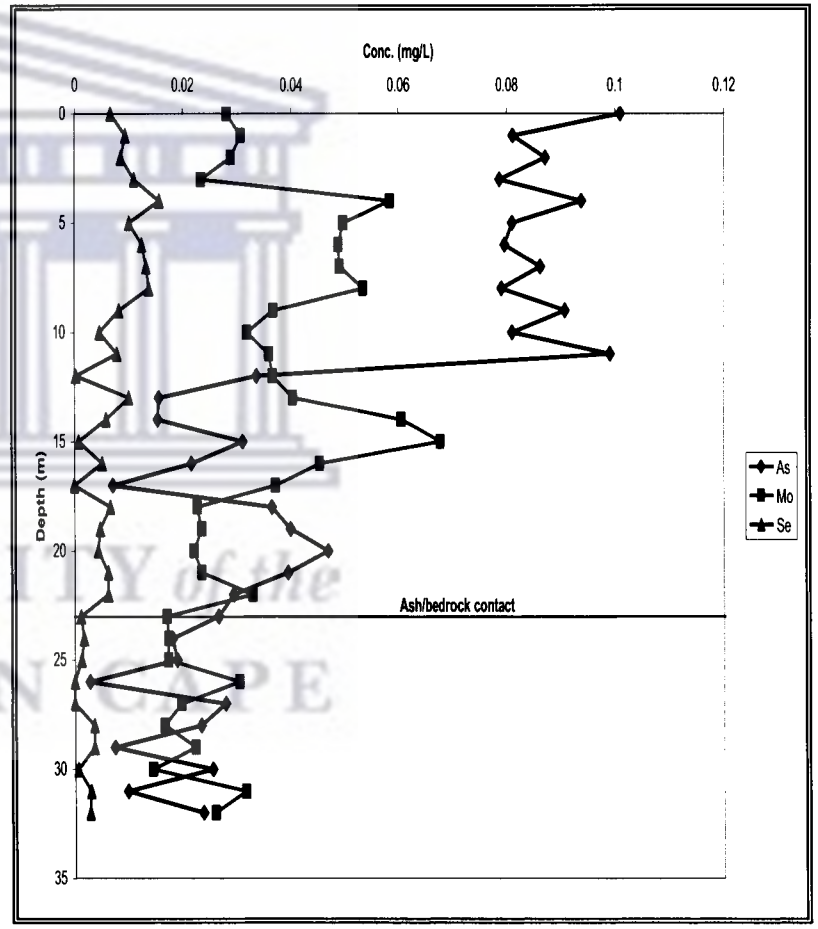

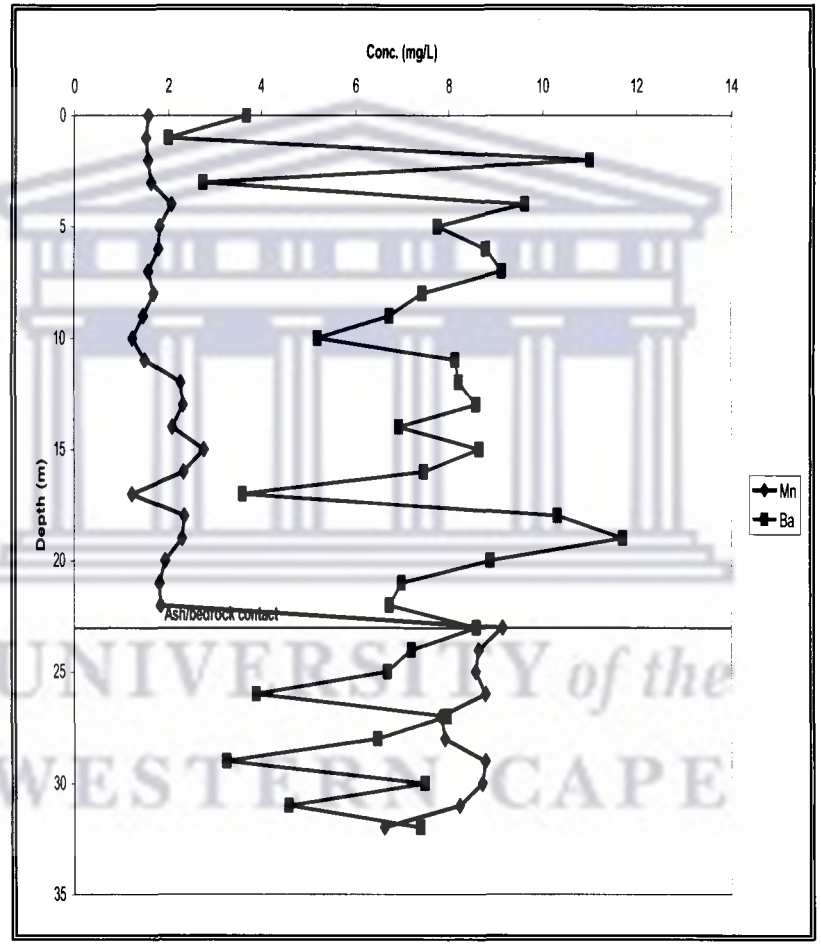

(d) Sample at 12m

(e) Sample at 16m

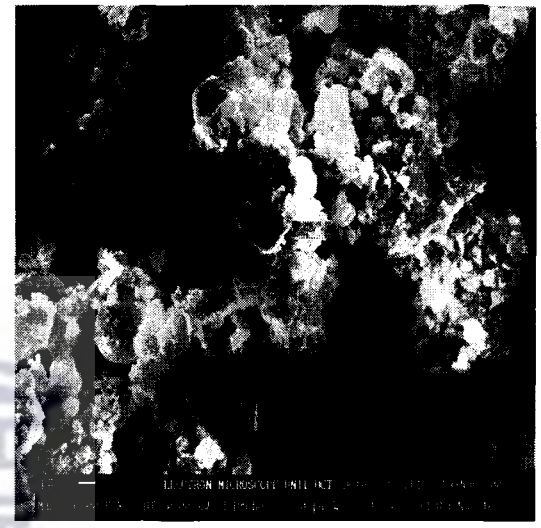

(f) Sample at 20m

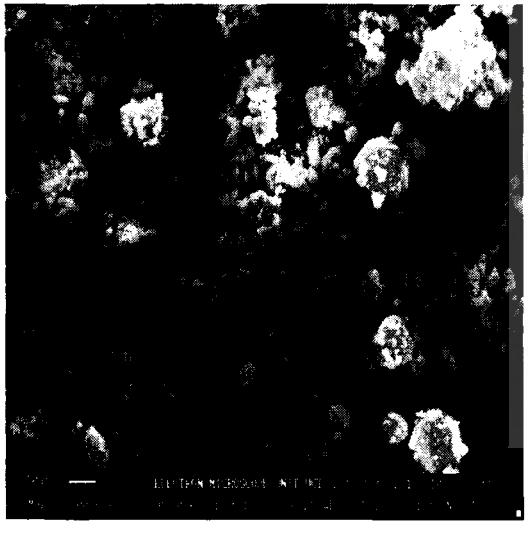

(g) Sample at 21m

(h) Sample at 22m

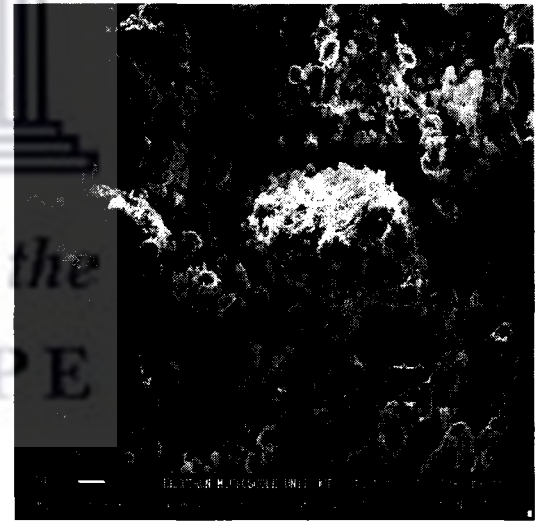

(i) Sample at 23m

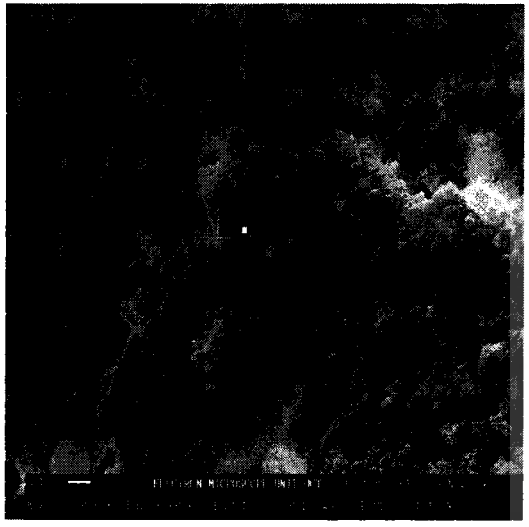

(j) Sample at 24m

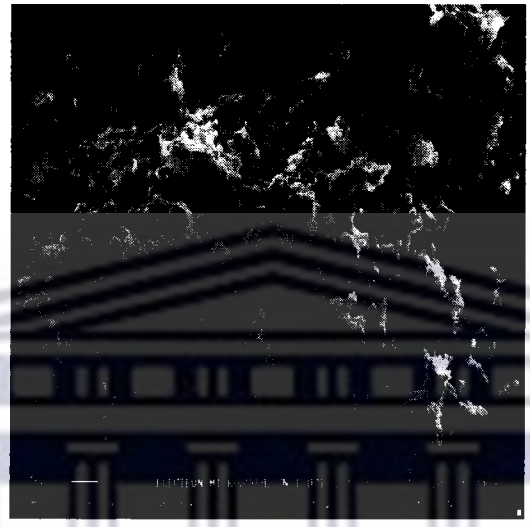

(k) Sample at 25m

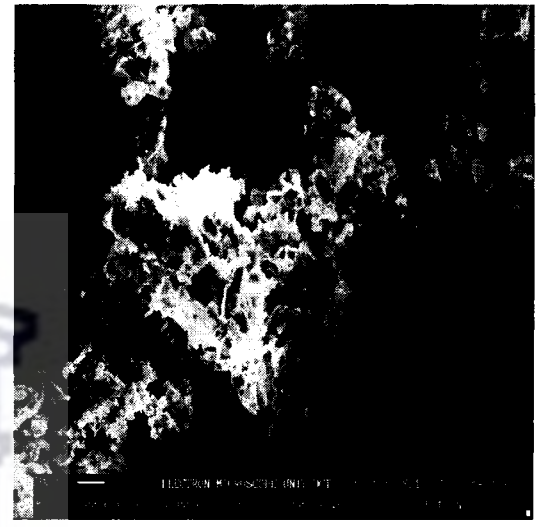

(l) Sample at 26m

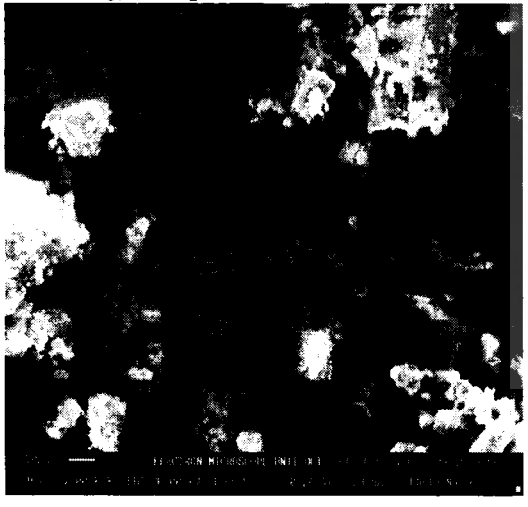

(m)Sample at 27m

(n) Sample at 28m

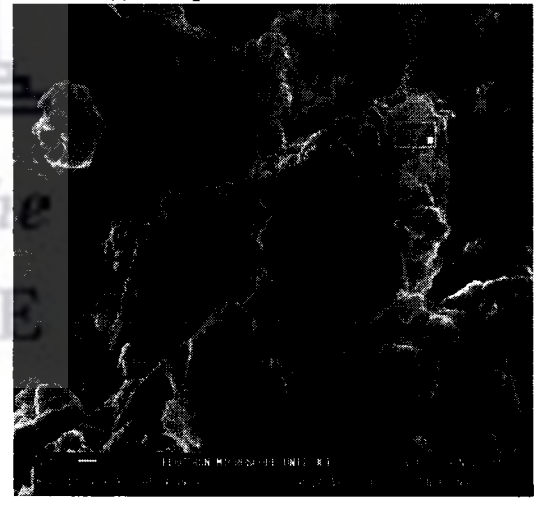

(o) Sample at 32m

APPENDIX F – Table for major elements from total acid digestion

Sample Names	Depth (m)	B (mg/L)	Fe (mg/L)	Al (mg/L)	Ti (mg/L)	Sr (mg/L)	Ca (mg/L)	K (mg/L)	Mg (mg/L)	Na (mg/L)	Si (mg/L)
KS0	0	111.78	86.20	144.47	75.82	10.89	160.96	16.73	31.25	10.46	106.83
KS1	1	90.14	80.41	138.18	69.97	10.67	152.34	12.84	29.97	7.15	121.80
KS2	2	101.29	93.37	133.97	74.62	11.15	160.67	25.18	23.81	12.70	118.87
KS3	3	161.33	95.94	137.74	73.52	10.60	173.56	14.01	21.23	7.42	109.14
KS4	4	279.25	153.52	136.61	75.00	17.49	250.83	46.49	25.96	11.47	151.97
KS5	5	255.52	128.04	128.22	75.67	15.71	172.58	36.10	27.44	7.50	161.70
KS6	6	219.72	139.17	132.28	65.83	16.49	236.92	38.45	25.92	8.93	166.36
KS7	7	251.59	138.10	131.84	75.11	14.93	169.44	34.93	27.73	9.59	142.83
KS8	8	251.72	142.95	129.56	79.47	14.61	209.25	28.44	24.61	11.46	143.62
KS9	9	88.03	102.97	145.63	77.85	11.68	214.32	13.05	22.00	7.55	148.83
KS10	10	87.01	90.83	134.27	76.94	10.60	208.03	12.98	15.62	5.38	189.40
KS11	11	94.50	91.65	140.38	83.25	12.34	228.25	14.18	22.12	7.00	167.31
KS12	12	138.83	119.48	127.92	75.07	15.55	241.51	20.67	25.50	9.33	134.03
KS13	13	214.52	145.15	132.84	64.43	17.33	277.75	34.40	29.27	7.81	157.10
KS14	14	257.92	113.17	125.94	70.72	16.71	195.02	33.21	29.48	9.88	136.95
KS15	15	282.41	174.15	140.66	76.66	18.48	213.41	21.15	25.67	9.02	136.38
KS16	16	292.48	154.70	133.25	57.30	18.61	332.46	34.13	26.82	9.14	152.66
KS17	17	73.73	71.14	152.13	26.34	13.17	327.36	9.52	21.33	8.95	168.21
KS18	18	42.58	115.60	193.22	59.62	15.74	377.95	6.11	23.58	10.95	222.17
KS19	19	40.05	173.69	136.73	59.13	19.65	513.87	16.25	27.22	8.74	164.22
KS20	20	86.28	87.03	151.96	63.68	15.42	251.65	9.71	22.35	15.47	154.29
KS21	21	90.76	103.60	156.02	66.86	12.20	215.81	8.61	21.85	14.38	210.10

KS22	22	116.37	97.85	156.42	62.50	14.94	196.49	11.28	22.24	13.28	181.27
KS23	23	71.58	211.63	169.13	40.69	11.47	188.40	50.11	33.86	19.54	152.60
KS24	24	52.11	251.94	181.49	43.94	10.70	190.45	45.73	44.44	23.36	145.45
KS25	25	88.15	311.82	157.71	45.05	8.95	281.30	38.27	39.07	22.84	137.74
KS26	26	116.96	344.48	155.79	56.25	9.04	304.55	39.23	54.38	21.76	142.74
KS27	27	25.77	321.35	178.39	49.65	7.93	184.52	39.66	41.07	24.66	202.63
KS28	28	31.62	295.49	149.68	38.86	8.51	171.61	40.80	41.13	18.49	180.91
KS29	29	49.40	397.51	174.92	38.92	6.78	205.31	45.60	103.27	28.54	167.13
KS30	30	44.62	272.85	171.47	43.48	8.03	159.87	40.67	36.37	16.93	186.26
KS31	31	77.26	338.99	161.28	45.128	9.71	197.72	83.00	65.44	22.98	193.33
KS32	32	54.13	264.89	160.78	31.38	10.61	160.17	119.82	30.91	17.12	166.15

APPENDIX G – Table for trace elements from total acid digestion

Sample Names	Depth (m)	V (mg/L)	Cr (mg/L)	Mn (mg/L)	Co (mg/L)	Ni (mg/L)	Cu (mg/L)	Zn (mg/L)	As (mg/L)	Se (mg/L)	Mo (mg/L)	Ba (mg/L)
KS0	0	0.10	1.29	1.59	0.17	0.42	0.33	0.97	0.10	0.01	0.03	3.68
KS1	1	0.96	1.44	1.55	0.15	0.40	0.23	0.95	0.08	0.01	0.03	2.01
KS2	2	1.05	1.63	1.59	0.14	0.36	0.26	1.03	0.09	0.01	0.03	11.01
KS3	3	1.05	1.34	1.66	0.16	0.38	0.28	0.60	0.08	0.01	0.02	2.75
KS4	4	1.09	1.80	2.08	0.18	0.40	0.32	0.56	0.09	0.02	0.06	9.64
KS5	5	0.99	1.65	1.83	0.16	0.35	0.26	0.60	0.08	0.01	0.05	7.77
KS6	6	0.98	1.69	1.80	0.16	0.36	0.26	0.60	0.08	0.01	0.05	8.81
KS7	7	0.98	1.63	1.59	0.14	0.33	0.24	0.77	0.09	0.01	0.05	9.15
KS8	8	1.03	1.78	1.71	0.14	0.31	0.25	0.74	0.08	0.01	0.05	7.45
KS9	9	0.95	1.49	1.49	0.12	0.37	0.26	1.04	0.09	0.01	0.04	6.74
KS10	10	0.90	1.38	1.27	0.11	0.26	0.24	0.85	0.08	0.00	0.03	5.21
KS11	11	1.05	1.61	1.52	0.13	0.32	0.27	1.06	0.10	0.01	0.04	8.17
KS12	12	0.78	1.63	2.29	0.08	0.36	0.18	0.66	0.03	0.00	0.04	8.24
KS13	13	0.67	1.59	2.33	0.06	0.33	0.16	0.45	0.02	0.01	0.04	8.60
KS14	14	0.70	1.71	2.09	0.06	0.34	0.16	0.34	0.02	0.01	0.06	6.95
KS15	15	0.71	1.85	2.78	0.09	0.51	0.19	0.46	0.03	0.00	0.07	8.67
KS16	16	0.62	1.42	2.34	0.08	0.45	0.16	0.39	0.02	0.01	0.05	7.48
KS17	17	0.27	0.94	1.25	0.04	0.33	0.06	0.27	0.01	0.00	0.04	3.60
KS18	18	0.50	1.09	2.36	0.09	0.42	0.15	0.64	0.04	0.01	0.02	10.32
KS19	19	0.57	1.35	2.31	0.10	0.41	0.17	0.61	0.04	0.00	0.02	11.72
KS20	20	0.59	1.27	1.95	0.10	0.45	0.18	0.69	0.05	0.00	0.02	8.91
KS21	21	0.56	1.16	1.83	0.10	0.43	0.17	0.71	0.04	0.01	0.02	7.01

KS22	22	0.58	1.26	1.85	0.10	0.43	0.17	0.40	0.03	0.01	0.03	6.74
KS23	23	1.75	2.45	9.16	0.32	0.57	0.34	1.28	0.03	0.00	0.02	8.61
KS24	24	1.81	2.25	8.66	0.32	0.54	0.37	1.04	0.02	0.00	0.02	7.22
KS25	25	1.70	1.91	8.60	0.31	0.53	0.36	0.93	0.02	0.00	0.02	6.70
KS26	26	1.86	2.79	8.80	0.33	0.58	0.40	0.62	0.00	0.00	0.03	3.91
KS27	27	1.67	1.68	7.84	0.30	0.53	0.39	1.08	0.03	0.00	0.02	7.98
KS28	28	1.67	1.72	7.92	0.32	0.52	0.40	1.01	0.02	0.00	0.02	6.47
KS29	29	1.85	2.52	8.79	0.33	0.53	0.44	0.70	0.01	0.00	0.02	3.25
KS30	30	1.83	2.02	8.73	0.33	0.55	0.46	1.23	0.03	0.00	0.01	7.49
KS31	31	1.83	2.64	8.24	0.31	0.51	0.42	0.80	0.01	0.00	0.03	4.60
KS32	32	1.31	1.76	6.62	0.24	0.39	0.29	0.96	0.02	0.00	0.02	7.40

APPENDIX H – Major elements in the water soluble fraction phase

Sample Names	Depth (m)	Ca (mg/kg)	Mg (mg/kg)	Na (mg/kg)	Si (mg/kg)	Sr (mg/kg)	B (mg/kg)	Al (mg/kg)	K (mg/kg)	Ti (mg/kg)	Fe (mg/kg)
KS0	0	1042.40	217.32	293.91	472.27	15.07	8.78	378.64	41.16	23.93	74.54
KS1	1	1487.80	214.63	303.74	292.61	16.68	68.02	245.36	20.45	2.77	15.78
KS2	2	1798.00	207.15	326.69	293.55	22.75	79.77	288.27	26.29	2.97	23.07
KS3	3	2034.00	205.68	266.81	320.75	25.17	74.30	352.88	25.93	5.00	24.22
KS4	4	2088.50	164.92	199.58	288.42	26.05	84.07	308.19	23.17	2.81	11.86
KS5	5	1536.80	173.46	408.66	335.79	19.03	78.55	305.34	31.83	4.97	19.28
KS6	6	1566.00	195.18	317.1	316.54	17.62	79.69	252.16	26.11	3.05	15.01
KS7	7	1434.50	136.31	302.24	345.92	20.90	62.89	327.66	19.37	7.523	24.16
KS8	8	1440.70	155.16	325.18	317.46	20.21	103.74	420.50	32.90	6.89	31.52
KS9	9	1735.20	218.77	326.9	341.49	24.78	89.86	271.92	25.32	3.93	21.94
KS10	10	1609.80	184.86	305.07	300.49	24.49	93.05	251.77	22.21	2.44	16.32
KS11	11	1650.20	181.66	318.29	284.28	24.65	110.86	283.81	25.46	5.10	20.31
KS12	12	1187.50	131.47	277.84	386.92	15.49	35.17	269.81	22.73	7.83	35.31
KS13	13	1287.40	143.5	314.77	476.41	14.86	28.42	286.78	24.98	8.52	37.74
KS14	14	1444.20	198.84	321.87	422.33	18.34	50.01	199.87	21.77	3.45	17.18
KS15	15	1431.50	175.01	305.12	374.38	13.01	31.08	210.77	33.49	0.80	8.27
KS16	16	1609.70	178.46	820.44	314.09	16.00	50.34	148.35	53.64	1.68	14.39
KS17	17	2078.00	150.19	295.66	376.98	19.38	43.43	382.64	19.14	1.47	14.89
KS18	18	2919.00	129.91	323.81	379.52	24.30	48.68	531.60	23.03	0.55	8.53
KS19	19	2280.40	137.57	402.11	412.84	22.22	52.84	377.20	29.52	1.25	13.34
KS20	20	2046.50	200.64	355.76	343.39	20.29	66.70	226.13	28.32	1.21	15.86
KS21	21	2067.40	169.86	389.25	349.48	21.87	66.70	226.13	28.323	1.21	15.86

KS22	22	1914.90	177.70	383.54	351.31	21.47	62.70	186.61	29.31	0.48	10.85
KS23	23	1159.30	366.88	422.7	1989.60	11.35	19.74	585.36	69.25	8.06	794.43
KS24	24	850.43	211.37	385.97	875.73	7.26	12.69	286.89	43.03	4.17	353.34
KS25	25	826.04	238.83	411.58	1114.00	7.064	16.11	359.76	50.10	6.16	514.11
KS26	26	514.32	261.42	673.54	1103.20	4.43	6.00	452.24	66.47	4.95	623.87
KS27	27	871.69	165.95	434.31	651.39	8.50	17.81	272.38	63.80	3.14	205.74
KS28	28	715.32	215.81	377.14	777.99	6.73	9.32	370.32	92.00	4.98	343.23
KS29	29	387.30	309.66	379.77	1150.80	3.07	7.21	380.08	75.19	5.82	596.03
KS30	30	775.54	346.20	315.42	983.06	8.28	11.41	368.56	79.22	5.04	560.35
KS31	31	278.06	317.69	332.21	1109.30	2.11	2.82	382.00	109.68	3.68	587.71
KS32	32	498.44	293.21	370.66	933.75	3.053	3.31	317.82	144.45	1.72	408.67

APPENDIX I – Trace elements in the water soluble fraction phase

Sample Names	Depth (m)	V(mg/kg)	Cr (mg/kg)	Mn (mg/kg)	Co (mg/kg)	Ni (mg/kg)	Cu (mg/kg)	Zn (mg/kg)	As (mg/kg)	Se (mg/kg)
KS0	0	4.20	2.00	4.21	0.11	1.03	2.07	1.35	1.13	0.34
KS1	1	5.88	2.49	2.17	0.02	0.50	1.81	1.07	2.09	0.54
KS2	2	5.37	2.93	2.75	0.02	0.59	3.17	1.94	1.96	0.78
KS3	3	5.64	3.18	2.32	0.03	0.54	2.05	0.90	2.04	0.89
KS4	4	5.01	2.35	1.11	0.02	0.29	0.28	0.58	2.34	0.80
KS5	5	4.85	2.42	2.25	0.02	0.46	1.57	0.65	2.27	0.83
KS6	6	5.05	2.79	2.01	0.02	0.61	1.30	0.43	2.25	0.63
KS7	7	4.53	1.96	1.84	0.02	0.25	1.53	0.27	2.00	0.68
KS8	8	5.87	3.29	2.95	0.04	0.66	0.92	0.00	2.86	1.10
KS9	9	4.26	2.47	2.02	0.02	0.90	2.26	2.05	2.24	0.91
KS10	10	4.09	2.01	1.71	0.01	0.46	2.73	1.30	2.31	0.78
KS11	11	4.76	2.29	2.26	0.02	0.42	1.75	0.56	2.26	0.73
KS12	12	1.69	1.21	2.64	0.02	0.34	1.16	0.12	0.54	0.49
KS13	13	1.38	1.35	2.38	0.01	0.47	1.57	0.44	0.37	0.37
KS14	14	2.15	1.33	2.00	0.01	0.38	0.87	0.00	0.61	0.58
KS14	15	1.33	1.10	1.75	0.00	0.39	1.04	3.48	0.42	0.27
KS16	16	1.01	1.32	2.61	0.02	0.59	1.47	2.71	0.37	0.25
KS17	17	1.34	2.49	1.89	0.01	236.49	1.02	2.20	0.52	0.21
KS18	18	1.45	1.63	2.18	0.00	0.26	1.73	3.72	0.43	0.22
KS19	19	1.72	2.60	2.24	0.01	0.83	1.77	2.90	0.57	0.31
KS20	20	1.77	3.74	2.67	0.04	1.58	1.27	2.34	0.72	0.31
KS21	21	1.77	3.74	2.67	0.04	1.58	1.27	2.34	0.72	0.31

KS22	22	1.80	2.59	2.12	0.01	1.64	1.49	3.38	0.64	0.28
KS23	23	6.42	3.16	21.49	0.65	2.66	4.54	5.87	0.23	0.11
KS24	24	3.37	1.51	10.44	0.28	1.07	4.17	6.47	0.21	0.13
KS25	25	3.83	2.08	15.41	0.42	1.77	2.24	2.69	0.26	0.20
KS26	26	2.54	1.74	12.96	0.45	1.83	4.02	2.06	0.14	0.09
KS27	27	2.01	1.23	6.33	0.18	0.87	1.73	1.23	0.36	0.16
KS28	28	1.76	1.46	8.38	0.28	1.35	2.16	1.29	0.24	0.21
KS28	29	2.59	2.24	11.87	0.41	2.06	2.54	2.07	0.23	0.12
KS30	30	2.71	1.99	11.43	0.43	2.00	3.34	2.00	0.24	0.05
KS31	31	1.81	1.65	8.16	0.38	1.90	4.35	3.06	0.11	0.07
KS32	32	1.79	1.36	10.77	0.33	1.37	2.08	1.79	0.13	0.12

APPENDIX J – Major elements in the exchangeable fraction phase

Sample Names	Depth (m)	Ca (mg/kg)	Mg (mg/kg)	Na (mg/kg)	Si (mg/kg)	Sr (mg/kg)	B (mg/kg)	Al (mg/kg)	K (mg/kg)	Ti (mg/kg)	Fe (mg/kg)
KS0	0	12882.00	632.73	347.64	198.37	166.30	32.78	24.80	1766.50	0.20	7.63
KS1	1	14552.00	873.16	389.42	430.88	174.65	95.64	23.40	1384.00	0.10	7.21
KS2	2	13974.00	921.30	350.10	514.71	197.85	95.74	24.90	1685.70	0.10	9.80
KS3	3	17732.00	1231.10	399.77	668.30	224.12	121.78	17.40	1782.10	0.10	5.74
KS4	4	16220.00	883.59	367.85	557.84	204.14	121.12	0.26	95.05	0.00	0.00
KS5	5	15296.00	938.90	356.79	614.09	200.72	115.20	2.78	90.26	0.20	0.00
KS6	6	14660.00	859.92	377.39	566.93	180.99	104.77	1.31	87.18	0.00	0.00
KS7	7	13228.00	947.12	361.48	604.34	185.15	105.87	23.50	1709.30	0.30	9.97
KS8	8	13579.00	838.61	363.37	520.76	206.63	101.14	0.20	76.10	0.00	0.00
KS9	9	14347.00	1020.10	368.10	552.36	209.16	119.66	16.70	1743.40	0.10	6.24
KS10	10	13293.00	829.73	364.45	554.04	202.39	124.89	0.00	86.83	0.00	0.00
KS11	11	13918.00	766.57	361.71	552.36	229.93	130.72	12.10	1381.60	0.10	3.88
KS12	12	12817.00	540.93	284.01	405.62	178.49	63.50	0.00	80.01	0.00	0.00
KS13	13	13002.00	770.37	345.74	467.06	150.64	43.24	0.06	88.67	0.00	0.00
KS14	14	23271.00	1272.70	389.19	551.93	304.69	94.07	7.61	1543.00	0.10	2.27
KS15	15	23548.00	1074.70	349.19	664.91	252.13	76.78	8.28	1389.10	0.10	1.82
KS16	16	16650.00	969.90	485.23	579.70	185.71	79.56	20.30	1885.60	0.30	7.24
KS17	17	24512.00	1024.00	326.29	792.63	263.39	98.78	6.80	1565.90	0.10	1.81
KS18	18	36245.00	1326.30	370.92	832.17	333.88	118.05	6.57	1821.90	0.10	1.29
KS19	19	29124.00	1235.10	408.44	792.25	310.70	111.98	7.97	1828.70	0.10	2.09
KS20	20	29824.00	1145.10	421.28	688.66	375.96	123.26	6.17	1852.50	0.10	1.49
KS21	21	28557.00	1041.50	335.51	711.58	346.85	112.45	5.54	1436.40	0.10	0.91

KS22	22	28199.00	1179.00	624.92	623.36	339.74	106.95	0.00	92.16	0.00	0.00
KS23	23	9333.70	783.90	352.91	277.85	83.36	13.95	18.70	1359.10	0.00	5.60
KS24	24	5020.50	580.02	384.43	225.58	58.98	10.25	6.27	62.28	0.00	0.00
KS25	25	5914.50	594.90	370.06	282.81	71.83	12.87	5.73	86.02	0.00	0.00
KS26	26	3630.10	671.65	569.46	162.80	32.54	4.92	20.80	85.51	0.00	0.85
KS27	27	6000.30	493.14	378.83	282.31	73.60	17.37	6.85	85.22	0.00	0.00
KS28	28	3560.60	409.03	351.51	185.53	42.92	11.06	13.10	92.36	0.00	0.28
KS29	29	3612.80	617.19	310.63	155.56	32.97	5.94	14.70	95.03	0.00	0.52
KS30	30	5231.70	636.22	374.19	195.18	51.80	8.02	10.10	97.79	0.00	0.00
KS31	31	3263.40	762.24	387.37	129.92	21.42	3.89	23.00	128.57	0.00	1.92
KS32	32	4086.40	613.64	351.50	103.78	22.02	3.22	15.20	123.23	0.00	0.61

APPENDIX K – Trace elements of the exchangeable fraction phase

Sample Names	Depth (m)	V(mg/kg)	Cr (mg/kg)	Mn (mg/kg)	Co (mg/kg)	Ni (mg/kg)	Cu (mg/kg)	Zn (mg/kg)	As (mg/kg)	Se (mg/kg)
KS0	0	6.77	2.23	11.98	0.08	0.38	0.82	1.34	8.17	2.61
KS1	1	7.94	3.86	19.62	0.20	1.21	2.27	1.65	6.92	2.22
KS2	2	8.07	4.05	17.28	0.17	1.08	2.32	1.64	7.21	2.16
KS3	3	9.97	5.44	27.04	0.21	1.23	2.85	1.70	8.59	2.32
KS4	4	8.48	3.34	25.72	0.18	0.71	2.25	4.06	8.67	2.74
KS5	5	7.86	3.29	19.65	0.19	0.83	2.24	2.18	8.17	2.29
KS6	6	8.07	3.15	19.48	0.17	0.72	2.16	2.06	8.69	2.50
KS7	7	8.61	3.35	16.92	0.12	0.78	2.01	1.82	9.13	2.34
KS8	8	7.87	2.62	15.97	0.12	0.52	2.28	2.82	8.65	2.33
KS9	9	7.80	3.69	16.03	0.13	0.84	2.68	1.77	8.79	2.43
KS10	10	8.00	3.25	14.18	0.13	0.56	2.10	2.51	9.13	2.86
KS11	11	8.44	3.67	14.61	0.12	0.71	2.34	1.74	9.13	2.47
KS12	12	2.53	0.77	15.15	0.07	0.50	1.92	2.85	2.24	1.39
KS13	13	1.54	0.44	16.15	0.06	0.59	1.34	1.38	1.07	0.93
KS14	14	2.95	1.54	20.49	0.11	1.65	2.42	1.77	2.91	2.10
KS15	15	2.70	2.01	29.99	0.13	1.57	1.83	1.03	2.49	1.51
KS16	16	2.05	1.23	25.92	0.08	1.09	1.54	0.90	2.08	0.94
KS17	17	2.71	2.26	34.64	0.14	1.82	2.32	1.27	3.05	1.06
KS18	18	2.70	2.94	36.40	0.18	2.23	2.31	1.40	3.23	1.26
KS19	19	3.14	2.91	32.05	0.17	1.88	2.64	2.25	3.47	1.27
KS20	20	3.48	3.37	31.12	0.14	1.51	2.64	1.37	3.51	1.35
KS21	21	3.23	2.94	28.49	0.14	1.37	2.28	1.74	3.42	1.40

KS22	22	3.24	2.71	28.02	0.15	1.23	1.56	1.30	3.20	1.39
KS23	23	1.10	0.38	165.20	0.33	0.95	1.85	1.84	0.57	0.33
KS24	24	0.52	0.53	23.55	0.09	0.55	4.21	1.96	0.35	0.34
KS25	25	0.58	0.59	24.34	0.09	0.72	3.44	1.72	0.49	0.20
KS26	26	0.25	0.43	26.76	0.26	1.47	6.29	3.65	0.09	0.08
KS27	27	0.68	0.68	27.78	0.30	1.69	6.12	2.50	0.65	0.26
KS28	28	0.39	0.55	32.87	0.65	3.17	8.53	4.08	0.33	0.12
KS29	29	0.22	0.43	23.61	0.23	1.29	5.61	1.89	0.13	0.02
KS30	30	0.30	0.50	19.61	0.10	0.78	3.53	1.23	0.30	0.14
KS31	31	0.13	0.37	20.10	0.16	0.94	5.57	4.53	0.03	0.09
KS32	32	0.15	0.42	36.73	0.15	0.73	6.15	3.19	0.09	0.03

APPENDIX L – Major elements of the carbonate fraction phase

Sample Names	Depth (m)	Ca (mg/kg)	Mg (mg/kg)	Na (mg/kg)	Si (mg/kg)	Sr (mg/kg)	Fe (mg/kg)	Al (mg/kg)	K (mg/kg)	Ti (mg/kg)	B (mg/kg)
KS0	0	2595.20	1023.10	15.30	1884.70	44.37	400.49	2037.50	469.00	7.35	15.38
KS1	1	2343.0	955.28	35.10	3116.90	36.33	659.86	3071.30	461.46	19.30	16.34
KS2	2	2067.60	793.95	30.20	3295.60	36.00	759.74	3104.20	453.75	19.30	13.57
KS3	3	2410.90	1046.50	27.20	3742.20	44.25	624.00	3472.40	477.77	18.20	13.76
KS4	4	2728.00	915.99	42.10	3357.50	45.86	692.02	3183.10	363.50	15.50	16.14
KS5	5	2469.90	844.36	37.90	3233.70	41.81	689.22	2984.60	439.05	13.70	16.30
KS6	6	2278.70	755.31	28.20	3021.00	37.41	640.67	2767.30	323.35	11.80	14.27
KS7	7	2169.50	608.09	11.90	2709.40	40.36	586.54	2418.50	0.00	9.66	11.94
KS8	8	2337.00	568.99	18.20	2503.40	46.46	510.29	2192.50	0.00	6.65	14.27
KS9	9	2444.40	715.07	22.10	2798.00	48.65	536.79	2493.20	62.47	11.20	17.50
KS10	10	2201.50	656.76	24.00	2746.20	46.07	503.89	2380.70	302.22	9.58	17.60
KS11	11	2330.70	629.71	62.70	2637.70	47.12	482.98	2288.20	308.93	9.65	19.77
KS12	12	2694.70	540.42	29.10	2819.90	44.29	807.67	2646.80	378.73	10.20	11.60
KS13	13	2825.20	500.56	24.60	2227.20	41.94	734.06	2118.10	452.34	9.33	10.58
KS14	14	5076.10	822.36	58.80	3598.80	84.25	940.25	3416.00	321.22	11.60	18.65
KS15	15	4152.90	745.40	13.50	3897.60	58.94	657.26	3358.30	0.00	13.80	13.35
KS16	16	3047.20	794.44	13.80	2699.30	46.17	464.72	2367.70	5.54	8.41	13.56
KS17	17	3847.00	733.28	7.00	3964.00	56.62	611.36	3289.30	0.00	14.90	13.89
KS18	18	7171.10	1059.30	28.60	6213.90	89.91	908.60	5153.20	53.16	27.90	18.51
KS19	19	5705.70	1013.20	19.90	5037.60	76.55	814.77	4313.50	16.97	23.00	17.67
KS20	20	4948.90	944.21	18.20	4940.20	80.30	643.60	4142.00	25.18	21.10	19.27
KS21	21	5129.80	948.31	16.70	4630.30	79.32	613.21	3783.20	11.92	18.10	20.45

KS22	22	4227.70	916.94	19.10	4736.40	69.24	632.11	3941.20	0.00	18.20	16.87
KS23	23	869.14	356.42	20.80	791.24	11.12	270.39	734.92	69.77	1.56	2.56
KS24	24	511.39	248.44	35.30	656.12	7.43	237.88	699.82	0.00	2.37	0.59
KS25	25	566.85	275.68	7.88	836.70	8.60	302.26	807.62	0.00	2.13	1.56
KS26	26	278.30	138.17	2.75	455.02	3.63	372.51	470.77	0.00	1.33	0.00
KS27	27	363.84	143.15	33.20	475.37	5.27	211.61	484.97	45.62	2.21	5.61
KS28	28	415.98	207.27	0.00	606.64	6.24	434.23	665.77	0.48	3.89	0.51
KS29	29	326.68	157.59	1.14	420.99	3.73	311.28	410.55	1.53	1.11	0.00
KS30	30	545.29	227.22	3.00	572.76	6.90	283.89	551.11	0.00	1.34	1.80
KS31	31	257.56	110.54	6.51	298.61	2.03	281.89	260.24	0.00	0.39	0.00
KS32	32	274.69	96.65	6.96	277.25	2.01	207.31	278.43	4.57	0.71	2.06

APPENDIX M – Trace elements of the carbonate fraction phase

Sample Names	Depth (m)	V (mg/kg)	Cr (mg/kg)	Mn (mg/kg)	Co (mg/kg)	Ni (mg/kg)	Cu (mg/kg)	Zn (mg/kg)	As (mg/kg)	Se (mg/kg)	Mo (mg/kg)
KS0	0	8.81	7.16	26.66	0.61	2.48	0.87	2.61	6.15	1.21	0.29
KS1	1	8.86	10.31	34.78	0.69	2.87	2.56	3.36	5.75	0.96	0.15
KS2	2	8.09	12.14	31.62	0.55	2.43	2.04	3.61	5.25	1.017	0.08
KS3	3	8.97	13.74	37.83	0.69	2.71	2.06	3.32	5.42	0.89	0.17
KS4	4	8.03	14.00	38.99	0.62	2.76	4.01	5.02	6.02	1.04	0.17
KS5	5	7.45	12.94	32.88	0.58	2.55	4.22	4.52	5.38	0.85	0.16
KS6	6	7.65	12.33	30.48	0.54	2.19	3.74	2.94	5.51	0.93	0.13
KS7	7	6.42	8.95	23.27	0.36	1.49	1.40	3.10	4.36	0.85	0.10
KS8	8	6.11	8.07	22.75	0.35	1.40	3.22	2.72	4.26	0.78	0.12
KS9	9	6.25	10.46	21.50	0.41	1.58	1.90	2.70	4.46	0.98	0.16
KS10	10	6.43	9.89	16.07	0.35	1.49	3.82	2.72	4.59	0.75	0.13
KS11	11	6.20	10.60	16.49	0.34	1.78	2.35	4.18	4.51	0.72	0.20
KS12	12	2.87	6.89	36.73	0.28	2.00	3.40	2.01	1.60	0.79	0.05
KS13	13	1.75	4.65	31.01	0.19	1.84	2.74	2.22	0.82	0.83	0.05
KS14	14	2.49	7.73	45.37	0.34	3.14	2.31	3.00	1.54	1.43	0.17
KS15	15	2.58	6.71	55.47	0.43	3.15	1.91	2.11	1.50	1.26	0.10
KS16	16	1.88	4.221	42.98	0.28	2.35	1.24	1.54	1.17	0.99	0.07
KS17	17	2.32	5.71	54.46	0.42	2.90	1.65	1.55	1.52	1.34	0.06
KS18	18	2.66	7.42	78.60	0.62	3.93	1.55	1.76	1.84	1.91	0.14

KS19	19	3.07	8.05	65.71	0.58	3.60	1.87	2.25	1.98	1.71	0.13
KS20	20	3.26	8.65	53.92	0.51	3.39	1.63	2.27	2.12	1.74	0.11
KS21	21	2.87	7.64	53.67	0.52	3.37	2.07	1.35	1.95	1.55	0.10
KS22	22	3.04	8.11	50.35	0.55	3.71	3.44	1.31	2.04	1.52	0.09
KS23	23	1.49	2.67	130.93	1.88	2.82	2.49	1.83	0.49	0.44	0.00
KS24	24	0.90	2.45	52.58	0.91	2.11	6.16	2.17	0.37	0.25	0.00
KS25	25	0.10	2.48	59.96	0.91	2.41	6.17	2.75	0.48	0.22	0.00
KS26	26	0.54	1.86	62.73	2.20	3.87	7.43	3.11	0.17	0.11	0.00
KS27	27	0.50	1.41	34.10	1.13	2.18	4.61	3.00	0.33	0.17	0.02
KS28	28	0.76	2.25	71.85	3.04	5.81	9.04	4.01	0.40	0.13	0.00
KS29	29	0.54	2.17	81.85	2.52	4.68	6.87	3.01	0.24	0.23	0.00
KS30	30	0.64	2.32	74.82	1.82	3.68	6.37	2.63	0.39	0.10	0.00
KS31	31	0.33	2.67	59.38	2.13	3.14	9.52	5.87	0.11	0.05	0.02
KS32	32	0.39	2.63	78.53	1.93	3.14	5.41	3.89	0.18	0.08	0.05

APPENDIX N – Major elements of the iron and manganese fraction phase

Sample Names	Depth (m)	Fe (mg/kg)	Al (mg/kg)	Ca (mg/kg)	Mg (mg/kg)	Si (mg/kg)	Na (mg/kg)	K (mg/kg)	B (mg/kg)	Ti (mg/kg)
KS0	0	589.00	1209.00	1031.00	436.00	1269.00	6.60	65.00	4.50	10.00
KS1	1	863.00	1257.00	898.00	319.00	1292.00	32.00	59.00	4.60	16.00
KS2	2	973.00	2371.00	1226.00	373.00	2444.00	34.00	39.00	6.50	10.00
KS3	3	757.00	1397.00	939.00	361.00	1436.00	28.00	56.00	5.30	11.00
KS4	4	861.00	1826.00	1249.00	356.00	1928.00	31.00	15.00	4.20	9.90
KS5	5	820.00	1223.00	1047.00	313.00	1329.00	23.00	67.00	4.70	15.00
KS6	6	812.00	1322.00	1102.00	292.00	1400.00	54.00	34.00	4.20	9.00
KS7	7	866.00	1386.00	1105.00	293.00	1517.00	14.00	6.90	4.60	9.50
KS8	8	880.00	1237.00	1156.00	292.00	1373.00	30.00	4.50	4.30	12.00
KS9	9	780.00	1180.00	1063.00	294.00	1382.00	29.00	52.00	4.60	10.00
KS10	10	729.00	1090.00	987.00	281.00	1265.00	26.00	36.00	5.00	11.00
KS11	11	796.00	1425.00	1082.00	278.00	1571.00	26.00	36.00	6.80	7.20
KS12	12	1348.00	2889.00	2270.00	395.00	3494.00	57.00	27.00	5.70	11.00
KS13	13	1183.00	1439.00	1673.00	244.00	1714.00	18.00	41.00	4.10	7.80
KS14	14	1430.00	1791.00	1851.00	285.00	2141.00	33.00	17.00	4.90	7.80
KS15	15	1201.00	1626.00	1624.00	276.00	1924.00	15.00	5.90	4.10	7.70
KS16	16	834.00	1395.00	1481.00	332.00	1651.00	7.90	4.60	3.60	7.10
KS17	17	1037.00	1359.00	1613.00	294.00	1697.00	0.50	4.50	3.50	9.90
KS18	18	1354.00	2406.00	2205.00	325.00	3138.00	6.20	7.40	4.30	4.70
KS19	19	1119.00	1974.00	1796.00	305.00	2458.00	7.00	5.40	3.60	4.40
KS20	20	890.00	1590.00	1429.00	315.00	1881.00	1.70	3.80	3.60	7.50
KS21	21	867.000	1306.00	1531.00	329.00	1684.00	8.00	8.20	3.50	11.00

KS22	22	1052.00	1553.00	1586.00	371.00	1908.00	30.00	12.00	4.00	10.00
KS23	23	2292.00	2054.00	1753.00	624.00	1929.00	41.00	10.00	2.50	3.80
KS24	24	1120.00	1035.00	1325.00	356.00	1046.00	17.00	2.90	1.10	0.90
KS25	25	1111.00	970.70	846.00	303.00	1003.00	11.00	9.90	2.20	1.00
KS26	26	1066.00	409.80	412.00	163.00	466.00	6.50	8.00	0.30	0.20
KS27	27	975.00	463.90	323.00	201.00	578.10	0.00	9.40	0.10	4.70
KS28	28	1414.00	569.40	446.00	257.00	539.60	15.00	7.70	0.00	1.00
KS29	29	1003.00	424.30	799.00	214.00	477.90	6.00	6.80	0.00	0.10
KS30	30	776.00	359.70	306.00	188.00	480.80	16.00	1.60	0.00	0.60
KS31	31	774.00	189.40	378.00	106.00	301.20	0.00	3.80	0.00	0.00
KS32	32	1025.00	552.80	949.00	186.00	437.80	25.00	16.00	0.00	0.20

APPENDIX O – Trace elements in the iron and manganese fraction phase

Sample Names	Depth (m)	V (mg/kg)	Cr (mg/kg)	Mn (mg/kg)	Sr (mg/kg)	Co (mg/kg)	Ni (mg/kg)	Cu (mg/kg)	Zn (mg/kg)	As (mg/kg)
KS0	0	18.10	4.57	33.16	13.94	0.51	1.42	0.00	0.31	1.20
KS1	1	17.59	8.55	27.07	13.76	0.40	1.58	0.00	0.00	1.08
KS2	2	17.39	8.60	21.01	22.44	0.45	1.71	1.75	1.77	1.28
KS3	3	15.78	7.01	27.10	17.11	0.41	1.25	0.00	0.00	0.91
KS4	4	15.20	7.06	23.24	21.85	0.39	1.30	0.06	0.00	1.21
KS5	5	13.63	7.54	23.45	16.54	0.34	1.22	0.00	0.00	0.98
KS6	6	13.59	7.54	20.27	17.30	0.33	1.54	0.00	0.00	1.01
KS7	7	12.44	5.79	16.37	18.63	0.26	1.32	0.00	0.00	0.90
KS8	8	11.87	6.60	17.20	19.96	0.27	1.14	0.00	0.00	0.78
KS9	9	10.83	6.44	12.76	19.32	0.24	1.01	0.00	0.00	0.73
KS10	10	10.17	6.12	10.69	19.06	0.22	0.92	0.00	0.00	0.73
KS11	11	11.30	6.84	11.72	20.54	0.25	1.09	0.00	0.00	0.80
KS12	12	7.65	9.19	25.26	33.12	0.32	2.05	1.14	0.00	0.48
KS13	13	5.29	7.23	22.18	21.88	0.19	1.56	0.00	0.00	0.18
KS14	14	6.99	10.38	26.84	26.58	0.28	2.16	0.00	0.00	0.25
KS15	15	6.77	7.30	39.11	21.96	0.35	1.97	0.00	0.00	0.28
KS16	16	4.80	3.75	32.28	18.38	0.26	1.47	0.00	0.00	0.25
KS17	17	5.44	5.15	38.85	20.45	0.31	1.75	0.00	0.00	0.24
KS18	18	8.24	4.29	48.90	25.89	0.44	1.84	0.00	0.00	0.37
KS19	19	7.28	4.99	33.22	22.09	0.34	1.67	0.00	0.00	0.38
KS20	20	7.11	4.39	33.19	18.05	0.31	1.43	0.00	0.00	0.36

KS21	21	6.18	4.15	33.63	19.28	0.32	1.45	0.00	0.00	0.30
KS22	22	7.37	5.88	37.18	20.49	0.39	2.89	0.00	0.00	0.35
KS23	23	12.88	7.21	116.66	18.36	6.42	8.97	6.06	0.00	0.33
KS24	24	8.96	3.97	258.04	7.84	8.93	9.95	5.66	0.00	0.25
KS25	25	9.47	2.91	326.60	6.25	9.65	15.48	4.61	0.23	0.20
KS26	26	4.94	2.65	88.43	2.27	3.60	5.37	2.71	0.00	0.07
KS27	27	4.43	3.22	65.70	3.96	2.34	3.63	0.00	0.00	0.12
KS28	28	3.90	4.42	42.46	3.57	1.67	3.43	1.42	0.00	0.11
KS29	29	4.37	2.35	105.56	2.42	3.85	5.61	2.58	0.00	0.12
KS30	30	4.79	1.94	157.26	2.69	5.31	7.28	1.87	0.00	0.07
KS31	31	2.94	3.26	38.30	0.81	1.71	2.26	1.09	0.00	0.06
KS32	32	3.55	5.25	93.08	2.15	3.26	4.92	3.50	0.00	0.15

APPENDIX P – Major elements in the residual fraction phase

Sample Names	Depth (m)	Ca (mg/kg)	Al (mg/kg)	Si (mg/kg)	Mg (mg/kg)	K (mg/kg)	Na (mg/kg)	Fe (mg/kg)	Mn (mg/kg)	Ba (mg/kg)	Sr (mg/kg)
KS0	0	8203.14	19468.18	29268.44	2691.52	334.19	1010.80	12721.12	178.29	353.72	1502.40
KS1	1	5092.79	17510.93	30354.97	2432.66	130.38	383.48	11318.94	163.69	91.315	1466.10
KS2	2	6641.85	15645.79	20472.19	1513.23	1824.10	1291.10	13173.78	181.00	1465.10	1504.30
KS3	3	4654.20	16798.22	27294.95	552.44	0.00	466.19	13940.05	170.15	142.31	1384.60
KS4	4	17846.70	16539.74	18182.37	1833.46	6941.50	1195.50	22997.77	243.79	1245.40	2501.10
KS5	5	7261.73	15998.90	20358.36	2120.20	5147.70	373.02	18958.10	214.78	994.08	2235.70
KS6	6	18300.90	16821.11	21312.63	2044.89	5680.70	652.16	20800.31	216.30	1179.70	2385.20
KS7	7	9173.63	16937.93	17676.12	2452.03	3854.00	843.72	20609.30	196.69	1246.9	2123.90
KS8	8	14967.30	16879.82	18264.34	2081.85	4437.00	1096.60	21450.30	214.47	940.42	2044.40
KS9	9	14702.30	19339.64	18738.94	1272.04	204.01	461.11	15129.35	186.46	818.21	1567.60
KS10	10	15193.10	17759.68	25438.63	547.38	1630.50	141.55	13283.37	159.80	580.82	1403.90
KS11	11	17540.00	18450.96	21723.63	1684.18	517.01	351.22	13361.60	198.90	1051.60	1652.50
KS12	12	19671.90	14661.02	14338.74	2473.23	2798.40	844.70	16926.58	286.21	1154.50	2217.20
KS13	13	25652.30	17410.91	20249.52	3025.32	4898.00	547.36	21268.00	301.07	1136.10	2542.80
KS14	14	0.00	14736.83	15198.42	2138.28	3409.60	776.87	15716.15	240.47	778.21	2239.80
KS15	15	3387.61	17301.93	14960.28	1836.72	1955.10	760.51	25995.96	318.14	1126.80	2610.30
KS16	16	30406.10	17388.65	19182.14	2017.50	3510.80	135.49	23432.00	270.51	1024.70	2711.20
KS17	17	20328.60	19303.31	20083.28	1211.57	0.00	802.23	9717.49	69.66	295.18	1747.10
KS18	18	11931.90	22817.64	24983.27	933.292	0.00	1022.20	16223.26	211.50	1233.40	2045.20
KS19	19	43313.40	15204.54	17574.54	1663.65	719.37	560.40	25841.47	236.03	1513.70	2712.10
KS20	20	2016.38	18349.15	16832.22	971.36	0.00	1678.30	12373.46	190.52	1099.30	1972.40
KS21	21	0.00	19642.07	26239.94	1007.45	0.00	1551.50	15079.36	174.40	788.30	1484.20
KS22	22	0.00	19346.54	21383.58	913.78	1671.40	1067.30	13961.28	178.79	748.18	1940.00
KS23	23	17028.40	23667.60	19427.76	3286.20	6509.40	2289.30	30497.71	1031.00	1198.80	1710.90
KS24	24	22764.80	27011.02	20468.18	5714.66	7208.50	2915.00	38598.27	1040.00	1018.40	1629.90

KS25	25	36853.90	23089.34	18801.76	4839.13	5977.00	2854.80	47963.73	949.18	918.79	1337.60
KS26	26	43893.10	23572.12	20650.71	7467.14	6116.10	2228.50	53054.11	1217.60	496.29	1403.50
KS27	27	21964.80	27313.80	30432.85	5568.23	6140.90	3099.10	50023.52	1120.90	1138.40	1177.80
KS28	28	22319.40	22330.94	26836.11	5491.49	6336.30	2213.90	45087.36	1111.50	902.47	1302.10
KS29	29	27722.90	26758.03	24534.75	15225.60	7116.80	3868.80	61690.56	1184.20	419.85	1042.20
KS30	30	18721.00	26145.05	27568.94	4421.75	6329.00	2000.50	42035.89	1133.00	1099.40	1214.50
KS31	31	27458.40	24950.59	29093.14	9174.12	13039.00	2950.80	52593.42	1192.70	658.30	1527.10
KS32	32	19818.40	24559.93	24831.48	3755.67	18883.00	1984.60	40741.46	840.14	1121.50	1668.30

APPENDIX Q – Trace elements in the residual fraction phase

Sample Names	Depth (m)	Zn (mg/kg)	Cu (mg/kg)	Mo (mg/kg)	Se (mg/kg)	As (mg/kg)	Ni (mg/kg)	Cr (mg/kg)	V (mg/kg)	Co (mg/kg)
KS0	0	154.40	49.44	3.37	0.00	0.00	61.55	190.48	121.34	25.46
KS1	1	151.54	30.92	3.37	0.00	0.00	57.96	205.64	113.30	22.95
KS2	2	162.80	32.95	3.33	0.00	0.00	51.06	233.13	128.90	20.92
KS3	3	95.42	37.81	1.73	0.00	0.00	55.46	185.31	127.80	24.13
KS4	4	88.95	45.10	7.46	0.00	0.00	58.61	260.81	137.19	27.91
KS5	5	94.84	32.91	5.90	0.00	0.00	50.67	238.18	123.46	25.15
KS6	6	96.57	33.98	5.83	0.00	0.00	52.51	244.79	121.67	25.22
KS7	7	123.47	32.95	6.17	0.00	0.00	49.02	240.48	124.96	21.25
KS8	8	119.11	32.84	6.59	0.00	0.00	46.59	264.83	132.75	21.41
KS9	9	166.81	34.15	3.80	0.00	0.00	55.09	215.54	122.94	19.05
KS10	10	136.70	29.89	3.15	0.00	0.00	38.98	199.90	115.63	17.09
KS11	11	170.33	37.40	3.75	0.00	0.00	47.49	234.56	137.92	19.59
KS12	12	106.08	21.37	4.83	0.00	0.53	52.72	242.87	108.79	11.94
KS13	13	72.62	19.48	5.46	0.00	0.08	49.09	241.19	97.58	8.64
KS14	14	54.87	20.06	7.90	0.00	0.00	47.24	252.59	97.86	9.21
KS15	15	74.17	25.75	9.66	0.00	0.29	74.09	278.12	100.62	13.81
KS16	16	62.04	20.83	6.02	0.00	0.00	66.50	216.89	89.05	12.24
KS17	17	43.91	4.63	4.76	0.00	0.00	0.00	134.97	31.22	6.24
KS18	18	102.00	17.90	2.26	0.00	0.00	58.31	157.36	65.19	13.64
KS19	19	97.99	20.39	2.45	0.00	0.00	58.11	196.77	75.55	14.51
KS20	20	109.74	23.82	2.40	0.00	0.79	63.67	182.06	78.80	15.55
KS21	21	112.95	22.08	2.71	0.00	0.00	60.65	166.86	76.23	14.55
KS22	22	64.19	20.60	4.12	0.00	0.00	58.17	183.00	76.93	14.88
KS23	23	204.41	39.30	2.43	0.00	2.65	75.23	378.87	257.54	42.55
KS24	24	165.69	38.63	2.44	0.00	1.72	72.04	352.31	275.27	41.22
KS25	25	148.88	40.82	2.53	0.00	1.61	63.74	298.22	257.43	38.89

KS26	26	98.90	44.00	4.66	0.00	0.00	80.46	438.96	289.96	45.92
KS27	27	172.89	49.50	2.72	0.00	3.01	77.16	262.38	259.73	44.78
KS28	28	161.13	42.11	2.14	0.04	2.67	69.47	266.49	261.02	44.89
KS29	29	111.58	53.34	3.34	0.03	0.46	71.64	395.66	287.62	45.80
KS30	30	196.09	58.19	2.11	0.00	3.09	74.02	316.92	284.90	45.70
KS31	31	128.15	46.13	4.74	0.21	1.26	73.28	414.49	287.90	45.89
KS32	32	153.77	28.93	3.65	0.00	3.26	52.90	271.91	204.03	31.94

APPENDIX R – Major elements in XRF data

Sample Names	Depth (m)	Si (mg/kg)	Al (mg/kg)	Fe (mg/kg)	Mn (mg/kg)	Mg (mg/kg)	Ca (mg/kg)	Na (mg/kg)	K (mg/kg)	P (mg/kg)	Ti (mg/kg)
KS0	0	225118.00	145434.00	19906.00	263.58	6099.30	38623.00	7451.90	4223.60	2128.40	19487.00
KS1	1	227097.00	176591.00	21212.00	260.90	5454.00	42005.00	6550.80	3667.10	1745.20	19775.00
KS2	2	220134.00	30149.00	20768.00	237.70	4865.20	45021.00	6471.60	3599.60	1636.60	20718.00
KS3	3	219269.00	48998.00	22582.00	295.36	5878.30	46969.00	5615.20	3968.60	2447.30	18923.00
KS4	4	225450.00	166630.00	21802.00	270.26	5132.80	45307.00	6535.20	3568.40	2042.10	19049.00
KS5	5	226071.00	169132.00	23157.00	279.00	5575.30	46211.00	6402.10	3911.70	2058.90	20234.00
KS6	6	227148.00	171565.00	22463.00	267.44	5319.20	45311.00	7025.40	3736.20	2090.60	20084.00
KS7	7	226666.00	173971.00	22303.00	224.83	4552.20	40507.00	6589.00	3235.50	2273.40	19622.00
KS8	8	226929.00	172521.00	23921.00	239.51	5011.90	42250.00	6695.40	3384.00	2500.40	20355.00
KS9	9	232736.00	164482.00	24090.00	217.63	5966.70	46033.00	7054.50	3861.00	2933.30	19961.00
KS10	10	235096.00	162249.00	22688.00	205.55	5919.80	44274.00	7178.80	3892.30	2975.20	19351.00
KS11	11	236138.00	160822.00	21091.00	195.03	5619.70	43634.00	6603.20	4079.00	2712.60	19001.00
KS12	12	238207.00	172711.00	21893.00	300.72	3950.00	45869.00	4382.00	2810.10	2183.80	18840.00
KS13	13	234508.00	169990.00	24068.00	342.53	3931.70	49200.00	3605.10	3062.60	2294.10	19254.00
KS14	14	228862.00	170997.00	22525.00	309.34	3951.10	46444.00	4036.50	2683.90	2508.60	18890.00
KS15	15	206042.00	162501.00	27139.00	371.13	4342.80	68825.00	3819.90	1836.30	4736.90	17892.00
KS16	16	212093.00	169198.00	26584.00	357.47	5547.00	60852.00	5251.30	2019.10	4310.30	18969.00
KS17	17	201723.00	161882.00	29861.00	393.32	4644.70	77910.00	4023.50	1705.20	5127.30	17453.00
KS18	18	183061.00	147976.00	28849.00	429.78	4628.90	94345.00	4112.60	1772.00	5505.50	16444.00
KS19	19	201061.00	147976.00	29489.00	385.43	4833.30	80075.00	4459.10	2093.30	4670.20	17201.00
KS20	20	208803.00	158354.00	23239.00	311.10	4457.00	73573.00	4329.40	2121.10	4659.90	17377.00
KS21	21	203031.00	158972.00	24532.00	329.34	4550.70	73050.00	4520.70	2192.30	4668.80	17488.00

KS22	22	203178.00	156836.00	25576.00	330.99	4799.20	71760.00	4519.10	2083.70	4436.00	17007.00
KS23	23	230472.00	99621.00	73033.00	1435.30	17381.00	70175.00	9495.00	4945.00	1751.50	11314.00
KS24	24	227259.00	99742.00	80166.00	1317.50	19808.00	71491.00	11851.00	5363.00	1685.70	10702.00
KS25	25	226170.00	101416.00	77128.00	1367.20	19328.00	68446.00	11177.00	5319.60	1730.70	11373.00
KS26	26	230008.00	90962.00	81075.00	1318.10	23539.00	79439.00	15360.00	6177.70	1394.90	9673.40
KS27	27	227171.00	106626.00	72977.00	1200.80	20171.00	75527.00	14187.00	5866.80	1951.30	11884.00
KS28	28	228301.00	97263.00	74692.00	1252.90	22571.00	73816.00	16606.00	646.28	1444.00	10821.00
KS29	29	229352.00	87118.00	82212.00	1326.50	23970.00	74390.00	14010.00	5954.80	1261.80	11052.00
KS30	30	232173.00	91778.00	81858.00	1256.40	23507.00	70638.00	12303.00	5351.80	1360.90	11731.00
KS31	31	247720.00	83992.00	9020.30	1049.60	22194.00	67055.00	14506.00	10034.00	992.39	9653.50
KS32	32	274819.00	80714.00	57325.00	981.91	17833.00	52745.00	13975.00	19932.00	840.58	8126.50

APPENDIX S – Trace elements in XRF data

Sample Names	Depth (m)	Pb (ppm)	As (ppm)	Ba (ppm)	Ce (ppm)	Co (ppm)	Cu (ppm)	Mo (ppm)	Nb (ppm)	Ni (ppm)	Sr (ppm)
KS0	0	115.61	29.29	51.48	279.66	29.01	86.56	6.01	42.32	85.01	1006.37
KS1	1	103.68	27.80	0.00	257.39	28.73	72.96	6.18	44.32	83.10	918.52
KS2	2	100.51	24.22	0.00	264.32	22.27	78.01	6.41	43.89	80.45	988.73
KS3	3	90.54	23.97	97.85	278.41	24.45	78.90	6.65	42.14	79.02	1085.43
KS4	4	104.18	26.67	0.00	267.79	24.28	76.66	6.12	44.43	75.46	1032.04
KS5	5	100.24	24.65	0.00	252.64	22.24	69.99	6.28	44.09	72.88	974.50
KS6	6	103.52	27.22	0.00	258.09	25.06	75.26	6.75	45.24	79.21	978.27
KS7	7	102.38	26.02	0.00	253.27	22.70	73.53	6.31	43.70	68.78	968.26
KS8	8	96.54	24.44	0.00	250.87	19.48	72.60	6.33	44.43	64.47	1039.15
KS9	9	97.37	24.31	28.63	267.86	22.67	73.65	6.08	43.62	61.98	1070.31
KS10	10	92.89	23.77	80.14	269.24	19.70	70.75	6.26	43.10	56.33	1101.56
KS11	11	93.17	24.93	57.30	265.72	18.87	78.84	6.34	45.25	63.73	1094.56
KS12	12	34.05	8.19	0.00	218.54	9.05	55.30	6.41	41.70	77.42	920.40
KS13	13	21.31	3.35	0.00	244.17	10.86	45.53	6.66	46.55	71.37	1040.07
KS14	14	28.02	6.93	0.00	232.92	10.27	48.91	6.61	43.26	73.64	1083.86
KS15	15	29.43	5.67	138.98	264.79	8.90	53.59	6.35	40.64	101.20	1332.26
KS16	16	25.28	5.60	0.00	238.72	14.60	48.24	6.21	43.55	97.18	1175.90
KS17	17	19.79	4.38	291.38	278.82	12.43	52.44	6.34	41.52	101.34	1389.18
KS18	18	17.14	3.81	632.92	305.93	16.55	47.74	6.24	39.04	92.45	1411.14

KS19	19	21.36	6.04	474.21	294.16	14.44	42.33	6.57	41.55	85.77	1351.56
KS20	20	22.10	5.32	411.02	294.35	13.64	56.69	5.98	41.42	93.76	1332.15
KS21	21	26.22	5.42	452.62	300.49	17.43	57.35	5.70	39.95	96.30	1350.63
KS22	22	25.36	7.47	486.46	316.11	17.33	54.49	6.60	42.20	96.07	1374.40
KS23	23	0.00	0.00	87.19	136.04	36.61	104.83	4.98	19.96	109.52	436.30
KS24	24	0.00	0.00	91.64	129.13	32.59	101.88	5.00	18.99	103.95	377.96
KS25	25	0.00	0.00	73.93	139.08	34.06	108.86	4.86	19.73	109.08	426.27
KS26	26	0.00	0.00	147.66	103.60	34.20	100.58	4.63	15.61	104.41	290.31
KS27	27	0.00	0.00	39.49	136.25	32.44	109.22	4.43	18.98	105.97	435.66
KS28	28	0.00	0.00	0.00	107.89	37.19	115.95	4.81	16.21	112.17	344.04
KS29	29	0.00	0.00	0.00	95.46	37.80	121.55	4.60	12.82	108.63	274.29
KS30	30	0.00	0.00	0.00	103.08	27.70	122.04	4.61	19.69	106.69	323.81
KS31	31	0.00	0.00	0.00	81.31	31.20	103.24	4.30	14.38	93.54	239.62
KS32	32	0.00	1.83	354.85	102.44	28.15	81.77	4.77	13.42	74.26	235.77

APPENDIX T

Major elements in surface sample in %

Fractions	Ca	Al	Si	Fe	Mg	Na	K	Sr	Ti	Ba
WE	4.05	1.64	1.43	0.54	4.35	17.55	1.54	0.87	0.20	1.84
XF	50.02	0.11	0.60	0.06	12.65	20.76	66.01	9.55	0.00	22.63
CF	10.08	8.81	5.70	2.90	20.46	0.91	17.52	2.55	0.06	11.47
Fe/MnF	4.00	5.23	3.83	4.27	8.71	0.39	2.44	0.80	0.08	4.03
RF	31.85	84.21	88.44	92.23	53.83	60.37	12.49	86.24	99.66	60.04

Major elements at 18 m in %

Fractions	Ca	Al	Si	Fe	Mg	Na	K	Sr	Ti	Ba
WE	4.83	1.72	1.07	0.05	3.44	18.55	1.21	0.96	0.01	0.22
XF	59.94	0.02	2.34	0.01	35.15	21.24	95.76	13.25	0.00	12.94
CF	11.86	16.67	17.48	4.91	28.07	1.64	2.80	3.57	0.29	9.91
Fe/MnF	3.65	7.78	8.83	7.32	8.60	0.029	0.24	1.03	0.05	1.58
Residual	19.73	73.81	70.28	87.71	24.73	58.55	0.00	81.19	99.65	75.35

Trace elements in the surface sample in %

Fractions	B	Mn	Co	Ni	V	Cu	Zn	As	Se	Cr	Mo	Cd	Pb
WE	0.05	1.66	0.42	1.54	2.64	3.89	0.84	6.77	8.11	0.97	4.52	0.00	0.69
XF	0.18	4.71	0.29	0.56	4.25	1.54	0.84	49.10	61.68	1.08	10.75	0.00	0.25
CF	0.09	10.48	2.27	3.70	5.53	1.63	1.63	36.94	28.50	2.22	6.50	9.96	1.31
Fe/MnF	0.03	13.04	1.90	2.12	11.37	0	0.19	7.20	1.71	2.22	3.49	0.00	0.20
RF	99.66	70.11	95.12	92.07	76.21	92.94	96.50	0.00	0.00	92.27	74.73	90.00	97.55

Trace elements at 18 m in %

	B	Mn	Co	Ni	V	Cu	Zn	As	Se	Cr	Mo	Cd	Pb
WE	0.71	0.58	0.02	0.39	1.81	7.37	3.42	7.38	5.87	0.94	10.79	0.00	0.35
XF	1.73	9.64	1.23	3.34	3.36	9.85	1.28	55.02	33.29	1.69	20.53	0.00	1.14
CF	0.27	20.82	4.14	5.91	3.32	6.58	1.62	31.34	50.33	4.27	3.772	0.00	3.61
Fe/MnF	0.06	12.95	2.99	2.765	10.26	0.00	0.00	6.27	10.51	2.47	2.761	0.00	0.06
RF	97.21	56.01	91.62	87.59	81.25	76.20	93.68	0.00	0.00	90.63	62.15	100.00	94.84

APPENDIX U – pH, EC and TDS data

Sample Names	Depth (m)	TDS (ppth)	EC (mS/cm)	pH
KS0	0	0.07	0.13	8.65
KS1	1	0.11	0.21	9.67
KS2	2	0.15	0.29	9.57
KS3	3	0.09	0.17	10.15
KS4	4	0.09	0.16	10.16
KS5	5	0.09	0.17	10.26
KS6	6	0.08	0.16	10.34
KS7	7	0.09	0.17	10.25
KS8	8	0.08	0.16	10.26
KS9	9	0.08	0.15	10.22
KS10	10	0.09	0.16	10.23
KS11	11	0.10	0.18	10.13
KS12	12	0.07	0.14	10.32
KS13	13	0.08	0.15	10.22
KS14	14	0.09	0.18	10.11
KS15	15	0.12	0.23	10.24
KS16	16	0.24	0.46	10.22
KS17	17	0.11	0.21	10.43
KS18	18	0.15	0.29	10.72
KS19	19	0.16	0.29	10.78
KS20	20	0.13	0.25	10.23
KS21	21	0.11	0.22	10.62
KS22	22	0.12	0.23	10.58
KS23	23	0.04	0.09	9.48
KS24	24	0.05	0.11	9.21
KS25	25	0.08	0.15	9.15
KS26	26	0.06	0.12	9.10
KS27	27	0.07	0.14	9.67
KS28	28	0.06	0.13	9.09
KS29	29	0.06	0.13	8.96
KS30	30	0.07	0.14	9.05
KS31	31	0.03	0.08	8.57
KS32	32	0.05	0.11	9.15